

Functional characterisation of Nudix hydrolase effectors from phytopathogenic fungi

Carl L. McCombe

November 2023

A thesis submitted for the degree of Doctor of Philosophy of The Australian National
University

© Copyright by Carl McCombe 2023

All Rights Reserved

Declaration

This thesis contains no material which has been accepted for the award of any other degree or diploma in any university. To the best of the author's knowledge, it contains no material previously published or written by another person, except where due reference is made in the text.

Carl McCombe

November 2023

Acknowledgements

First and foremost, thank you to my primary supervisor Dr Simon Williams. The support, guidance, enthusiasm, and independence you have provided me was instrumental for my success and happiness throughout this journey.

I would like to thank all past and present Williams Lab members, Megan Outram, Daniel Yu, Emma Crean, Ash Smith, Sean Broderick, Julian Greenwood, Helana Trantino, Nuren Tasneem, Shouvik Aditya, Zhao Li, and Erin Hill, for ensuring the time spent in the lab was always welcoming, fun, and entertaining. Thank you to our remote lab member and one of my co-supervisors, Daniel Eriksson. I submitted four protein structures to the PDB during my PhD, Daniel provided expert support and graciously checked all my data files before submission. Furthermore, I would like to acknowledge the entire plant-microbe interactions floor for fostering a productive, friendly, and collaborative environment.

I had the opportunity to supervise three wonderful undergraduate students, Elly, Sascha, and Riley. Thank you for injecting enthusiasm and curiosity into the research, your involvement was incredibly motivating.

Many *Nicotiana benthamiana* plants were utilised for my research, a big thank you to the incredible plant services team for their continuous provision of seedlings. I've also enjoyed working as a weekend waterer for plant services throughout this year, many of my better ideas have been thought-up while watering plants.

I'm grateful to my parents for their constant support, it has been almost eight years since I moved away from home and throughout my university education my parents have always been there for me. My incredible fiancée Madi has been both an anchor and inspiration throughout this journey, bringing happiness and unwavering support into my life; for that, I am profoundly grateful. I would also like to express my gratitude for the two cutest rabbits, Ginny and Lyra, whose comforting presence and playful antics provided immeasurable joy.

With everyone's help, I have thoroughly enjoyed my PhD experience.

This research was supported by an AINSE Ltd. Postgraduate Research Award (PGRA), and Australian Government Research Training Program (RTP) Scholarship.

Abstract

Agricultural crop production is persistently constrained by plant-pathogenic fungi, threatening the ability of society to feed a growing global population. Central to the intricate molecular interactions occurring between plants and pathogenic fungi are small pathogen-secreted proteins (effectors). While these effectors typically exhibit vast sequence diversity due to intense evolutionary pressures, there are instances where similar effector groups are shared across multiple unrelated pathogens. The Nudix hydrolase effectors are one such group. Understanding the functions of conserved effector families offers a potential pathway towards unravelling the sophisticated interplay that occurs between multiple cropping plant species and their devastating fungal pathogens. Effector functional characterisation may also offer invaluable insights into potential strategies to improve crop disease resistance. In this thesis, I have identified and characterised effectors from pathogenic fungi that are functional Nudix hydrolase enzymes.

AvrM14, a Nudix hydrolase effector from *Melampsora lini* (flax rust), is recognised by the *Linum usitatissimum* (flax) immune receptors M1 and M4. An exhaustive substrate screen was conducted prior to my thesis, including 70 compounds often hydrolysed by Nudix hydrolases. The *in vitro* screen revealed AvrM14's remarkable substrate selectivity, the effector only hydrolysed $^{m7}Gp_5G$ (P1-(5'-7-methyl-guanosyl)-P5-(5'-guanosyl)-pentaphosphate). While $^{m7}Gp_5G$ does not occur naturally, 7-methyl guanosine (^{m7}G) is a distinctive molecular structure from the 5' cap of mRNA transcribed by eukaryotic RNA polymerase II. I conducted a sensitive *in vitro* radiolabelled assay and determined that AvrM14 can remove the protective 5' cap from mRNA and this activity requires a glutamate amino acid within the putative active site. Notably, homodimerisation of AvrM14 promoted biologically relevant mRNA cap cleavage and mRNA decapping activity is conserved in related Nudix hydrolase effectors across the *Melampsora* genus. When expressed *in planta*, AvrM14 suppresses the immune-related reactive oxygen species burst and hypersensitive cell-death response triggered by M1. Significantly, the same pivotal glutamate amino acid is indispensable both for the mRNA decapping and the immune-suppressive activities. My findings support a model whereby the Nudix hydrolase effectors from *Melampsora* spp. decap plant mRNA to suppress immune responses and ultimately promote the infection process.

Predicted Nudix hydrolase effectors also exist in *Magnaporthe oryzae* (rice blast) and multiple *Colletotrichum* spp. The Nudix effectors from *Magnaporthe* and *Colletotrichum* are more closely related to each other than the mRNA decapping effectors of *Melampsora* spp. Substrate

screening with purified effector proteins revealed that the *Magnaporthe* and *Colletotrichum* effectors hydrolyse inositol pyrophosphate signalling molecules. To understand substrate binding, I determined the crystal structure of the *M. oryzae* Nudix effector (*MoNudix*). Structural similarity searches revealed that *Homo sapiens* diphosphoinositol polyphosphate phosphohydrolase 1 (*HsDIPP1*) is remarkably similar to *MoNudix* in both overall structure and surface charge properties. *HsDIPP1* also hydrolyses inositol pyrophosphates, and using targeted mutagenesis I demonstrate that like *HsDIPP1*, *MoNudix* utilises basic amino acids to facilitate selective inositol pyrophosphate binding and hydrolysis. Inositol pyrophosphates are signalling molecules that indicate the availability of phosphate: diminished inositol pyrophosphate levels activate phosphate starvation response transcription factors, thereby driving the expression of genes responsive to phosphate deprivation. Consistent with this, the production of Nudix hydrolase effectors from *M. oryzae* and *Colletotrichum* spp. in *Nicotiana benthamiana* elevated the expression of phosphate starvation responsive genes as measured by RT-qPCR. Phosphate starvation induction was dependant on amino acids required for the hydrolysis of inositol pyrophosphates *in vitro*, and all qPCR data was corroborated using an innovative promoter/reporter system developed during the study. Work from our collaborators demonstrated that when the expression of one inositol pyrophosphate hydrolysing effector from *M. oryzae* was reduced using RNAi, there was a significant decline in the pathogen's virulence on rice. Live cell-imaging also indicates that the inositol pyrophosphate hydrolase effector is translocated into the host rice cell during infection. Collectively, the results indicate that *Magnaporthe* and *Colletotrichum* Nudix hydrolase effectors function as intracellular hydrolases, targeting inositol pyrophosphate signalling molecules which initiates plant phosphate starvation responses.

To date, the virulence functions of fungal effectors have remained largely unidentified. Through this study, I have established that the predicted Nudix hydrolase effectors from pathogenic fungi act as enzymes, likely targeting mRNA caps and inositol pyrophosphates. Collectively, my work has led to significant advances in our understanding of fungal effector function and the complex interplay occurring between pathogenic fungi and their plant hosts.

List of Abbreviations

6 x His	-	hexahistidine protein tag
ACRF	-	Australian Cancer Research Foundation
ADP	-	adenosine diphosphate
ADPR	-	adenosine diphosphate ribose
AINSE	-	Australian Institute of Nuclear Science and Engineering
AMF	-	arbuscular mycorrhizal fungi
AMP	-	adenosine monophosphate
ANOVA	-	analysis of variance
AP	-	appressoria
APIP	-	AvrPiz-t Interacting Protein
Ap _n A	-	diadenosine polyphosphate
ARC	-	Australian Research Council
ATP	-	adenosine triphosphate
AU	-	absorbance units
Avr	-	avirulence effector protein
BFA	-	brefeldin A
BIC	-	biotrophic interfacial complex
BLAST	-	basic local alignment search tool
CC	-	coiled-coil
cDNA	-	complementary DNA
CDP	-	cytidine diphosphate
CDS	-	coding sequence
CE-ESI-MS	-	capillary electrophoresis electrospray ionization mass spectrometry
CEBiP	-	chitin elicitor binding protein
CERK1	-	chitin elicitor receptor kinase 1
cNMP	-	cyclic nucleotide monophosphate
DAMP	-	damage-associated molecular pattern
DE	-	differential expression
DNA	-	deoxyribonucleic acid
dpi	-	days-post infiltration
ECD	-	extracellular domain
EIHM	-	extra-invasive hyphal membrane
ER	-	endoplasmic reticulum
ETI	-	effector-triggered immunity
FAD	-	flavin adenine dinucleotide
FDR	-	false discovery rate
GDP	-	guanosine diphosphate
GFP	-	green fluorescent protein
GMP	-	guanosine monophosphate
GO	-	gene ontology
G _p ₅ G	-	diguanosine pentaphosphate
GTP	-	guanosine triphosphate
hpi	-	hours-post inoculation
HR	-	hypersensitive response
ID	-	integrated domain
InsP ₆	-	inositol hexakisphosphate
InsP ₈	-	1/3,5-PP-InsP ₄
IQR	-	interquartile range

ITP	-	inosine triphosphate
JA-Ile	-	(3R,7S)-jasmonoyl-L-isoleucine
JGI	-	Joint Genome Institute
Kd	-	disassociation constant
kDa	-	kilodalton
LB	-	Luria-Bertani broth
LRR	-	leucine-rich repeat
LysM	-	lysin motif
^{m7} G	-	7-methyl guanosine
^{m7} Gp ₅ G	-	P1-(5'-7-methyl-guanosyl)-P5-(5'-guanosyl)-pentaphosphate
MALS	-	multi-angle light scattering
MAMP	-	microbe-associated molecular pattern
MAPK	-	mitogen-activated protein kinase
MEC	-	membranous effector compartment
mL	-	millilitre
mM	-	millimolar
MR	-	molecular replacement
mRFP	-	monomeric red fluorescent protein
mRNA	-	messenger RNA
MST	-	micro-scale thermophoresis
NAD ⁺ /NADH	-	nicotinamide adenine dinucleotide
NB	-	nucleotide binding
NCBI	-	National Centre for Biotechnology Information
ng	-	nanogram
NLR	-	nucleotide binding leucine-rich repeat receptor
nm	-	nanometre
nM	-	nanomolar
NMD	-	nonsense-mediated mRNA decay
NRD	-	N-terminal regulatory domain
ns	-	not significant
Nudix	-	nucleoside diphosphate linked to moiety-X
OD	-	optical density
ORF	-	open reading frame
p-RNA	-	5'-monophosphate RNA
P1BS	-	PHR binding sequence
PAGE	-	polyacrylamide gel electrophoresis
PCR	-	polymerase chain reaction
PDB	-	protein data bank
pEG	-	pEarleyGate
PGRA	-	Postgraduate Research Award
PHR	-	phosphate starvation response transcription factor
Pi	-	inorganic phosphate
PMSF	-	phenylmethylsulfonyl fluoride
PP-InsP	-	inositol pyrophosphate
pp-RNA	-	5'-diphosphate RNA
PPI	-	protein-protein interaction
pRib-ADP	-	2'-(5''-phosphoribosyl)-5'-adenosine diphosphate
pRib-AMP	-	2'-(5''-phosphoribosyl)-5'-adenosine monophosphate
PSI	-	phosphate starvation induced
PSR	-	phosphate starvation response

PTI	-	pattern-triggered immunity
qPCR	-	quantitative polymerase chain reaction
qRT-PCR	-	quantitative reverse transcription polymerase chain reaction
RALF	-	rapid alkalinisation factor
Rf	-	retention factor
RLCK	-	receptor-like cytoplasmic kinase
RLK	-	receptor-like kinase
RLP	-	receptor-like protein
RLU	-	relative luminescence units
RNA	-	ribonucleic acid
RNA-Seq	-	RNA-Sequencing
RNAi	-	RNA interference
ROS	-	reactive oxygen species
RTP	-	Research Training Program
S1P	-	site-1 protease
SAD	-	single-wavelength anomalous diffraction
SD	-	standard deviation
SEC	-	size-exclusion chromatography
SEM	-	standard error of the mean
T-DNA	-	transfer DNA
TB	-	terrific broth
TDP	-	thymidine diphosphate
TIR	-	toll/interleukin-1 receptor
TLC	-	thin-layer chromatography
TNT	-	tuberculosis necrotizing toxin
TPM	-	transcripts per million
tRNA	-	transfer RNA
TPP	-	thymidine triphosphate
UDP	-	uridine diphosphate
UTR	-	untranslated region
WAK	-	wall-associated-kinase
WT	-	wild-type
XTP	-	xanthosine triphosphate
Y2H	-	yeast-two hybrid
YFP	-	yellow fluorescent protein
μ L	-	microlitre

Table of contents

1. Introduction	12
1.1 Plant diseases	12
1.1.1 <i>Melampsora</i> spp.	12
1.1.2 <i>Magnaporthe</i> spp.	14
1.2 Molecular plant immunity	17
1.2.1 Pathogen recognition	17
1.2.2 Plant immune signaling	18
1.2.3 Overcoming plant defence with effectors	21
1.3 Nudix hydrolase effectors	23
1.3.1 Avr3b	25
1.3.2 RipN	26
1.3.3 HopAG1	27
1.3.4 MoNudix	28
1.3.5 AvrM14	29
1.4 Aims of this thesis	30
1.5 References	31
2. A rust-fungus Nudix hydrolase effector decaps mRNA <i>in vitro</i> and interferes with plant immune pathways	41
3. A family of fungal effectors induce plant phosphate starvation responses by hydrolysing inositol pyrophosphates	86
4. Discussion	140
4.1 Summary of key findings	140
4.2 Enzymatic effectors from pathogenic fungi	141
4.3 Substrate selectivity mechanisms in Nudix hydrolases	142
4.4 Evidence for RNA decapping influencing plant immune signalling	143
4.5 The influence of phosphate homeostasis on plant-microbe interactions	144
4.6 Are Nudix effectors critical pathogenicity factors in <i>Colletotrichum</i> ?	146
4.7 Links between phosphate status and mRNA decay	148
4.8 Targeting Nudix effectors to achieve disease resistance	149
4.9 Conclusion	151
4.10 References	152
5. Appendix	156

Disclaimer: Section 1.2 of this introduction contains text adapted from: McCombe CL, Greenwood JR, Solomon PS, Williams SJ. Molecular plant immunity against biotrophic, hemibiotrophic, and necrotrophic fungi. *Essays Biochem.* 2022 Sep 30;66(5):581-593.

All text represents original writing that I completed during my candidature at The Australian National University.

Carl McCombe

November 2023

1. Introduction

1.1 Plant diseases

In 2021, the Food and Agricultural Organisation of the United Nations estimated the global economic cost of plant diseases to be US\$220 billion annually (Fao 2021). The impact of these diseases, however, extends beyond financial losses. Recent outbreaks of coffee rust in Central America contributed to coffee farmers and labourers losing their livelihoods, leading to increased poverty and hunger (Avelino *et al.*, 2015). Notable historical events like the Irish potato famine and the Great Bengal famine underscore the catastrophic potential of crop diseases. In the Great Bengal famine alone, it is estimated that two million people died of starvation (Padmanabhan 1973). With a predicted 60% increase in global food production required by 2050 to feed the growing population (Fao 2019), society needs to detect, monitor, and control plant diseases to ensure future food security. Complicating matters further are forecasts of pathogen spread to new geographical areas prompted by changing climates (Bebber *et al.*, 2013, Bebber 2015, Delgado-Baquerizo *et al.*, 2020), the evolution of novel pathogen lineages (Singh *et al.*, 2011, Cooke *et al.*, 2012, Inoue *et al.*, 2017), and the emergence of pesticide resistance (Chen *et al.*, 2007, Castroagudín *et al.*, 2015, Dooley *et al.*, 2016). In the fight against plant pathogens, it is imperative that we understand our enemy.

1.1.1 *Melampsora* spp.

Melampsora belongs to the order *Pucciniales*, which is composed of >7000 identified species of foliar plant pathogens (Aime and Mctaggart 2021). The *Pucciniales* are commonly referred to as rust diseases, due to their characteristic rust (yellow/orange/red/brown) colouration on infected plants. Rusts sap their host plants of important nutrients, promote water loss by rapidly increasing plant transpiration during fungal sporulation, and ultimately reduce the yield of important crops (Voegele and Mendgen 2003, Grimmer *et al.*, 2012). The historical footprint of rust diseases on human society traces back over 3000 years, as indicated by archaeological evidence (Kislev, 1982). In ancient Rome, the Robigalia festival involved sacrificial offerings aimed at preventing epidemics of cereal rust diseases. Today, cereal rusts alongside other rust diseases continue to pose significant threats to agricultural productivity and are the focus of intensive characterisation and research (Singh *et al.*, 2011, Langenbach *et al.*, 2016, Moscou and Van Esse 2017, Talhinhias *et al.*, 2017, Figueroa *et al.*, 2018, Duplessis *et al.*, 2021, Petre and Duplessis 2022).

Rust fungi are obligate biotrophs, they subsist exclusively on living plant tissue. Their lifestyle is remarkably complex, with up to 5 distinct spore stages. Furthermore, many rust fungi are heteroecious, meaning they infect multiple plant host species during different stages of development (Aime *et al.*, 2017). The combination of obligate biotrophy and a complex lifestyle place rust fungi among the most difficult plant pathogens to study in a modern research environment. Therefore, to study the molecular interactions occurring during plant infection, researchers typically rely heavily on heterologous systems (reviewed in (Lorrain *et al.*, 2018)). A key player in the molecular interactions occurring between rust fungi and their host plants are small proteins secreted from the fungus called effectors, which play a pivotal role in promoting disease. However, some effectors can be recognised by host plant receptor proteins which typically leads to disease resistance (see section 1.2 for a detailed introduction to plant immunity receptors and effectors). Recognised effectors are often called Avrs (avirulence effector).

Melampsora lini is considered the ‘model’ rust species with respect to studies on effector-dependent virulence/avirulence (Lawrence *et al.*, 2007). *M. lini* is an autoecious fungus, its entire lifecycle is completed on a single host plant. Although *M. lini* infection of flax (*Linum usitatissimum*) can result in severe seed yield losses and reduced flax fibre quality, flax rust has been described as ‘more famous than infamous’ (Dean *et al.*, 2012). This description reflects the profound and fundamental knowledge studies of the flax/flax rust interaction have provided society regarding plant-microbe interactions. Harold Flor’s seminal research into the interactions between flax and flax rust in the mid-20th century (Flor 1935, 1940, 1941, 1942, 1946, 1947), mapped the ability of flax rust races to infect various flax genotypes. During this research, Flor proposed that the ‘pathogenicity of a physiologic race of *Melampsora lini* is determined by pathogenic factors specific for each resistance factor possessed by the host’. This is known as the ‘gene-for-gene’ relationship (reviewed in (Lawrence *et al.*, 2007)). The pathogenic factors have since been identified as effectors and the resistance factors as plant immunity receptors.

Over the past few decades various avirulence effectors from flax rust and their cognate receptor proteins in flax have been identified (Lawrence *et al.*, 1995, Anderson *et al.*, 1997, Ellis *et al.*, 1999, Dodds *et al.*, 2001, Dodds *et al.*, 2004, Catanzariti *et al.*, 2006, Lawrence *et al.*, 2010) and their interactions characterised (Catanzariti *et al.*, 2010, Ravensdale *et al.*, 2012, Ve *et al.*, 2013, Anderson *et al.*, 2016, Zhang *et al.*, 2018). These studies have revealed important details regarding the recognition of Avrs. However, a comprehensive understanding of how rust effectors promote virulence in the absence of recognition remains elusive. The presented thesis

will provide an in-depth analysis into how a group of *Melampsora* effectors act as enzymes to promote virulence. Understanding the virulence activities of rust effectors is essential for a comprehensive understanding rust disease.

1.1.2 *Magnaporthe* spp.

Species within the *Magnaporthe* (*syn. Pyricularia*) genus are the causal agents of blast disease afflicting various monocot grass species, including vital crops such as rice, wheat, barley, and finger millet. Of particular concern to the global economy and food security is *Magnaporthe oryzae*, which restrains rice yield (Talbot 2003, Fernandez and Orth 2018), can devastate finger millet crops (Mbinda and Masaki 2020), and poses an emerging threat to wheat production (Cruz and Valent 2017, Ceresini *et al.*, 2018, Ceresini *et al.*, 2019). Annually, this one fungal species is responsible for the destruction of enough food to sustain hundreds of millions of people (Fisher *et al.*, 2012). *M. oryzae* can be separated into several host-adapted lineages, including *Oryza* (rice), *Triticum* (wheat), *Setaria* (foxtail millet), *Eleusine* (finger millet), and *Lolium* (ryegrass) lineages (Gladieux *et al.*, 2018). Isolates within each lineage are typically associated with aggressive blast disease on their preferred host plant, although there are instances of isolates straying beyond their typical lineages to target alternative hosts (Farman *et al.*, 2017, Gladieux *et al.*, 2018). Concerningly, *M. oryzae* is poised for further host expansion and specialisation (Valent *et al.*, 2019). The combination of gene flow between lineages (Gladieux *et al.*, 2018), the ability to infect multiple hosts (Mackill and Bonman 1986, Chung *et al.*, 2020, Paul *et al.*, 2022), and the proximity in which various *M. oryzae* hosts often grow, could expedite the emergence of novel and aggressive *M. oryzae* strains. This threat is exemplified by the recent development of wheat blast disease, which was first reported in Brazil in 1985 (Igarashi 1986) and spread to Bangladesh in 2016 (Surovy *et al.*, 2023) and Zambia in 2017 (Tembo *et al.*, 2020).

M. oryzae is a hemibiotrophic pathogen, initially extracting nutrients from living host tissue before causing plant cell death. Detailed analysis of the rice infection process has revealed that infection begins by three-celled spores (conidia) actively attaching to the surface of a leaf (Hamer *et al.*, 1988). These conidia germinate and extend a germ tube across the leaf surface (Figure 1). An infection structure called an appressorium forms at the tip of the germ tube; the appressorium generates extreme turgor pressure (up to 8.0 MPa) (Howard *et al.*, 1991) to drive a penetration peg through the host cuticle, breaching the epidermal cells beneath (Dagdas *et al.*, 2012). In a successful infection, *M. oryzae* develops intimate connections with living plant

cells (Figure 1). Live-cell imaging suggests that *M. oryzae* transits between plant cells by penetrating pit fields, where plasmodesmata cluster (Kankanala *et al.*, 2007, Sakulkoo *et al.*, 2018) (Figure 1). *M. oryzae* interacts with invaded rice cells using intracellular hyphae sealed within a plant-derived membrane, named the extra-invasive hyphal membrane (EIHM) (Kankanala *et al.*, 2007) (Figure 1). A dome-shaped region of the EIHM, the biotrophic interfacial complex (BIC), is the site of effector translocation from the fungus into the host cell (Khang *et al.*, 2010) (Figure 1). The functions of most *M. oryzae* effectors are unknown, although some have demonstrated roles interfering with plant immunity (Park *et al.*, 2012, Kim *et al.*, 2020), and preventing pathogen recognition (Mentlak *et al.*, 2012). Identifying how *M. oryzae* effectors promote intracellular colonisation will provide a more comprehensive understanding of this critically important fungal species and may direct the development of cropping plants with enhanced blast disease resistance.

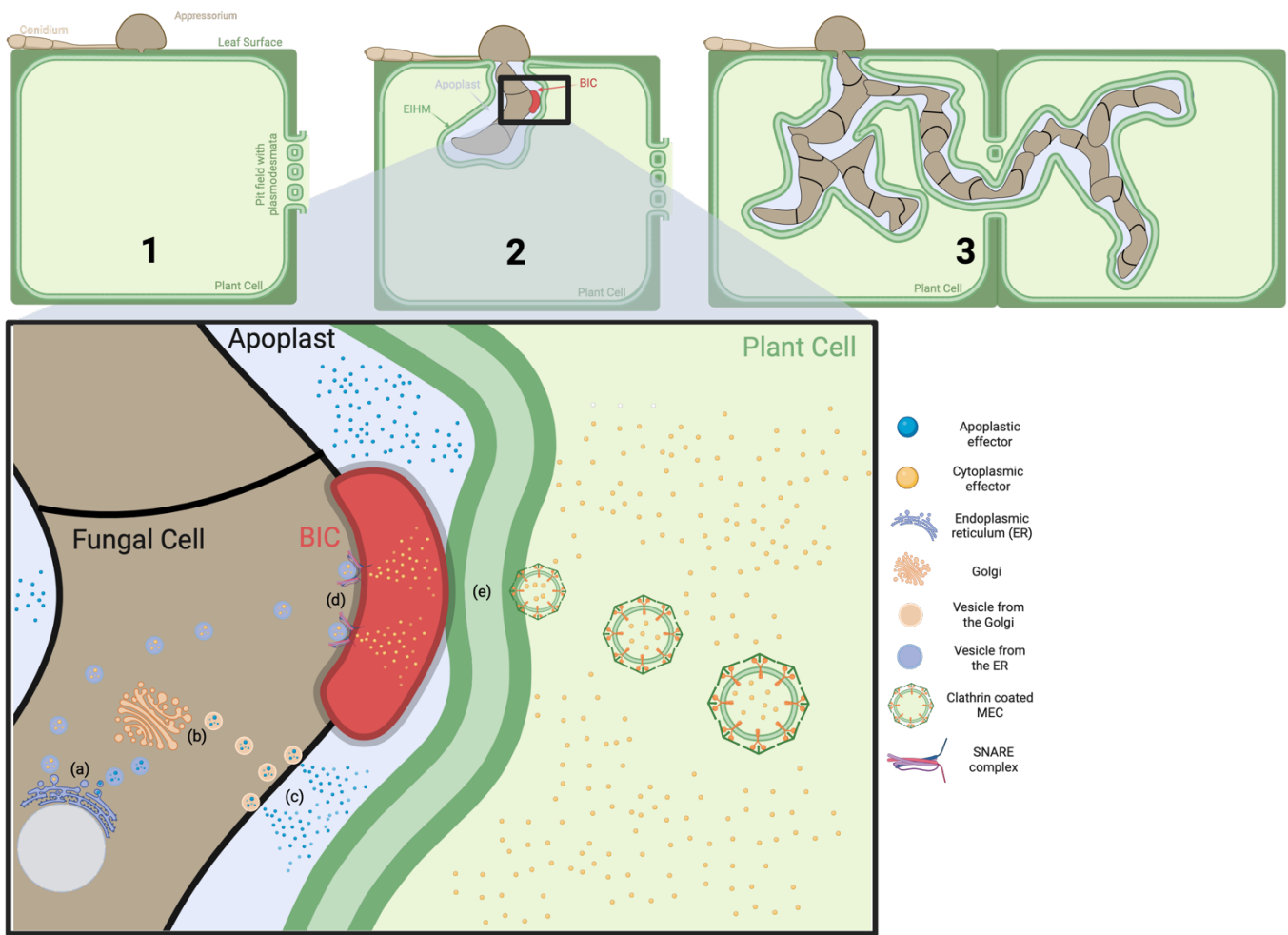


Figure 1: The rice blast infection process and *Magnaporthe oryzae* effector secretion pathways. (Top) (1) Infection begins when a fungal spore (conidium) attaches to the surface of a leaf. The spore extends a germ tube across the leaf surface, at the tip of the germ tube an appressorium is formed. The appressorium generates extreme turgor pressure to drive a penetration peg through the host cuticle and into the epidermal plant cells beneath. (2) A fungal hypha grows into the breached plant cell. Fungal hyphae are sealed within a plant-derived membrane, named the extra-invasive hyphal membrane (EIHM). The region between the fungal cell wall and the plant plasma membrane is known as the apoplast. A dome-shaped region of the EIHM, the biotrophic interfacial complex (BIC), is the site of effector translocation from the fungus into the host cell. (3) As the infection progresses, *M. oryzae* hyphae transit between plant cells by penetrating pit fields, where the cell wall is thinner and where plasmodesmata cluster. (Bottom) Apoplastic and cytoplasmic effectors are secreted by distinct mechanisms in *M. oryzae*. (a) The translation of apoplastic and cytoplasmic effectors may occur in divergent subcellular environments, as only cytoplasmic effector expression is sensitive to changes in ribosomal pausing during codon decoding by tRNAs. (b and c) Apoplastic effectors are secreted into the apoplast from the endoplasmic reticulum via a Golgi-dependant mechanism. (d) The translocation of cytoplasmic effectors into the BIC requires the exocyst complex including SNAREs. (e) To cross the plant membrane at the BIC, cytoplasmic effectors are packaged into clathrin-coated vesicle-like membranous effector compartments (MECs) derived from plant membranes.

1.2 Molecular plant immunity

To detect pathogens and initiate immune responses, plants rely on receptor proteins at the cell surface and within the cell (Kanyuka and Rudd 2019, Van Der Burgh and Joosten 2019, Mccombe *et al.*, 2022). The receptors sense molecules characteristic of pathogen infection, including microbe-associated molecular patterns (MAMPs), damage-associated molecular patterns (DAMPs), plant-derived immunomodulatory peptides called phytocytokines, and effectors. The responses activated by plant receptors can include the production of reactive oxygen species (ROS) and anti-microbial compounds, the influx of Ca^{2+} into the cytosol, immune signalling via mitogen-activated protein kinase (MAPK) cascades, transcriptional reprogramming, and a hypersensitive response (HR) leading to localised plant cell death (Tsuda and Katagiri 2010, Peng *et al.*, 2018). To undermine and overcome the innate plant immune system, pathogens utilise effectors.

1.2.1 Pathogen recognition

The apoplast, the region situated between the fungal cell wall and plant plasma membrane, can be monitored by plant cells to enable pathogen detection early during infection. Apoplastic pathogen recognition is controlled by a network of receptors embedded in the plant plasma-membrane. Most cell-surface pathogen-recognition receptors are categorised as either receptor-like proteins (RLPs) or receptor-like kinases (RLKs), depending on the absence or presence of an intracellular kinase domain. Both receptor classes exhibit a membrane-embedded domain and an extracellular ligand-binding domain. RLPs and RLKs can be further classified into subfamilies based on their extracellular domain (ECD). Identified ECDs of plant pathogen recognition receptors include lysin motif (LysM), leucine-rich repeat (LRR), lectin, epidermal growth factor-like, galacturonan-binding wall-associated-kinase (WAK) and WAK-associated C-terminal domains (Macho and Zipfel 2014, Stephens *et al.*, 2022). In the fight against fungal pathogens, LysM-RLP/RLKs are crucial as they can detect chitin oligomers released from the cell-wall of invading fungi. Chitin elicitor receptor kinase 1 (CERK1) is a LysM-RLK involved in chitin-induced defense responses and is present in both monocot and dicot plants (Miya *et al.*, 2007, Shimizu *et al.*, 2010). In rice, CERK1 is recruited by the chitin elicitor binding protein (CEBiP), a LysM-RLP, following homodimerisation of CEBiP promoted by binding to long-chain chitin oligomers (Hayafune *et al.*, 2014). The CERK1 and CEBiP complex activates immune signalling pathways and ultimately promotes fungal disease resistance (Hayafune *et al.*, 2014). Rice CERK1 is also implicated in symbiosis with arbuscular

mycorrhizal fungi (AMF) (Miyata *et al.*, 2014, Zhang *et al.*, 2015) and can also detect short-chain chitin oligomers produced by AMF when in complex with MYR1 (another LysM-RLK) (Carotenuto *et al.*, 2017, He *et al.*, 2019). A recent discovery demonstrated that MYR1/CERK1 complex formation reduces the chitin-induced immune response by inhibiting the recruitment of CERK1 by CEBiP (Zhang *et al.*, 2021). By recognising highly conserved fungal cell wall components, LysM-RLPs/RLKs can inhibit the growth of a diverse range of pathogenic fungi, including biotrophs like *Melampsora spp.*, and hemibiotrophs like *Magnaporthe spp.*, while also supporting interactions with beneficial fungi.

In addition to detecting wide-spread and conserved fungal molecules like chitin and other MAMPs, plants can detect rapidly evolving and diverse effector proteins secreted by pathogenic fungi. While there are examples of apoplastic fungal effectors being recognised by extracellular receptors (Jones *et al.*, 1994, Dixon *et al.*, 1996, Thomas *et al.*, 1997, Dixon *et al.*, 1998, Takken *et al.*, 1999, Kawchuk *et al.*, 2001, De Jonge *et al.*, 2012), most identified receptors for rust and blast Avrs are cytosolic nucleotide binding (NB) leucine-rich repeat (LRR) receptors (NLRs) (Periyannan *et al.*, 2017, Wang *et al.*, 2017). Typically, NLRs are composed of a C-terminal LRR domain, central nucleotide-binding (NB) domain, and variable N-terminal domain. The two major classes of NLR are CC-NLRs that have a coiled-coil N-terminal domain and TIR-NLRs with a toll/interleukin-1 receptor N-terminal domain. In general, the CC and TIR domains are required for immune signalling following activation, and the NB and LRR domains regulate NLR activation. There are 6 *M. lini* avirulence effectors identified that are recognised by 19 flax NLRs. Interestingly, all identified flax NLRs that recognise flax rust effectors are TIR-NLRs. In contrast, monocot species like rice lack TIR-NLRs (Shao *et al.*, 2016). In rice, most identified *M. oryzae* effector recognising receptors are CC-NLRs, with some containing additional integrated domains (IDs) required for effector recognition (reviewed in (Marchal *et al.*, 2022)). The activation of an NLR by fungal effector recognition often results in a HR that prevents the growth of biotrophic and hemibiotrophic pathogens (Balint-Kurti 2019).

1.2.2 Plant immune signalling

Upon recognition of MAMPs/DAMPs/phytocytokines, extracellular receptors initiate a series of immune responses broadly classified as pattern-triggered immunity (PTI). Our knowledge of PTI is mostly informed by studies on the bacterial MAMP flg-22 (a small peptide from bacterial flagellin). However, there is clear overlap between the PTI signalling pathways

activated by bacterial and fungal MAMP recognition (Nühse *et al.*, 2000, Zhang *et al.*, 2010, Kadota *et al.*, 2014). In all characterised examples, elicitor binding triggers an oligomerisation event that brings the intracellular domains of multiple membrane-bound receptor proteins into proximity (Chinchilla *et al.*, 2007, Liu *et al.*, 2012, Sun *et al.*, 2013, Tang *et al.*, 2015). The activated receptors recruit members of the receptor-like cytoplasmic kinase (RLCK) subfamily and participate in intricate auto- and/or trans-phosphorylation events of the intracellular receptor domains and RLCKs to facilitate downstream signalling (Lu *et al.*, 2010, Petutschnig *et al.*, 2010, Liu *et al.*, 2013, Cao *et al.*, 2014, Shinya *et al.*, 2014, Kong *et al.*, 2016, Suzuki *et al.*, 2016, Yamada *et al.*, 2016, Erwig *et al.*, 2017, Lal *et al.*, 2018). BIK1 is a well-studied and central *Arabidopsis thaliana* RLCK that integrates signals from multiple extracellular receptors, including those detecting diverse bacterial, fungal, and plant derived molecules (Lu *et al.*, 2010, Zhang *et al.*, 2010, Liu *et al.*, 2013). Following phosphorylation events, BIK1 undergoes monoubiquitination prior to release from the receptor complex (Ma *et al.*, 2020). BIK1 then goes on to directly regulate ROS generation (Kadota *et al.*, 2014, Li *et al.*, 2014), calcium ion channel activation (Tian *et al.*, 2019), and hormone production (Lal *et al.*, 2018). Immune-related ROS generation is primarily controlled by the plasma membrane-localised NADPH oxidase RBOHD (Nühse *et al.*, 2007, Zhang *et al.*, 2007). BIK1 interacts with and phosphorylates RBOHD to activate ROS signalling (Kadota *et al.*, 2014, Li *et al.*, 2014). ROS have been proposed to possess a multitude of functions in promoting plant immunity, including acting as antimicrobial compounds (Peng and Kuc 1992), regulating stomatal closure (Macho *et al.*, 2012), catalysing reactions involved in cell wall remodelling (Brown *et al.*, 1998), and acting as important secondary messenger molecules to trigger further immune responses (Wu *et al.*, 2023). One mechanism by which ROS transduce signalling is via oxidation of plant proteins. For example, a cysteine amino acid in the thiol peroxidase protein PRXIIB is oxidised by ROS produced during plant immune signalling (Bi *et al.*, 2022), the oxidised PRXIIB cysteine subsequently conjugates with a free cysteine on the protein serine/threonine phosphatase ABSCISIC ACID-INSENSITIVE2 (ABI2). The conjugation of PRXIIB and ABI2 reduces the phosphatase activity of ABI2 and promotes stomata-mediated immunity against the bacterial pathogen *Pseudomonas syringae* (Bi *et al.*, 2022).

Effector recognition by NLRs also involves protein oligomerization events, prior to signal transduction and the activation of immune responses known as effector-triggered immunity (ETI) (Wang *et al.*, 2019, Li *et al.*, 2020, Ma *et al.*, 2020, Martin *et al.*, 2020, Förderer *et al.*, 2022, Zhao *et al.*, 2022, Contreras *et al.*, 2023). The recent structures of two CC-NLRs, ZAR1

from *A. thaliana* and Sr35 from wheat, demonstrate that the activated receptors form a pentameric complex (termed resistosome) with a characteristic funnel shaped structure that associates with the plant plasma membrane (Wang *et al.*, 2019, Förderer *et al.*, 2022, Zhao *et al.*, 2022). Current models indicate that CC-NLR resistosomes function as calcium-ion channels that cause an influx of Ca^{2+} into the cytosol to trigger immune signalling that culminates in cell death (Bi *et al.*, 2021, Jacob *et al.*, 2021, Förderer *et al.*, 2022). TIR-NLRs also form oligomeric complexes following effector recognition. The structures of two TIR-NLRs, ROQ1 from *Nicotiana benthamiana* and RPP1 from *A. thaliana*, demonstrate tetrameric complex formation (Ma *et al.*, 2020, Martin *et al.*, 2020). The TIR-NLR tetramers revealed binding sites for small nucleotide molecules, consistent with the ability of multiple TIR-domains to hydrolyse NAD^+ (nicotinamide adenine dinucleotide) into ADPR (adenosine diphosphate ribose) and cyclic ADPR isomers (Horsefield *et al.*, 2019, Wan *et al.*, 2019). Recent advances have identified that TIR-NLRs can also use NAD^+ and ATP to produce multiple nucleotide molecules including pRib-AMP, pRib-ADP, ADPR-ATP, and di-ADPR (Huang *et al.*, 2022, Jia *et al.*, 2022). For *A. thaliana* and *N. benthamiana*, TIR-catalysed nucleotide molecules can function as signals that ultimately lead to the activation of CC-NLR NRG1 and calcium-ion channel formation (Qi *et al.*, 2018, Jacob *et al.*, 2021). It is notable that plant TIR domains can also produce cyclic nucleotide monophosphates (cNMPs) from nucleic acid, which are required for TIR-NLR mediated plant cell death (Yu *et al.*, 2022). However, how cNMPs integrate with the other TIR-catalysed small molecule signalling and induce plant immune responses requires clarification (Essuman *et al.*, 2022).

Both PTI and ETI responses ultimately converge on similar cellular responses (Jacob *et al.*, 2018), albeit often with differences in amplitude (Yuan *et al.*, 2021, Bernoux *et al.*, 2022). One example is the intracellular influx of Ca^{2+} , which occurs in tightly controlled bursts during PTI but in a long, sustained influx during ETI (Kim *et al.*, 2022). PTI and ETI are also intertwined, with the two pathways requiring and potentiating each other (Ngou *et al.*, 2021, Pruitt *et al.*, 2021, Tian *et al.*, 2021, Yuan *et al.*, 2021, Lang *et al.*, 2022). Overall, the plant immune system is incredibly successful at recognising incoming threats and halting infection. To overcome the host immune system and facilitate colonisation, adapted pathogens rely on effector proteins that often interfere with PTI and ETI.

1.2.3 Overcoming plant defences with effectors

Fungal effectors are generally small proteins (< 300 amino acids), have signal peptides to ensure translocation out of the fungal cell, and often demonstrate positive evolutionary selection pressures (Joly *et al.*, 2010, Stukenbrock *et al.*, 2011, Wicker *et al.*, 2013, Menardo *et al.*, 2017, Beckerson *et al.*, 2019). The rapid evolution of effectors likely reflects the need to prevent recognition by plant immune receptors while continuing to optimise virulence function (Lo Presti *et al.*, 2015). Effectors can be broadly split into two groups, those localised to the apoplast and the effectors that move across the plant plasma membrane into the plant cell cytoplasm. Recent progress in predicting fungal effector localisation using machine-learning models, suggests that approximately two-thirds of all *M. lini* effectors and over half of all *M. oryzae* effectors translocate into the host plant cell cytoplasm (Sperschneider and Dodds 2022). Fungal effector secretion systems and the mechanisms differing between cytoplasmic and apoplastic effector secretion are perhaps best characterised in the *M. oryzae*-rice pathosystem. In *M. oryzae*, apoplastic effectors travel through the endoplasmic reticulum (ER) to the Golgi prior to secretion (Giraldo *et al.*, 2013) (Figure 1). Treatment with brefeldin A (BFA), a potent inhibitor of Golgi trafficking (Chardin and McCormick 1999), prevents the secretion of apoplastic *M. oryzae* effectors (Giraldo *et al.*, 2013). These data indicate that apoplastic effectors follow the well-studied conventional protein secretion pathway, involving signal-peptide dependant co-translational insertion of the nascent polypeptide chain into the ER membrane, trafficking through the ER and vesicle-mediated transport to the Golgi, protein sorting at the Golgi, and finally transport to the surface of the fungal cell (Rodrigues *et al.*, 2013) (Figure 1). In contrast, cytoplasmic effector secretion is BFA-insensitive and therefore Golgi-independent (Giraldo *et al.*, 2013). Furthermore, recent evidence indicates that cytoplasmic and apoplastic effectors from *M. oryzae* are translated in different sub-cellular environments, as cytoplasmic but not apoplastic effectors are sensitive to changes in ribosomal pausing during codon decoding by tRNAs (Li *et al.*, 2023). After translation, the secretion of cytoplasmic effectors to the BIC requires components of the fungal exocyst complex (Giraldo *et al.*, 2013) (Figure 1). To then cross the plant membrane at the BIC, cytoplasmic effectors are packaged into vesicle-like membranous effector compartments (MECs) derived from plant membranes and lined with CLATHRIN LIGHT CHAIN 1 (Oliveira-Garcia *et al.*, 2023), indicating that *M. oryzae* co-opts plant clathrin-mediated endocytosis pathways to facilitate the uptake of cytoplasmic effectors (Figure 1). While most rice blast and rust effectors likely localise within the host cytoplasm, our knowledge of their functions remains limited.

For rust fungi, the best-characterised cytoplasmic effectors are AvrL567 and AvrP. Yeast two-hybrid (Y2H) screens identified *LuCKX1.1* as a potential target of AvrL567 (Wan *et al.*, 2019). *LuCKX1.1* is a member of the cytokinin oxidase/dehydrogenase family, enzymes responsible for the inactivation of cytokinin phytohormones (Schmülling *et al.*, 2003). In *in vitro* enzymatic assays, the incubation of *LuCKX1.1* with AvrL567 enhances *LuCKX1.1* activity, suggesting that AvrL567 may function by inhibiting cytokinin signalling (Wan *et al.*, 2019). However, no changes could be detected in cytokinin levels in whole flax plants overexpressing AvrL567 (Wan *et al.*, 2019). In flax rust, knock out of AvrL567 did not reduce pathogen virulence, indicating that either AvrL567's activity only makes a very minor or no contribution to rust virulence, or that there are functionally redundant effectors which make up for the loss of AvrL567 (Lawrence *et al.*, 2010). For AvrP, the protein's crystal structure revealed three zinc ions co-ordinated by cysteine and histidine amino acids (Zhang *et al.*, 2018). Confocal microscopy analysis of *N. benthamiana* leaves expressing fluorescent-protein tagged AvrP identified a mostly nuclear localisation, despite the absence of a nuclear localisation signal (Zhang *et al.*, 2018). The localisation of AvrP may be influenced by interactions with flax proteins. Y2H experiments identified three flax proteins (a phosphoglucomutase, peptidyl-prolyl cis-trans isomerase, and DEAD-box ATP-dependent RNA helicase) capable of interacting with AvrP (Farah 2018). All AvrP interactions could be reconstituted in *N. benthamiana* plants using bimolecular fluorescence complementation (Akram 2023). Using purified recombinant proteins, *in vitro* experimentation demonstrates that AvrP can modulate the activity of a flax phosphoglucomutase to increase the conversion of glucose-1-phosphate to glucose-6-phosphate (Akram 2023). Furthermore, AvrP can inhibit the ATPase and helicase activity of a flax DEAD-box ATP-dependent RNA helicase and expression of AvrP in flax results in major transcriptional changes. The initial characterisation of AvrP suggests it is a multifunctional effector with diverse host targets (Akram 2023).

M. oryzae effector AvrPiz-t also interacts with multiple intracellular host proteins, with 12 putative interactors identified in Y2H screens named APIP1-12 (AvrPiz-t Interacting Protein 1-12) (Park *et al.*, 2012). AvrPiz-t can be ubiquitinated by and suppresses the ubiquitin ligase activity of APIP6 and APIP10, two rice RING E3 ubiquitin ligases (Park *et al.*, 2012, Park *et al.*, 2016). AvrPiz-t can also bind to the rice plasma membrane K⁺-channel protein OsAKT1 (APIP7), interfering with the association between OsAKT1 and the cytoplasmic kinase OsCIPK23, leading to reduced K⁺ influx into the plant cell (Shi *et al.*, 2018). Interestingly, two of the AvrPiz-t interactors are involved in the recognition of AvrPiz-t and activation of ETI by the NLR Piz-t (Park *et al.*, 2016, Wang *et al.*, 2016). APIP10 promotes the degradation of Piz-

t, and therefore AvrPiz-t-mediated suppression of ubiquitin ligase activity promotes the accumulation of Piz-t. Likewise, APIP5, a bZIP-type transcription factor, also interacts with Piz-t to protect against the virulence activities of AvrPiz-t (Wang *et al.*, 2016). It is remarkable that such a small protein, comprising 90 amino acids after signal peptide removal, can interact with and modulate the activity of various plant proteins with diverse sequences. The findings from AvrPiz-t suggest that the currently uncharacterised approximately 500 predicted *M. oryzae* effectors (Sperschneider and Dodds 2022) could target over 6000 unique plant processes. However, this number is likely much smaller, as many effectors are predicted to be functionally redundant (Giraldo and Valent 2013, Lanver *et al.*, 2017). Functional redundancy, where multiple effectors can perform the same function, is often cited as the reason for the observed lack of virulence phenotypes in effector gene knockout experiments. For instance, in a large-scale single-gene knockout screen of predicted *M. oryzae* effectors, only one out of the 78 tested effectors significantly contributed to pathogen virulence on the susceptible rice cultivar Shin No. 2 (Saitoh *et al.*, 2012). Functional redundancy makes characterising the importance of a specific virulence function for pathogenicity difficult. To expedite the identification and characterisation of important effector virulence functions in multiple plant pathogen interactions, it could be advantageous to focus on effector families predicted to have conserved functions across diverse pathosystems. This thesis delves into the virulence functions of the putative Nudix hydrolase effector families in multiple pathogenic fungi, including in *M. lini* and *M. oryzae*.

1.3 Nudix hydrolase effectors

The Nudix (**nucleoside diphosphate linked to moiety-X**) hydrolase superfamily is ubiquitous in prokaryotic and eukaryotic organisms. These enzymes play key roles in diverse physiological processes and in the maintenance of cellular homeostasis (Mclennan 2006). Nudix hydrolases typically function as pyrophosphohydrolase enzymes, catalysing the hydrolysis of pyrophosphate bonds. The highly conserved Nudix-box consensus sequence: GX5EX7REUXEEXGU (Figure 2A) is required for Nudix hydrolase activity. In this sequence, 'U' typically represents a hydrophobic residue, while 'X' can be any amino acid (Mclennan 2006). The first glutamate and arginine form a stabilising salt bridge between a flexible loop region and α -helix, and the remaining glutamates are generally responsible for divalent metal cation binding (Figure 2A); most Nudix enzymes are hypothesised to bind to Mg^{2+} in physiological environments (Mclennan 2006). The metal cations bind to the pyrophosphate of

the substrate, neutralising and orienting it towards a general base. This base, often a glutamate or aspartate, extracts a proton from H₂O, producing a free hydroxide ion. The nucleophilic hydroxide ion hydrolyses the bound pyrophosphate (Mildvan *et al.*, 2005). Nudix hydrolases can act on several well-characterised substrates. These include intact and oxidatively damaged nucleoside triphosphates (Sakumi *et al.*, 1993, Ito *et al.*, 2005, Jemth *et al.*, 2018), ADPR (O'handley *et al.*, 1998, Gabelli *et al.*, 2002, Kang *et al.*, 2003, Perraud *et al.*, 2003), diadenosine polyphosphates (Ap_nAs) (Bessman *et al.*, 2001, Leslie *et al.*, 2002, Iwai *et al.*, 2004), and the 5' cap of mRNA transcripts (Van Dijk *et al.*, 2002, Wang *et al.*, 2002, Song *et al.*, 2013). Despite their diverse range of substrates and sequences, all structurally characterised Nudix hydrolases possess the Nudix fold with an approximately 130 amino acid α - β - α sandwich domain architecture (Srouji *et al.*, 2017) (Figure 2B). The Nudix fold is also present in isopentenyl diphosphate isomerasases and adenine glycosylases, although these families notably lack the Nudix motif sequence (Srouji *et al.*, 2017).

Nudix hydrolase domains have been predicted in effectors from multiple fungal, oomycete, and bacterial plant pathogens (Dong and Wang 2016). The putative Nudix hydrolase effectors were identified through their similarities with the Nudix-box consensus sequence (Figure 2A). Experimentally, a subset of these Nudix effectors have been confirmed to hydrolyse pyrophosphate bonds in substrates containing nucleosides.

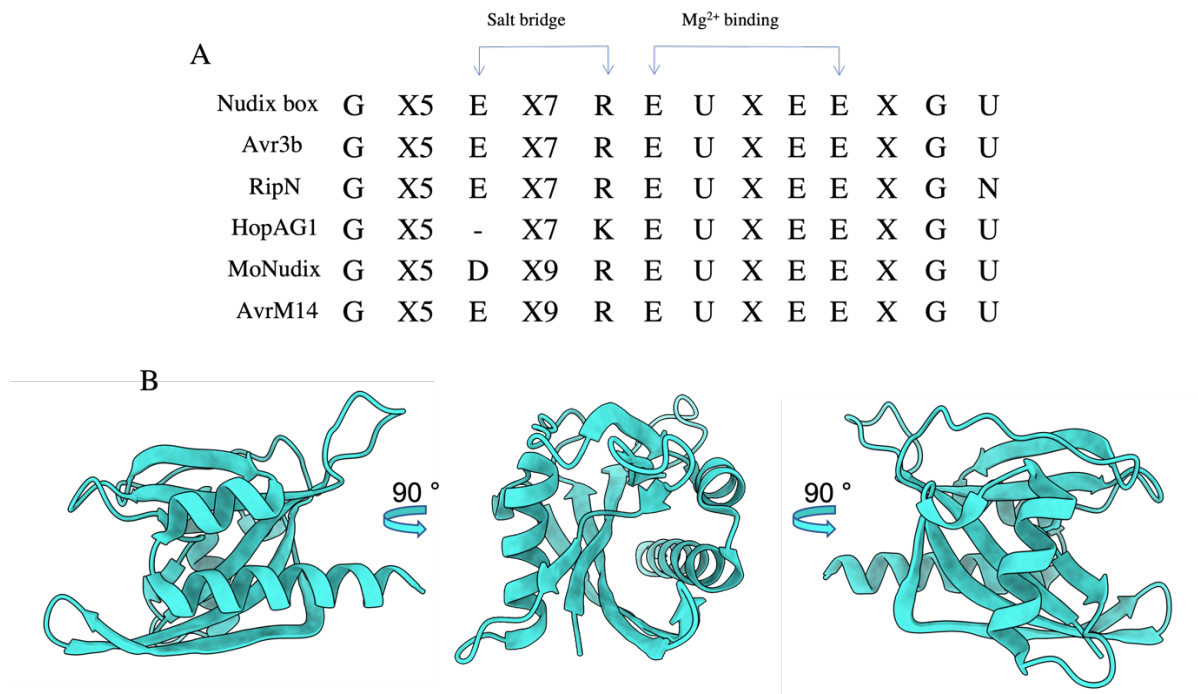


Figure 2: Characteristic features of Nudix hydrolase enzymes and Nudix box sequences from predicted effectors. (A) The conventional Nudix box consensus sequence (top) and the putative Nudix box sequences identified in effectors from phytopathogens. The glutamate and arginine which typically form a stabilising salt bridge, and the glutamates often involved in Mg²⁺ binding, are indicated with arrows. (B) The α - β - α sandwich Nudix fold, the example shown is from *Homo sapiens* Nudix hydrolase 2 (PDB ID: 3U53) (Ge *et al.*, 2013).

1.3.1 Avr3b

Avr3b from the oomycete *Phytophthora sojae*, a destructive soybean pathogen, was the first Nudix hydrolase effector to be experimentally validated. The mature Avr3b protein consists of 297 amino acids and can be recognised by soybean cultivars with the Rps3b resistance gene (Dong *et al.*, 2011). Pathogen strains virulent on Rps3b-soybean display multiple polymorphisms in their Avr3b gene. The polymorphisms include a premature stop codon that truncates 85 amino acids from the C-terminus of the protein, preventing recognition by Rps3b (Dong *et al.*, 2011). When Avr3b is transiently expressed in *N. benthamiana*, it increases susceptibility to *Phytophthora capsica* and *Phytophthora parasitica* infection. Avr3b also reduces ROS accumulation around invasion sites and suppresses plant cell death during infection (Dong *et al.*, 2011). In soybean, the expression of Avr3b suppresses cell-death triggered by the recognition of Avr1b (Dong *et al.*, 2011). For enzymatic activation, Avr3b requires a plant cyclophilin which likely catalyses the isomerisation of a proline in the Avr3b protein. Both the cyclophilin-targeted proline and the Nudix-box are essential for the observed virulence activities of Avr3b (Dong *et al.*, 2011, Kong *et al.*, 2015). Avr3b has been tested with a limited range of substrates and was able to hydrolyse NADH and ADPR (Dong *et al.*, 2011).

Notably, even though the truncated form of Avr3b is not recognised by Rps3b, it still maintains Nudix hydrolase activity. There are also related Nudix effector genes in other *Phytophthora* spp. as well as in *Hyaloperonospora parasitica*, another phytopathogenic oomycete (Dong and Wang 2016). Recently, Yu *et al.*, (2022) demonstrated that Avr3b also has cyclic nucleotide phosphodiesterase activity against the cNMPs produced by plant TIR-domains and suggest that this enzymatic activity is a virulence function of the effector. The study also identified *A. thaliana* Nudix hydrolase 7 (*AtNudx7*) as a plant cNMP phosphodiesterase (Yu *et al.*, 2022). *AtNudx7* is a well-known negative regulator of EDS1-dependant immune signalling, a pathway which is activated by the small nucleotide molecules produced by TIR-NLRs (Bartsch *et al.*, 2006, Ge *et al.*, 2007, Huang *et al.*, 2022, Jia *et al.*, 2022). Yu *et al* (2022) propose that *AtNudx7* negatively regulates TIR-NLR signalling by hydrolysing cNMPs. Alternatively, other *in vitro* substrates for *AtNudx7* have been identified previously (including ADPR, NADH, NAD⁺, AP₃A, AP₄A, AP₅A, FAD, UDP-glucose, and ADP-glucose) (Ogawa *et al.*, 2005, Olejnik and Kraszewska 2005) and these substrates share greater structural similarities with other TIR-produced and pyrophosphate-containing immunomodulatory molecules such as di-ADPR, ADPR-ATP, and pRib-ADP. The promiscuous *in vitro* enzymatic activity of both *AtNudx7* and Avr3b is a trait often observed in Nudix hydrolases (McLennan 2013) and complicates the identification of *in vivo* substrates.

1.3.2 RipN

The pathogenic bacterium *Ralstonia solanacearum* is responsible for bacterial wilt disease in various crops, including potato, tomato, and banana. *R. solanacearum* secretes RipN, a 473-amino acid Nudix hydrolase effector that hydrolyses a variety of nucleoside diphosphate substrates *in vitro* (Sun *et al.*, 2019). Similar to *AtNudx7* and Avr3b, the preferred *in vitro* substrates of RipN are NADH and ADPR; however, overexpression of RipN in *A. thaliana* did not result in significant changes to ADPR, NAD⁺ or NADH levels (Sun *et al.*, 2019). Unlike Avr3b, it is unlikely that RipN mimics the activity of *AtNudx7* to negatively regulate plant immunity. This is because RipN localises to the nuclear and endoplasmic reticulum membranes when expressed in *N. tabacum* and *A. thaliana* with a GFP tag, whereas GFP-tagged *AtNudx7* localises in the aqueous cytoplasm/nucleus (Olejnik *et al.*, 2011, Sun *et al.*, 2019). The localisation of RipN does not require the Nudix domain and is dependent on the c-terminus, which has no homology to proteins of known function or identifiable localisation sequences (Sun *et al.*, 2019). Transgenic *A. thaliana* plants expressing RipN demonstrate compromised

PTI, including reduced defence gene-induction and callose deposition following treatment with flg-22. RipN with a mutated Nudix box was unable to interfere with PTI, indicating the importance of Nudix hydrolase activity (Sun *et al.*, 2019). The large size of RipN suggests that the Nudix box is not the only functional region in the effector, perhaps identifying protein interactors will provide further insight into the virulence function/s of RipN.

1.3.3 HopAG1

HopAG1 (previously known as HolPsyAG) was identified as a potential Nudix effector in *Pseudomonas syringae* pv. *syringae* strain B728a, which causes brown spot disease in snap bean (Greenberg and Vinatzer 2003). In the well characterised *Pseudomonas syringae* pv. *tomato* DC3000 strain, the insertion of a transposon into the HopAG1 open reading frame (ORF) results in the loss of the C-terminal Nudix hydrolase domain from the effector (Greenberg and Vinatzer 2003, Schechter *et al.*, 2004). Similarly, *Pseudomonas syringae* pv. *avellanae* strain Ve037 has a frameshift mutation which disrupts the HopAG1 effector sequence (O'brien *et al.*, 2012). The loss of HopAG1 in multiple *Pseudomonas syringae* pathovars indicates that the effector is not essential for pathogen virulence. The translocation of HopAG1 into *A. thaliana* leaves was confirmed by fusing the C-terminus of the recognised effector AvrRpt2 to HopAG1 in *P. syringae* pv. *tomato* DC3000, which resulted in a Rpt2-dependant HR (Vinatzer *et al.*, 2005). HopAG1 is a large effector (716 amino acids) with three predicted domains. At the C-terminus is the Nudix hydrolase domain, at the N-terminus is a predicted ADP-ribosyltransferase domain (Hulin *et al.*, 2023), and the middle domain has a predicted structure similar to proteins that utilise ATPase activity to transfer phosphate to a target (e.g. protein kinases and aminoglycoside phosphotransferases) (Figure 3). The enzymatic activities and roles of the three domains of HopAG1 remain unknown. However, the combination of domains predicted to act on similar substrates suggests HopAG1 may couple multiple enzymatic reactions together, to create small nucleotide/sugar molecules (Figure 3). For example, ADP-ribosyltransferases cleave the N-glycoside bond in NAD⁺, resulting in ADPR. Aminoglycoside phosphotransferases can transfer phosphate to free hydroxyl groups on sugars, from ADPR this may result in ADPR 1-phosphate. The Nudix domain could then hydrolyse the pyrophosphate bond, producing the metabolic activators ribose 1,5-bisphosphate and AMP (Figure 3). While the HopAG1 effector is not essential for the virulence of all *Pseudomonas syringae* pathovars, the intriguing three domain structure is worthy of further investigation.

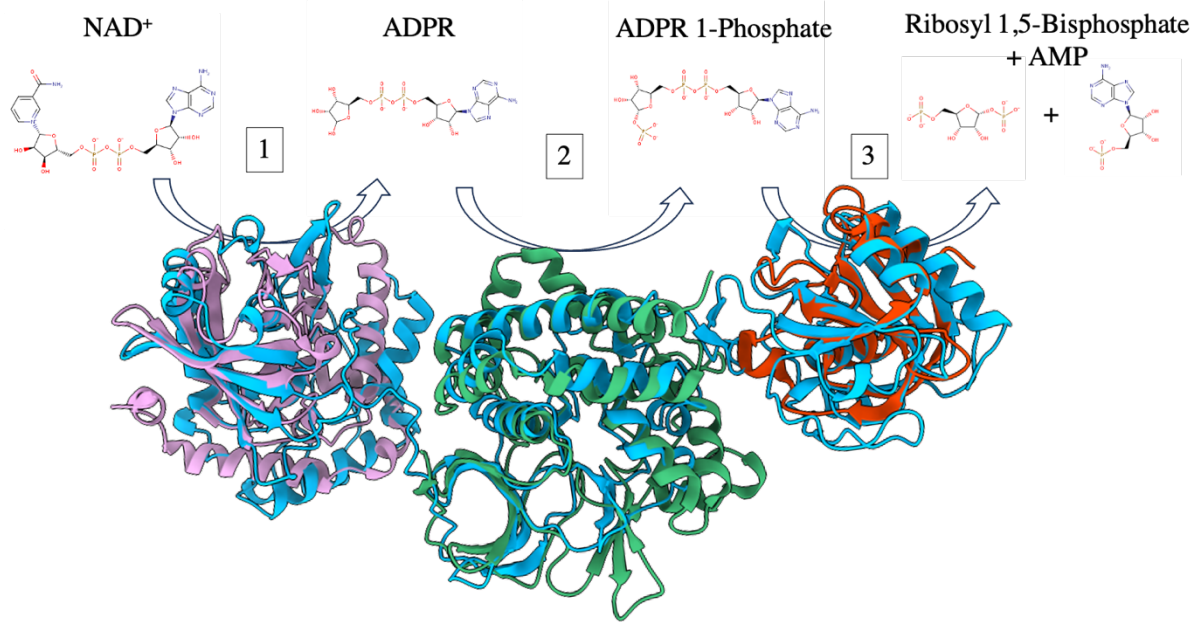


Figure 3: The *Pseudomonas syringae* HopAG1 effector consists of three predicted enzymatic domains. (Top) A hypothetical reaction catalysed by the three predicted enzymatic domains in HopAG1. (1) NAD⁺ could be cleaved by the predicted ADP-ribosyltransferase domain, resulting in ADPR and nicotinamide (not shown). (2) The predicted phosphotransferase domain could transfer a phosphate from ATP (not shown) to ADPR, creating ADPR 1-Phosphate. (3) The predicted Nudix hydrolase domain could use H₂O (not shown) to hydrolyse the pyrophosphate bond in ADPR 1-Phosphate, resulting in Ribosyl 1,5-Bisphosphate and AMP. (Bottom) The predicted structure of *Pseudomonas syringae* pv. *papulans* HopAG1 from the AlphaFold Protein Structure Database (ID: A0A0P9XY22) (cyan) (Jumper *et al.*, 2021, Varadi *et al.*, 2022) aligned with the crystal structures of a *Vibrio splendidus* ADP-ribosyltransferase (PDB ID: 4XZJ) (pink), a *Helicobacter pylori* proinflammatory kinase CTKA (PDB ID: 3AKK) (green), and a *Homo sapiens* Nudix hydrolase MTH1 (PDB ID: 5GHI) (red).

1.3.3 MoNudix

The Nudix effectors predicted in pathogenic fungi are smaller than Avr3b, RipN, and HopAG1, with only slightly more amino acids in the mature effector proteins than that required to achieve the Nudix fold (approximately 130 amino acids are required for the α - β - α sandwich domain architecture). For example, *M. oryzae* has two identical Nudix effector genes (MGG_14344 and MGG_14156, called *MoNudix*) encoding a predicted mature protein of 138 amino acids. *MoNudix* is one of the most highly upregulated effectors during *M. oryzae* infection of rice (Yan *et al.*, 2023), suggesting it may play an important role in promoting pathogen virulence. No substrates have been identified for *MoNudix*, nor is there any experimental evidence indicating *MoNudix* is an active Nudix hydrolase enzyme. However, a potential homologue of *MoNudix*, *CtNudix* from *Colletotrichum lenti*s, elicits a cell-death response when transiently

overexpressed in *N. tabacum* (Bhaduria *et al.*, 2013). When the Nudix motif was deleted from the effector it abolished the cell death phenotype (Bhaduria *et al.*, 2013). However, the deletion of 23 amino acids from the core of the protein likely resulted in major structural changes and therefore it is unclear if the cell death response is dependent on hydrolase activity or a non-enzymatic function of the protein. It is unknown if *CtNudix* possesses hydrolase activity or what substrate it might hydrolyse during infection. Cell-death also required secretion of the effector protein out of the plant cell; this suggests that cell death may be unrelated to the virulence function of the Nudix effector as all Nudix effectors are predicted to act within the plant cell during infection. Likewise, all *A. thaliana* Nudix hydrolases are intracellular proteins (Yoshimura and Shigeoka 2015). More research is required to uncover the roles of *MoNudix*, *CtNudix* and other Nudix effectors from *Colletotrichum* and *Magnaporthe* spp. during plant infection.

1.3.4 AvrM14

In 1965, Harold Flor demonstrated that flax rust isolates with the pathogenicity factors A-M1 and A-M4 show identical segregation on flax cultivars with M1 and M4 resistance (Flor 1965). Over 50 years later, Anderson *et al.*, (2016) demonstrated that flax M1 and M4 resistance proteins both recognise the same flax rust effector protein (named AvrM14), explaining the inseparable genetic linkage between A-M1 and A-M4 observed in Flor's experiments. M1 encodes a TIR-NLR, M4 is yet to be cloned (Lawrence *et al.*, 2010). *M. lini* produces AvrM14 early during the flax infection process (Wu *et al.*, 2019), and other *Melampsora* species encode predicted AvrM14 homologues. AvrM14 has a mature protein size of 146 amino acids and possesses a Nudix box motif (Anderson *et al.*, 2016). The AvrM14 effector has two identified allelic variants, AvrM14-A which is recognised by M1 and M4, and AvrM14-B which is not recognised and enables the infection of M1 and M4 flax cultivars (Anderson *et al.*, 2016). Only six amino acid substitutions distinguish AvrM14-A from AvrM14-B, and both have an identical Nudix box sequence. The recognition of AvrM14-A in M1 and M4 flax when the effector is transiently expressed by agrobacterium-mediated transformation, requires removal of the signal peptide. This demonstrates that AvrM14-A must be retained in the plant cell to enable effector recognition, indicating that AvrM14 is translocated inside flax cells during infection (Anderson *et al.*, 2016). AvrM14 has no identified or predicted substrates.

Table 1: Nudix hydrolase effectors in phytopathogens.

Nudix effector*	Pathogenic species	Mature protein size (amino acids)	Identified <i>in vitro</i> substrates
Avr3b	<i>Phytophthora sojae</i>	297	cNMPs, NADH, ADPR
RipN	<i>Ralstonia solanacearum</i>	473	ADPR, NADH, NAD, FAD, Ap ₄ A
HopAG1	<i>Pseudomonas syringae</i>	716	None
MoNudix	<i>Magnaporthe oryzae</i>	138	None
AvrM14	<i>Melampsora lini</i>	146	None

* Where multiple effectors with greater than 30% protein sequence identity have been identified, only one of the effectors is listed. For example, *CtNudix* is not listed as it has a similar sequence to *MoNudix*.

1.4 Aims of this thesis

The overall aim of the work presented in this thesis is to characterise the virulence function/s of the Nudix effectors from phytopathogenic fungi, focusing on AvrM14 from *M. lini* and *MoNudix* from *M. oryzae*. I hypothesise that the Nudix effectors from phytopathogenic fungi are enzymes, and that enzymatic activity is important for their virulence function in plants.

To identify molecules hydrolysed by the Nudix effectors, I expressed and purified AvrM14 and *MoNudix* without their signal peptides from *E. coli* to enable characterisation of their enzymatic activity. I also determined crystal structures of both AvrM14 and *MoNudix* proteins to aid in substrate identification and characterisation. I complemented the *in vitro* experimentation with *in planta* analysis, and extended my findings to homologous Nudix effectors in other pathogenic fungal species identified throughout the course of this study.

1.5 References

- Aime, M. C. and A. R. McTaggart (2021). "A higher-rank classification for rust fungi, with notes on genera." *Fungal Syst Evol* **7**: 21-47.
- Aime, M. C., A. R. McTaggart, S. J. Mondo and S. Duplessis (2017). "Phylogenetics and Phylogenomics of Rust Fungi." *Adv Genet* **100**: 267-307.
- Akram, A. (2023). "Functional characterisation of the flax rust AvrP effector protein." For the degree of Doctor of Philosophy of The Australian National University. <https://anulib.anu.edu.au/collections/theses>.
- Anderson, C., M. A. Khan, A.-M. Catanzariti, C. A. Jack, A. Nemri, G. J. Lawrence, N. M. Upadhyaya, A. R. Hardham, J. G. Ellis, P. N. Dodds and D. A. Jones (2016). "Genome analysis and avirulence gene cloning using a high-density RADseq linkage map of the flax rust fungus, *Melampsora lini*." *BMC Genomics* **17**(1): 667.
- Anderson, P. A., G. J. Lawrence, B. C. Morrish, M. A. Ayliffe, E. J. Finnegan and J. G. Ellis (1997). "Inactivation of the flax rust resistance gene M associated with loss of a repeated unit within the leucine-rich repeat coding region." *Plant Cell* **9**(4): 641-651.
- Avelino, J., M. Cristancho, S. Georgiou, P. Imbach, L. Aguilar, G. Bornemann, P. Läderach, F. Anzueto, A. J. Hruska and C. Morales (2015). "The coffee rust crises in Colombia and Central America (2008–2013): impacts, plausible causes and proposed solutions." *Food Security* **7**(2): 303-321.
- Balint-Kurti, P. (2019). "The plant hypersensitive response: concepts, control and consequences." *Mol Plant Pathol* **20**(8): 1163-1178.
- Bartsch, M., E. Gobbato, P. Bednarek, S. Debey, J. L. Schultze, J. Bautor and J. E. Parker (2006). "Salicylic acid-independent ENHANCED DISEASE SUSCEPTIBILITY1 signaling in *Arabidopsis* immunity and cell death is regulated by the monooxygenase FMO1 and the Nudix hydrolase NUDT7." *Plant cell* **18**(4): 1038-1051.
- Bebber, D. P. (2015). "Range-expanding pests and pathogens in a warming world." *Annu Rev Phytopathol* **53**: 335-356.
- Bebber, D. P., M. A. T. Ramotowski and S. J. Gurr (2013). "Crop pests and pathogens move polewards in a warming world." *Nature Climate Change* **3**(11): 985-988.
- Beckerson, W. C., R. C. Rodríguez de la Vega, F. E. Hartmann, M. Duhamel, T. Giraud and M. H. Perlin (2019). "Cause and Effectors: Whole-Genome Comparisons Reveal Shared but Rapidly Evolving Effector Sets among Host-Specific Plant-Castrating Fungi." *mBio* **10**(6): e02391-02319.
- Bernoux, M., H. Zetsche and J. Stuttmann (2022). "Connecting the dots between cell surface- and intracellular-triggered immune pathways in plants." *Curr Opin Plant Biol* **69**: 102276.
- Bessman, M. J., J. D. Walsh, C. A. Dunn, J. Swaminathan, J. E. Weldon and J. Shen (2001). "The gene *ygdP*, associated with the invasiveness of *Escherichia coli* K1, designates a Nudix hydrolase, *Orf176*, active on adenosine-pentaphospho-(5')-adenosine (Ap5A)." *The Journal of biological chemistry* **276**(41): 37834-37838.
- Bhaduria, V., S. Banniza, A. Vandenberg, G. Selvaraj and Y. Wei (2013). "Overexpression of a novel biotrophy-specific *Colletotrichum truncatum* effector, CtNUDIX, in hemibiotrophic fungal phytopathogens causes incompatibility with their host plants." *Eukaryotic cell* **12**(1): 2-11.
- Bi, G., M. Hu, L. Fu, X. Zhang, J. Zuo, J. Li, J. Yang and J. M. Zhou (2022). "The cytosolic thiol peroxidase PRXIIB is an intracellular sensor for H(2)O(2) that regulates plant immunity through a redox relay." *Nat Plants* **8**(10): 1160-1175.
- Bi, G., M. Su, N. Li, Y. Liang, S. Dang, J. Xu, M. Hu, J. Wang, M. Zou, Y. Deng, Q. Li, S. Huang, J. Li, J. Chai, K. He, Y. H. Chen and J. M. Zhou (2021). "The ZAR1 resistosome is a calcium-permeable channel triggering plant immune signaling." *Cell* **184**(13): 3528-3541.e3512.
- Brown, I., J. Trethowan, M. Kerry, J. Mansfield and G. P. Bolwell (1998). "Localization of components of the oxidative cross-linking of glycoproteins and of callose synthesis in papillae formed during the interaction between non-pathogenic strains of *Xanthomonas campestris* and French bean mesophyll cells." *The Plant Journal* **15**(3): 333-343.
- Cao, Y., Y. Liang, K. Tanaka, C. T. Nguyen, R. P. Jedrzejczak, A. Joachimiak and G. Stacey (2014). "The kinase LYK5 is a major chitin receptor in *Arabidopsis* and forms a chitin-induced complex with related kinase CERK1." *Elife* **3**: e03766.
- Carotenuto, G., M. Chabaud, K. Miyata, M. Capozzi, N. Takeda, H. Kaku, N. Shibuya, T. Nakagawa, D. G. Barker and A. Genre (2017). "The rice LysM receptor-like kinase OsCERK1 is required for the perception of short-chain chitin oligomers in arbuscular mycorrhizal signaling." *New Phytol* **214**(4): 1440-1446.
- Castroagudín, V. L., P. C. Ceresini, S. C. de Oliveira, J. T. Reges, J. L. Maciel, A. L. Bonato, A. F. Dorigan and B. A. McDonald (2015). "Resistance to QoI Fungicides Is Widespread in Brazilian Populations of the Wheat Blast Pathogen *Magnaporthe oryzae*." *Phytopathology* **105**(3): 284-294.

Catanzariti, A.-M., P. N. Dodds, G. J. Lawrence, M. A. Ayliffe and J. G. Ellis (2006). "Haustorially expressed secreted proteins from flax rust are highly enriched for avirulence elicitors." *The Plant Cell* **18**(1): 243-256.

Catanzariti, A.-M., P. N. Dodds, T. Ve, B. Kobe, J. G. Ellis and B. J. Staskawicz (2010). "The AvrM effector from flax rust has a structured C-terminal domain and interacts directly with the M resistance protein." *Molecular Plant-Microbe Interactions* **23**(1): 49-57.

Ceresini, P. C., V. L. Castroagudín, F. Rodrigues, J. A. Rios, C. E. Aucique-Pérez, S. I. Moreira, D. Croll, E. Alves, G. de Carvalho, J. L. N. Maciel and B. A. McDonald (2019). "Wheat blast: from its origins in South America to its emergence as a global threat." *Mol Plant Pathol* **20**(2): 155-172.

Ceresini, P. C., V. L. Castroagudín, F. Rodrigues, J. A. Rios, C. Eduardo Aucique-Pérez, S. I. Moreira, E. Alves, D. Croll and J. L. N. Maciel (2018). "Wheat Blast: Past, Present, and Future." *Annu Rev Phytopathol* **56**: 427-456.

Chardin, P. and F. McCormick (1999). "Brefeldin A: the advantage of being uncompetitive." *Cell* **97**(2): 153-155.

Chen, W. J., F. Delmotte, S. Richard-Cervera, L. Douence, C. Greif and M. F. Corio-Costet (2007). "At least two origins of fungicide resistance in grapevine downy mildew populations." *Appl Environ Microbiol* **73**(16): 5162-5172.

Chinchilla, D., C. Zipfel, S. Robatzek, B. Kemmerling, T. Nürnberg, J. D. Jones, G. Felix and T. Boller (2007). "A flagellin-induced complex of the receptor FLS2 and BAK1 initiates plant defence." *Nature* **448**(7152): 497-500.

Chung, H., J. Goh, S. S. Han, J. H. Roh, Y. Kim, S. Heu, H. K. Shim, D. G. Jeong, I. J. Kang and J. W. Yang (2020). "Comparative Pathogenicity and Host Ranges of Magnaporthe oryzae and Related Species." *Plant Pathol J* **36**(4): 305-313.

Contreras, M. P., H. Pai, Y. Tumtas, C. Duggan, E. L. H. Yuen, A. V. Cruces, J. Kourelis, H. K. Ahn, K. T. Lee, C. H. Wu, T. O. Bozkurt, L. Derevnina and S. Kamoun (2023). "Sensor NLR immune proteins activate oligomerization of their NRC helpers in response to plant pathogens." *Embo J* **42**(5): e111519.

Cooke, D. E., L. M. Cano, S. Raffaele, R. A. Bain, L. R. Cooke, G. J. Etherington, K. L. Deahl, R. A. Farrer, E. M. Gilroy, E. M. Goss, N. J. Grünwald, I. Hein, D. MacLean, J. W. McNicol, E. Randall, R. F. Oliva, M. A. Pel, D. S. Shaw, J. N. Squires, M. C. Taylor, V. G. Vleeshouwers, P. R. Birch, A. K. Lees and S. Kamoun (2012). "Genome analyses of an aggressive and invasive lineage of the Irish potato famine pathogen." *PLoS Pathog* **8**(10): e1002940.

Cruz, C. D. and B. Valent (2017). "Wheat blast disease: danger on the move." *Tropical Plant Pathology* **42**(3): 210-222.

Dagdas, Y. F., K. Yoshino, G. Dagdas, L. S. Ryder, E. Bielska, G. Steinberg and N. J. Talbot (2012). "Septin-mediated plant cell invasion by the rice blast fungus, Magnaporthe oryzae." *Science* **336**(6088): 1590-1595.

de Jonge, R., H. P. van Esse, K. Maruthachalam, M. D. Bolton, P. Santhanam, M. K. Saber, Z. Zhang, T. Usami, B. Lievens, K. V. Subbarao and B. P. Thomma (2012). "Tomato immune receptor Ve1 recognizes effector of multiple fungal pathogens uncovered by genome and RNA sequencing." *Proc Natl Acad Sci U S A* **109**(13): 5110-5115.

Dean, R., J. A. Van Kan, Z. A. Pretorius, K. E. Hammond-Kosack, A. Di Pietro, P. D. Spanu, J. J. Rudd, M. Dickman, R. Kahmann, J. Ellis and G. D. Foster (2012). "The Top 10 fungal pathogens in molecular plant pathology." *Mol Plant Pathol* **13**(4): 414-430.

Delgado-Baquerizo, M., C. A. Guerra, C. Cano-Díaz, E. Egidi, J.-T. Wang, N. Eisenhauer, B. K. Singh and F. T. Maestre (2020). "The proportion of soil-borne pathogens increases with warming at the global scale." *Nature Climate Change* **10**(6): 550-554.

Dixon, M. S., K. Hatzixanthis, D. A. Jones, K. Harrison and J. D. Jones (1998). "The tomato Cf-5 disease resistance gene and six homologs show pronounced allelic variation in leucine-rich repeat copy number." *Plant Cell* **10**(11): 1915-1925.

Dixon, M. S., D. A. Jones, J. S. Keddie, C. M. Thomas, K. Harrison and J. D. Jones (1996). "The tomato Cf-2 disease resistance locus comprises two functional genes encoding leucine-rich repeat proteins." *Cell* **84**(3): 451-459.

Dodds, P. N., G. J. Lawrence, A.-M. Catanzariti, M. A. Ayliffe and J. G. Ellis (2004). "The Melampsora lini AvrL567 Avirulence Genes Are Expressed in Haustoria and Their Products Are Recognized inside Plant Cells." *The Plant Cell* **16**(3): 755-768.

Dodds, P. N., G. J. Lawrence and J. G. Ellis (2001). "Contrasting modes of evolution acting on the complex N locus for rust resistance in flax." *The Plant Journal* **27**(5): 439-453.

Dong, S. and Y. Wang (2016). "Nudix effectors: a common weapon in the arsenal of plant pathogens." *PLoS pathogens* **12**(8): e1005704-e1005704.

Dong, S., W. Yin, G. Kong, X. Yang, D. Qutob, Q. Chen, S. D. Kale, Y. Sui, Z. Zhang, D. Dou, X. Zheng, M. Gijzen, B. M. Tyler and Y. Wang (2011). "Phytophthora sojae avirulence effector Avr3b is a secreted NADH and ADP-ribose pyrophosphorylase that modulates plant immunity." *PLoS pathogens* **7**(11): e1002353-e1002353.

Dooley, H., M. W. Shaw, J. Mehenni-Ciz, J. Spink and S. Kildea (2016). "Detection of Zymoseptoria tritici SDHI-insensitive field isolates carrying the SdhC-H152R and SdhD-R47W substitutions." *Pest Manag Sci* **72**(12): 2203-2207.

Duplessis, S., C. Lorrain, B. Petre, M. Figueroa, P. N. Dodds and M. C. Aime (2021). "Host Adaptation and Virulence in Heteroecious Rust Fungi." *Annu Rev Phytopathol* **59**: 403-422.

Ellis, J. G., G. J. Lawrence, J. E. Luck and P. N. Dodds (1999). "Identification of Regions in Alleles of the Flax Rust Resistance Gene *L* That Determine Differences in Gene-for-Gene Specificity." *The Plant Cell* **11**(3): 495.

Erwig, J., H. Ghareeb, M. Kopischke, R. Hacke, A. Matei, E. Petutschnig and V. Lipka (2017). "Chitin-induced and CHITIN ELICITOR RECEPTOR KINASE1 (CERK1) phosphorylation-dependent endocytosis of *Arabidopsis thaliana* LYSIN MOTIF-CONTAINING RECEPTOR-LIKE KINASE5 (LYK5)." *New Phytol* **215**(1): 382-396.

Essuman, K., J. Milbrandt, J. L. Dangl and M. T. Nishimura (2022). "Shared TIR enzymatic functions regulate cell death and immunity across the tree of life." *Science* **377**(6605): eab0001.

FAO. (2019). "The state of food and agriculture 2019. Moving forward on food loss and waste reduction." from <http://www.fao.org/3/ca6030en/ca6030en.pdf>.

FAO. (2021). "New standards to curb the global spread of plant pests and diseases." from <https://www.fao.org/news/story/en/item/1187738/icode/>.

Farah, N. (2018). "Functional Characterisation of the Flax Rust AvrP/AvrP123 Avirulence Proteins." For the degree of Doctor of Philosophy of *The Australian National University*. <https://anulib.anu.edu.au/collections/theses>.

Farmam, M., G. Peterson, L. Chen, J. Starnes, B. Valent, P. Bachi, L. Murdock, D. Hershman, K. Pedley, J. M. Fernandes and J. Bavaresco (2017). "The *Lolium* Pathotype of *Magnaporthe oryzae* Recovered from a Single Blasted Wheat Plant in the United States." *Plant Dis* **101**(5): 684-692.

Fernandez, J. and K. Orth (2018). "Rise of a Cereal Killer: The Biology of *Magnaporthe oryzae* Biotrophic Growth." *Trends Microbiol* **26**(7): 582-597.

Figueroa, M., K. E. Hammond-Kosack and P. S. Solomon (2018). "A review of wheat diseases—a field perspective." *Molecular plant pathology* **19**(6): 1523-1536.

Fisher, M. C., D. A. Henk, C. J. Briggs, J. S. Brownstein, L. C. Madoff, S. L. McCraw and S. J. Gurr (2012). "Emerging fungal threats to animal, plant and ecosystem health." *Nature* **484**(7393): 186-194.

Flor, H. (1935). "Physiologic specialization of *Melampsora lini* on *Linum usitatissimum*." *J. agric. Res* **51**: 819-837.

Flor, H. (1940). "New physiologic races of Flax rust." *J Agric Res* **9**: 579-591.

Flor, H. (1941). "Pathogenicity of aeciospores obtained by selfing and crossing known physiologic races of *Melampsora lini*." *Phytopathology* **31**: 852-854.

Flor, H. (1942). "Inheritance of pathogenicity in *Melampsora lini*." *Phytopathology* **32**: 653-669.

Flor, H. (1946). "Genetics of pathogenicity in *Melampsora lini*." *J Agric Res* **73**: 335-357.

Flor, H. (1947). "Inheritance of reaction to rust in flax." *J Agric Res* **74**: 241-262.

Flor, H. (1965). "Inheritance of smooth-spore-wall and pathogenicity in *Melampsora lini*." *Phytopathology* **55**(7): 724.

Förderer, A., E. Li, A. W. Lawson, Y. N. Deng, Y. Sun, E. Logemann, X. Zhang, J. Wen, Z. Han, J. Chang, Y. Chen, P. Schulze-Lefert and J. Chai (2022). "A wheat resistosome defines common principles of immune receptor channels." *Nature* **610**(7932): 532-539.

Gabelli, S. B., M. A. Bianchet, Y. Ohnishi, Y. Ichikawa, M. J. Bessman and L. M. Amzel (2002). "Mechanism of the *Escherichia coli* ADP-ribose pyrophosphatase, a Nudix hydrolase." *Biochemistry* **41**(30): 9279-9285.

Ge, H., X. Chen, W. Yang, L. Niu and M. Teng (2013). "Crystal structure of wild-type and mutant human Ap4A hydrolase." *Biochem Biophys Res Commun* **432**(1): 16-21.

Ge, X., G. J. Li, S. B. Wang, H. Zhu, T. Zhu, X. Wang and Y. Xia (2007). "AtNUDT7, a negative regulator of basal immunity in *Arabidopsis*, modulates two distinct defense response pathways and is involved in maintaining redox homeostasis." *Plant Physiol* **145**(1): 204-215.

Giraldo, M. C., Y. F. Dagdas, Y. K. Gupta, T. A. Mentlak, M. Yi, A. L. Martinez-Rocha, H. Saitoh, R. Terauchi, N. J. Talbot and B. Valent (2013). "Two distinct secretion systems facilitate tissue invasion by the rice blast fungus *Magnaporthe oryzae*." *Nat Commun* **4**: 1996.

Giraldo, M. C. and B. Valent (2013). "Filamentous plant pathogen effectors in action." *Nat Rev Microbiol* **11**(11): 800-814.

Gladieux, P., B. Condon, S. Ravel, D. Soanes, J. L. N. Maciel, A. Nhani, Jr., L. Chen, R. Terauchi, M. H. Lebrun, D. Tharreau, T. Mitchell, K. F. Pedley, B. Valent, N. J. Talbot, M. Farman and E. Fournier (2018). "Gene Flow between Divergent Cereal- and Grass-Specific Lineages of the Rice Blast Fungus Magnaporthe oryzae." *mBio* **9**(1): e01219-01217.

Greenberg, J. T. and B. A. Vinatzer (2003). "Identifying type III effectors of plant pathogens and analyzing their interaction with plant cells." *Curr Opin Microbiol* **6**(1): 20-28.

Grimmer, M. K., M. John Foulkes and N. D. Paveley (2012). "Foliar pathogenesis and plant water relations: a review." *J Exp Bot* **63**(12): 4321-4331.

Hamer, J. E., R. J. Howard, F. G. Chumley and B. Valent (1988). "A mechanism for surface attachment in spores of a plant pathogenic fungus." *Science* **239**(4837): 288-290.

Hayafune, M., R. Berisio, R. Marchetti, A. Silipo, M. Kayama, Y. Desaki, S. Arima, F. Squeglia, A. Ruggiero, K. Tokuyasu, A. Molinaro, H. Kaku and N. Shibuya (2014). "Chitin-induced activation of immune signaling by the rice receptor CEBiP relies on a unique sandwich-type dimerization." *Proc Natl Acad Sci U S A* **111**(3): E404-413.

He, J., C. Zhang, H. Dai, H. Liu, X. Zhang, J. Yang, X. Chen, Y. Zhu, D. Wang, X. Qi, W. Li, Z. Wang, G. An, N. Yu, Z. He, Y. F. Wang, Y. Xiao, P. Zhang and E. Wang (2019). "A LysM Receptor Heteromer Mediates Perception of Arbuscular Mycorrhizal Symbiotic Signal in Rice." *Mol Plant* **12**(12): 1561-1576.

Horsefield, S., H. Burdett, X. Zhang, M. K. Manik, Y. Shi, J. Chen, T. Qi, J. Gilley, J. S. Lai, M. X. Rank, L. W. Casey, W. Gu, D. J. Ericsson, G. Foley, R. O. Hughes, T. Bosanac, M. von Itzstein, J. P. Rathjen, J. D. Nanson, M. Boden, I. B. Dry, S. J. Williams, B. J. Staskawicz, M. P. Coleman, T. Ve, P. N. Dodds and B. Kobe (2019). "NAD(+) cleavage activity by animal and plant TIR domains in cell death pathways." *Science* **365**(6455): 793-799.

Howard, R. J., M. A. Ferrari, D. H. Roach and N. P. Money (1991). "Penetration of hard substrates by a fungus employing enormous turgor pressures." *Proc Natl Acad Sci U S A* **88**(24): 11281-11284.

Huang, S., A. Jia, W. Song, G. Hessler, Y. Meng, Y. Sun, L. Xu, H. Laessle, J. Jirschitzka, S. Ma, Y. Xiao, D. Yu, J. Hou, R. Liu, H. Sun, X. Liu, Z. Han, J. Chang, J. E. Parker and J. Chai (2022). "Identification and receptor mechanism of TIR-catalyzed small molecules in plant immunity." *Science* **377**(6605): eabq3297.

Hulin, M. T., L. Hill, J. D. G. Jones and W. Ma (2023). "Pangenomic analysis reveals plant NAD(+) manipulation as an important virulence activity of bacterial pathogen effectors." *Proc Natl Acad Sci U S A* **120**(7): e2217114120.

Igarashi, S. (1986). "Pyricularia em trigo. 1. Ocorrencia de Pyricularia sp no estado do Parana." *Fitopatol. Bras* **11**: 351-352.

Inoue, Y., T. T. P. Vy, K. Yoshida, H. Asano, C. Mitsuoka, S. Asuke, V. L. Anh, C. J. R. Cumagun, I. Chuma, R. Terauchi, K. Kato, T. Mitchell, B. Valent, M. Farman and Y. Tosa (2017). "Evolution of the wheat blast fungus through functional losses in a host specificity determinant." *Science* **357**(6346): 80-83.

Ito, R., H. Hayakawa, M. Sekiguchi and T. Ishibashi (2005). "Multiple Enzyme Activities of Escherichia coli MutT Protein for Sanitization of DNA and RNA Precursor Pools." *Biochemistry* **44**(17): 6670-6674.

Iwai, T., S. Kuramitsu and R. Masui (2004). "The Nudix hydrolase Ndx1 from *Thermus thermophilus* HB8 is a diadenosine hexaphosphate hydrolase with a novel activity" *The Journal of biological chemistry* **279**(21): 21732-21739.

Jacob, F., B. Kracher, A. Mine, C. Seyfferth, S. Blanvillain-Baufumé, J. E. Parker, K. Tsuda, P. Schulze-Lefert and T. Maekawa (2018). "A dominant-interfering camta3 mutation compromises primary transcriptional outputs mediated by both cell surface and intracellular immune receptors in *Arabidopsis thaliana*." *New Phytol* **217**(4): 1667-1680.

Jacob, P., N. H. Kim, F. Wu, F. El-Kasmi, Y. Chi, W. G. Walton, O. J. Furzer, A. D. Lietzan, S. Sunil, K. Kempthorn, M. R. Redinbo, Z. M. Pei, L. Wan and J. L. Dangl (2021). "Plant "helper" immune receptors are Ca(2+)-permeable nonselective cation channels." *Science* **373**(6553): 420-425.

Jemth, A.-S., R. Gustafsson, L. Bräutigam, L. Henriksson, K. S. A. Vallin, A. Sarno, I. Almlöf, E. Homan, A. Rasti, U. Warpman Berglund, P. Stenmark and T. Helleday (2018). "MutT homologue 1 (MTH1) catalyzes the hydrolysis of mutagenic O6-methyl-dGTP." *Nucleic Acids Research* **46**(20): 10888-10904.

Jia, A., S. Huang, W. Song, J. Wang, Y. Meng, Y. Sun, L. Xu, H. Laessle, J. Jirschitzka, J. Hou, T. Zhang, W. Yu, G. Hessler, E. Li, S. Ma, D. Yu, J. Gebauer, U. Baumann, X. Liu, Z. Han, J. Chang, J. E. Parker and J. Chai (2022). "TIR-catalyzed ADP-ribosylation reactions produce signaling molecules for plant immunity." *Science* **377**(6605): eabq8180.

Joly, D. L., N. Feau, P. Tanguay and R. C. Hamelin (2010). "Comparative analysis of secreted protein evolution using expressed sequence tags from four poplar leaf rusts (*Melampsora* spp.)." *BMC Genomics* **11**: 422.

Jones, D. A., C. M. Thomas, K. E. Hammond-Kosack, P. J. Balint-Kurti and J. D. Jones (1994). "Isolation of the tomato Cf-9 gene for resistance to *Cladosporium fulvum* by transposon tagging." *Science* **266**(5186): 789-793.

Jumper, J., R. Evans, A. Pritzel, T. Green, M. Figurnov, O. Ronneberger, K. Tunyasuvunakool, R. Bates, A. Žídek, A. Potapenko, A. Bridgland, C. Meyer, S. A. A. Kohl, A. J. Ballard, A. Cowie, B. Romera-Paredes, S. Nikolov, R. Jain, J. Adler, T. Back, S. Petersen, D. Reiman, E. Clancy, M. Zielinski, M. Steinegger, M. Pacholska, T. Berghammer, S. Bodenstein, D. Silver, O. Vinyals, A. W. Senior, K. Kavukcuoglu, P. Kohli and D. Hassabis (2021). "Highly accurate protein structure prediction with AlphaFold." *Nature* **596**(7873): 583-589.

Kadota, Y., J. Sklenar, P. Derbyshire, L. Stransfeld, S. Asai, V. Ntoukakis, J. D. Jones, K. Shirasu, F. Menke, A. Jones and C. Zipfel (2014). "Direct regulation of the NADPH oxidase RBOHD by the PRR-associated kinase BIK1 during plant immunity." *Mol Cell* **54**(1): 43-55.

Kang, L.-W., S. B. Gabelli, J. E. Cunningham, S. F. O'Handley and L. M. Amzel (2003). "Structure and mechanism of MT-ADPRase, a Nudix hydrolase from *Mycobacterium tuberculosis*." *Structure* **11**(8): 1015-1023.

Kankanala, P., K. Czymbek and B. Valent (2007). "Roles for rice membrane dynamics and plasmodesmata during biotrophic invasion by the blast fungus." *The Plant Cell* **19**(2): 706-724.

Kanyuka, K. and J. J. Rudd (2019). "Cell surface immune receptors: the guardians of the plant's extracellular spaces." *Curr Opin Plant Biol* **50**: 1-8.

Kawchuk, L. M., J. Hachey, D. R. Lynch, F. Kulcsar, G. van Rooijen, D. R. Waterer, A. Robertson, E. Kokko, R. Byers, R. J. Howard, R. Fischer and D. Prufer (2001). "Tomato Ve disease resistance genes encode cell surface-like receptors." *Proc Natl Acad Sci U S A* **98**(11): 6511-6515.

Khang, C. H., R. Berruyer, M. C. Giraldo, P. Kankanala, S. Y. Park, K. Czymbek, S. Kang and B. Valent (2010). "Translocation of Magnaporthe oryzae effectors into rice cells and their subsequent cell-to-cell movement." *The Plant Cell* **22**(4): 1388-1403.

Kim, N. H., P. Jacob and J. L. Dangl (2022). "Con-Ca(2+) -tenating plant immune responses via calcium-permeable cation channels." *New Phytol* **234**(3): 813-818.

Kim, S., C. Y. Kim, S. Y. Park, K. T. Kim, J. Jeon, H. Chung, G. Choi, S. Kwon, J. Choi, J. Jeon, J. S. Jeon, C. H. Khang, S. Kang and Y. H. Lee (2020). "Two nuclear effectors of the rice blast fungus modulate host immunity via transcriptional reprogramming." *Nat Commun* **11**(1): 5845.

Kong, G., Y. Zhao, M. Jing, J. Huang, J. Yang, Y. Xia, L. Kong, W. Ye, Q. Xiong, Y. Qiao, S. Dong, W. Ma and Y. Wang (2015). "The activation of Phytophthora effector Avr3b by plant cyclophilin is required for the Nudix hydrolase activity of Avr3b." *PLoS pathogens* **11**(8): e1005139-e1005139.

Kong, Q., T. Sun, N. Qu, J. Ma, M. Li, Y. T. Cheng, Q. Zhang, D. Wu, Z. Zhang and Y. Zhang (2016). "Two Redundant Receptor-Like Cytoplasmic Kinases Function Downstream of Pattern Recognition Receptors to Regulate Activation of SA Biosynthesis." *Plant Physiol* **171**(2): 1344-1354.

Lal, N. K., U. Nagalakshmi, N. K. Hurlburt, R. Flores, A. Bak, P. Sone, X. Ma, G. Song, J. Walley, L. Shan, P. He, C. Casteel, A. J. Fisher and S. P. Dinesh-Kumar (2018). "The Receptor-like Cytoplasmic Kinase BIK1 Localizes to the Nucleus and Regulates Defense Hormone Expression during Plant Innate Immunity." *Cell Host Microbe* **23**(4): 485-497.e485.

Lang, J., B. Genot, J. Bigeard and J. Colcombet (2022). "MPK3 and MPK6 control salicylic acid signaling by up-regulating NLR receptors during pattern- and effector-triggered immunity." *J Exp Bot* **73**(7): 2190-2205.

Langenbach, C., R. Campe, S. F. Beyer, A. N. Mueller and U. Conrath (2016). "Fighting Asian Soybean Rust." *Front Plant Sci* **7**: 797.

Lanver, D., M. Tollot, G. Schweizer, L. Lo Presti, S. Reissmann, L. S. Ma, M. Schuster, S. Tanaka, L. Liang, N. Ludwig and R. Kahmann (2017). "Ustilago maydis effectors and their impact on virulence." *Nat Rev Microbiol* **15**(7): 409-421.

Lawrence, G. J., P. A. Anderson, P. N. Dodds and J. G. Ellis (2010). "Relationships between rust resistance genes at the M locus in flax." *Molecular Plant Pathology* **11**(1): 19-32.

Lawrence, G. J., P. N. Dodds and J. G. Ellis (2007). "Rust of flax and linseed caused by *Melampsora lini*." *Mol Plant Pathol* **8**(4): 349-364.

Lawrence, G. J., P. N. Dodds and J. G. Ellis (2010). "Transformation of the flax rust fungus, *Melampsora lini*: selection via silencing of an avirulence gene." *Plant J* **61**(2): 364-369.

Lawrence, G. J., E. J. Finnegan, M. A. Ayliffe and J. G. Ellis (1995). "The L6 gene for flax rust resistance is related to the *Arabidopsis* bacterial resistance gene RPS2 and the tobacco viral resistance gene N." *The Plant Cell* **7**(8): 1195-1206.

Leslie, N. R., A. G. McLennan and S. T. Safrany (2002). "Cloning and characterisation of hAps1 and hAps2, human diadenosine polyphosphate-metabolising Nudix hydrolases." *BMC Biochemistry* **3**(1): 20.

Li, G., N. Dulal, Z. Gong and R. A. Wilson (2023). "Unconventional secretion of Magnaporthe oryzae effectors in rice cells is regulated by tRNA modification and codon usage control." *Nat Microbiol* **8**(9): 1706-1716.

Li, L., A. Habring, K. Wang and D. Weigel (2020). "Atypical Resistance Protein RPW8/HR Triggers Oligomerization of the NLR Immune Receptor RPP7 and Autoimmunity." *Cell Host Microbe* **27**(3): 405-417.e406.

Li, L., M. Li, L. Yu, Z. Zhou, X. Liang, Z. Liu, G. Cai, L. Gao, X. Zhang, Y. Wang, S. Chen and J. M. Zhou (2014). "The FLS2-associated kinase BIK1 directly phosphorylates the NADPH oxidase RbohD to control plant immunity." *Cell Host Microbe* **15**(3): 329-338.

Liu, T., Z. Liu, C. Song, Y. Hu, Z. Han, J. She, F. Fan, J. Wang, C. Jin, J. Chang, J. M. Zhou and J. Chai (2012). "Chitin-induced dimerization activates a plant immune receptor." *Science* **336**(6085): 1160-1164.

Liu, Z., Y. Wu, F. Yang, Y. Zhang, S. Chen, Q. Xie, X. Tian and J. M. Zhou (2013). "BIK1 interacts with PEPRs to mediate ethylene-induced immunity." *Proc Natl Acad Sci U S A* **110**(15): 6205-6210.

Lo Presti, L., D. Lanver, G. Schweizer, S. Tanaka, L. Liang, M. Tollot, A. Zuccaro, S. Reissmann and R. Kahmann (2015). "Fungal effectors and plant susceptibility." *Annual reviews plant biology* **66**: 513-545.

Lorrain, C., B. Petre and S. Duplessis (2018). "Show me the way: rust effector targets in heterologous plant systems." *Curr Opin Microbiol* **46**: 19-25.

Lu, D., S. Wu, X. Gao, Y. Zhang, L. Shan and P. He (2010). "A receptor-like cytoplasmic kinase, BIK1, associates with a flagellin receptor complex to initiate plant innate immunity." *Proc Natl Acad Sci U S A* **107**(1): 496-501.

Ma, S., D. Lapin, L. Liu, Y. Sun, W. Song, X. Zhang, E. Logemann, D. Yu, J. Wang, J. Jirschitzka, Z. Han, P. Schulze-Lefert, J. E. Parker and J. Chai (2020). "Direct pathogen-induced assembly of an NLR immune receptor complex to form a holoenzyme." *Science* **370**(6521): eabe3069.

Ma, X., L. A. N. Claus, M. E. Leslie, K. Tao, Z. Wu, J. Liu, X. Yu, B. Li, J. Zhou, D. V. Savatin, J. Peng, B. M. Tyler, A. Heese, E. Russinova, P. He and L. Shan (2020). "Ligand-induced monoubiquitination of BIK1 regulates plant immunity." *Nature* **581**(7807): 199-203.

Macho, A. P., F. Boutrot, J. P. Rathjen and C. Zipfel (2012). "Aspartate oxidase plays an important role in *Arabidopsis* stomatal immunity." *Plant Physiol* **159**(4): 1845-1856.

Macho, A. P. and C. Zipfel (2014). "Plant PRRs and the activation of innate immune signaling." *Mol Cell* **54**(2): 263-272.

Mackill, A. and J. Bonman (1986). "New hosts of *Pyricularia oryzae*." *Plant Disease* **70**(2): 125-127.

Marchal, C., V. A. Michalopoulou, Z. Zou, V. Cevik and P. F. Sarris (2022). "Show me your ID: NLR immune receptors with integrated domains in plants." *Essays Biochem* **66**(5): 527-539.

Martin, R., T. Qi, H. Zhang, F. Liu, M. King, C. Toth, E. Nogales and B. J. Staskawicz (2020). "Structure of the activated ROQ1 resistosome directly recognizing the pathogen effector XopQ." *Science* **370**(6521): eabd9993.

Mbinda, W. and H. Masaki (2020). "Breeding Strategies and Challenges in the Improvement of Blast Disease Resistance in Finger Millet. A Current Review." *Front Plant Sci* **11**: 602882.

McCombe, C. L., J. R. Greenwood, P. S. Solomon and S. J. Williams (2022). "Molecular plant immunity against biotrophic, hemibiotrophic, and necrotrophic fungi." *Essays Biochem* **66**(5): 581-593.

McLennan, A. G. (2006). "The Nudix hydrolase superfamily." *Cell Mol Life Sci* **63**(2): 123-143.

McLennan, A. G. (2013). "Substrate ambiguity among the nudix hydrolases: biologically significant, evolutionary remnant, or both?" *Cellular and molecular life sciences : CMLS* **70**(3): 373-385.

Menardo, F., C. R. Praz, T. Wicker and B. Keller (2017). "Rapid turnover of effectors in grass powdery mildew (*Blumeria graminis*)."*BMC Evol Biol* **17**(1): 223.

Mentlak, T. A., A. Kombrink, T. Shinya, L. S. Ryder, I. Otomo, H. Saitoh, R. Terauchi, Y. Nishizawa, N. Shibuya, B. P. Thomma and N. J. Talbot (2012). "Effector-mediated suppression of chitin-triggered immunity by magnaporthe oryzae is necessary for rice blast disease." *The Plant Cell* **24**(1): 322-335.

Mildvan, A. S., Z. Xia, H. F. Azurmendi, V. Saraswat, P. M. Legler, M. A. Massiah, S. B. Gabelli, M. A. Bianchet, L. W. Kang and L. M. Amzel (2005). "Structures and mechanisms of Nudix hydrolases." *Archives of Biochemistry and Biophysics* **433**(1): 129-143.

Miya, A., P. Albert, T. Shinya, Y. Desaki, K. Ichimura, K. Shirasu, Y. Narusaka, N. Kawakami, H. Kaku and N. Shibuya (2007). "CERK1, a LysM receptor kinase, is essential for chitin elicitor signaling in *Arabidopsis*." *Proc Natl Acad Sci U S A* **104**(49): 19613-19618.

Miyata, K., T. Kozaki, Y. Kouzai, K. Ozawa, K. Ishii, E. Asamizu, Y. Okabe, Y. Umehara, A. Miyamoto, Y. Kobae, K. Akiyama, H. Kaku, Y. Nishizawa, N. Shibuya and T. Nakagawa (2014). "The bifunctional plant receptor, OsCERK1, regulates both chitin-triggered immunity and arbuscular mycorrhizal symbiosis in rice." *Plant Cell Physiol* **55**(11): 1864-1872.

- Moscou, M. J. and H. P. van Esse (2017). "The quest for durable resistance." *Science* **358**(6370): 1541-1542.
- Ngou, B. P. M., H. K. Ahn, P. Ding and J. D. G. Jones (2021). "Mutual potentiation of plant immunity by cell-surface and intracellular receptors." *Nature* **592**(7852): 110-115.
- Nühse, T. S., A. R. Bottrill, A. M. Jones and S. C. Peck (2007). "Quantitative phosphoproteomic analysis of plasma membrane proteins reveals regulatory mechanisms of plant innate immune responses." *Plant J* **51**(5): 931-940.
- Nühse, T. S., S. C. Peck, H. Hirt and T. Boller (2000). "Microbial elicitors induce activation and dual phosphorylation of the *Arabidopsis thaliana* MAPK 6." *J Biol Chem* **275**(11): 7521-7526.
- O'Brien, H. E., S. Thakur, Y. Gong, P. Fung, J. Zhang, L. Yuan, P. W. Wang, C. Yong, M. Scorticini and D. S. Guttman (2012). "Extensive remodeling of the *Pseudomonas syringae* pv. *avellanae* type III secretome associated with two independent host shifts onto hazelnut." *BMC Microbiol* **12**: 141.
- O'Handley, S. F., D. N. Frick, C. A. Dunn and M. J. Bessman (1998). "Orf186 represents a new member of the Nudix hydrolases, active on adenosine (5') triphospho (5') adenosine, ADP-ribose, and NADH." *The Journal of biological chemistry* **273**(6): 3192-3197.
- Ogawa, T., Y. Ueda, K. Yoshimura and S. Shigeoka (2005). "Comprehensive analysis of cytosolic Nudix hydrolases in *Arabidopsis thaliana*." *Journal of biological chemistry* **280**(26): 25277-25283.
- Olejnik, K., M. Bucholc, A. Anielska-Mazur, A. Lipko, M. Kujawa, M. Modzelan, A. Augustyn and E. Kraszewska (2011). "Arabidopsis thaliana Nudix hydrolase AtNUDT7 forms complexes with the regulatory RACK1A protein and Ggamma subunits of the signal transducing heterotrimeric G protein." *Acta Biochim Pol* **58**(4): 609-616.
- Olejnik, K. and E. Kraszewska (2005). "Cloning and characterization of an *Arabidopsis thaliana* Nudix hydrolase homologous to the mammalian GFG protein." *Biochim Biophys Acta* **1752**(2): 133-141.
- Oliveira-Garcia, E., T. M. Tamang, J. Park, M. Dalby, M. Martin-Urdiroz, C. Rodriguez Herrero, A. H. Vu, S. Park, N. J. Talbot and B. Valent (2023). "Clathrin-mediated endocytosis facilitates the internalization of Magnaporthe oryzae effectors into rice cells." *The Plant Cell* **35**(7): 2527-2551.
- Padmanabhan, S. (1973). "The great Bengal famine." *Annual Review of Phytopathology* **11**(1): 11-24.
- Park, C. H., S. Chen, G. Shirsekar, B. Zhou, C. H. Khang, P. Songkumarn, A. J. Afzal, Y. Ning, R. Wang, M. Bellizzi, B. Valent and G. L. Wang (2012). "The Magnaporthe oryzae effector AvrPiz-t targets the RING E3 ubiquitin ligase APIP6 to suppress pathogen-associated molecular pattern-triggered immunity in rice." *The Plant Cell* **24**(11): 4748-4762.
- Park, C. H., G. Shirsekar, M. Bellizzi, S. Chen, P. Songkumarn, X. Xie, X. Shi, Y. Ning, B. Zhou, P. Suttipiriya, M. Wang, K. Umemura and G. L. Wang (2016). "The E3 Ligase APIP10 Connects the Effector AvrPiz-t to the NLR Receptor Piz-t in Rice." *PLoS Pathog* **12**(3): e1005529.
- Paul, S. K., N. U. Mahmud, D. R. Gupta, K. Rani, H. Kang, G.-L. Wang, L. Jankuloski and T. Islam (2022). "Oryzae pathotype of Magnaporthe oryzae can cause typical blast disease symptoms on both leaves and spikes of wheat under a growth room condition." *Phytopathology Research* **4**(1): 9.
- Peng, M. and J. Kuc (1992). "Peroxidase-generated hydrogen peroxide as a source of antifungal activity in vitro and on tobacco leaf disks." *Phytopathology* **82**(6): 696-699.
- Peng, Y., R. van Wersch and Y. Zhang (2018). "Convergent and Divergent Signaling in PAMP-Triggered Immunity and Effector-Triggered Immunity." *Mol Plant Microbe Interact* **31**(4): 403-409.
- Periyannan, S., R. J. Milne, M. Figueroa, E. S. Lagudah and P. N. Dodds (2017). "An overview of genetic rust resistance: From broad to specific mechanisms." *PLoS Pathog* **13**(7): e1006380.
- Perraud, A.-L., B. Shen, C. A. Dunn, K. Rippe, M. K. Smith, M. J. Bessman, B. L. Stoddard and A. M. Scharenberg (2003). "NUDT9, a member of the Nudix hydrolase family, is an evolutionarily conserved mitochondrial ADP-ribose pyrophosphatase." *The Journal of biological chemistry* **278**(3): 1794-1801.
- Petre, B. and S. Duplessis (2022). "A decade after the first *Pucciniales* genomes: A bibliometric snapshot of (post) genomics studies in three model rust fungi." *Front Microbiol* **13**: 989580.
- Petutschnig, E. K., A. M. Jones, L. Serazetdinova, U. Lipka and V. Lipka (2010). "The lysin motif receptor-like kinase (LysM-RLK) CERK1 is a major chitin-binding protein in *Arabidopsis thaliana* and subject to chitin-induced phosphorylation." *J Biol Chem* **285**(37): 28902-28911.
- Pruitt, R. N., F. Locci, F. Wanke, L. Zhang, S. C. Saile, A. Joe, D. Karelina, C. Hua, K. Fröhlich, W. L. Wan, M. Hu, S. Rao, S. C. Stolze, A. Harzen, A. A. Gust, K. Harter, M. Joosten, B. Thomma, J. M. Zhou, J. L. Dangl, D. Weigel, H. Nakagami, C. Oecking, F. E. Kasmi, J. E.

Parker and T. Nürnberger (2021). "The EDS1-PAD4-ADR1 node mediates Arabidopsis pattern-triggered immunity." *Nature* **598**(7881): 495-499.

Qi, T., K. Seong, D. P. T. Thomazella, J. R. Kim, J. Pham, E. Seo, M. J. Cho, A. Schultink and B. J. Staskawicz (2018). "NRG1 functions downstream of EDS1 to regulate TIR-NLR-mediated plant immunity in Nicotiana benthamiana." *Proc Natl Acad Sci U S A* **115**(46): E10979-e10987.

Ravensdale, M., M. Bernoux, T. Ve, B. Kobe, P. H. Thrall, J. G. Ellis and P. N. Dodds (2012). "Intramolecular interaction influences binding of the Flax L5 and L6 resistance proteins to their AvrL567 ligands." *PLoS pathogens* **8**(11): e1003004.

Rodrigues, M. L., A. J. Franzen, L. Nimrichter and K. Miranda (2013). "Vesicular mechanisms of traffic of fungal molecules to the extracellular space." *Curr Opin Microbiol* **16**(4): 414-420.

Saitoh, H., S. Fujisawa, C. Mitsuoka, A. Ito, A. Hirabuchi, K. Ikeda, H. Irieda, K. Yoshino, K. Yoshida, H. Matsumura, Y. Tosa, J. Win, S. Kamoun, Y. Takano and R. Terauchi (2012). "Large-scale gene disruption in Magnaporthe oryzae identifies MC69, a secreted protein required for infection by monocot and dicot fungal pathogens." *PLoS Pathog* **8**(5): e1002711.

Sakulkoo, W., M. Osés-Ruiz, E. Oliveira Garcia, D. M. Soanes, G. R. Littlejohn, C. Hacker, A. Correia, B. Valent and N. J. Talbot (2018). "A single fungal MAP kinase controls plant cell-to-cell invasion by the rice blast fungus." *Science* **359**(6382): 1399-1403.

Sakumi, K., M. Furuichi, T. Tsuzuki, T. Kakuma, S. Kawabata, H. Maki and M. Sekiguchi (1993). "Cloning and expression of cDNA for a human enzyme that hydrolyzes 8-oxo-dGTP, a mutagenic substrate for DNA synthesis." *The Journal of biological chemistry* **268**(31): 23524-23530.

Schechter, L. M., K. A. Roberts, Y. Jamir, J. R. Alfano and A. Collmer (2004). "Pseudomonas syringae type III secretion system targeting signals and novel effectors studied with a Cya translocation reporter." *J Bacteriol* **186**(2): 543-555.

Schmülling, T., T. Werner, M. Riefler, E. Krupková and I. Bartrina y Manns (2003). "Structure and function of cytokinin oxidase/dehydrogenase genes of maize, rice, Arabidopsis and other species." *J Plant Res* **116**(3): 241-252.

Shao, Z. Q., J. Y. Xue, P. Wu, Y. M. Zhang, Y. Wu, Y. Y. Hang, B. Wang and J. Q. Chen (2016). "Large-Scale Analyses of Angiosperm Nucleotide-Binding Site-Leucine-Rich Repeat Genes Reveal Three Anciently Diverged Classes with Distinct Evolutionary Patterns." *Plant Physiol* **170**(4): 2095-2109.

Shi, X., Y. Long, F. He, C. Zhang, R. Wang, T. Zhang, W. Wu, Z. Hao, Y. Wang, G. L. Wang and Y. Ning (2018). "The fungal pathogen Magnaporthe oryzae suppresses innate immunity by modulating a host potassium channel." *PLoS Pathog* **14**(1): e1006878.

Shimizu, T., T. Nakano, D. Takamizawa, Y. Desaki, N. Ishii-Minami, Y. Nishizawa, E. Minami, K. Okada, H. Yamane, H. Kaku and N. Shibuya (2010). "Two LysM receptor molecules, CEBiP and OsCERK1, cooperatively regulate chitin elicitor signaling in rice." *Plant J* **64**(2): 204-214.

Shinya, T., K. Yamaguchi, Y. Desaki, K. Yamada, T. Narisawa, Y. Kobayashi, K. Maeda, M. Suzuki, T. Tanimoto, J. Takeda, M. Nakashima, R. Funama, M. Narusaka, Y. Narusaka, H. Kaku, T. Kawasaki and N. Shibuya (2014). "Selective regulation of the chitin-induced defense response by the Arabidopsis receptor-like cytoplasmic kinase PBL27." *Plant J* **79**(1): 56-66.

Singh, R. P., D. P. Hodson, J. Huerta-Espino, Y. Jin, S. Bhavani, P. Njau, S. Herrera-Foessel, P. K. Singh, S. Singh and V. Govindan (2011). "The emergence of Ug99 races of the stem rust fungus is a threat to world wheat production." *Annu Rev Phytopathol* **49**: 465-481.

Song, M.-G., S. Bail and M. Kiledjian (2013). "Multiple Nudix family proteins possess mRNA decapping activity." *RNA* **19**(3): 390-399.

Sperschneider, J. and P. N. Dodds (2022). "EffectorP 3.0: Prediction of Apoplastic and Cytoplasmic Effectors in Fungi and Oomycetes." *Mol Plant Microbe Interact* **35**(2): 146-156.

Srouji, J. R., A. Xu, A. Park, J. F. Kirsch and S. E. Brenner (2017). "The evolution of function within the Nudix homology clan." *Proteins* **85**(5): 775-811.

Stephens, C., K. E. Hammond-Kosack and K. Kanyuka (2022). "WAKsing plant immunity, waning diseases." *J Exp Bot* **73**(1): 22-37.

Stukenbrock, E. H., T. Bataillon, J. Y. Dutheil, T. T. Hansen, R. Li, M. Zala, B. A. McDonald, J. Wang and M. H. Schierup (2011). "The making of a new pathogen: insights from comparative population genomics of the domesticated wheat pathogen *Mycosphaerella graminicola* and its wild sister species." *Genome Res* **21**(12): 2157-2166.

Sun, Y., L. Li, A. P. Macho, Z. Han, Z. Hu, C. Zipfel, J. M. Zhou and J. Chai (2013). "Structural basis for flg22-induced activation of the Arabidopsis FLS2-BAK1 immune complex." *Science* **342**(6158): 624-628.

Sun, Y., P. Li, D. Shen, Q. Wei, J. He and Y. Lu (2019). "The Ralstonia solanacearum effector RipN suppresses plant PAMP-triggered immunity, localizes to the endoplasmic reticulum and nucleus, and alters the NADH/NAD(+) ratio in Arabidopsis." *Molecular plant pathology* **20**(4): 533-546.

Surovy, M. Z., T. Islam and A. von Tiedemann (2023). "Role of seed infection for the near and far distance dissemination of wheat blast caused by Magnaporthe oryzae pathotype Triticum." *Front Microbiol* **14**: 1040605.

Suzuki, M., M. Shibuya, H. Shimada, N. Motoyama, M. Nakashima, S. Takahashi, K. Suto, I. Yoshida, S. Matsui, N. Tsujimoto, M. Ohnishi, Y. Ishibashi, Z. Fujimoto, Y. Desaki, H. Kaku, K. Kito and N. Shibuya (2016). "Autophosphorylation of Specific Threonine and Tyrosine Residues in Arabidopsis CERK1 is Essential for the Activation of Chitin-Induced Immune Signaling." *Plant Cell Physiol* **57**(11): 2312-2322.

Takken, F. L., C. M. Thomas, M. H. Joosten, C. Golstein, N. Westerink, J. Hille, H. J. Nijkamp, P. J. De Wit and J. D. Jones (1999). "A second gene at the tomato Cf-4 locus confers resistance to cladosporium fulvum through recognition of a novel avirulence determinant." *Plant J* **20**(3): 279-288.

Talbot, N. J. (2003). "On the trail of a cereal killer: Exploring the biology of Magnaporthe grisea." *Annu Rev Microbiol* **57**: 177-202.

Talhahas, P., D. Batista, I. Diniz, A. Vieira, D. N. Silva, A. Loureiro, S. Tavares, A. P. Pereira, H. G. Azinheira, L. Guerra-Guimarães, V. Várzea and M. D. C. Silva (2017). "The coffee leaf rust pathogen Hemileia vastatrix: one and a half centuries around the tropics." *Mol Plant Pathol* **18**(8): 1039-1051.

Tang, J., Z. Han, Y. Sun, H. Zhang, X. Gong and J. Chai (2015). "Structural basis for recognition of an endogenous peptide by the plant receptor kinase PEPR1." *Cell Res* **25**(1): 110-120.

Tembo, B., R. M. Mulenga, S. Sichilima, K. M'Siska K, M. Mwale, P. C. Chikoti, P. K. Singh, X. He, K. F. Pedley, G. L. Peterson, R. P. Singh and H. J. Braun (2020). "Detection and characterization of fungus (Magnaporthe oryzae pathotype Triticum) causing wheat blast disease on rain-fed grown wheat (Triticum aestivum L.) in Zambia." *PLoS One* **15**(9): e0238724.

Thomas, C. M., D. A. Jones, M. Parniske, K. Harrison, P. J. Balint-Kurti, K. Hatzixanthis and J. D. Jones (1997). "Characterization of the tomato Cf-4 gene for resistance to Cladosporium fulvum identifies sequences that determine recognitional specificity in Cf-4 and Cf-9." *The Plant Cell* **9**(12): 2209-2224.

Tian, H., Z. Wu, S. Chen, K. Ao, W. Huang, H. Yaghmaiean, T. Sun, F. Xu, Y. Zhang, S. Wang, X. Li and Y. Zhang (2021). "Activation of TIR signalling boosts pattern-triggered immunity." *Nature* **598**(7881): 500-503.

Tian, W., C. Hou, Z. Ren, C. Wang, F. Zhao, D. Dahlbeck, S. Hu, L. Zhang, Q. Niu, L. Li, B. J. Staskawicz and S. Luan (2019). "A calmodulin-gated calcium channel links pathogen patterns to plant immunity." *Nature* **572**(7767): 131-135.

Tsuda, K. and F. Katagiri (2010). "Comparing signaling mechanisms engaged in pattern-triggered and effector-triggered immunity." *Curr Opin Plant Biol* **13**(4): 459-465.

Valent, B., M. Farman, Y. Tosa, D. Begerow, E. Fournier, P. Gladieux, M. T. Islam, S. Kamoun, M. Kemler, L. M. Kohn, M. H. Lebrun, J. E. Stajich, N. J. Talbot, R. Terauchi, D. Tharreau and N. Zhang (2019). "Pyricularia graminis-tritici is not the correct species name for the wheat blast fungus: response to Ceresini et al. (MPP 20:2)." *Mol Plant Pathol* **20**(2): 173-179.

van der Burgh, A. M. and M. Joosten (2019). "Plant Immunity: Thinking Outside and Inside the Box." *Trends Plant Sci* **24**(7): 587-601.

Van Dijk, E., N. Cougot, S. Meyer, S. Babajko, E. Wahle and B. Séraphin (2002). "Human Dcp2: a catalytically active mRNA decapping enzyme located in specific cytoplasmic structures." *The EMBO Journal* **21**(24): 6915-6924.

Varadi, M., S. Anyango, M. Deshpande, S. Nair, C. Natassia, G. Yordanova, D. Yuan, O. Stroe, G. Wood, A. Laydon, A. Žídek, T. Green, K. Tunyasuvunakool, S. Petersen, J. Jumper, E. Clancy, R. Green, A. Vora, M. Lutfi, M. Figurnov, A. Cowie, N. Hobbs, P. Kohli, G. Kleywegt, E. Birney, D. Hassabis and S. Velankar (2022). "AlphaFold Protein Structure Database: massively expanding the structural coverage of protein-sequence space with high-accuracy models." *Nucleic Acids Res* **50**(D1): D439-d444.

Ve, T., S. J. Williams, A.-M. Catanzariti, M. Rafiqi, M. Rahman, J. G. Ellis, A. R. Hardham, D. A. Jones, P. A. Anderson and P. N. Dodds (2013). "Structures of the flax-rust effector AvrM reveal insights into the molecular basis of plant-cell entry and effector-triggered immunity." *Proceedings of the National Academy of Sciences* **110**(43): 17594-17599.

Vinatzer, B. A., J. Jelenska and J. T. Greenberg (2005). "Bioinformatics correctly identifies many type III secretion substrates in the plant pathogen *Pseudomonas syringae* and the biocontrol isolate *P. fluorescens* SBW25." *Mol Plant Microbe Interact* **18**(8): 877-888.

Voegele, R. T. and K. Mendgen (2003). "Rust haustoria: nutrient uptake and beyond." *New Phytol* **159**(1): 93-100.

Wan, L., K. Essuman, R. G. Anderson, Y. Sasaki, F. Monteiro, E. H. Chung, E. Osborne Nishimura, A. DiAntonio, J. Milbrandt, J. L. Dangl and M. T. Nishimura (2019). "TIR domains of plant immune receptors are NAD(+) -cleaving enzymes that promote cell death." *Science* **365**(6455): 799-803.

Wan, L., M. Koeck, S. J. Williams, A. R. Ashton, G. J. Lawrence, H. Sakakibara, M. Kojima, C. Böttcher, D. J. Ericsson, A. R. Hardham, D. A. Jones, J. G. Ellis, B. Kobe and P. N. Dodds (2019). "Structural and functional insights into the modulation of the activity of a flax cytokinin oxidase by flax rust effector AvrL567-A." *Mol Plant Pathol* **20**(2): 211-222.

Wang, B.-h., D. J. Ebbole and Z.-h. Wang (2017). "The arms race between Magnaporthe oryzae and rice: Diversity and interaction of Avr and R genes." *Journal of Integrative Agriculture* **16**(12): 2746-2760.

Wang, J., M. Hu, J. Wang, J. Qi, Z. Han, G. Wang, Y. Qi, H. W. Wang, J. M. Zhou and J. Chai (2019). "Reconstitution and structure of a plant NLR resistosome conferring immunity." *Science* **364**(6435): eaav5870.

Wang, R., Y. Ning, X. Shi, F. He, C. Zhang, J. Fan, N. Jiang, Y. Zhang, T. Zhang, Y. Hu, M. Bellizzi and G. L. Wang (2016). "Immunity to Rice Blast Disease by Suppression of Effector-Triggered Necrosis." *Curr Biol* **26**(18): 2399-2411.

Wang, Z., X. Jiao, A. Carr-Schmid and M. Kiledjian (2002). "The hDcp2 protein is a mammalian mRNA decapping enzyme." *Proc Natl Acad Sci U S A* **99**(20): 12663-12668.

Wicker, T., S. Oberhaensli, F. Parlange, J. P. Buchmann, M. Shatalina, S. Roffler, R. Ben-David, J. Doležel, H. Šimková, P. Schulze-Lefert, P. D. Spanu, R. Bruggmann, J. Amselem, H. Quesneville, E. Ver Loren van Themaat, T. Paape, K. K. Shimizu and B. Keller (2013). "The wheat powdery mildew genome shows the unique evolution of an obligate biotroph." *Nat Genet* **45**(9): 1092-1096.

Wu, B., F. Qi and Y. Liang (2023). "Fuels for ROS signaling in plant immunity." *Trends Plant Sci* **28**(10): 1124-1131.

Wu, W., A. Nemri, L. M. Blackman, A.-M. Catanzariti, J. Sperschneider, G. J. Lawrence, P. N. Dodds, D. A. Jones and A. R. Hardham (2019). "Flax rust infection transcriptomics reveals a transcriptional profile that may be indicative for rust Avr genes." *PLoS one* **14**(12): e0226106.

Yamada, K., K. Yamaguchi, T. Shirakawa, H. Nakagami, A. Mine, K. Ishikawa, M. Fujiwara, M. Narusaka, Y. Narusaka, K. Ichimura, Y. Kobayashi, H. Matsui, Y. Nomura, M. Nomoto, Y. Tada, Y. Fukao, T. Fukamizo, K. Tsuda, K. Shirasu, N. Shibuya and T. Kawasaki (2016). "The Arabidopsis CERK1-associated kinase PBL27 connects chitin perception to MAPK activation." *Embo J* **35**(22): 2468-2483.

Yan, X., B. Tang, L. S. Ryder, D. MacLean, V. M. Were, A. B. Eseola, N. Cruz-Mireles, W. Ma, A. J. Foster, M. Osés-Ruiz and N. J. Talbot (2023). "The transcriptional landscape of plant infection by the rice blast fungus Magnaporthe oryzae reveals distinct families of temporally co-regulated and structurally conserved effectors." *The Plant Cell* **35**(5): 1360-1385.

Yoshimura, K. and S. Shigeoka (2015). "Versatile physiological functions of the Nudix hydrolase family in Arabidopsis." *Biosci Biotechnol Biochem* **79**(3): 354-366.

Yu, D., W. Song, E. Y. J. Tan, L. Liu, Y. Cao, J. Jirschitzka, E. Li, E. Logemann, C. Xu, S. Huang, A. Jia, X. Chang, Z. Han, B. Wu, P. Schulze-Lefert and J. Chai (2022). "TIR domains of plant immune receptors are 2',3'-cAMP/cGMP synthetases mediating cell death." *Cell* **185**(13): 2370-2386.e2318.

Yuan, M., Z. Jiang, G. Bi, K. Nomura, M. Liu, Y. Wang, B. Cai, J. M. Zhou, S. Y. He and X. F. Xin (2021). "Pattern-recognition receptors are required for NLR-mediated plant immunity." *Nature* **592**(7852): 105-109.

Yuan, M., B. P. M. Ngou, P. Ding and X. F. Xin (2021). "PTI-ETI crosstalk: an integrative view of plant immunity." *Curr Opin Plant Biol* **62**: 102030.

Zhang, C., J. He, H. Dai, G. Wang, X. Zhang, C. Wang, J. Shi, X. Chen, D. Wang and E. Wang (2021). "Discriminating symbiosis and immunity signals by receptor competition in rice." *Proc Natl Acad Sci U S A* **118**(16): e2023738118.

Zhang, J., W. Li, T. Xiang, Z. Liu, K. Laluk, X. Ding, Y. Zou, M. Gao, X. Zhang, S. Chen, T. Mengiste, Y. Zhang and J. M. Zhou (2010). "Receptor-like cytoplasmic kinases integrate signaling from multiple plant immune receptors and are targeted by a *Pseudomonas syringae* effector." *Cell Host Microbe* **7**(4): 290-301.

Zhang, J., F. Shao, Y. Li, H. Cui, L. Chen, H. Li, Y. Zou, C. Long, L. Lan, J. Chai, S. Chen, X. Tang and J. M. Zhou (2007). "A *Pseudomonas syringae* effector inactivates MAPKs to suppress PAMP-induced immunity in plants." *Cell Host Microbe* **1**(3): 175-185.

Zhang, X., W. Dong, J. Sun, F. Feng, Y. Deng, Z. He, G. E. Oldroyd and E. Wang (2015). "The receptor kinase CERK1 has dual functions in symbiosis and immunity signalling." *Plant J* **81**(2): 258-267.

Zhang, X., N. Farah, L. Rolston, D. J. Ericsson, A.-M. Catanzariti, M. Bernoux, T. Ve, K. Bendak, C. Chen, J. P. Mackay, G. J. Lawrence, A. Hardham, J. G. Ellis, S. J. Williams, P. N. Dodds, D. A. Jones and B. Kobe (2018). "Crystal structure of the *Melampsora lini* effector AvrP reveals insights into a possible nuclear function and recognition by the flax disease resistance protein P." *Molecular Plant Pathology* **19**(5): 1196-1209.

Zhao, Y. B., M. X. Liu, T. T. Chen, X. Ma, Z. K. Li, Z. Zheng, S. R. Zheng, L. Chen, Y. Z. Li, L. R. Tang, Q. Chen, P. Wang and S. Ouyang (2022). "Pathogen effector AvrSr35 triggers Sr35 resistosome assembly via a direct recognition mechanism." *Sci Adv* **8**(36): eabq5108.

Chapter 2 A rust-fungus Nudix hydrolase effector decaps mRNA *in vitro* and interferes with plant immune pathways

To understand the roles of fungal Nudix hydrolase effectors, I sought to characterise AvrM14 from *M. lini*. For the purposes of my thesis, I present this work as a published manuscript. Below is a detailed description of the experimental work performed by myself and others.

Prior to my PhD, Dr Ann-Maree Catanzariti, Dr Simon Williams, and Dr Anna Desai performed experiments to understand the function and recognition of AvrM14. Dr Catanzariti created a series of reciprocal single and double amino acid substitutions in AvrM14-A and AvrM14-B to identify the requirements for recognition by the M1 and M4 resistance proteins. Dr Williams determined the crystal structure of AvrM14-A revealing a Nudix fold, and Dr Desai completed an extensive substrate screening experiment with purified AvrM14-A protein and identified ^{m7}Gp₅G as a substrate of AvrM14-A. The hydrolysis of ^{m7}Gp₅G in the screening experiment suggested that AvrM14 may remove the protective 5' cap from eukaryotic mRNA. During my Honours research year in the Williams lab, I reproduced the results showing hydrolysis of ^{m7}Gp₅G by AvrM14-A and demonstrated that this activity is conserved in AvrM14-B and dependant on a predicted Mg²⁺ co-ordinating glutamate within the Nudix motif. Utilizing the Australian Synchrotron, I collected X-ray diffraction data from crystals of monomeric and homodimeric AvrM14-B proteins to enable structural determination and comparative analysis. I also identified that both AvrM14-A and AvrM14-B could remove the protective 5' cap structure from mRNA *in vitro*.

During my PhD, I refined the previously collected X-ray diffraction data to create accurate models of the crystal structures and deposited these to the protein data bank (PDB) (IDs: 8DP8, 8DP9, and 8DPA). I repeated all mRNA decapping assays with AvrM14-A and AvrM14-B with new preparations of purified protein and different mRNA sequences to ensure the data is robust, reproducible, and to obtain clear images for publication.

Furthermore, I:

1. demonstrate that homodimerisation alters the pyrophosphate bond in the mRNA cap hydrolysed by AvrM14-A and -B,
2. analysed the oligomeric state of AvrM14 when expressed in *N. benthamiana* plants,
3. determined that four additional related Nudix effectors from other *Melampsora* species retain mRNA decapping activity,

4. generated and analysed RNA-Sequencing datasets to investigate the impact of AvrM14 enzymatic activity on flax leaves,
5. identified that AvrM14-A enzymatic activity can suppress the HR triggered by the M1 resistance protein in flax,
6. repeated experiments initially completed by Dr Catanzariti demonstrating that the Nudix hydrolase activity of AvrM14 suppresses flg-22 and chitin triggered ROS production in *N. benthamiana*.

For publication, I assembled all data collected on the function and recognition of AvrM14. I wrote the initial draft of the manuscript and created all the figures. The draft was subsequently edited and approved by all authors. This chapter includes the main text and supporting information as published in *New Phytologist* and available online at <https://doi.org/10.1111/nph.18727>. The statement of contribution details my pivotal role in this work.



Statement of Contribution

I declare that the research presented in this Thesis represents original work that I carried out during my candidature at the Australian National University, except for contributions to multi-author papers incorporated in the Thesis where my contributions are specified in this Statement of Contribution.

Title: A rust-fungus Nudix hydrolase effector decaps mRNA *in vitro* and interferes with plant immune pathways

Authors: Carl L. McCombe, Ann-Maree Catanzariti, Julian R. Greenwood, Anna M. Desai, Megan A. Outram, Daniel S. Yu, Daniel J. Ericsson, Steven E. Brenner, Peter N. Dodds, Bostjan Kobe, David A. Jones and Simon J. Williams

Publication outlet: New Phytologist

Current status of paper: Not Yet Submitted/Submitted/Under Revision/Accepted/**Published**

Contribution to paper: I generated ~ 80% of the data presented in the manuscript. I produced all figures, and wrote the initial draft of the paper, which was subsequently edited and approved by all co-authors. For Figure 1B and C, I reproduced the data originally generated by Ann-Maree Catanzariti.

Data generated by others that I used to produce figures include:

Figures 1B, 1C, 6A – C, S2, S3, S11, and S12 (Ann-Maree Catanzariti)

Senior author or collaborating authors endorsement: _____

Carl McCombe

Candidate – Print Name

13/11/2023

Signature

Date

Endorsed

Simon Williams

Primary Supervisor – Print Name

13/11/2023

Signature

Date



A rust-fungus Nudix hydrolase effector decaps mRNA *in vitro* and interferes with plant immune pathways

Carl L. McCombe^{1*} , Ann-Maree Catanzariti^{1*} , Julian R. Greenwood¹ , Anna M. Desai²,
Megan A. Outram¹ , Daniel S. Yu¹ , Daniel J. Ericsson³ , Steven E. Brenner² , Peter N. Dodds⁴ ,
Bostjan Kobe⁵ , David A. Jones¹  and Simon J. Williams¹ 

¹Plant Sciences Division, Research School of Biology, The Australian National University, Canberra, ACT 2601, Australia; ²Plant and Microbial Biology Department, University of California, Berkeley, CA 94720, USA; ³Australian Synchrotron, Macromolecular Crystallography, Clayton, Vic. 3168, Australia; ⁴Black Mountain Science and Innovation Park, CSIRO Agriculture and Food, Canberra, ACT 2601, Australia; ⁵School of Chemistry and Molecular Biosciences, Institute for Molecular Bioscience and Australian Infectious Diseases Research Centre, University of Queensland, Brisbane, Qld 4072, Australia

Summary

Authors for correspondence:
Simon J. Williams
Email: simon.williams@anu.edu.au

David A. Jones
Email: david.jones@anu.edu.au

Received: 20 September 2022
Accepted: 2 January 2023

New Phytologist (2023) **239**: 222–239
doi: 10.1111/nph.18727

Key words: AvrM14, fungal effectors, *Melampsora lini*, mRNA decapping, Nudix hydrolase, plant immunity.

- To infect plants, pathogenic fungi secrete small proteins called effectors. Here, we describe the catalytic activity and potential virulence function of the Nudix hydrolase effector AvrM14 from the flax rust fungus (*Melampsora lini*).
- We completed extensive *in vitro* assays to characterise the enzymatic activity of the AvrM14 effector. Additionally, we used *in planta* transient expression of wild-type and catalytically dead AvrM14 versions followed by biochemical assays, phenotypic analysis and RNA sequencing to unravel how the catalytic activity of AvrM14 impacts plant immunity.
- AvrM14 is an extremely selective enzyme capable of removing the protective 5' cap from mRNA transcripts *in vitro*. Homodimerisation of AvrM14 promoted biologically relevant mRNA cap cleavage *in vitro* and this activity was conserved in related effectors from other *Melampsora* spp. *In planta* expression of wild-type AvrM14, but not the catalytically dead version, suppressed immune-related reactive oxygen species production, altered the abundance of some circadian-rhythm-associated mRNA transcripts and reduced the hypersensitive cell-death response triggered by the flax disease resistance protein M1.
- To date, the decapping of host mRNA as a virulence strategy has not been described beyond viruses. Our results indicate that some fungal pathogens produce Nudix hydrolase effectors with *in vitro* mRNA-decapping activity capable of interfering with plant immunity.

Introduction

Infectious diseases represent a significant threat to global crop production. To facilitate and maintain infection, plant pathogens secrete an array of proteins (termed effectors; Lo Presti *et al.*, 2015). Effectors are either delivered to the apoplast or translocated inside host cells, to modulate cellular processes. Plants have evolved resistance genes (*R*-genes) to defend against pathogen infection. Resistance genes encode effector-detecting resistance proteins (R-proteins) capable of inducing a strong immune response, known as effector-triggered immunity (ETI; Jones & Dangl, 2006; Dodds & Rathjen, 2010). The activation of ETI typically prevents pathogen growth, and recognised effectors are therefore referred to as avirulence (Avr) proteins. The ability of effectors to promote infection while avoiding recognition is crucial for successful infection. Consequently, understanding the pathogenicity function of effectors and how they are

perceived by R-proteins remains a major focus in the study of plant–pathogen interactions.

Nucleoside diphosphate linked to moiety-X (Nudix) hydrolase domains have been predicted in effectors from multiple fungal, oomycete and bacterial plant pathogens (Dong & Wang, 2016). The putative Nudix hydrolase effectors were identified based on similarities with the Nudix-box consensus sequence (GX₃EX₇-REUXEEXGU, where *U* is usually a hydrophobic residue and *X* is any amino acid). Nudix hydrolases typically hydrolyse nucleoside diphosphates bound to an additional moiety and substrate specificity is generally controlled by residues outside the Nudix box (McLennan, 2006; Srouji *et al.*, 2017). Well-characterised substrates of Nudix hydrolases include nucleoside triphosphates (Sakumi *et al.*, 1993; Ito *et al.*, 2005; Jemth *et al.*, 2018), adenosine diphosphate ribose (ADPR) (O'Handley *et al.*, 1998; Gabelli *et al.*, 2002; Kang *et al.*, 2003; Perraud *et al.*, 2003), diadenosine polyphosphates (ApnAs; Bessman *et al.*, 2001; Leslie *et al.*, 2002; Iwai *et al.*, 2004) and the 5' cap of mRNA transcripts (Van Dijk

*These authors contributed equally to this work.

et al., 2002; Wang et al., 2002; Song et al., 2013). Nudix hydrolases are ubiquitous in prokaryotic and eukaryotic organisms and are involved in diverse physiological processes and cellular homeostasis (McLennan, 2006).

The first Nudix hydrolase effector to be experimentally validated was Avr3b from the oomycete *Phytophthora sojae*, a destructive pathogen of soybean. Transient expression of Avr3b in *Nicotiana benthamiana* increased susceptibility to *Phytophthora capsica* and *Phytophthora parasitica* infection, diminished reactive oxygen species (ROS) accumulation around invasion sites, and reduced plant cell death during infection (Dong et al., 2011). In soybean, the expression of Avr3b suppressed cell death triggered by the recognition of Avr1b (Dong et al., 2011). Avr3b requires a plant cyclophilin for enzymatic activation, and both the cyclophilin and the Nudix box are required for the identified Avr3b virulence activities (Dong et al., 2011; Kong et al., 2015). Avr3b hydrolyses multiple nucleoside diphosphate compounds *in vitro* (Dong et al., 2011). Recently, Yu et al. (2022) demonstrated that Avr3b also has phosphodiesterase activity against 2',3'-cAMP/GMP and suggest that this enzymatic activity is a virulence function of the effector (Yu et al., 2022). The promiscuous *in vitro* enzymatic activity of Avr3b is common among Nudix hydrolases (McLennan, 2013) and complicates the identification of the true substrates of the effector during infection. RipN, a Nudix hydrolase effector from the bacterial pathogen *Ralstonia solanacearum*, also hydrolyses a variety of nucleoside diphosphate substrates *in vitro* (Sun et al., 2019). The preferred *in vitro* substrates of RipN are NADH and ADPR; however, overexpression of RipN in *Arabidopsis thaliana* did not result in significant changes to ADPR, NAD⁺ or NADH levels (Sun et al., 2019). CtNUDIX, a putative Nudix hydrolase effector from the hemibiotrophic fungus *Colletotrichum truncatum*, elicits a cell-death response when transiently expressed in *Nicotiana tabacum* (Bhaduria et al., 2013). However, it is unknown whether CtNUDIX possesses hydrolase activity and what it targets during infection. Putative Nudix hydrolase effectors have also been identified in biotrophic fungal pathogens. The flax rust-fungus *Melampsora lini* expresses AvrM14 early in infection of flax. AvrM14 encodes a predicted Nudix hydrolase effector (Anderson et al., 2016; Wu et al., 2019). The AvrM14 effector is recognised by the flax immune receptors M1 and M4, with previous research on AvrM14 immune recognition indicating that the effector is translocated inside flax cells during infection (Anderson et al., 2016). Here, we report the structure, biochemical activity and likely virulence function of the AvrM14 protein.

Materials and Methods

Cloning

AvrM14-A and AvrM14-B, without the predicted signal sequence (residues 22–166), were PCR-amplified from *Melampsora lini* cDNA (primers listed in Supporting Information Table S1) to facilitate respective downstream cloning processes.

AvrM14 mutants were generated using the Phusion Site-Directed Mutagenesis Kit (Thermo Fisher Scientific, Waltham, MA, USA) and 5' phosphorylated primers (Table S1).

For transient expression of AvrM14 *in planta*, T-DNA plasmids were generated using Gateway cloning. The constructs were initially cloned into the pENTR/D-TOPO entry vector and then into the pEarleyGate (pEG) destination vectors pEG102 or pEG104 (Earley et al., 2006). All constructs were cloned with 3' stop codons after the coding sequence, resulting in the expression of untagged (pEG102) or N-terminal YFP-tagged (pEG104) proteins *in planta*. The M1 sequence was cloned into the pTN35S plant expression vector (Dodds et al., 2004).

For recombinant protein production in *Escherichia coli*, the AvrM14-A, AvrM14-B, AvrM14-A^{E82Q} and AvrM14-B^{E82Q} sequences were cloned into the pMCSG7 vector using ligation-independent cloning (Stols et al., 2002). The resulting plasmids encoded an N-terminal hexahistidine (6×His) tag, followed by a tobacco etch virus protease cleavage site allowing 6×His tag removal. AvrM14 homologues from other *Melampsora* spp. were ordered as *E. coli* codon-optimised double-stranded DNA fragments without the predicted signal sequences from Integrated DNA Technologies Inc. (IDT®, Coralville, IA, USA). The DNA fragments were cloned into a modified pOPIN vector (Bentham et al., 2021), resulting in an N-terminal 6×His tagged construct with a 3C protease site in-between the 6×His tag and the coding sequence for each homologue. All protein sequences following purification and tag-cleavage are listed in Table S1.

Protein production

Recombinant HsNudt16 protein was purchased from Abcam (Cambridge, UK). All other proteins were expressed in *E. coli* BL21 (DE3) cells and purified using nickel metal affinity chromatography, followed by size-exclusion chromatography. For full details of protein production, see Methods S1.

Crystallisation and structure determination

Initial crystallisation screening with purified AvrM14-A and AvrM14-B monomeric proteins was conducted using a Mosquito robot (STP LabTech, Melbourn, UK) in a 96-well plate format using sparse matrix screens. The hanging drop vapour-diffusion method of crystallisation was used and drops consisting of 100 nl 10 mg ml⁻¹ protein solution and 100 nl reservoir solution were equilibrated against 100 µl reservoir solution. The final optimised condition for monomeric AvrM14-A (10 mg ml⁻¹) was 2.4 M sodium malonate pH 6.0 and 2% glycerol. For monomeric and homodimeric AvrM14-B, the condition utilised for crystallisation was 1.8 M (NH₄)₂SO₄, 100 mM sodium acetate (pH 4.33) and 100 mM MgCl₂.

Before X-ray data collection, AvrM14-A crystals were transferred to 2.4 M sodium malonate pH 6.0 and 10% glycerol, before flash-cooling in liquid nitrogen. To enable phasing, some AvrM14-A crystals were soaked in a solution of 2.4 M sodium malonate pH 6.0, 10% glycerol and 1 M NaBr. AvrM14-B

crystals were transferred to the same condition used for crystallisation supplemented with 20% glycerol, before flash-cooling in liquid nitrogen.

Single-wavelength anomalous diffraction (SAD) and native datasets were collected on the MX1 and MX2 beamlines at the Australian Synchrotron (Table S2; Cowieson *et al.*, 2015; Aragão *et al.*, 2018). The datasets were processed in XDS (Kabsch, 2010) and scaled using AIMLESS in the CCP4 suite (Evans & Murshudov, 2013). For SAD phasing of AvrM14-A, the CRANK2 pipeline (Skubák & Pannu, 2013) was used in the CCP4 suite. The best chain from the autobuilt model was then used as a search model to solve the structure of a native dataset using maximum-likelihood molecular replacement (MR) with Phaser in Phenix (Liebschner *et al.*, 2019).

The crystal structure of monomeric and homodimeric AvrM14-B was determined using maximum-likelihood MR with Phaser in Phenix (Liebschner *et al.*, 2019). The MR search model was chain A of the AvrM14-A crystal structure. For all native datasets, automated model building and initial refinement were completed using either Phenix AutoBuild (Terwilliger *et al.*, 2008) or ARP/wARP (Langer *et al.*, 2008). Subsequent model building was carried out manually in Coot (Casañal *et al.*, 2020) in-between rounds of automated refinement using Phenix refine (Afonine *et al.*, 2012). MolProbity was used for validation of the final models (Williams *et al.*, 2018). Analysis of the final structures was performed with Coot (Casañal *et al.*, 2020), PyMOL, APBS (Jurrus *et al.*, 2018) and ESPRIPT v.3.0 (Robert & Gouet, 2014).

Map coordinates and structure files have been deposited in the Protein Data Bank (AvrM14-A Monomer: 8DP8, AvrM14-B Monomer: 8DP9, AvrM14-B Homodimer: 8DPA).

Nudix hydrolase substrate screening assays

To assess phosphohydrolase activity against ADPR, NADH, Ap₄A, FAD and NAD⁺, 6 μM of recombinant protein was incubated with 2 mM substrate in a reaction buffer containing 50 mM Tris-HCl pH 8.5, 5 mM MgCl₂, 1 mM DTT and 40 U ml⁻¹ of alkaline phosphatase at 37°C for 30 min. To detect inorganic phosphate produced from the reactions, a phosphomolybdate method was used (Ames, 1966). Sulphuric acid was added to a final concentration of 500 mM; ammonium molybdate was added to a final concentration of 2 mM and ascorbic acid to a final concentration of 60 mM; the solution was then incubated at 45°C for 10 min, and the absorbance at 820 nm was recorded.

A kinetic screening method with a phosphate sensing fluorophore (Nguyen *et al.*, 2016) was used to measure phosphohydrolase activity against 69 unique nucleoside diphosphates (substrates and their groups are listed in Table S3). In short, the standard reaction contained 10 mM Tris-HCl pH 7.6, 1 mM MgCl₂, 5 μM phosphate sensor (Thermo Fisher Scientific), 0.05 U ml⁻¹ of yeast pyrophosphatase (PPase) when pyrophosphate was a predicted product or 1 U ml⁻¹ of alkaline phosphatase (APase) when a nucleoside monophosphate was a predicted product. Each substrate concentration was 5 μM in both grouped and ungrouped reactions. AvrM14-A recombinant protein concentration was 50 nM. The

mixtures were incubated at 37°C and monitored continuously for 30 min on a Tecan GENios Microplate Reader with the following parameters: λ-excitation = 425 nm, λ-emission = 465 nm, gain 60, 100 cycles, 37°C.

The subsequent kinetic screen to assess AvrM14-A, AvrM14-B, AvrM14-A^{E82Q} and AvrM14-B^{E82Q} hydrolase activity against ^{m7}Gp₅G (Jena Bioscience, Jena, Germany) was completed as above, with some modifications to optimise activity. The reaction mixture contained 10 mM Tris-HCl (pH 7.6), 2 mM MnCl₂, 1 U ml⁻¹ alkaline phosphatase, 5 μM ^{m7}Gp₅G, 2.5 μM phosphate sensor (Thermo Fisher Scientific) and 100 nM purified recombinant protein in a total volume of 100 μl. Fluorescence measurements (excitation at 425 nm and emission at 465 nm) were recorded every 10 s for 30 min using a Tecan Infinite® M1000 (Tecan, Männedorf, Switzerland) plate reader at room temperature.

RNA synthesis, purification, capping and decapping

A 231-nt synthetic RNA sequence (sequence in Table S1) was synthesised using the HiScribe™ T7 High Yield RNA Synthesis Kit (NEB, Ipswich, MA, USA) following the recommended protocol. The RNA was purified using RNAClean XP beads (Beckman Coulter, Brea, CA, USA). Purified RNA was capped using the Vaccinia Capping System (NEB) with GTP spiked with (α-³²P)-GTP (PerkinElmer, Waltham, MA, USA). To purify the capped RNA, the Monarch® RNA Cleanup Kit (NEB) was used, and two purifications were completed per capping reaction to ensure near-complete removal of (α-³²P)-GTP.

RNA-decapping assays were completed as described previously, with some minor modifications (Song *et al.*, 2013). In brief, 2 μM recombinant protein was incubated with capped RNA in a reaction buffer with 10 mM HEPES (pH 7.5), 150 mM NaCl, 2 mM MnCl₂, 1 mM DTT and 40 U ml⁻¹ RNase Inhibitor (Merck, Rahway, NJ, USA) for 30 min at 37°C. The reaction products were separated using PEI-cellulose TLC plates (Merck) with 0.45 M (NH₄)₂SO₄ as the liquid phase. Dried plates were placed into a cassette with a K-screen (Bio-Rad) and left for 14–18 h before imaging using a PharosFX™ scanner (Bio-Rad). To identify the reaction products, known standards of ^{m7}GMP (Jena Bioscience), ^{m7}GDP (Jena Bioscience), GMP (Merck) and GDP (Merck) were separated using the same TLC conditions and imaged using UV shadowing.

Plant materials and growth conditions

Nicotiana benthamiana and *N. tabacum* L. plants were grown in soil in a controlled environment at 25°C with a 16-h day length. Flax (*Linum usitatissimum* L.) plants were grown in soil in glasshouses with natural light at a constant temperature of 24°C. Infiltration experiments were completed on 4–5-wk-old *N. benthamiana*, c. 7-wk-old *N. tabacum* and c. 3-wk-old *L. usitatissimum*.

Agroinfiltrations

Agroinfiltrations were completed as described previously (Catanarziti *et al.*, 2015). In brief, *Agrobacterium* strain GV3101

(pMP90) containing the pEG102, pEG104 or pTN35S DNA constructs (see 'Cloning' in the Materials and Methods section) were suspended in infiltration buffer (10 mM MES pH 5.6, 10 mM MgCl₂ and 200 μM acetosyringone) to a final optical density at 600 nm of 1.0. All cultures were incubated in the dark at room temperature for 2 h before syringe-infiltration into either *N. benthamiana*, *N. tabacum* or *L. usitatissimum* leaves. Infiltrated plants were kept in the same growing conditions as before infiltration.

ROS burst assays

Measurement of ROS was completed as described previously with some minor modifications (Heese *et al.*, 2007). In brief, *N. benthamiana* leaf discs (4 mm diameter) were floated on water overnight in a 96-well plate. The water was replaced with an elicitor solution (100 μM luminol, 10 μg ml⁻¹ horseradish peroxidase and 100 nM flg-22 or 5 μg ml⁻¹ chitin), and luminescence was measured over time using a Tecan Infinite® M1000 Pro (Tecan) plate reader at room temperature.

Immunoblot analysis

Rabbit polyclonal antibodies against recombinant AvrM14-A protein were produced and affinity purified by the Walter & Eliza Hall Institute of Medical Research (WEHI, Melbourne, Vic., Australia). Protein extraction from plant tissue for Western blotting was performed as described previously (108). Blots were probed with either rabbit anti-AvrM14 (pEG102 constructs) or mouse anti-GFP (pEG104 constructs; Roche) and detected by goat anti-rabbit-HRP (Merck) or goat anti-mouse-HRP (Cytiva, Marlborough, MA, USA). Clarity™ Western ECL substrate (Bio-Rad) was added to the immunoblots and chemiluminescence detected using a ChemiDoc imager (Bio-Rad).

SEC-MALS analysis

SEC-MALS was performed as described previously (Casey *et al.*, 2016). In brief, the purified protein samples were loaded onto a Superdex 75 Increase 10/300 size-exclusion column (Cytiva) pre-equilibrated in buffer (10 mM HEPES pH 7.5, 150 mM NaCl), connected to a Dawn Heleos II 18-angle light-scattering detector and an Optilab rEX refractive index detector (Wyatt Technology, Santa Barbara, CA, USA). The molecular masses of the proteins were calculated using ASTRA 6.1 software (Wyatt Technology).

RNA extractions, sequencing and analysis

Twenty flax leaves from a single plant (per replicate, with a total of four replicates for both the AvrM14-A and AvrM14-A^{E82Q} treatments and three replicates for the vector-only treatment) were collected 3 d post-infiltration with either the pEG102 AvrM14-A, pEG102 AvrM14-A^{E82Q} or empty vector (pEG102) GV3101 *Agrobacterium* constructs. Each replicate (20 leaves) was placed into a plastic tube with stainless steel beads and frozen in

liquid nitrogen. Plant tissue was lysed using the TissueLyser II (Qiagen). TRIzol™ reagent and the PureLink™ RNA Mini Kit (Thermo Fisher Scientific) were used for RNA purification from the lysed sample following the manufacturer's protocol.

Whole transcriptome RNA sequencing was conducted by Novogene (Beijing, China) using the Ribo-Zero Magnetic Kit (Illumina, San Diego, CA, USA) for rRNA depletion, random hexamers for cDNA synthesis, the NEBNext® Ultra™ Directional RNA Library Prep Kit (NEB) for library preparation and the Illumina Novaseq 6000 platform for sequencing. Raw sequencing data is available from the NCBI (GEO: GSE207874, SRA: SRX16112399, SRX16112400, SRX16112401, SRX16112402, SRX16112403, SRX16112404, SRX16112405, SRX16112406, SRX16112384, SRX16112385 and SRX16112386). For full details of RNA-Seq data analysis, see Methods S1.

Results

AvrM14 is an active Nudix hydrolase capable of interfering with plant immune responses

The AvrM14 effector from flax rust contains 146 amino acids as a mature protein that includes a Nudix-box consensus sequence (Anderson *et al.*, 2016). Two allelic variants of AvrM14 have been identified (AvrM14-A and AvrM14-B). AvrM14-A is recognised by flax R-proteins M1 and M4, while AvrM14-B possesses six amino acid polymorphisms and has escaped recognition (Anderson *et al.*, 2016). To understand the virulence function(s) of AvrM14 and how the AvrM14-B effector escapes recognition by M1 and M4, we determined the crystal structures of AvrM14-A and AvrM14-B at a resolution of 2.3 and 1.8 Å, respectively (see Table S2 for data collection and refinement statistics; the higher-resolution structure of AvrM14-B will be used for structure analyses unless indicated otherwise). The structures revealed that AvrM14 proteins display a characteristic Nudix-fold architecture, consisting of a β-grasp fold surrounding an α-helix (Fig. 1a; Lin *et al.*, 1997; Gabelli *et al.*, 2001). In typical Nudix hydrolases, the Nudix box folds into a loop-α-helix-loop structure, but for AvrM14, a 3₁₀-helix is present before the α-helix (Figs 1a, S1a). The 3₁₀-helix appears to compensate for the double amino acid insertion in the AvrM14 Nudix box (Anderson *et al.*, 2016), allowing the protein to maintain a salt bridge between a conserved Nudix-box glutamate (E71) and arginine (R81) found in canonical Nudix hydrolase structures (Fig. S1a; Gabelli *et al.*, 2001; Xu *et al.*, 2004). Nudix hydrolases require divalent metal ions for catalysis (Mildvan *et al.*, 2005; McLennan, 2006). While Mg²⁺ cations were included in our crystallisation solution for AvrM14-B, we did not observe clear density to suggest metal ion binding in the structures. Despite this, two of the three Nudix-box glutamate residues typically required for divalent metal binding (E85 and E86) are positioned in a similar location to previously determined metal-bound Nudix hydrolase structures (Fig. S1c; Gabelli *et al.*, 2002). The third Nudix-box glutamate, also often implicated in metal binding (E82), has dual conformations in our crystal structures. In one conformation, the side chain is buried under a β-sheet, whereas in the other, it is solvent-exposed (Fig. S1c). Based on previously determined metal-bound

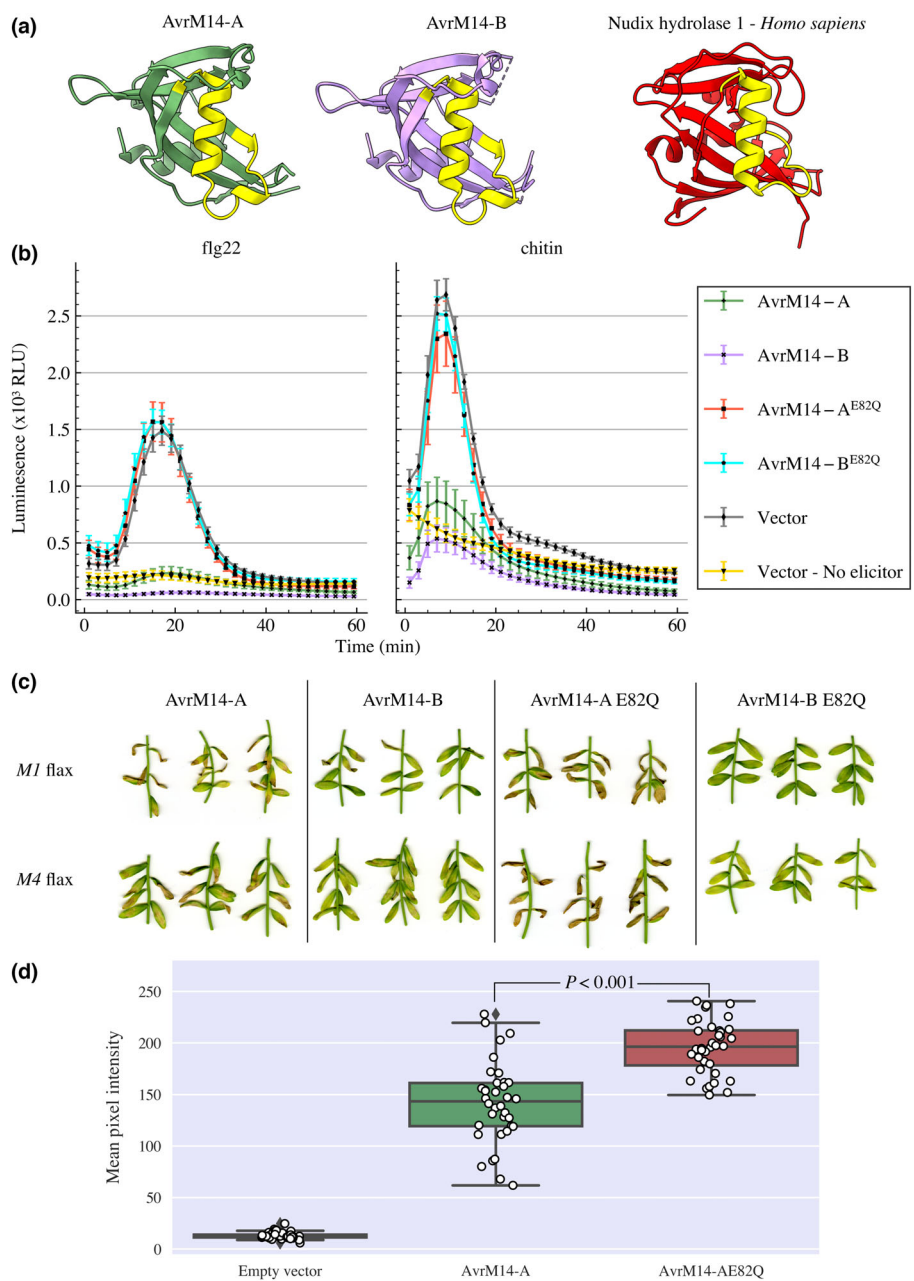


Fig. 1 Enzymatic activity of AvrM14, a Nudix hydrolase, suppresses reactive oxygen species (ROS) production, triggered by flg22 or chitin, and the hypersensitive response, triggered by the M1 resistance protein. (a) Ribbon diagrams of the AvrM14-A and AvrM14-B crystal structures, (PDB ID: 8DP8 and 8DP9) showing they adopt a Nudix fold. The Nudix-box region that typically folds into a loop-α-helix-loop is coloured yellow. For comparison to a prototypical Nudix hydrolase, the structure of Nudix hydrolase 1 (MTH1) from *Homo sapiens* is shown on the right (PDB ID: 5GHI) in analogous orientation (Waz et al., 2017). (b) *Nicotiana benthamiana* leaves were infiltrated with *Agrobacterium* (GV3101) harbouring either an empty vector (pEG104) or pEG104 constructs encoding AvrM14-A, AvrM14-B, AvrM14-AE82Q or AvrM14-BE82Q proteins with YFP N-terminal tags expressed under the 35 S promoter from the cauliflower mosaic virus. At 4 d post-infiltration (dpi), leaf tissue was exposed to 100 nM flg-22 or 1 µg ml⁻¹ chitin (except in the no-elicitor treatment) and ROS production was recorded as relative luminescence units over time. Results are means ± SEs (n = 12). (c) Bison × M1 (Williston Brown) or M4 (Victory 'A') flax lines were agroinfiltrated to transiently express either wild-type or mutant AvrM14 proteins (AvrM14-A, AvrM14-B, AvrM14-AE82Q and AvrM14-BE82Q). Multiple leaves from three independent plants were infiltrated with each construct. The agroinfiltrated leaves were photographed 7 dpi. (d) Bison × M1 (Williston Brown) flax leaves were agroinfiltrated with an empty vector or with constructs to transiently express either wild-type or mutant AvrM14-A proteins (AvrM14-A and AvrM14-AE82Q). At 6 dpi, all infiltrated leaves were collected and the cell-death response for each leaf was assessed by pixel intensity analysis using IMAGEJ after imaging the leaves with a Chemidoc MP imager. There were 36 replicates for each treatment, as indicated by the white dots on top overlaying the boxplots. In the boxplots the horizontal line in the middle of the box represents the median value, the box represents the interquartile range (IQR), the whiskers extend to 1.5 × IQR, and the grey diamonds indicate outlying values (defined as <Q1 - 1.5 × IQR or >Q3 + 1.5 × IQR). To determine whether there was a significant difference between the AvrM14-A and AvrM14-AE82Q treatments, an unpaired t-test was completed and the two-tailed P-value is displayed.

Nudix hydrolase structures, we propose that metal ion binding would lock E82 in the solvent-exposed conformation (Gabelli *et al.*, 2002). Overall, the Nudix fold and positioning of the putative metal-binding glutamates suggest that the AvrM14 effectors are enzymatically active Nudix hydrolases.

The RipN and Avr3b effectors both interfere with plant immunity in a Nudix-box-dependent manner, when expressed in *A. thaliana* and *N. benthamiana*, respectively (Dong *et al.*, 2011; Sun *et al.*, 2019). To determine whether AvrM14 can use Nudix hydrolase activity to interfere with plant immunity, we used *Agrobacterium*-mediated transformation in *N. benthamiana* to transiently express AvrM14-A, AvrM14-B, and both proteins with glutamate 82 mutated to glutamine (AvrM14-A^{E82Q} and AvrM14-B^{E82Q}) as YFP fusions and assessed their effect on plant immune responses. Numerous studies have demonstrated this equivalent mutation drastically reduces the catalytic activity of Nudix hydrolases, without altering protein structure or stability (Lin *et al.*, 1996; Perraud *et al.*, 2003; Mildvan *et al.*, 2005; Parrish *et al.*, 2007; Gunawardana *et al.*, 2008; Höfer *et al.*, 2016). Our results demonstrate that the expression of AvrM14-A and AvrM14-B, but not the E82Q mutants, inhibits the production of ROS, following exposure of *N. benthamiana* leaf tissue to either flg-22 or chitin (Fig. 1b). Both AvrM14 and E82Q mutant proteins were expressed and accumulate to similar levels in agroinfiltrated plant tissue (Fig. S2).

As both AvrM14-A and AvrM14-B suppress ROS production, and AvrM14-B is not recognised by the flax M1 and M4 R-proteins, we hypothesised that hydrolase activity would not be required for the recognition of AvrM14-A by M1 and M4. In support of this hypothesis, transient expression of AvrM14-A and AvrM14-A^{E82Q}, but not AvrM14-B or AvrM14-B^{E82Q}, triggered cell-death responses in near-isogenic lines of the flax variety Bison containing either *M1* (*M1* flax) or *M4* (*M4* flax) (Fig. 1c). *M1* and *M4* were introgressed into the Bison genetic background by 12 backcrosses, see Islam & Mayo (1990).

Analogous results were observed in tobacco when the effector was transiently co-expressing with *M1* (Fig. S3). Interestingly, AvrM14-A^{E82Q} expression appeared to result in a stronger cell-death response when compared to the wild-type protein in both *M1* and *M4* flax (Fig. 1c). We confirmed this result by expressing AvrM14-A and AvrM14-A^{E82Q} in a total of 36 *M1* flax leaves per treatment and the HR cell-death response was assessed by determining the mean signal intensity of each infiltrated area following green-light imaging of the leaves (Fig. 1d). The results demonstrate that AvrM14-A^{E82Q} expression results in a greater cell-death response than AvrM14-A (Fig. 1d). Our results indicate that while the integrity of the Nudix box is dispensable for M1 and M4 detection, the AvrM14-A E82Q mutation does influence the severity of the M1 activated immune response. Collectively, these data suggest that AvrM14 can suppress both PTI and ETI pathways, via an unknown Nudix hydrolase activity.

RNA cap analogues and capped RNA transcripts are selectively hydrolysed by AvrM14

To determine the compound(s) hydrolysed by AvrM14, we conducted a comprehensive substrate search, utilising a sensitive

fluorometric assay (Xu *et al.*, 2013), which tested AvrM14-A protein against 69 unique nucleoside diphosphate compounds (listed in Table S3). AvrM14-A only exhibited hydrolysis activity with a single substrate, ^{m7}Gp₅G (P1-(5'-7-methyl-guanosyl)-P5-(5'-guanosyl)-pentaphosphate). AvrM14-A did not hydrolyse diguanosine pentaphosphate (Gp₅G), indicating a preference for the methyl group.

To determine whether substrate hydrolysis was dependent on the Nudix box present in AvrM14-A and conserved in AvrM14-B, we assessed the hydrolytic activity of recombinant AvrM14-A, AvrM14-B, AvrM14-A^{E82Q} and AvrM14-B^{E82Q} against ^{m7}Gp₅G and monitored fluorescence over time (Fig. 2a). AvrM14-A and AvrM14-B hydrolysed ^{m7}Gp₅G, whereas the catalytic site mutants did not (Fig. 2a). ^{m7}Gp₅G is not found in nature; however, 7-methyl guanosine (^{m7}G) is a unique molecular structure present on the 5' cap of eukaryotic RNA transcribed by RNA polymerase II (Müller-McNicoll & Neugebauer, 2014); ^{m7}Gp₅G is used as an mRNA cap analogue in assays. Therefore, the results from the substrate screening experiments suggest that AvrM14 may function as an mRNA-decapping enzyme.

To determine whether the AvrM14 proteins hydrolyse ^{m7}G-capped RNA, we conducted a radiolabelled assay utilising a known decapping enzyme, *Homo sapiens* Nudt16 (HsNudt16) (Song *et al.*, 2010; Li *et al.*, 2011), as a positive control. AvrM14-A and AvrM14-B both efficiently decapped the labelled mRNA substrate, whereas the active site mutants (AvrM14-A^{E82Q} and AvrM14-B^{E82Q}) did not (Fig. 2b). These data demonstrate that AvrM14 is an active Nudix hydrolase with specificity for capped mRNA *in vitro*.

AvrM14 homodimerisation via domain swapping optimises RNA decapping

The AvrM14-A and AvrM14-B crystal structures display a common crystal packing interface despite different crystallisation conditions and crystallographic space groups (Table S2; Fig. S4c). Interestingly, the position of the interface, with respect to the Nudix-box helix, is similar to previously identified homodimeric RNA-decapping enzymes HsNudt16 and X29 (a Nudt16 ortholog from *Xenopus laevis*; Scarsdale *et al.*, 2006; Trésaugues *et al.*, 2015; Fig. S5). We aimed to determine whether homodimerisation of AvrM14 is important for mRNA decapping. Based on SEC (size-exclusion chromatography) chromatograms, we show that both recombinant AvrM14-A and AvrM14-B proteins exist in two stable and distinct oligomeric states that can be purified to near homogeneity (Fig. S4a,b). To determine the molecular mass of each oligomeric state more accurately, we utilised SEC coupled to a multi-angle light-scattering detector (SEC-MALS; Fig. 3). Our SEC-MALS data demonstrate that, in solution, recombinant AvrM14-B forms stable monomers and homodimers, which can be readily separated and purified (Fig. 3a).

The initial crystallisation and activity assays reported above were completed with monomeric AvrM14 proteins, which are the predominant forms after purification from *E. coli* (Fig. S4a). The fact that previous research indicates that HsNudt16 and X29 Nudix hydrolase mRNA-decapping enzymes act as homodimers,

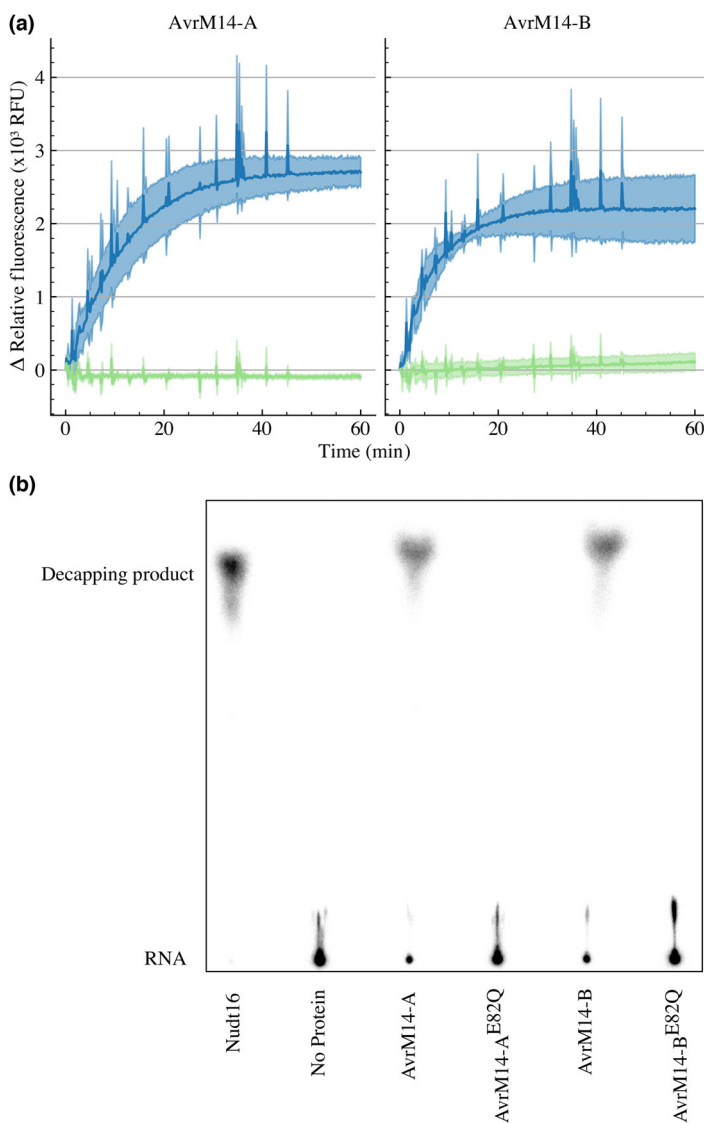


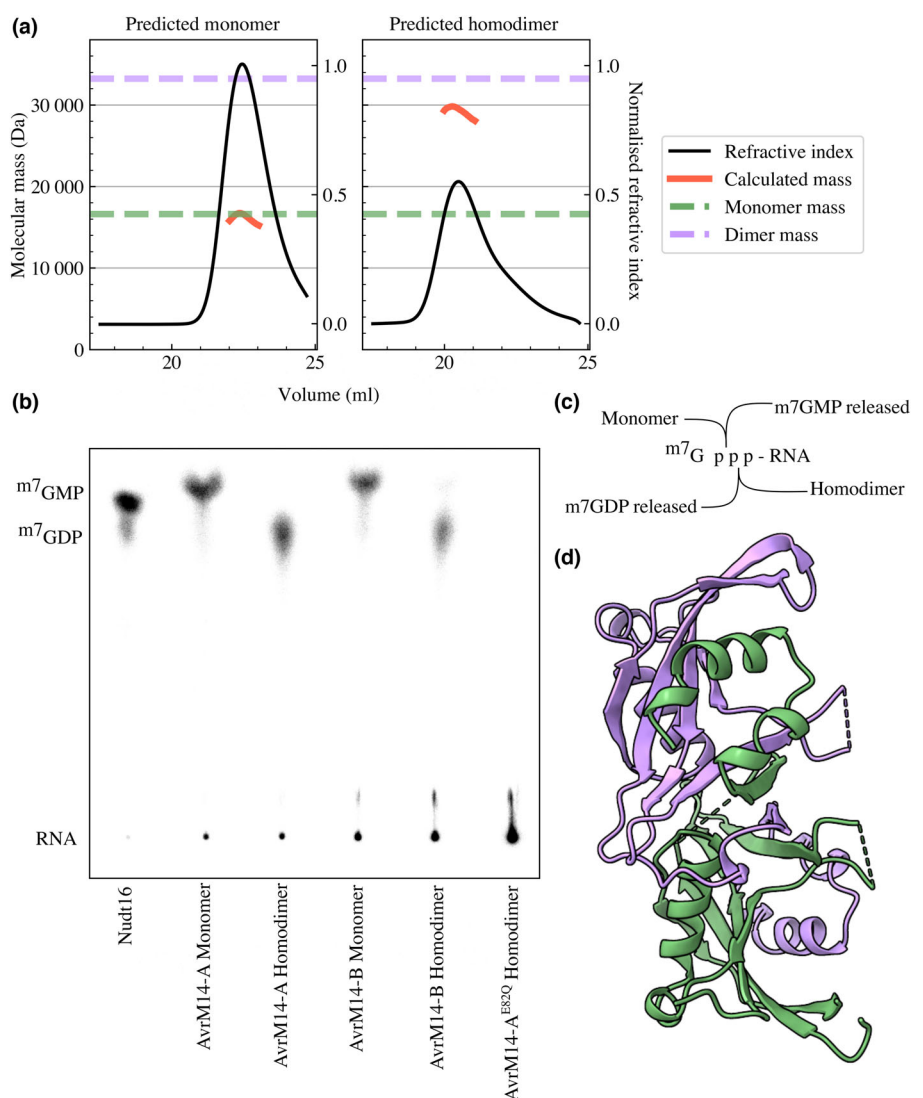
Fig. 2 AvrM14-A and AvrM14-B hydrolyse RNA cap analogues and capped mRNA *in vitro*. (a) Recombinant AvrM14-A (left) and AvrM14-B (right) (data in blue) and the corresponding mutant AvrM14^{E82Q} proteins (green) were incubated with the mRNA cap analogue m^7Gp_5G . Hydrolysis activity was measured over 60 min using a phosphate-binding fluorophore. Results are means (solid line) \pm SDs (shaded area), where $n = 3$. (b) Recombinant proteins (HsNudt16, AvrM14-A, AvrM14-A^{E82Q}, AvrM14-B and AvrM14-B^{E82Q}) were incubated with $m^7Gp^{32}pp$ -RNA and the reaction products analysed by thin-layer chromatography (TLC). Capped RNA remains at the origin of the TLC plate, whereas decapping products (m^7GDP and/or m^7GMP) migrate up the plate.

prompted us to further characterise the homodimeric form of AvrM14. To determine whether homodimerisation alters substrate specificity, we performed substrate screening with five common Nudix hydrolase substrates (Fig. S6). Consistent with the monomeric forms of the protein, homodimeric AvrM14-A and AvrM14-B did not hydrolyse any of the substrates tested (Fig. S6). To determine whether homodimeric AvrM14 proteins could decap RNA, we performed activity assays with m^7G -capped RNA. Both AvrM14-A and -B homodimers hydrolysed capped RNA efficiently, whereas homodimeric AvrM14-A^{E82Q} did not (Fig. 3b). Intriguingly, the product produced by the homodimers migrated to a lower position following separation by thin-layer chromatography (TLC), compared with the product released by the monomers (Fig. 3b). To identify the products released by the mRNA-decapping proteins, we measured the migration of m^7GMP , m^7GDP , GMP and GDP standards using UV shadowing under our TLC conditions (Fig. S7). The Rf values recorded for the m^7GMP , m^7GDP , GMP and GDP standards were used to place the labels on Figs 3(b) and 4(d). Our data indicate that the

major product released by homodimeric AvrM14 is m^7GDP , whereas the major product released by monomeric protein is m^7GMP . Thus, mRNA decapping by homodimeric AvrM14 generates 5'-monophosphate RNA (p-RNA), whereas monomeric AvrM14 generates 5'-diphosphate RNA (pp-RNA) (Fig. 3c). To promote mRNA decay, decapping enzymes are hypothesised to release p-RNA *in vivo*, that can be degraded by 5'-3' exoribonucleases, whereas pp-RNA is resistant to exoribonuclease degradation (Fujimura & Esteban, 2010; Schoenberg & Maquat, 2012; Grudzien-Nogalska & Kiledjian, 2017). Our *in vitro* results therefore suggest that to promote host mRNA decay, AvrM14 would function as a homodimer.

To understand how the AvrM14 proteins homodimerise, we sought to determine the crystal structure of homodimeric AvrM14-B. To ensure any differences observed in the structure were independent of the crystallisation process, we crystallised homodimeric AvrM14-B in identical conditions to monomeric AvrM14-B. The crystal structure demonstrates that homodimerisation is mediated by domain swapping (Fig. 3d). The

Fig. 3 Homodimerisation of AvrM14 is mediated by domain swapping, which alters RNA cap-cleavage location, compared with the monomer. (a) Size-exclusion chromatography coupled with multi-angle light scattering (SEC-MALS) was used to determine the molecular mass of the different oligomeric forms of AvrM14-B in solution. For all plots, the black lines refer to the right y-axis and indicate the protein elution traces (normalised refractive index) for proteins eluted from the Superdex S75 10/300 increase column. The red bands correspond to the average molecular-mass distribution across the refractive index peak, all molecular masses refer to the left y-axis. The green and purple dashed lines indicate the theoretical molecular mass of monomeric (16.6 kDa) and homodimeric (33.2 kDa) AvrM14 protein, respectively. (b) The separate monomeric and homodimeric forms of AvrM14-A and AvrM14-B were incubated with $m^7Gp^{32}pp$ -RNA and the reaction products were separated using thin-layer chromatography. *HsNudt16* was included as a positive control. The predicted identity of each ^{32}P -labelled compound is indicated on the left, based on the Rf value determined for standard solutions of m^7GMP and m^7GDP . (c) The pyrophosphate bond predominantly hydrolysed by monomeric and homodimeric AvrM14 proteins based on the RNA cap-cleavage assay results. (d) Ribbon model of the crystal structure of homodimeric AvrM14-B (PDB ID: 8DPA), showing C-terminal domain swapping. Chain A is coloured green and chain B purple.

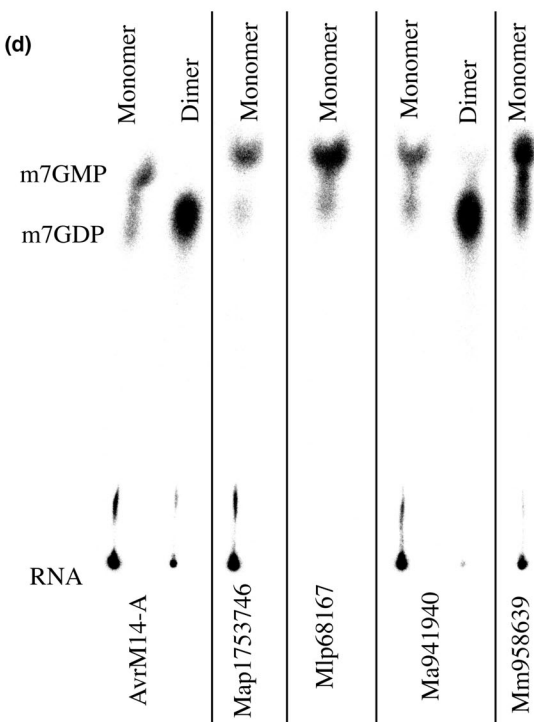
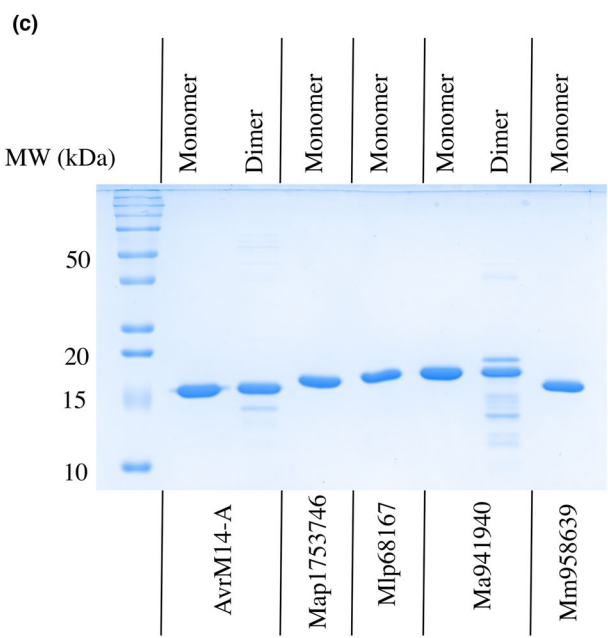
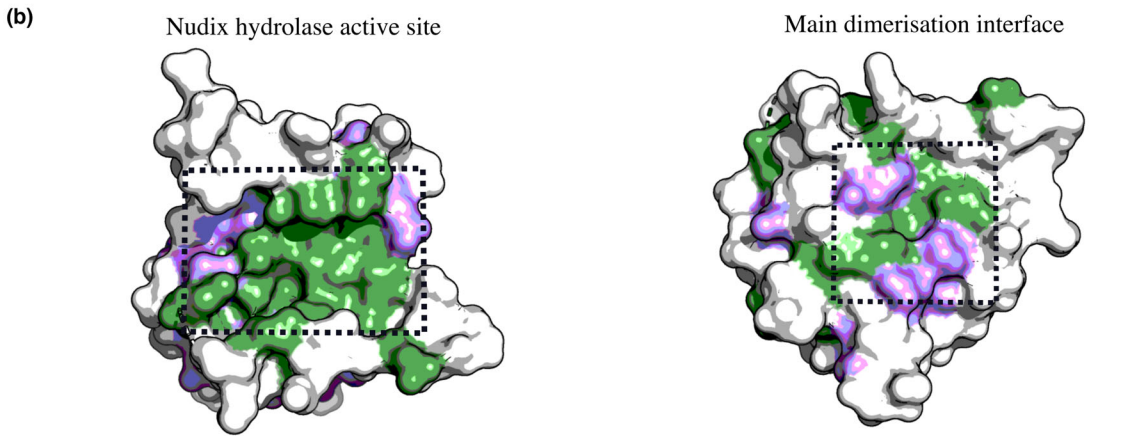
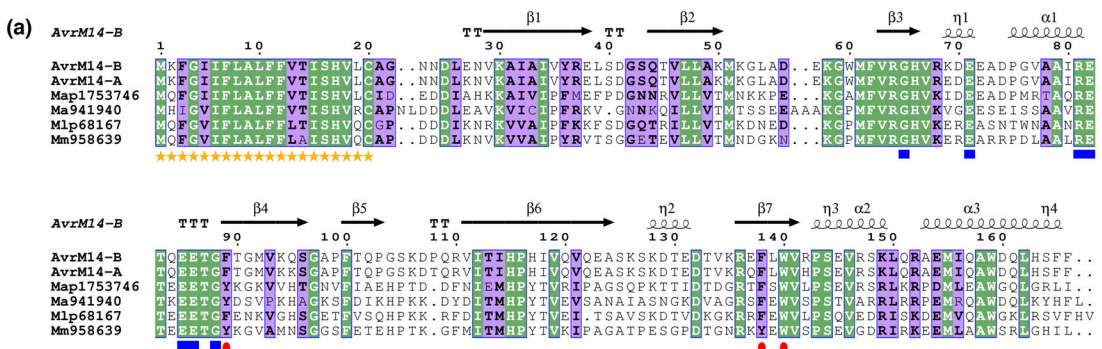


C-terminal regions (residues 124 to 166) from each of the monomeric proteins swap positions to form an intertwined homodimer (Fig. 3d). Domain-swapped homodimeric structures have been reported previously for ADPR-specific Nudix hydrolases (Gabelli *et al.*, 2001; Kang *et al.*, 2003; Yoshioka *et al.*, 2004; Zha *et al.*, 2006; Wakamatsu *et al.*, 2008; Tang *et al.*, 2015). However, the position of each monomeric subunit in the AvrM14 structure differs substantially from the previously reported domain-swapped Nudix hydrolases. The overall positioning of each monomeric subunit and the corresponding dimerisation interface are almost identical to the crystal packing observed in the asymmetric units of monomeric AvrM14-A and AvrM14-B and therefore are similar to the *HsNudt16/X29* homodimers (Figs 3d, S4c, S5). Buried in the main interface between the two monomeric subunits is an aromatic core composed of F⁸⁹, F¹³⁸ and W¹⁴⁰ from both monomers, which we hypothesise promote self-association (Fig. S4c). We attempted to mutate these amino acids to prevent homodimerisation for further experiments; however, the mutant proteins were not stable when expressed in *E. coli*.

To investigate whether stable dimeric forms of AvrM14 are produced *in planta*, we performed native protein extractions from *N. benthamiana* tissue expressing untagged AvrM14 protein. We separated these proteins using SEC, followed by western blot analysis with specific polyclonal antibodies raised against AvrM14 protein (Fig. S8). Using this approach, we observed AvrM14 protein elution from SEC at a volume consistent with monomeric forms of the protein. These data suggest that AvrM14 does not form stable dimers *in planta*, mediated by the domain-swapping mechanism observed in *E. coli*. However, these results do not preclude the potential for AvrM14 to function as a homodimer via transient association with other proteins that cannot be detected using these methods.

RNA-decapping activity is conserved in Nudix effectors from other pathogenic *Melampsora* spp.

We next wanted to determine whether other plant pathogens secrete similar Nudix hydrolase effectors with RNA-decapping activity. BLAST searches with JGI and NCBI databases yielded



proteins homologous to AvrM14 from all genome-sequenced *Melampsora* species. Their sequence identity to the AvrM14 proteins is c. 50%, with all sequences demonstrating conservation of the signal peptide, Nudix box and residues involved in the

dimerisation interface (Fig. 4a). Mapping the sequence conservation onto the structure of monomeric AvrM14-B demonstrates extremely high conservation around the Nudix hydrolase active site, suggesting that the homologues are active Nudix hydrolases

Fig. 4 Predicted effectors homologous to AvrM14 from multiple *Melampsora* species decap RNA *in vitro*. (a) Sequence alignment (produced using ESPRIPT 3.0) of AvrM14 variants and homologous proteins from other *Melampsora* species (Robert & Gouet, 2014). Each sequence is labelled with the relevant unique protein ID from the JGI database and the first letter of their genus and species name (Mm for *Melampsora medusae*, Mlp for *Melampsora larcini-populina*, Map for *Melampsora allii-populina*, and Ma for *Melampsora americana*). Residues with 100% conservation are coloured green, residues with conserved substitutions are coloured purple, white are nonconserved residues, the predicted signal peptide region is indicated by orange stars, the aromatic residues in the AvrM14 dimeric interface are indicated by red dots, and the conserved Nudix box residues are indicated by blue squares. Above the sequence alignment is the secondary structure of AvrM14-B (black arrows indicating β -strands, squiggles indicating helices, and the TT and TTT symbols indicating β -turns and α -turns respectively). (b) The structure of monomeric AvrM14-B, demonstrating the surface regions with the highest conservation across the homologues. Residue colouring is the same as in the sequence alignment. The Nudix hydrolase active site and the major interface involved in dimerisation are indicated. (c) Coomassie-stained SDS-PAGE analysis demonstrating the purity of each protein used in the RNA-decapping assays. (d) Recombinant AvrM14-A and the homologous proteins were incubated with m7 Gp 32 pp-RNA and the reaction products were separated using thin-layer chromatography. The oligomeric state of each protein, as predicted by size-exclusion chromatography, is indicated along the top. The predicted identity of each 32 P labelled compound is indicated on the left, based on the Rf value determined for standard solutions of m7 GMP and m7 GDP. A middle lane not relevant to the analysis has been removed from the image.

featuring similar substrate specificity (Fig. 4b). The surface involved in dimerisation is also highly conserved (Fig. 4b). No Nudix hydrolases with similarity to AvrM14 were identified outside of the genus *Melampsora*.

The predicted AvrM14 homologues from *Melampsora americana*, *Melampsora medusae*, *Melampsora allii-populina* and *Melampsora larici-populina* were selected for biochemical analysis (sequences in Table S1). Size-exclusion chromatography indicated that all homologues were predominantly in a monomeric state, following purification from *E. coli* (Fig. S9). All monomeric proteins could be purified to near homogeneity and decapped mRNA *in vitro* (Fig. 5). The assay results demonstrate that RNA-decapping activity has been conserved throughout the evolution of this gene family in *Melampsora* spp. The AvrM14 homologues from all species, except *M. medusae*, also showed a SEC absorbance peak at a position consistent with a homodimeric protein (Fig. S9). However, low yields of the putative homodimeric proteins meant that only one (the homologue from *M. americana*) could be purified (Fig. 4c). Analogous to homodimeric AvrM14 from *M. lini*, the homologous *M. americana* homodimer released predominantly m7 GDP from capped RNA *in vitro*, whereas the monomeric protein released predominantly m7 GMP (Fig. 4d).

AvrM14 expression in flax promotes the expression of genes involved in growth and metabolic processes while inhibiting aspects of plant immunity

To better characterise how the AvrM14 effector impacts host plant physiology, we transiently expressed AvrM14-A in flax leaves and conducted transcriptome-wide RNA-sequencing (RNA-Seq) analysis. The RNA was extracted from leaves recently infiltrated with *Agrobacterium*, to enable AvrM14 expression. Therefore, our data are representative of the changes induced by AvrM14 following the activation of plant immune responses by *Agrobacterium* exposure. Our differential expression (DE) analysis identified 488 and 312 significantly (q value <0.05) more abundant ($\log_2\text{fc} > 0.5$) and less abundant ($\log_2\text{fc} < -0.5$) transcripts, respectively, in leaves agroinfiltrated with *AvrM14-A*, compared with the vector-only control (Table S4). Gene Ontology (GO) enrichment analysis indicates that AvrM14 expression promotes the expression of genes involved in carbon fixation, photosynthetic reactions and various metabolic processes (Fig. 5a), and suppresses the expression of genes involved in cell-

recognition, hypoxia, salt and biotic stress responses (Fig. 5a). To identify which changes are due to the enzymatic activity of AvrM14, we also conducted RNA-Seq on flax leaves expressing *AvrM14-A^{E82Q}* and compared the *AvrM14-A* and *AvrM14-A^{E82Q}* datasets. Both *AvrM14-A* and *AvrM14-A^{E82Q}* were expressed at similar levels (Fig. S10). The DE analysis indicates that many of the differences between the *AvrM14-A* and vector-only datasets are unrelated to enzymatic activity, with only 90 significantly more abundant and 36 significantly less abundant transcripts in leaves agroinfiltrated with *AvrM14-A*, compared with *AvrM14-A^{E82Q}* (Table S5). There is multiple significantly less abundant transcripts homologous to pseudo-response regulator 5 (APRR5) from *A. thaliana* (Fig. 5b). Consistent with changes to APRR5 levels, there is an overrepresentation of transcripts homologous to *A. thaliana* APRR5 targets (Nakamichi *et al.*, 2012) in the significantly less abundant transcripts (Fig. 5c). APRR5 is an important regulator of *A. thaliana* circadian rhythm (Nakamichi *et al.*, 2005; Rawat *et al.*, 2011); our results therefore suggest that the enzymatic activity of AvrM14 effectors could impact circadian rhythm processes.

Surface-exposed residues required for M1 and M4 recognition

In addition to characterising the virulence function of AvrM14, we were interested in understanding the requirements for recognition of AvrM14 by M1 and M4. Flax M1 belongs to the TIR-NLR class of R-proteins. M4 has not yet been cloned, but is expected to encode a protein closely related to M1 (Lawrence *et al.*, 2010).

The AvrM14 structures reveal that the six amino acid polymorphisms differentiating the A and B alleles map to the protein surface (Fig. 6a). To understand which polymorphisms are important for recognition, we transiently expressed various AvrM14 proteins with single or double mutations at the six polymorphic residues in tobacco co-expressing *M1* (*M1* tobacco) and in near-isogenic lines of the flax variety Bison containing either *M1* (*M1* flax) or *M4* (*M4* flax), using *Agrobacterium*-mediated transformation (sequences in Table S1).

The expression and accumulation of all mutant AvrM14 proteins in plant tissue were confirmed via Western blotting (Fig. S2). Most of the mutations had only a minor or no effect on the observed phenotype (Figs S11, S12; Table S6). Only by

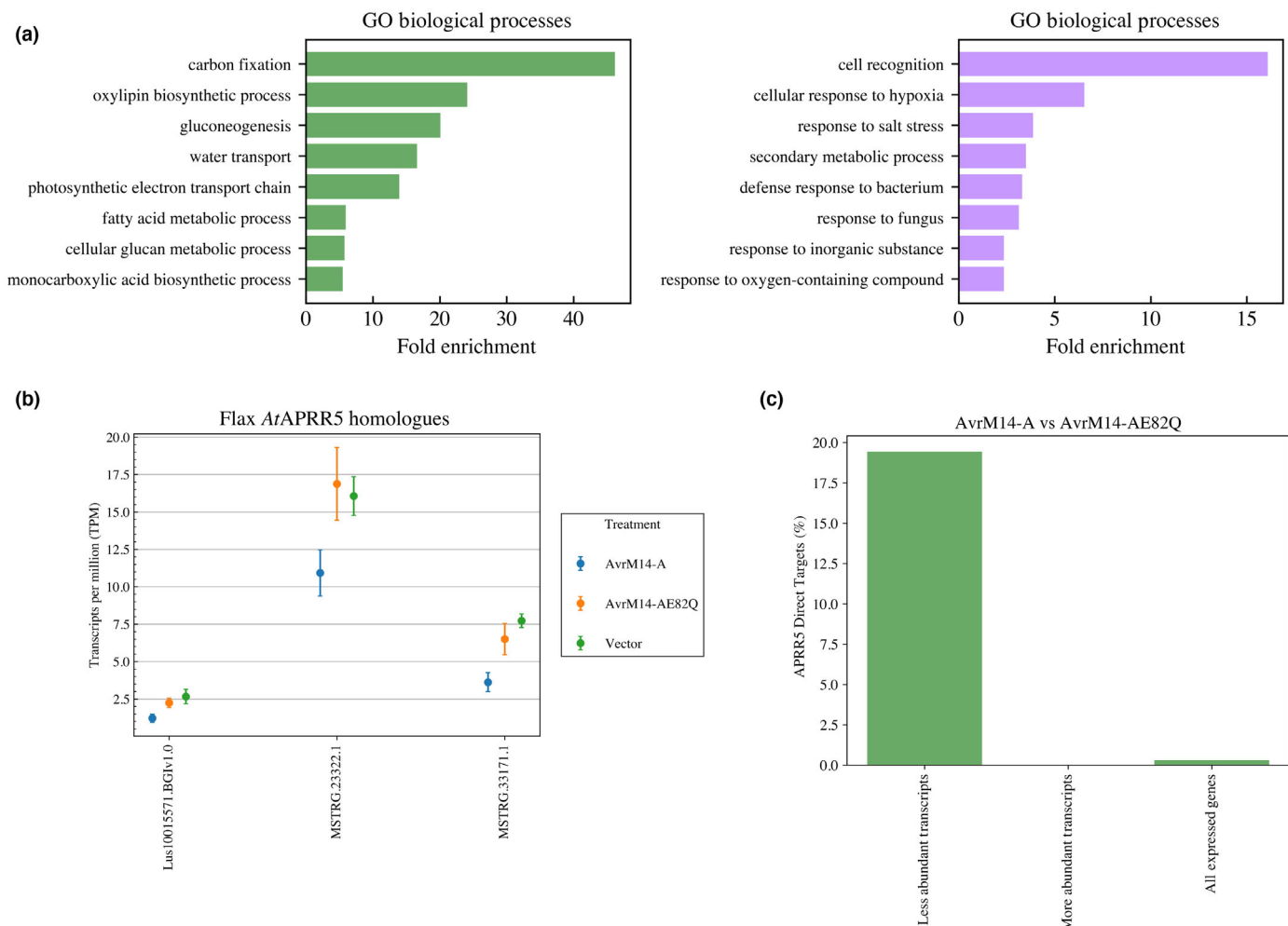


Fig. 5 Enzymatic activity of AvrM14-A in flax leaves reduces the relative abundance of transcripts homologous to *Arabidopsis thaliana* APPR5 and APPR5 direct targets. (a) The Gene Ontology biological processes that are enriched ($FDR < 0.05$) in the list of transcripts significantly ($q < 0.05$) more abundant (left, green; $\log_2 fc > 0.5$) and less abundant (right, purple; $\log_2 fc < -0.5$), when comparing flax leaves transformed with AvrM14-A to an empty vector. Only the top 10 (sorted by fold enrichment) processes are shown, after filtering out redundant terms using REVIGO (Supek *et al.*, 2011). (b) The average expression levels ($\pm SDs$) are displayed as transcripts per million (TPM) for transcripts homologous to *A. thaliana* PRR5 that are significantly less abundant ($q < 0.05$, $\log_2 fc < -0.5$) when comparing the AvrM14-A (blue) ($n = 4$) and AvrM14-AE82Q (orange) ($n = 4$) RNA-Seq datasets, the mean TPM ($\pm SDs$) are also displayed for the vector-only dataset (green) ($n = 3$). The x-axis label indicates the name of the transcript as listed in Supporting Information Tables S4 and S5. (c) The percentage of transcripts homologous to *A. thaliana* APPR5 direct targets, as identified by Nakamichi *et al.* (2012), present in the list of transcripts significantly ($q < 0.05$) less abundant (left; $\log_2 fc < -0.5$), or more abundant (middle) ($\log_2 fc > 0.5$) when comparing flax leaves expressing AvrM14-A to leaves expressing AvrM14-AE82Q. The percentage of transcripts homologous to *A. thaliana* APPR5 direct targets present among all expressed genes included in the differential expression analysis is indicated on the right.

mutating residues 95 and 108, we were able to completely and consistently reverse recognition by both *M1* and *M4* in flax (i.e. AvrM14-A^{K95Q/T108P} expression resulted in a HR similar to AvrM14-B expression and AvrM14-B^{Q95K/P108T} expression resulted in a HR similar to AvrM14-A expression; Fig. 6c; Table S6).

Overall, our results indicate that both *M1* and *M4* R-proteins recognise AvrM14-A using a mechanism that can be evaded by mutating residues 95 and 108, suggesting that the currently uncharacterised *M4* is highly similar to *M1*, consistent with the observation that *M1* and *M4* are likely to be allelic (Lawrence *et al.*, 2010). According to the crystal structure of monomeric and homodimeric AvrM14, residues 95 and 108 do not localise to the same surface region (Fig. 6b). If *M1* and *M4* interact

directly with AvrM14, our results suggest that the R-proteins have multiple contact points with the effector, like previous data suggest occurs with other flax/flax rust R-protein/effector pairs, AvrM and M, and AvrL567 and L5/L6 (Ravensdale *et al.*, 2012; Ve *et al.*, 2013).

Discussion

In this study, we have demonstrated that the AvrM14 effector from *M. lini* is a Nudix hydrolase that is able to suppress plant immunity, modify host transcriptome composition and uncap mRNAs in a manner that would render them susceptible to degradation by host exoribonucleases. No plant pathogens have been previously reported to use mRNA-decapping enzymes to

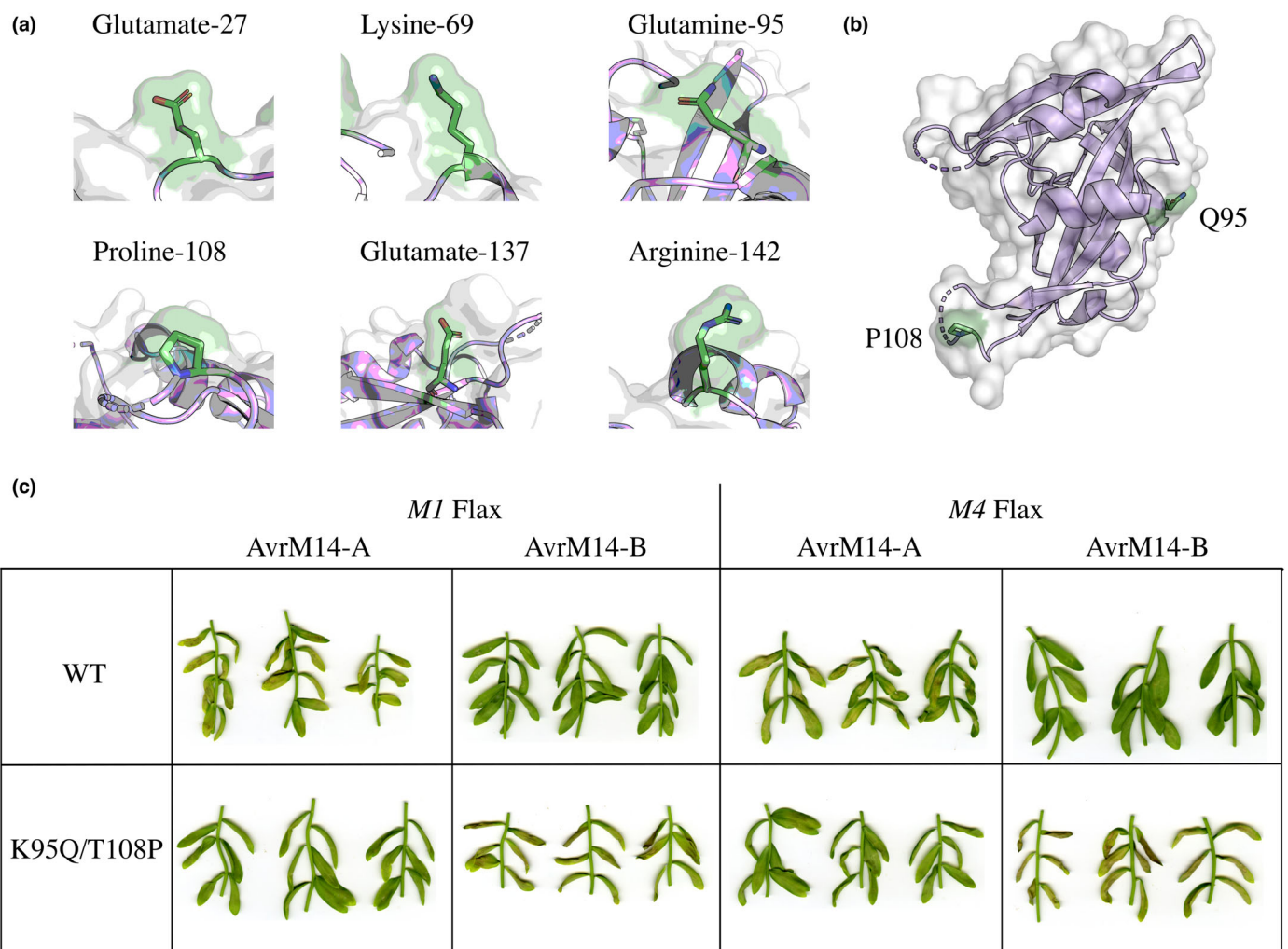


Fig. 6 AvrM14 polymorphic residues are surface-exposed, with residues 95 and 108 involved in resistance protein recognition. (a) The six polymorphic residues differentiating AvrM14-A and AvrM14-B all localise to the protein surface, as demonstrated here using the AvrM14-B structure displayed in ribbon representation, superimposed on a surface representation, with side chains of polymorphic residues coloured green. (b) The crystal structure of AvrM14-B with the side chains of residues important for evading M1 and M4 detection (Q95 and P108) coloured green. (c) Bison \times M1 (Williston Brown) or M4 (Victory 'A') flax (*Linum usitatissimum*) lines were infiltrated with *Agrobacterium* harbouring constructs encoding either wild-type or mutant YFP-tagged AvrM14 proteins (AvrM14-A, AvrM14-B, AvrM14-A^{K95Q/T108P} or AvrM14-B^{Q95K/P108T}). The agroinfiltrated leaves were photographed 5 d post-infiltration to assess the cell-death response.

inhibit plant immunity. Before the present study, only certain animal viruses, including vaccinia and African swine fever viruses, have been known to produce mRNA-decapping Nudix hydrolases during host-cell infection (Parrish & Moss, 2006; Quintas *et al.*, 2017). Our findings have implications for understanding genetic post-transcriptional regulation in plants, in addition to helping understand how *Melampsora* pathogens circumvent plant immunity during successful infection.

Host and pathogen Nudix hydrolases influence plant immunity

Diverse pathogens of plants secrete effectors with Nudix domains and prior research have confirmed that two of these (Avr3b and RipN) can inhibit plant immune function (Dong *et al.*, 2011; Dong & Wang, 2016; Sun *et al.*, 2019). We have demonstrated

that a third effector, AvrM14 from flax rust, is also a Nudix hydrolase that can suppress plant immunity. The Nudix hydrolase activity of AvrM14 inhibits the MAMP-induced ROS burst in the nonhost plant *N. benthamiana* and reduces the HR cell-death response triggered by M1 in flax. However, it is currently unknown whether the suppressive effect of AvrM14 on plant immunity promotes the virulence of flax rust during infection.

Plant Nudix hydrolases also play important roles in regulating plant immune responses. *Arabidopsis thaliana* Nudix hydrolases 6, 7 and 8 (AtNUDX6/7/8) have all been implicated in modulating plant immune function (Bartsch *et al.*, 2006; Ge *et al.*, 2007; Ishikawa *et al.*, 2010; Fonseca & Dong, 2014). Additionally, wheat Nudix hydrolase 23 (TaNUDX23) suppresses ROS accumulation and is stabilised by an effector protein from *Puccinia striiformis* f. sp. *tritici* (Yang *et al.*, 2020). Recently, it was reported that AtNUDX7 and the Avr3b effector can degrade

cyclic nucleotide monophosphates (cNMPs) by acting as phosphodiesterases (Yu *et al.*, 2022). Yu *et al.* (2022) demonstrated that cNMPs are important for TIR-NLR-mediated plant immunity and that NUDX7 can suppress the cell-death response triggered by the TIR-only disease R-protein RBA1 (Yu *et al.*, 2022). AvrM14 does not hydrolyse similar substrates to AtNUDX7, TaNUDX23 or Avr3b *in vitro* and is not structurally similar to AtNUDX7 (Tang *et al.*, 2015); our data support a different mechanism of immunity suppression.

AvrM14 is a highly selective Nudix hydrolase

Nudix hydrolases are renowned for their broad substrate specificity, with many enzymes readily hydrolysing multiple substrates *in vitro* (McLennan, 2013). Avr3b, AtNUDX7, TaNUDX23 and RipN were tested against a limited subset of potential substrates and all hydrolysed multiple substrates (Ogawa *et al.*, 2005; Dong *et al.*, 2011; Sun *et al.*, 2019; Yang *et al.*, 2020), complicating the identification of physiologically relevant substrates. By contrast, we found that AvrM14 does not exhibit broad substrate specificity *in vitro*, based on extensive screening of a total of 70 potential substrates. AvrM14 only hydrolysed mRNA cap analogues and capped mRNA. In our broad screen, AvrM14 effectively hydrolysed m^7 Gp₅G but not Gp₅G, suggesting that AvrM14 achieves substrate specificity by selecting for the methylated guanosine. Nudix hydrolases with specificity for methylated guanosine have been reported previously and experimental evidence indicates that these proteins function as mRNA-decapping enzymes (Van Dijk *et al.*, 2002; Wang *et al.*, 2002; Piccirillo *et al.*, 2003; Parrish *et al.*, 2007; Parrish & Moss, 2007). The canonical mRNA-decapping enzyme in eukaryotes, DCP2, demonstrates improved mRNA-decapping activity with m^7 Gp₃RNA, when compared to Gp₃RNA (Van Dijk *et al.*, 2002; Wang *et al.*, 2002; Piccirillo *et al.*, 2003). Additionally, two mRNA-decapping enzymes from the vaccinia virus, D9 and D10, both demonstrate specificity for methylated guanosine substrates (Parrish *et al.*, 2007; Parrish & Moss, 2007). Structural studies with mRNA cap analogues indicate that the N-terminal regulatory domain (NRD) of DCP2 is important for binding to the cap region (Charenton *et al.*, 2016; Mugridge *et al.*, 2016; Wurm *et al.*, 2017). AvrM14 lacks an NRD, therefore binding cannot be controlled by the same mechanism as DCP2. We attempted cocrystallisation of AvrM14 with the mRNA cap analogues m^7 Gp₃G and m^7 Gp₅G to understand the molecular basis of substrate selectivity, but were unable to capture them bound to the enzyme.

AvrM14 likely functions as a homodimer to ensure the correct mRNA cap pyrophosphate bond is hydrolysed

We found that a proportion of AvrM14 protein was produced in *E. coli* as a stable dimer and demonstrated via X-ray crystallography that this was mediated via domain swapping. Dimerisation via domain swapping has been shown previously for other Nudix hydrolases (Gabelli *et al.*, 2001; Kang *et al.*, 2003; Yoshioka *et al.*, 2004; Zha *et al.*, 2006; Wakamatsu *et al.*, 2008; Tang

et al., 2015), and we were interested in investigating the biological relevance of this, if any, for AvrM14. Our *in planta* experiments show that AvrM14 is monomeric when expressed in *N. benthamiana*, indicating that homodimerisation of AvrM14 via the domain-swapping mechanism in plants is unlikely. Unfortunately, the method we used to discriminate monomeric and homodimeric AvrM14 is not sensitive enough to investigate what the fungus itself delivers into flax cells during infection. Despite this, we suggest that AvrM14 functions as a dimer to decap mRNA. Our *in vitro* and *in silico* analyses provide multiple lines of evidence for AvrM14 functioning as a homodimer. We demonstrate that homodimeric AvrM14 releases m^7 GDP and 5'-monophosphate RNA from capped mRNA. It is well established that following decapping, mRNA transcripts in cells are subject to 5'-3' decay by exoribonucleases (XRN4 in plants), which target a 5' end monophosphate RNA substrate, and that 5' diphosphate RNA is not a direct target for 5' decay (Grudzien-Nogalska & Kiledjian, 2017). In support of this, the structurally related decapping enzyme Nudt16, homodimerises and preferentially releases m^7 GDP (Song *et al.*, 2010, 2013; Trésagues *et al.*, 2015). There are also strong similarities between the homodimerisation interface observed in the Nudt16 crystal structure (PDB ID: 3MGM) and the crystal packing, and domain-swapping dimer, observed for AvrM14-A and AvrM14-B. In addition, the aromatic residues involved in the dimeric interface of AvrM14 are highly conserved in homologous effectors from other *Melampsora* species, suggesting that this protein–protein interaction surface is important for effector function. Collectively, based on our *in vitro* and *in silico* analysis of AvrM14 and the homologous effectors, we suggest that these proteins are biologically active as dimers, but how this is achieved in a natural setting, that is domain swapping, interactions with other proteins or mRNA itself, remain unknown.

Controlling plant immunity by decapping mRNA

AvrM14 decaps mRNA *in vitro* and the mRNA-decapping activity requires glutamate-82 (E82). We also demonstrated that E82 is required for suppression of ROS production in *N. benthamiana* and for the reduction in the cell-death response following AvrM14 recognition by M1 in flax. Our results are consistent with AvrM14 acting as an mRNA-decapping enzyme, to inhibit aspects of plant immunity. This suggests that AvrM14 can selectively decap transcripts involved in plant immunity, rather than destabilising the entire transcriptome. We speculate that AvrM14 may interact with other proteins in the plant cell to enable transcript selectivity, as occurs with DCP2 in yeast (He *et al.*, 2018). Alternatively, AvrM14 may be hydrolysing another unknown compound *in planta* that also requires E82 to inhibit plant immunity. However, due to the selectivity of AvrM14 for methylated guanosine substrates *in vitro*, our substrate screening data suggest that this is unlikely.

The decapping and decay of plant mRNA are known to be important for plant immune function. For example, following immune activation, phosphorylation of the DCP2-interacting protein DCP1 (decapping 1) enhances DCP2-dependent decay

of multiple transcripts encoding negative regulators of plant immunity (Yu *et al.*, 2019; He *et al.*, 2022). By contrast, during periods of normal growth, mRNA decapping and decay can prevent immune activation via nonsense-mediated mRNA decay (NMD) of numerous *R*-gene transcripts (Gloggnitzer *et al.*, 2014; Jung *et al.*, 2020). Nonsense-mediated mRNA decay regulation for many of these *R*-genes requires VARICOSE (VCS), a scaffolding protein for decapping machinery (Xu *et al.*, 2006; Raxwal *et al.*, 2020).

Our RNA-Seq analysis identified that the enzymatic activity of AvrM14-A decreases the abundance of multiple transcripts homologous to *A. thaliana* circadian network-related genes. Plant defence responses, including ROS production and the HR triggered by R-proteins, are linked to circadian rhythm (Lu *et al.*, 2017; Westwood *et al.*, 2019; Butt *et al.*, 2020). For example, the expression of some *A. thaliana* *R*-genes is controlled by the circadian regulator, CIRCADIAN CLOCK-ASSOCIATED 1 (Wang *et al.*, 2011) and the amplitude of ROS production following flg-22 exposure is time-of-day-dependant (Korneli *et al.*, 2014). The suppression of ROS production and reduction in the M1-activated HR by the enzymatic activity of AvrM14 may be a result of AvrM14 altering plant circadian rhythm.

The transcript level of regulators of circadian rhythm in *A. thaliana* has recently been identified to be controlled by 5'-3' mRNA decay requiring the cytoplasmic exoribonuclease XRN4 (Careno *et al.*, 2022). We speculate that AvrM14 decreases the abundance of flax circadian rhythm regulator transcripts by removing their 5' cap and promoting their XRN4-dependant decay. Further research is required to confirm that the decrease in the abundance of APRR5 and other circadian-rhythm-related transcripts due to the enzymatic activity of AvrM14 is a direct result of these transcripts being decapped by AvrM14.

Acknowledgements

This work was supported by funding from the Australian Research Council (ARC) (Discovery Projects DP120100685, DP160102244 and DP200100387) and the Australian National University (ANU) Future Scheme (35665). SW was supported by ARC DECRA (DE160100893) and Future Fellowships (FT200100135). BK was supported by a Laureate Fellowship (FL180100109). CM and DY were recipients of the Australian Government Research Training Programme (RTP) Stipend Scholarship and the Australian Institute of Nuclear Science and Engineering (AINSE) Ltd. Postgraduate Research Award (PGRA). We thank Ayesha Akram for providing mature flax plants for the RNA-Seq experiment, and the Plant Services Team at the Australian National University for providing *Nicotiana benthamiana* seedlings. We thank Jeffrey Ellis for support during the early stages of the work and scientific discussion. The authors acknowledge the use of the ANU crystallisation facility. The authors also acknowledge the use of the Australian Synchrotron MX facility and thank the staff for their support. This research was undertaken in part using the MX2 beamline at the Australian Synchrotron, part of ANSTO, and made use of the Australian Cancer Research Foundation (ACRF) detector. Open access

publishing facilitated by Australian National University, as part of the Wiley - Australian National University agreement via the Council of Australian University Librarians.

Competing interests

None declared.

Author contributions

CLM, A-MC, PND, BK, DAJ and SJW planned and designed the research study. CLM, A-MC, JRG, AMD, MAO, DSY and SJW performed the experiments; CLM, A-MC, JRG, DJE, SEB, PND, DAJ and SJW analysed the data. CLM wrote the original draft and all authors contributed to writing, reviewing and editing of the manuscript. CLM and A-MC contributed equally to this work.

ORCID

Steven E. Brenner  <https://orcid.org/0000-0001-7559-6185>
Ann-Maree Catanzariti  <https://orcid.org/0000-0001-8518-044X>

Peter N. Dodds  <https://orcid.org/0000-0003-0620-5923>
Daniel J. Ericsson  <https://orcid.org/0000-0001-5101-9244>
Julian R. Greenwood  <https://orcid.org/0000-0003-0497-0541>

David A. Jones  <https://orcid.org/0000-0001-8809-5822>
Bostjan Kobe  <https://orcid.org/0000-0001-9413-9166>
Carl L. McCombe  <https://orcid.org/0000-0001-9347-8879>
Megan A. Outram  <https://orcid.org/0000-0003-4510-3575>
Simon J. Williams  <https://orcid.org/0000-0003-4781-6261>
Daniel S. Yu  <https://orcid.org/0000-0003-0454-7989>

Data availability

The data that support the protein structures described in this study are openly available under accession nos. 8DP8, 8DP9 and 8DPA at the PDB. RNA-sequencing data are available from the NCBI (GEO: GSE207874, SRA: SRX16112399, SRX16112400, SRX16112401, SRX16112402, SRX16112403, SRX16112404, SRX16112405, SRX16112406, SRX16112384, SRX16112385 and SRX1611238).

References

- Afonine PV, Grosse-Kunstleve RW, Echols N, Head JJ, Moriarty NW, Mustyakimov M, Terwilliger TC, Urzhumtsev A, Zwart PH, Adams PD. 2012. Towards automated crystallographic structure refinement with phenix.refine. *Acta Crystallographica. Section D, Biological Crystallography* 68: 352–367.
- Ames BN. 1966. Assay of inorganic phosphate, total phosphate and phosphatases. In: *Methods in enzymology*. Cambridge, MA, USA: Academic Press, 115–118.
- Anderson C, Khan MA, Catanzariti A-M, Jack CA, Nemri A, Lawrence GJ, Upadhyaya NM, Hardham AR, Ellis JG, Dodds PN *et al.* 2016. Genome analysis and avirulence gene cloning using a high-density RADseq linkage map of the flax rust fungus, *Melampsora lini*. *BMC Genomics* 17: 667–668.

- Aragão D, Aishima J, Cherukuvada H, Clarken R, Clift M, Cowieson NP, Ericsson DJ, Gee CL, Macedo S, Mudie N. 2018. MX2: a high-flux undulator microfocus beamline serving both the chemical and macromolecular crystallography communities at the Australian Synchrotron. *Journal of Synchrotron Radiation* 25: 885–891.
- Bartsch M, Gobbato E, Bednarek P, Debey S, Schultze JL, Bautista J, Parker JE. 2006. Salicylic acid-independent ENHANCED DISEASE SUSCEPTIBILITY1 signaling in *Arabidopsis* immunity and cell death is regulated by the monooxygenase *FMO1* and the Nudix hydrolase *NUDT7*. *Plant Cell* 18: 1038–1051.
- Bentham AR, Youles M, Mendel MN, Varden FA, JCDI C, Banfield MJ. 2021. pOPIN-GG: a resource for modular assembly in protein expression vectors. *BioRxiv*. doi: 10.1101/2021.08.10.455798.
- Bessman MJ, Walsh JD, Dunn CA, Swaminathan J, Weldon JE, Shen J. 2001. The gene *ygdP*, associated with the invasiveness of *Escherichia coli* K1, designates a Nudix hydrolase, Orf176, active on adenosine-pentaphospho-(5')-adenosine (Ap5A). *The Journal of Biological Chemistry* 276: 37834–37838.
- Bhaduria V, Banniza S, Vandenberg A, Selvaraj G, Wei Y. 2013. Overexpression of a novel biotrophy-specific *Colletotrichum truncatum* effector, CtNUDIX, in hemibiotrophic fungal phytopathogens causes incompatibility with their host plants. *Eukaryotic Cell* 12: 2–11.
- Butt GR, Qayyum ZA, Jones MA. 2020. Plant defence mechanisms are modulated by the circadian system. *Biology* 9: 454.
- Careno DA, Santangelo SP, Macknight RC, Yanovsky MJ. 2022. The 5'-3' mRNA decay pathway modulates the plant circadian network in *Arabidopsis*. *Plant & Cell Physiology* 63: 1709–1719.
- Casañal A, Lohkamp B, Emsley P. 2020. Current developments in Coot for macromolecular model building of electron cryo-microscopy and crystallographic data. *Protein Science* 29: 1069–1078.
- Casey LW, Lavrencic P, Bentham AR, Cesari S, Ericsson DJ, Croll T, Turk D, Anderson PA, Mark AE, Dodds PN *et al.* 2016. The CC domain structure from the wheat stem rust resistance protein Sr33 challenges paradigms for dimerization in plant NLR proteins. *Proceedings of the National Academy of Sciences, USA* 113: 12856–12861.
- Catanzariti A-M, Lim GTT, Jones DA. 2015. The tomato I-3 gene: a novel gene for resistance to Fusarium wilt disease. *New Phytologist* 207: 106–118.
- Charenton C, Taverniti V, Gaudon-Plesse C, Back R, Séraphin B, Graillat M. 2016. Structure of the active form of Dcp1–Dcp2 decapping enzyme bound to m7GDP and its Edc3 activator. *Nature Structural & Molecular Biology* 23: 982–986.
- Cowieson NP, Aragão D, Clift M, Ericsson DJ, Gee C, Harrop SJ, Mudie N, Panjikar S, Price JR, Riboldi-Tunnicliffe A. 2015. MX1: a bending-magnet crystallography beamline serving both chemical and macromolecular crystallography communities at the Australian Synchrotron. *Journal of Synchrotron Radiation* 22: 187–190.
- Dodds PN, Lawrence GJ, Catanzariti AM, Ayliffe MA, Ellis JG. 2004. The *Melampsora lini* AvrL567 avirulence genes are expressed in haustoria and their products are recognized inside plant cells. *Plant Cell* 16: 755–768.
- Dodds PN, Rathjen JP. 2010. Plant immunity: towards an integrated view of plant–pathogen interactions. *Nature Reviews. Genetics* 11: 539–548.
- Dong S, Wang Y. 2016. Nudix effectors: a common weapon in the arsenal of plant pathogens. *PLoS Pathogens* 12: e1005704.
- Dong S, Yin W, Kong G, Yang X, Qutob D, Chen Q, Kale SD, Sui Y, Zhang Z, Dou D *et al.* 2011. *Phytophthora sojae* avirulence effector Avr3b is a secreted NADH and ADP-ribose pyrophosphorylase that modulates plant immunity. *PLoS Pathogens* 7: e1002353.
- Earley KW, Haag JR, Pontes O, Opper K, Juehne T, Song K, Pikaard CS. 2006. Gateway-compatible vectors for plant functional genomics and proteomics. *The Plant Journal* 45: 616–629.
- Evans PR, Murshudov GN. 2013. How good are my data and what is the resolution? *Acta crystallographica Section D, Biological Crystallography* 69: 1204–1214.
- Fonseca JP, Dong X. 2014. Functional characterization of a Nudix hydrolase AtNUDX8 upon pathogen attack indicates a positive role in plant immune responses. *PLoS ONE* 9: e114119.
- Fujimura T, Esteban R. 2010. Yeast double-stranded RNA virus LA deliberately synthesizes RNA transcripts with 5'-diphosphate. *The Journal of Biological Chemistry* 285: 22911–22918.
- Gabelli SB, Bianchet MA, Bessman MJ, Amzel LM. 2001. The structure of ADP-ribose pyrophosphatase reveals the structural basis for the versatility of the Nudix family. *Nature Structural Biology* 8: 467–472.
- Gabelli SB, Bianchet MA, Ohnishi Y, Ichikawa Y, Bessman MJ, Amzel LM. 2002. Mechanism of the *Escherichia coli* ADP-ribose pyrophosphatase, a Nudix hydrolase. *Biochemistry* 41: 9279–9285.
- Ge X, Li G-J, Wang S-B, Zhu H, Zhu T, Wang X, Xia Y. 2007. AtNUDT7, a negative regulator of basal immunity in *Arabidopsis*, modulates two distinct defense response pathways and is involved in maintaining redox homeostasis. *Plant Physiology* 145: 204–215.
- Gloggnitzer J, Akimcheva S, Srinivasan A, Kusenda B, Riehs N, Stampfli H, Bautista J, Dekrout B, Jonak C, Jiménez-Gómez JM *et al.* 2014. Nonsense-mediated mRNA decay modulates immune receptor levels to regulate plant antibacterial defense. *Cell Host & Microbe* 16: 376–390.
- Grudzien-Nogalska E, Kiledjian M. 2017. New insights into decapping enzymes and selective mRNA decay. *Wiley Interdisciplinary Reviews. RNA* 8: e1379.
- Gunawardana D, Cheng H-C, Gayler KR. 2008. Identification of functional domains in *Arabidopsis thaliana* mRNA decapping enzyme (AtDcp2). *Nucleic Acids Research* 36: 203–216.
- He F, Celik A, Wu C, Jacobson A. 2018. General decapping activators target different subsets of inefficiently translated mRNAs. *eLife* 7: e34409.
- He F, Wu C, Jacobson A. 2022. Dcp2 C-terminal cis-binding elements control selective targeting of the decapping enzyme by forming distinct decapping complexes. *eLife* 11: e74410.
- Heese A, Hann DR, Giménez-Ibanez S, Jones AME, He K, Li J, Schroeder JI, Peck SC, Rathjen JP. 2007. The receptor-like kinase SERK3/BAK1 is a central regulator of innate immunity in plants. *Proceedings of the National Academy of Sciences, USA* 104: 12217–12222.
- Höfer K, Li S, Abele F, Frindert J, Schlotthauer J, Gräfenhoff J, Du J, Patel DJ, Jäschke A. 2016. Structure and function of the bacterial decapping enzyme NudC. *Nature Chemical Biology* 12: 730–734.
- Ishikawa K, Yoshimura K, Harada K, Fukusaki E, Ogawa T, Tamoi M, Shigeoka S. 2010. AtNUDX6, an ADP-ribose/NADH pyrophosphohydrolase in *Arabidopsis*, positively regulates NPR1-dependent salicylic acid signaling. *Plant Physiology* 152: 2000–2012.
- Islam MR, Mayo GME. 1990. A compendium on host genes in flax conferring resistance to flax rust. *Plant Breeding* 104: 89–100.
- Ito R, Hayakawa H, Sekiguchi M, Ishibashi T. 2005. Multiple enzyme activities of *Escherichia coli* MutT protein for sanitization of DNA and RNA precursor pools. *Biochemistry* 44: 6670–6674.
- Iwai T, Kuramitsu S, Masui R. 2004. The Nudix hydrolase Ndx1 from *Thermus thermophilus* HB8 is a diadenosine hexaphosphate hydrolase with a novel activity. *The Journal of Biological Chemistry* 279: 21732–21739.
- Jemth A-S, Gustafsson R, Bräutigam L, Henriksson L, Vallin KSA, Sarno A, Almlöf J, Homan E, Rasti A, Warpmann Berglund U *et al.* 2018. MutT homologue 1 (MTH1) catalyzes the hydrolysis of mutagenic O6-methyl-dGTP. *Nucleic Acids Research* 46: 10888–10904.
- Jones JDG, Dangl JL. 2006. The plant immune system. *Nature* 444: 323–329.
- Jung HW, Panigrahi GK, Jung GY, Lee YJ, Shin KH, Sahoo A, Choi ES, Lee E, Man Kim K, Yang SH *et al.* 2020. Pathogen-associated molecular pattern-triggered immunity involves proteolytic degradation of core nonsense-mediated mRNA decay factors during the early defense response. *Plant Cell* 32: 1081–1101.
- Jurrus E, Engel D, Star K, Monson K, Brandi J, Felberg LE, Brookes DH, Wilson L, Chen J, Liles K *et al.* 2018. Improvements to the APBS biomolecular solvation software suite. *Protein Science* 27: 112–128.
- Kabsch W. 2010. XDS. *Acta crystallographica Section D, Biological Crystallography* 66: 125–132.
- Kang L-W, Gabelli SB, Cunningham JE, O'Handley SF, Amzel LM. 2003. Structure and mechanism of MT-ADPRase, a Nudix hydrolase from *Mycobacterium tuberculosis*. *Structure* 11: 1015–1023.
- Kong G, Zhao Y, Jing M, Huang J, Yang J, Xia Y, Kong L, Ye W, Xiong Q, Qiao Y *et al.* 2015. The activation of *Phytophthora* effector Avr3b by plant

- cyclophilin is required for the Nudix hydrolase activity of Avr3b. *PLoS Pathogens* 11: e1005139.
- Korneli C, Danisman S, Staiger D. 2014. Differential control of pre-invasive and post-invasive antibacterial defense by the *Arabidopsis* circadian clock. *Plant & Cell Physiology* 55: 1613–1622.
- Langer G, Cohen SX, Lamzin VS, Perrakis A. 2008. Automated macromolecular model building for X-ray crystallography using ARP/wARP v.7. *Nature Protocols* 3: 1171–1179.
- Lawrence GJ, Anderson PA, Dodds PN, Ellis JG. 2010. Relationships between rust resistance genes at the M locus in flax. *Molecular Plant Pathology* 11: 19–32.
- Leslie NR, McLennan AG, Safrany ST. 2002. Cloning and characterisation of hAps1 and hAps2, human diadenosine polyphosphate-metabolising Nudix hydrolases. *BMC Biochemistry* 3: 20.
- Li Y, Song M, Kiledjian M. 2011. Differential utilization of decapping enzymes in mammalian mRNA decay pathways. *RNA* 17: 419–428.
- Liebschner D, Afonine PV, Baker ML, Bunkóczki G, Chen VB, Croll TI, Hintze B, Hung L-W, Jain S, McCoy AJ. 2019. Macromolecular structure determination using X-rays, neutrons and electrons: recent developments in Phenix. *Acta Crystallographica. Section D, Structural Biology* 75: 861–877.
- Lin J, Abeygunawardana C, Frick DN, Bessman MJ, Mildvan AS. 1996. The role of Glu 57 in the mechanism of the *Escherichia coli* MutT enzyme by mutagenesis and heteronuclear NMR. *Biochemistry* 35: 6715–6726.
- Lin J, Abeygunawardana C, Frick DN, Bessman MJ, Mildvan AS. 1997. Solution structure of the quaternary MutT–M²⁺–AMPcPP–M²⁺ complex and mechanism of its pyrophosphohydrolase action. *Biochemistry* 36: 1199–1211.
- Lo Presti L, Lanver D, Schweizer G, Tanaka S, Liang L, Tollot M, Zuccaro A, Reissmann S, Kahmann R. 2015. Fungal effectors and plant susceptibility. *Annual Review of Plant Biology* 66: 513–545.
- Lu H, McClung CR, Zhang C. 2017. Tick Tock: circadian regulation of plant innate immunity. *Annual Review of Phytopathology* 55: 287–311.
- McLennan AG. 2006. The Nudix hydrolase superfamily. *Cellular and Molecular Life Sciences* 63: 123–143.
- McLennan AG. 2013. Substrate ambiguity among the nudix hydrolases: biologically significant, evolutionary remnant, or both? *Cellular and Molecular Life Sciences* 70: 373–385.
- Mildvan AS, Xia Z, Azurmendi HF, Saraswat V, Legler PM, Massiah MA, Gabelli SB, Bianchet MA, Kang LW, Amzel LM. 2005. Structures and mechanisms of Nudix hydrolases. *Archives of Biochemistry and Biophysics* 433: 129–143.
- Mugridge JS, Ziemniak M, Jemielity J, Gross JD. 2016. Structural basis of mRNA-cap recognition by Dcp1–Dcp2. *Nature Structural & Molecular Biology* 23: 987–994.
- Müller-McNicoll M, Neugebauer KM. 2014. Good cap/bad cap: how the cap-binding complex determines RNA fate. *Nature Structural & Molecular Biology* 21: 9–12.
- Nakamichi N, Kiba T, Kamioka M, Suzuki T, Yamashino T, Higashiyama T, Sakakibara H, Mizuno T. 2012. Transcriptional repressor PRR5 directly regulates clock-output pathways. *Proceedings of the National Academy of Sciences, USA* 109: 17123–17128.
- Nakamichi N, Kita M, Ito S, Sato E, Yamashino T, Mizuno T. 2005. The *Arabidopsis* pseudo-response regulators, PRR5 and PRR7, coordinately play essential roles for circadian clock function. *Plant & Cell Physiology* 46: 609–619.
- Nguyen VN, Park A, Xu A, Srouji JR, Brenner SE, Kirsch JF. 2016. Substrate specificity characterization for eight putative nudix hydrolases. Evaluation of criteria for substrate identification within the Nudix family. *Proteins* 84: 1810–1822.
- Ogawa T, Ueda Y, Yoshimura K, Shigeoka S. 2005. Comprehensive analysis of cytosolic Nudix hydrolases in *Arabidopsis thaliana*. *The Journal of Biological Chemistry* 280: 25277–25283.
- O'Handley SF, Frick DN, Dunn CA, Bessman MJ. 1998. Orf186 represents a new member of the Nudix hydrolases, active on adenosine (5') triphospho (5') adenosine, ADP-ribose, and NADH. *The Journal of Biological Chemistry* 273: 3192–3197.
- Parrish S, Moss B. 2006. Characterization of a vaccinia virus mutant with a deletion of the D10R gene encoding a putative negative regulator of gene expression. *Journal of Virology* 80: 553–561.
- Parrish S, Moss B. 2007. Characterization of a second vaccinia virus mRNA-decapping enzyme conserved in poxviruses. *Journal of Virology* 81: 12973–12978.
- Parrish S, Resch W, Moss B. 2007. Vaccinia virus D10 protein has mRNA-decapping activity, providing a mechanism for control of host and viral gene expression. *Proceedings of the National Academy of Sciences, USA* 104: 2139–2144.
- Perraud A-L, Shen B, Dunn CA, Rippe K, Smith MK, Bessman MJ, Stoddard BL, Scharenberg AM. 2003. NUDT9, a member of the Nudix hydrolase family, is an evolutionarily conserved mitochondrial ADP-ribose pyrophosphatase. *The Journal of Biological Chemistry* 278: 1794–1801.
- Piccirillo C, Khanna R, Kiledjian M. 2003. Functional characterization of the mammalian mRNA decapping enzyme hDcp2. *RNA* 9: 1138–1147.
- Quintas A, Pérez-Núñez D, Sánchez EG, Nogal ML, Hentze MW, Castelló A, Revilla Y. 2017. Characterization of the African swine fever virus decapping enzyme during Infection. *Journal of Virology* 91: e00990-17.
- Ravensdale M, Bernoux M, Ve T, Kobe B, Thrall PH, Ellis JG, Dodds PN. 2012. Intramolecular interaction influences binding of the Flax L5 and L6 resistance proteins to their AvrL567 ligands. *PLoS Pathogens* 8: e1003004.
- Rawat R, Takahashi N, Hsu PY, Jones MA, Schwartz J, Salemi MR, Phinney BS, Harmer SL. 2011. REVEILLE8 and PSEUDO-REPONSE REGULATOR5 form a negative feedback loop within the *Arabidopsis* circadian clock. *PLoS Genetics* 7: e1001350.
- Raxwal VK, Simpson CG, Gloggnitzer J, Entinze JC, Guo W, Zhang R, Brown JWS, Riha K. 2020. Nonsense-mediated RNA decay factor UPF1 is critical for posttranscriptional and translational gene regulation in *Arabidopsis*. *Plant Cell* 32: 2725–2741.
- Robert X, Gouet P. 2014. Deciphering key features in protein structures with the new ENDscript server. *Nucleic Acids Research* 42: W320–W324.
- Sakumi K, Furuichi M, Suzuki T, Kakuma T, Kawabata S, Maki H, Sekiguchi M. 1993. Cloning and expression of cDNA for a human enzyme that hydrolyses 8-oxo-dGTP, a mutagenic substrate for DNA synthesis. *The Journal of Biological Chemistry* 268: 23524–23530.
- Scarsdale JN, Peculis BA, Wright HT. 2006. Crystal structures of U8 snoRNA decapping Nudix hydrolase, X29, and its metal and cap complexes. *Structure* 14: 331–343.
- Schoenberg DR, Maquat LE. 2012. Regulation of cytoplasmic mRNA decay. *Nature Reviews. Genetics* 13: 246–259.
- Skubák P, Pannu NS. 2013. Automatic protein structure solution from weak X-ray data. *Nature Communications* 4: 2777.
- Song M-G, Bail S, Kiledjian M. 2013. Multiple Nudix family proteins possess mRNA decapping activity. *RNA* 19: 390–399.
- Song M-G, Li Y, Kiledjian M. 2010. Multiple mRNA decapping enzymes in mammalian cells. *Molecular Cell* 40: 423–432.
- Srouji JR, Xu A, Park A, Kirsch JF, Brenner SE. 2017. The evolution of function within the Nudix homology clan. *Proteins* 85: 775–811.
- Stols L, Gu M, Dieckman L, Raffen R, Collart FR, Donnelly MI. 2002. A new vector for high-throughput, ligation-independent cloning encoding a tobacco etch virus protease cleavage site. *Protein Expression and Purification* 25: 8–15.
- Sun Y, Li P, Shen D, Wei Q, He J, Lu Y. 2019. The *Ralstonia solanacearum* effector RipN suppresses plant PAMP-triggered immunity, localizes to the endoplasmic reticulum and nucleus, and alters the NADH/NAD(+) ratio in *Arabidopsis*. *Molecular Plant Pathology* 20: 533–546.
- Supek F, Bošnjak M, Škunca N, Šmuc T. 2011. REVIGO summarizes and visualizes long lists of gene ontology terms. *PLoS ONE* 6: e21800.
- Tang Q, Liu C, Zhong C, Ding J. 2015. Crystal structures of *Arabidopsis thaliana* Nudix hydrolase NUDT7 reveal a previously unobserved conformation. *Molecular Plant* 8: 1557–1559.
- Terwilliger TC, Grosse-Kunstleve RW, Afonine PV, Moriarty NW, Zwart PH, Hung L-W, Read RJ, Adams PD. 2008. Iterative model building, structure refinement and density modification with the PHENIX AutoBuild wizard. *Acta Crystallographica. Section D, Biological Crystallography* 64: 61–69.
- Trésautes L, Lundbäck T, Welin M, Flodin S, Nyman T, Silvander C, Gräslund S, Nordlund P. 2015. Structural basis for the specificity of human NUDT16 and its regulation by inosine monophosphate. *PLoS ONE* 10: e0131507.

- Van Dijk E, Cougot N, Meyer S, Babajko S, Wahle E, Séraphin B. 2002. Human Dcp2: a catalytically active mRNA decapping enzyme located in specific cytoplasmic structures. *EMBO Journal* 21: 6915–6924.
- Ve T, Williams SJ, Catanzariti A-M, Rafiqi M, Rahman M, Ellis JG, Hardham AR, Jones DA, Anderson PA, Dodds PN *et al.* 2013. Structures of the flax-rust effector AvrM reveal insights into the molecular basis of plant-cell entry and effector-triggered immunity. *Proceedings of the National Academy of Sciences, USA* 110: 17594–17599.
- Wakamatsu T, Nakagawa N, Kuramitsu S, Masui R. 2008. Structural basis for different substrate specificities of two ADP-ribose pyrophosphatases from *Thermus thermophilus* HB8. *Journal of Bacteriology* 190: 1108–1117.
- Wang W, Barnaby JY, Tada Y, Li H, Tör M, Caldelari D, Lee DU, Fu XD, Dong X. 2011. Timing of plant immune responses by a central circadian regulator. *Nature* 470: 110–114.
- Wang Z, Jiao X, Carr-Schmid A, Kiledjian M. 2002. The hDcp2 protein is a mammalian mRNA decapping enzyme. *Proceedings of the National Academy of Sciences, USA* 99: 12663–12668.
- Waz S, Nakamura T, Hirata K, Koga-Ogawa Y, Chirifu M, Arimori T, Tamada T, Ikemizu S, Nakabeppu Y, Yamagata Y. 2017. Structural and kinetic studies of the human nudix hydrolase MTH1 reveal the mechanism for its broad substrate specificity. *Journal of Biological Chemistry* 292: 2785–2794.
- Westwood ML, O'Donnell AJ, de Bekker C, Lively CM, Zuk M, Reece SE. 2019. The evolutionary ecology of circadian rhythms in infection. *Nature Ecology and Evolution* 3: 552–560.
- Williams CJ, Headd JJ, Moriarty NW, Prisant MG, Videau LL, Deis LN, Verma V, Keedy DA, Hintze BJ, Chen VB *et al.* 2018. MolProbity: more and better reference data for improved all-atom structure validation. *Protein Science* 27: 293–315.
- Wu W, Nemri A, Blackman LM, Catanzariti A-M, Sperschneider J, Lawrence GJ, Dodds PN, Jones DA, Hardham AR. 2019. Flax rust infection transcriptomics reveals a transcriptional profile that may be indicative for rust Avr genes. *PLoS ONE* 14: e0226106.
- Wurm JP, Holdermann I, Overbeck JH, Mayer PH, Sprangers R. 2017. Changes in conformational equilibria regulate the activity of the Dcp2 decapping enzyme. *Proceedings of the National Academy of Sciences, USA* 114: 6034–6039.
- Xu A, Desai AM, Brenner SE, Kirsch JF. 2013. A continuous fluorescence assay for the characterization of Nudix hydrolases. *Analytical Biochemistry* 437: 178–184.
- Xu J, Yang J-Y, Niu Q-W, Chua N-H. 2006. Arabidopsis DCP2, DCP1, and VARICOSE form a decapping complex required for postembryonic development. *Plant Cell* 18: 3386–3398.
- Xu W, Dunn CA, Jones CR, D'Souza G, Bessman MJ. 2004. The 26 Nudix hydrolases of *Bacillus cereus*, a close relative of *Bacillus anthracis*. *The Journal of Biological Chemistry* 279: 24861–24865.
- Yang Q, Huai B, Lu Y, Cai K, Guo J, Zhu X, Kang Z, Guo J. 2020. A stripe rust effector Pst18363 targets and stabilises TaNUDX23 that promotes stripe rust disease. *New Phytologist* 225: 880–895.
- Yoshiba S, Ooga T, Nakagawa N, Shibata T, Inoue Y, Yokoyama S, Kuramitsu S, Masui R. 2004. Structural insights into the *Thermus thermophilus* ADP-ribose pyrophosphatase mechanism via crystal structures with the bound substrate and metal. *The Journal of Biological Chemistry* 279: 37163–37174.
- Yu D, Song W, Tan EYJ, Liu L, Cao Y, Jirschitzka J, Li E, Logemann E, Xu C, Huang S *et al.* 2022. TIR domains of plant immune receptors are 2',3'-cAMP/cGMP synthases mediating cell death. *Cell* 185: 2370–2386.
- Yu X, Li B, Jang G-J, Jiang S, Jiang D, Jang J-C, Wu S-H, Shan L, He P. 2019. Orchestration of processing body dynamics and mRNA decay in *Arabidopsis* immunity. *Cell Reports* 28: 2194–2205.
- Zha M, Zhong C, Peng Y, Hu H, Ding J. 2006. Crystal structures of human NUDT5 reveal insights into the structural basis of the substrate specificity. *Journal of Molecular Biology* 364: 1021–1033.

Supporting Information

Additional Supporting Information may be found online in the Supporting Information section at the end of the article.

Fig. S1 Structural features of AvrM14.

Fig. S2 Western blots demonstrating the expression and accumulation of the AvrM14 wild-type (WT) and mutant proteins in agroinfiltrated plant tissue.

Fig. S3 Mutation of Nudix-box glutamate E82 to glutamine does not alter the recognition of AvrM14-A or AvrM14-B by M1 when co-expressed in tobacco.

Fig. S4 Recombinant AvrM14 proteins elute as two distinct peaks during size-exclusion chromatography (SEC); all AvrM14 crystal structures display similar self-association interfaces.

Fig. S5 AvrM14-B crystal packing dimer (A, purple) compared with homodimeric *Homo sapiens* Nudt16 (PDB ID: 3MGM) (B, gold) with the Nudix helices coloured green.

Fig. S6 Screening of common Nudix hydrolase substrates using monomeric and homodimeric AvrM14 protein.

Fig. S7 Migration and Rf values for standard solutions of potential mRNA-decapping products.

Fig. S8 Identifying stable multimeric AvrM14 protein complexes from *Nicotiana benthamiana* protein extracts.

Fig. S9 Size-exclusion chromatograms displaying the elution profile of each of the AvrM14 homologues assessed in our study.

Fig. S10 Average expression level (\pm SD) in transcripts per million for AvrM14 genes in each of the RNA-sequencing datasets.

Fig. S11 Co-expression of AvrM14 wild-type and mutant proteins with M1 in tobacco.

Fig. S12 Expression of wild-type and mutant AvrM14 proteins in M1 and M4 flax.

Methods S1 Extended Materials and Methods.

Table S1 DNA and protein sequences used in this study.

Table S2 Crystallography data collection and structure refinement statistics.

Table S3 Substrates and secondary enzymes used in the phosphate sensing fluorophore-based hydrolysis assays with recombinant AvrM14-A.

Table S4 Average read counts with standard deviations in TPM as determined by Salmon, the differential expression (DE) analysis output (\log_2 fc and *q*-values) as determined by fishpond when comparing the AvrM14-A and vector-only datasets and the BLAST-2-Go best hit for all transcripts.

Table S5 Average read counts with standard deviations in TPM as determined by Salmon, the differential expression (DE) analysis output ($\log_2\text{fc}$ and q -values) as determined by fishpond when comparing the AvrM14-A and AvrM14-AE82Q datasets, and the BLAST-25Go best hit for all transcripts.

Table S6 Summary of the cell-death results recorded during this study following the expression of various AvrM14 proteins in M1 flax, M4 flax and tobacco co-expressing M1.

Please note: Wiley is not responsible for the content or functionality of any Supporting Information supplied by the authors. Any queries (other than missing material) should be directed to the *New Phytologist* Central Office.

See also the Commentary on this article by [Banfield, 239: 7–9](#).

New Phytologist Supporting Information

Article title: A rust-fungus Nudix hydrolase effector decaps mRNA *in vitro* and interferes with plant immune pathways

Authors: Carl L. McCombe, Ann-Maree Catanzariti, Julian R. Greenwood, Anna M. Desai, Megan A. Outram, Daniel S. Yu, Daniel J. Ericsson, Steven E. Brenner, Peter N. Dodds, Bostjan Kobe, David A. Jones and Simon J. Williams

Article acceptance date: 02 January 2023

The following Supporting Information is available for this article:

Extended Materials and Methods

Fig. S1 Structural features of AvrM14.

Fig. S2 Western blots demonstrating the expression and accumulation of the AvrM14 wild-type (WT) and mutant proteins in agroinfiltrated plant tissue.

Fig. S3 The mutation of Nudix box glutamate E82 to glutamine does not alter the recognition of AvrM14-A or AvrM14-B by M1 when co-expressed in tobacco.

Fig. S4 Recombinant AvrM14 proteins elute as two distinct peaks during size-exclusion chromatography (SEC); all AvrM14 crystal structures display similar self-association interfaces.

Fig. S5 The AvrM14-B crystal packing dimer (A, purple) compared to homodimeric *Homo sapiens* Nudt16 (PDB ID: 3MGM) (B, gold) with the Nudix helices coloured green.

Fig. S6 Screening of common Nudix hydrolase substrates using monomeric and homodimeric AvrM14 protein.

Fig. S7 The migration and Rf values for standard solutions of potential mRNA decapping products.

Fig. S8 Identifying stable multimeric AvrM14 protein complexes from *N. benthamiana* protein extracts.

Fig. S9 Size-exclusion chromatograms displaying the elution profile of each of the AvrM14 homologues assessed in our study.

Fig. S10 The average expression level (\pm SD) in transcripts per million for AvrM14 genes in each of the RNA-Sequencing datasets.

Fig. S11 Co-expression of AvrM14 wild-type and mutant proteins with M1 in tobacco.

Fig. S12 Expression of wild-type and mutant AvrM14 proteins in M1 and M4 flax.

Table S1 DNA and protein sequences used in this study.

Table S2 Crystallography data collection and structure refinement statistics.

Table S3 The substrates and secondary enzymes used in the phosphate sensing fluorophore-based hydrolysis assays with recombinant AvrM14-A.

Table S4 The average read counts with standard deviations in TPM as determined by Salmon, the differential expression analysis output (log2fc and q-values) as determined by fishpond when comparing the AvrM14-A and vector only datasets, and the blast-2-go best hit for all transcripts.

Table S5 The average read counts with standard deviations in TPM as determined by Salmon, the differential expression analysis output (log2fc and q-values) as determined by fishpond when comparing the AvrM14-A and AvrM14-AE82Q datasets, and the blast-2-go best hit for all transcripts.

Table S6 Summary of the cell death results recorded during this study following the expression of various AvrM14 proteins in M1 flax, M4 flax, and tobacco co-expressing M1.

Extended Materials and Methods:

Protein production

Recombinant *HsNudt16* protein was purchased from Abcam (Cambridge, United Kingdom). All other proteins were expressed in *E. coli* BL21 (DE3) cells using ZYP-5052 (AvrM14 wild-type and mutant proteins) or ZYM-5052 (*Melampsora* homologues) autoinduction media (Studier, 2005). Cells were grown by continuous shaking at 37°C until the OD_{600nm} reached 0.6 – 0.8. The temperature was then dropped to 18°C and incubated with shaking for another 18 hours. The cells were harvested by centrifugation and resuspended in lysis buffer containing 50 mM HEPES pH 7 (Ma941940, Mlp68167) or 8 (AvrM14-A, AvrM14-B, AvrM14-A^{E82Q}, AvrM14-B^{E82Q}, Map1753746, Mm958639), 150 mM NaCl, and 1 mM DTT. Cells were lysed using sonication and cellular debris pelleted by centrifugation. The resulting supernatant was applied to a 5 mL HisTrap FF crude column (Cytiva, Marlborough, Massachusetts). To remove loosely bound proteins, the column was washed with the lysis buffer containing 30 mM imidazole. The remaining bound proteins were eluted with a continuous gradient of imidazole from 30 mM to 250 mM over 10 minutes, using an Äkta pure chromatography system. Fractions were analysed by Coomassie-stained SDS-PAGE and fractions containing the protein of interest were pooled and buffer exchanged to remove the imidazole before the addition of recombinant 6xHis-tagged TEV (AvrM14 proteins) or 3C protease (*Melampsora* homologs) for overnight tag cleavage at 4°C. Protease cleavage was confirmed via SDS-PAGE and the protein solution reapplied to the HisTrap FF column to remove the protease, cleaved 6xHis tag, and any other contaminants. Proteins were then purified further by SEC using a HiLoad 26/600 Superdex® 75 pg column (Cytiva) pre-equilibrated with 10 mM HEPES pH 7 (Ma941940, Mlp68167) or 8 (AvrM14-A, AvrM14-B, AvrM14-A^{E82Q}, AvrM14-B^{E82Q}, Map1753746, Mm958639), 150 mM NaCl, and 1 mM DTT using an Äkta pure chromatography system (Cytiva). After SEC, fractions containing the protein of interest were identified using SDS-PAGE and concentrated using Amicon® Ultra Centrifugal filters (Merck, Darmstadt, Germany) before storage at -80 °C.

In planta oligomeric state analysis (relates to Fig. S8)

N. benthamiana tissue 4-days post agroinfiltration with either the pEG102 AvrM14-A, pEG102 AvrM14-B or a pEG102 empty vector construct, was ground in liquid nitrogen to a fine powder.

The powder was combined with an equal volume of protein extraction buffer (25 mM Tris-HCl (pH 7.5), 1 mM EDTA, 2% w/v PVPP, 5 mM DTT, 1 mM PMSF, and 1X cOmplete protease inhibitor) and thoroughly mixed. Insoluble material was pelleted by centrifugation. The supernatant was concentrated to 25% of the starting volume using 10kDa Amicon® Ultra centrifugal filters (Merck). The solution was filtered and then passed over a S75 10/300 analytical size-exclusion chromatography column equilibrated in buffered solution (10 mM HEPES pH 8.0, 150 mM NaCl, and 1 mM DTT). Immunoblot analysis as described above was completed on the elution fractions to detect AvrM14 protein.

RNA sequencing analysis

Reads were aligned to the flax reference genome (Lusitatissimum_200_BGIv1.0.fa) (Wang *et al.*, 2012) using Hisat2 (Kim *et al.*, 2019). Sequence alignment map files (.sam) were sorted and converted to binary format (.bam) using samtools (Danecek *et al.*, 2021). Transcripts were assembled using Scallop2 (Zhang *et al.*, 2021). Reference annotations in General Feature Format (.gff3) were converted to General Transfer Format (.gtf) using gffread (Pertea & Pertea, 2020) and were merged with the Scallop2 annotations for all samples using stringtie (Pertea *et al.*, 2015). Unique transcripts that were not present in the reference annotation were identified using gff compare and were separated into a new .gtf file using gtcuff. The sequences of unique transcripts were extracted from the reference genome using gffread and then merged with the reference transcript file. This transcriptome was used for read quantification.

To aid in data analysis, each transcript was compared against the *Arabidopsis* TAIR10 protein list using Blast2GO within OmicsBox (v2.0) to provide a functional annotation (e-value cutoff: 1.0E-25, minimum length of match 50 amino acids) (the best hit for each transcript is available in Supplementary Table S4 and S5).

Salmon (v1.6.0) was used for transcript quantification following recommended procedures for the mapping-based mode (Patro *et al.*, 2017). First, a decoy transcriptome was created using our transcriptome and the entire flax genome (Wang *et al.*, 2012) (v1.0). A Salmon index was then generated using the recommended kmer length of 31. The quant command was used to quantify reads for each dataset using the generated index with validateMappings and gcBias flags activated and numGibbsSamples set to 20. Differential expression analysis was then completed using Swish within the fishpond R package (v1.8.0) (Zhu *et al.*, 2019), utilising tximeta (v1.10) (Love *et al.*, 2020) for data importation, the seed value was set to 1, and only transcripts with at least 10 reads

for three of the replicates for both conditions were analysed, as recommended by the developers (see output log2fc, p- and q-values in Supplementary Tables S4 and S5, transcripts excluded from DE analysis have no values listed in these columns). Gene ontology (GO) enrichment analysis using the Gene Ontology online resource (Ashburner *et al.*, 2000; Consortium, 2020) and Panther Overrepresentation Test (v16) (Mi *et al.*, 2020), was completed on the significantly upregulated (q value < 0.05; log2fc > 0.5) and downregulated (q value < 0.05 and log2fc < -0.5) groups of transcripts (using the gene name of the *Arabidopsis* homologue from the Blast2GO results and *Arabidopsis* as the reference organism). GO biological processes were overrepresented when the FDR was < 0.05. REVIGO (Supek *et al.*, 2011) was used to remove redundant GO terms.

Fig. S1 Structural features of AvrM14. Cartoon representation of the crystal structure of AvrM14-B, with key residues displayed in stick representation. (a) The unusual 3_{10} -helix (red) present in AvrM14's Nudix-box region. (b) The salt bridge observed between E⁷¹ and R⁸¹, with the hydrogen bonds displayed as yellow dashed lines. (c) The putative metal-ion binding glutamates (E⁸², E⁸⁵, E⁸⁶) of AvrM14-B (purple) superimposed onto the structure of a Mg²⁺ bound ADPR-hydrolysing Nudix enzyme (green; PDB ID: 1KHZ).

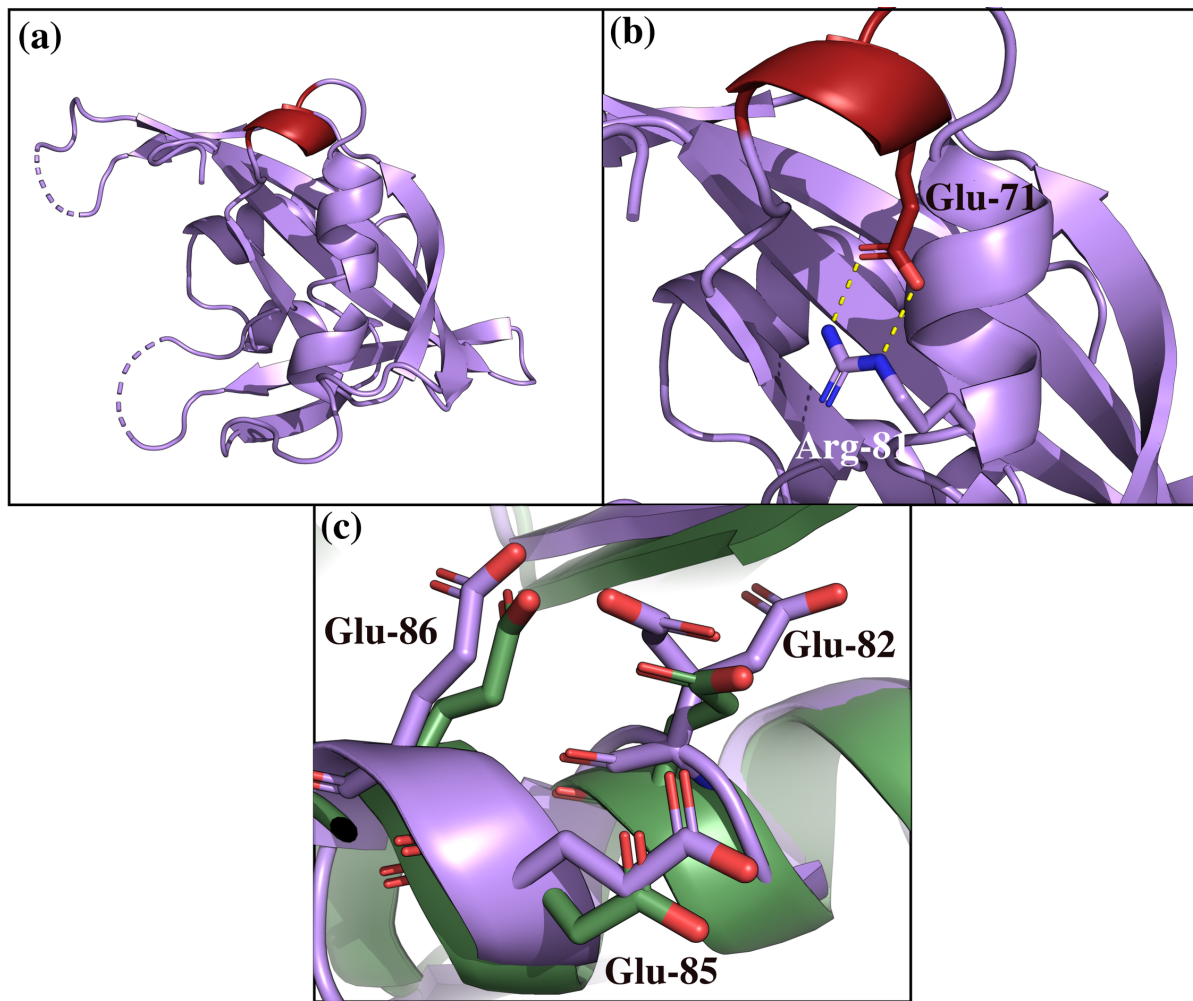


Fig. S2 Western blots demonstrating the expression and accumulation of the AvrM14 wild-type (WT) and mutant proteins in agroinfiltrated plant tissue. Total protein extracts from *Nicotiana tabacum* leaf tissue agroinfiltrated with a construct to express a YFP-tagged AvrM14 protein or with an empty pEG104 vector, were analysed by western blotting. Mouse anti-GFP (Roche) and goat anti-mouse-HRP (Amersham) were used as the primary and secondary antibodies, respectively. Ponceau S staining shows protein loading. The numbers on the left of each blot indicate the sizes of molecular weight markers. The top row of blots are AvrM14-A protein variants, and the bottom row of blots are AvrM14-B protein variants, the expected size of YFP-tagged AvrM14 is approximately 44 kDa.

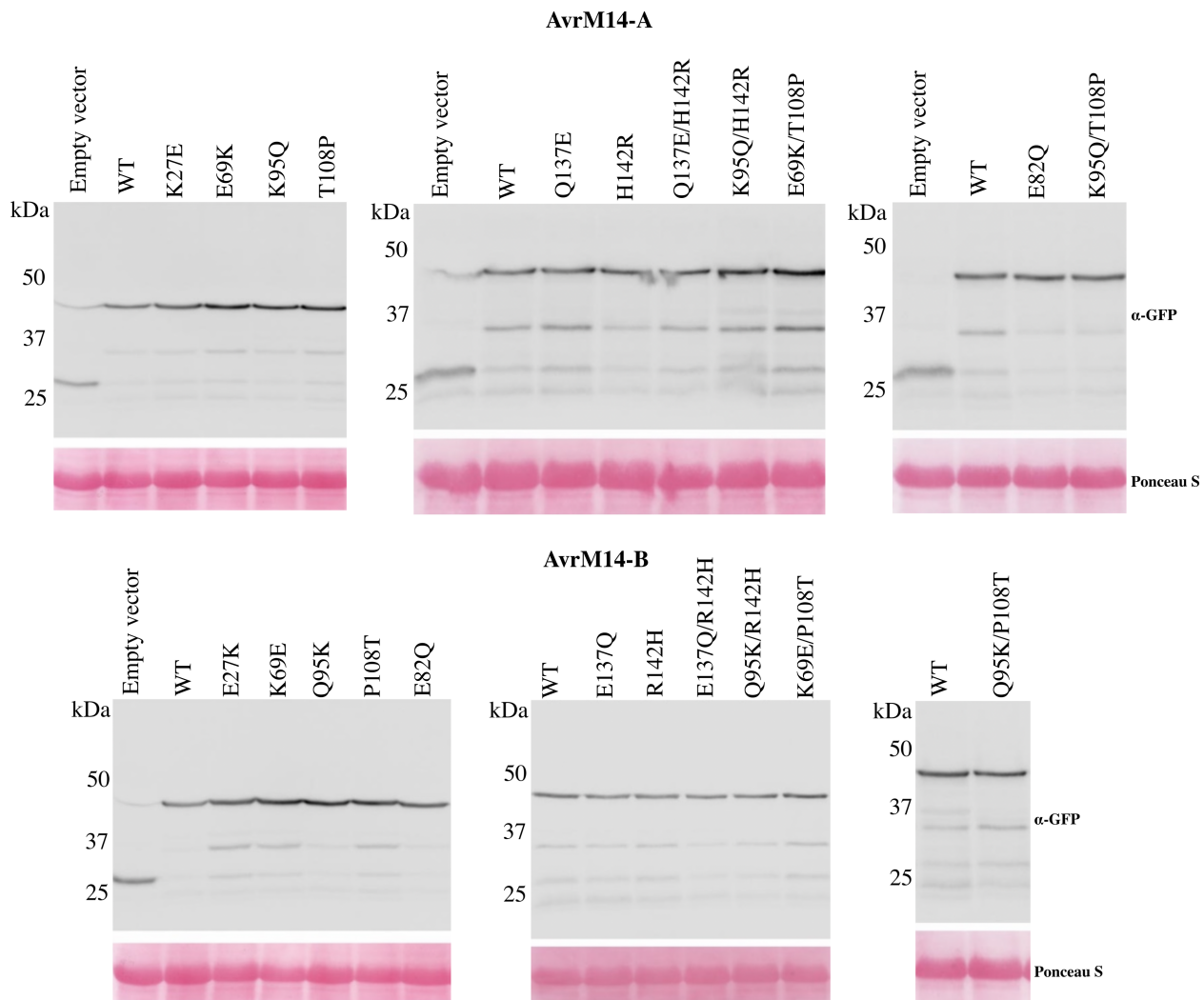


Fig. S3 The mutation of Nudix box glutamate E82 to glutamine does not alter the recognition of AvrM14-A or AvrM14-B by M1 when co-expressed in tobacco. (a) *Nicotiana tabacum* leaf sections were agroinfiltrated with a construct to express either M1, AvrM14-A, AvrM14-B, AvrM14-A^{E82Q} or AvrM14-B^{E82Q}. (b) *N. tabacum* leaf sections were co-agroinfiltrated with M1 and one of the AvrM14 constructs. Each leaf section is labelled with the name/s of the agroinfiltrated construct/s. Both leaves were imaged 6 days post-infiltration. The infiltrations were repeated 5 times with similar results obtained.

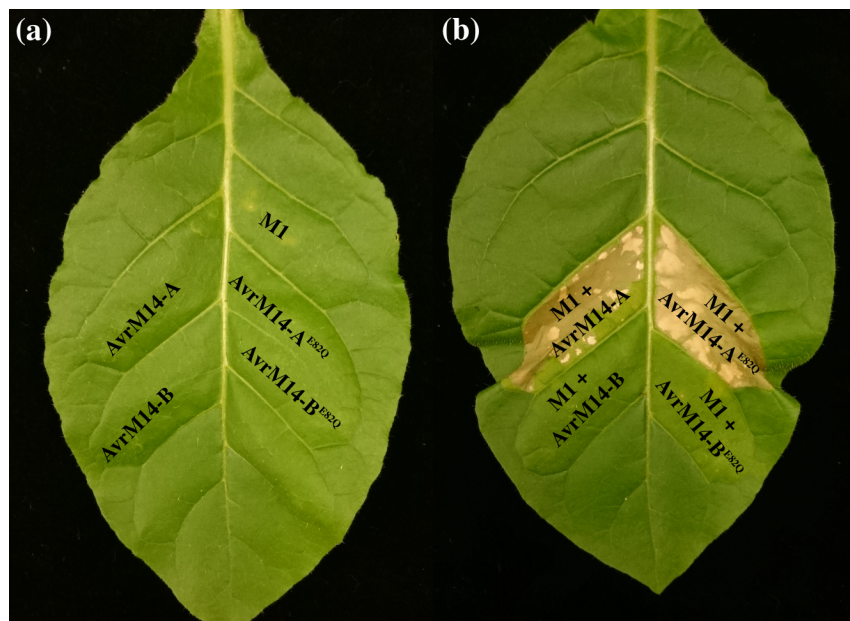


Fig. S4 Recombinant AvrM14 proteins elute as two distinct peaks during size-exclusion chromatography (SEC); all AvrM14 crystal structures display similar self-association interfaces.

(a) Size-exclusion chromatograms displaying the elution profile of each recombinant AvrM14 protein purified during this study. The green and purple shading indicate the peak representing monomeric and homodimeric protein, respectively. (b) Coomassie-stained SDS-PAGE analysis demonstrating the purity of the monomeric and homodimeric wild-type AvrM14 protein samples. (c) The crystal structures of monomeric AvrM14-A (left), AvrM14-B (middle) and homodimeric AvrM14-B (right) in cartoon form, demonstrating the similarities between the crystal packing dimers and the domain-swapped dimer. A zoomed-in view of the common dimeric interface observed in both AvrM14-B structures is shown in the middle, with the aromatic residues (F⁸⁹, F¹³⁸, and W¹⁴⁰) displayed as sticks.

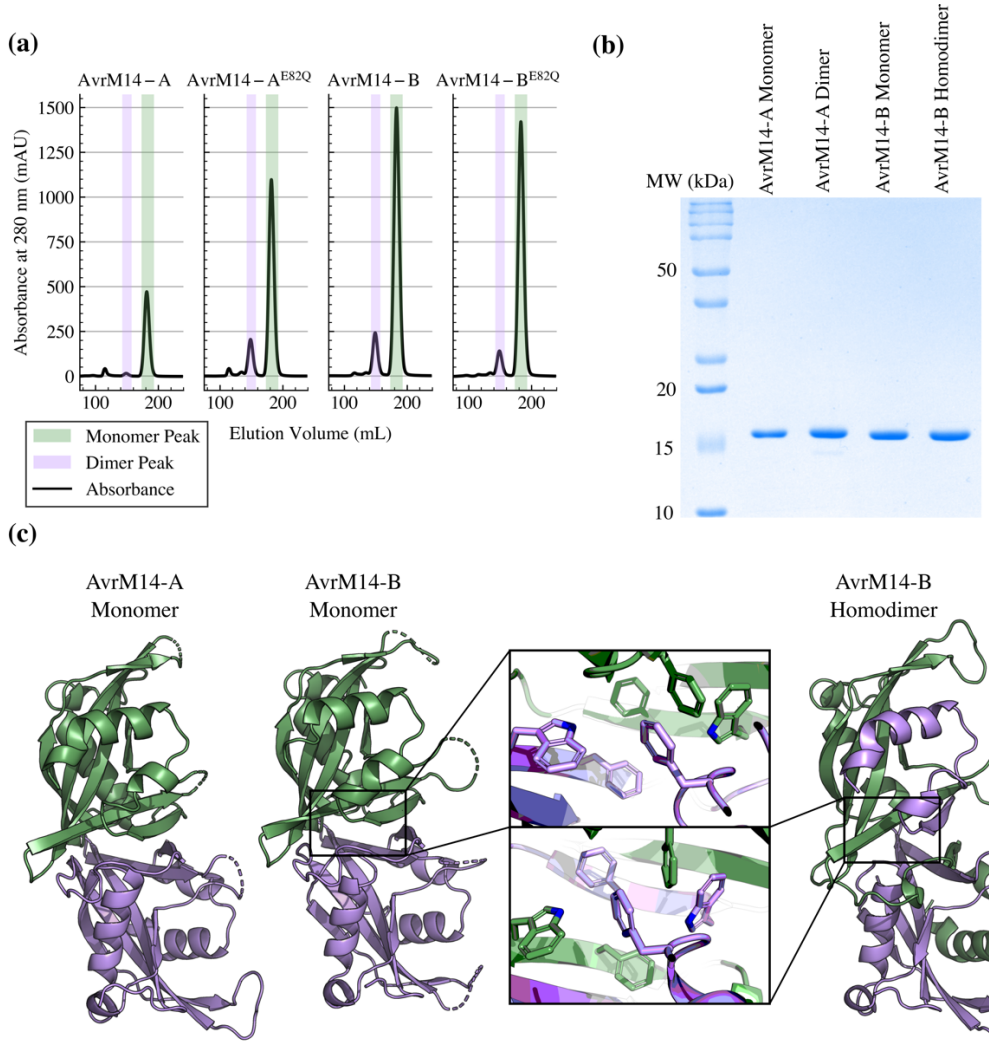


Fig. S5 The AvrM14-B crystal packing dimer (A, purple) compared to homodimeric *Homo sapiens* Nudt16 (PDB ID: 3MGM) (B, gold) with the Nudix helices coloured green.

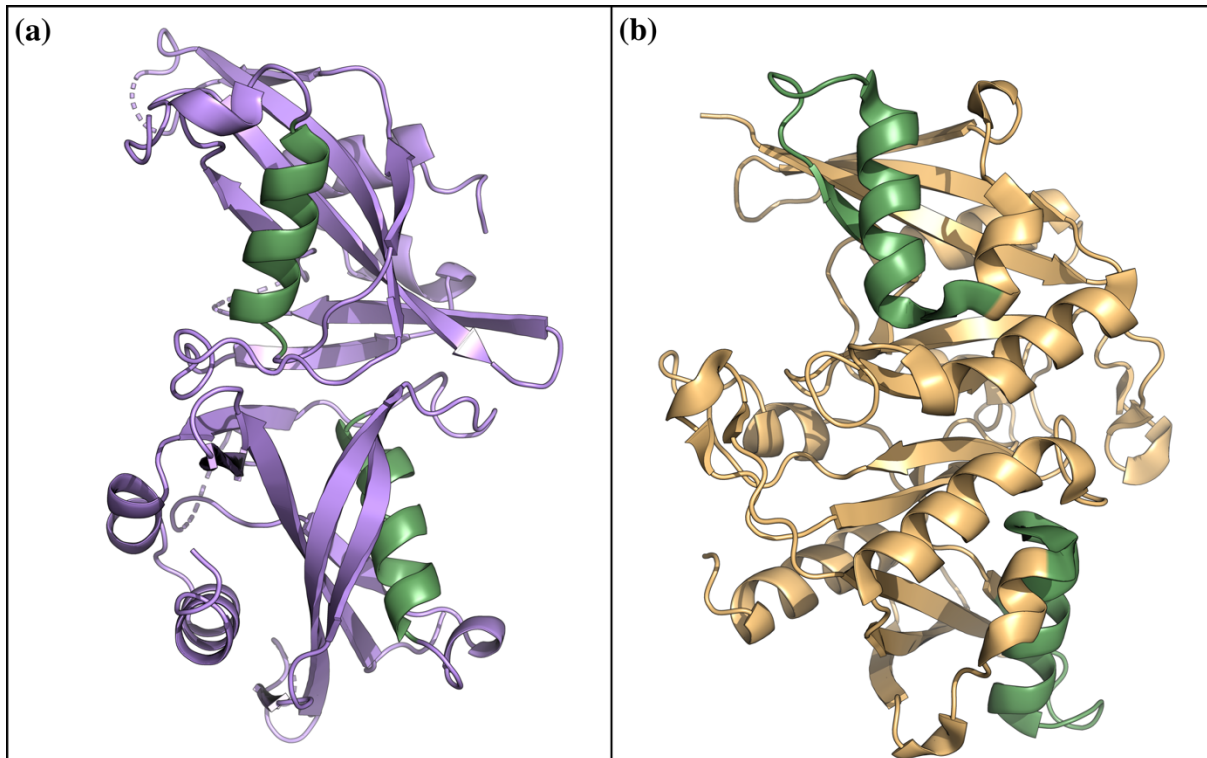


Fig. S6 Screening of common Nudix hydrolase substrates using monomeric and homodimeric AvrM14 protein. Recombinant AvrM14 monomeric and homodimeric proteins were incubated in a reaction buffer with potential substrate at 2 mM concentration for 30 minutes at 37 °C. Substrate hydrolysis was detected via the production of a blue-coloured phosphomolybdate complex that absorbs light with a wavelength of 820 nm; presented as mean absorbance \pm standard deviation ($n = 5$). A buffer only control without any Nudix hydrolase protein was used to blank the spectrophotometer before measurement. Recombinant AtNUDX7 and AtNUDX7^{E154Q} were used as positive and negative controls, respectively; the substrate hydrolysed is indicated at the top of each subplot.

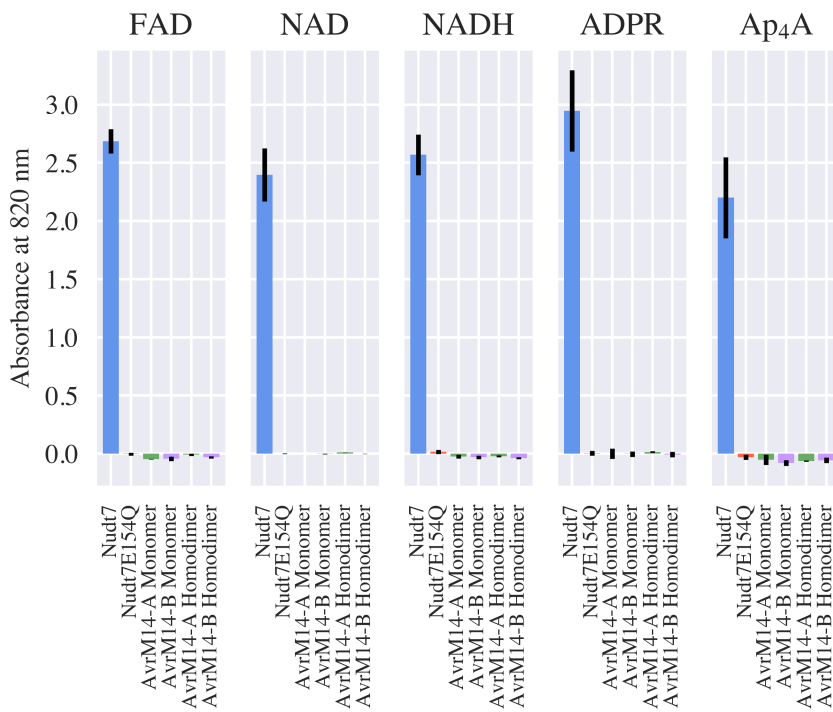
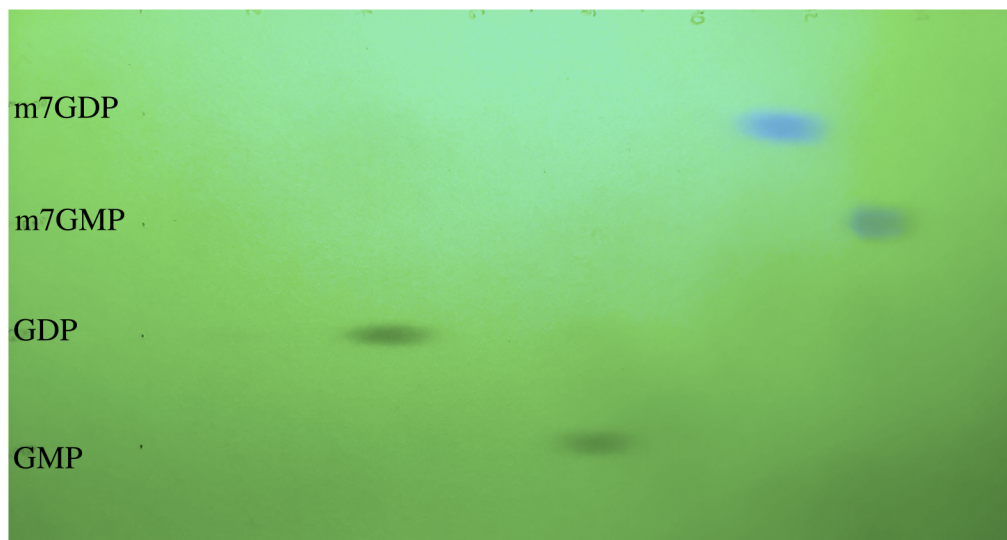


Fig. S7 The migration and Rf values for standard solutions of potential mRNA decapping products. (a) A thin-layer chromatography plate demonstrating the migration of standard solutions of m^7 GDP, m^7 GMP, GDP, and GMP. The plate was illuminated with 254 nm light to enable visualisation of the standards. (b) The migration of each standard was used to determine an Rf value. The mean Rf value from three replicates is listed.

(a)



(b)

Standard	Mean Rf Value
GMP	0.475
GDP	0.245
m^7 GMP	0.784
m^7 GDP	0.676

Fig. S8 Identifying stable multimeric AvrM14 protein complexes from *N. benthamiana* protein extracts. *Nicotiana benthamiana* leaves were infiltrated with *Agrobacterium* (GV3101) harbouring either an empty vector (pEG102) or pEG102 constructs encoding untagged AvrM14-A or AvrM14-B expressed under the 35S promoter from the cauliflower mosaic virus. At four days post-infiltration (dpi) leaf tissue was collected and total soluble protein was extracted. The protein solutions were loaded over a S75 10/300 analytical size-exclusion chromatography column. (a) The elution profile of the protein extract from plants transformed with AvrM14-A (red), AvrM14-B (gold), and the empty vector (blue). The peaks observed with purified recombinant AvrM14 monomeric and homodimeric under the same chromatography conditions are displayed in green and purple, respectively. (b) Immunoblot analysis with antibodies raised against AvrM14 was completed to determine the volume at which AvrM14 proteins were eluting from the column, from the plant tissue transformed with AvrM14-A (top), AvrM14-B (middle), and the empty vector (bottom). In all blots the lanes labelled with an 'A' contain 50 ng of recombinantly purified AvrM14-A and lanes labelled with a 'B' contain the plant protein extract before it was loaded onto the column. The numbers above the lanes indicate the elution volume of each fraction, as labelled on the chromatogram in (a).

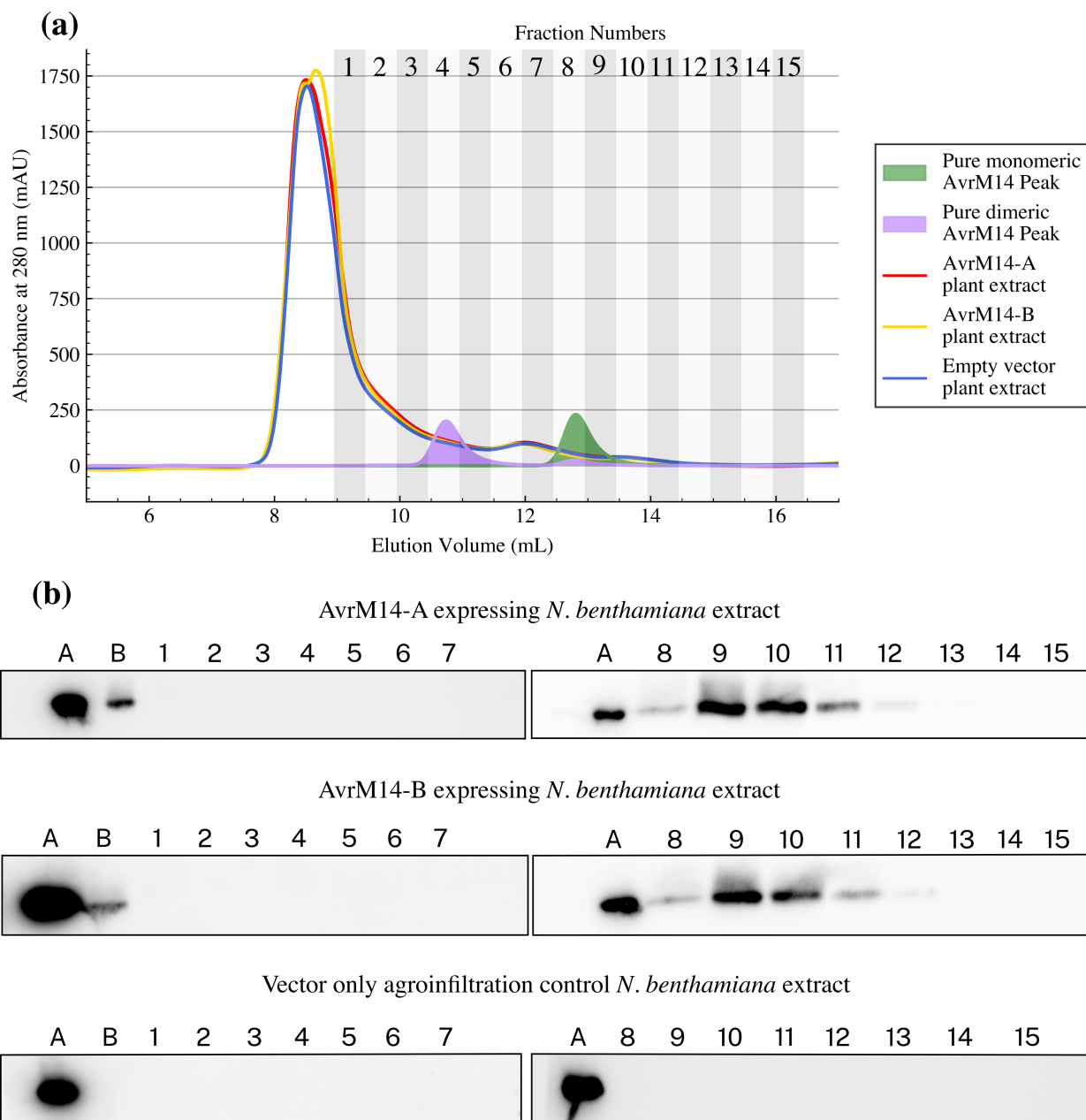


Fig. S9 Size-exclusion chromatograms displaying the elution profile of each of the AvrM14 homologues assessed in our study. For comparison, the elution volumes of monomeric and homodimeric AvrM14, using the same Superdex S75 26/600 column, are indicated by green and purple shading, respectively.

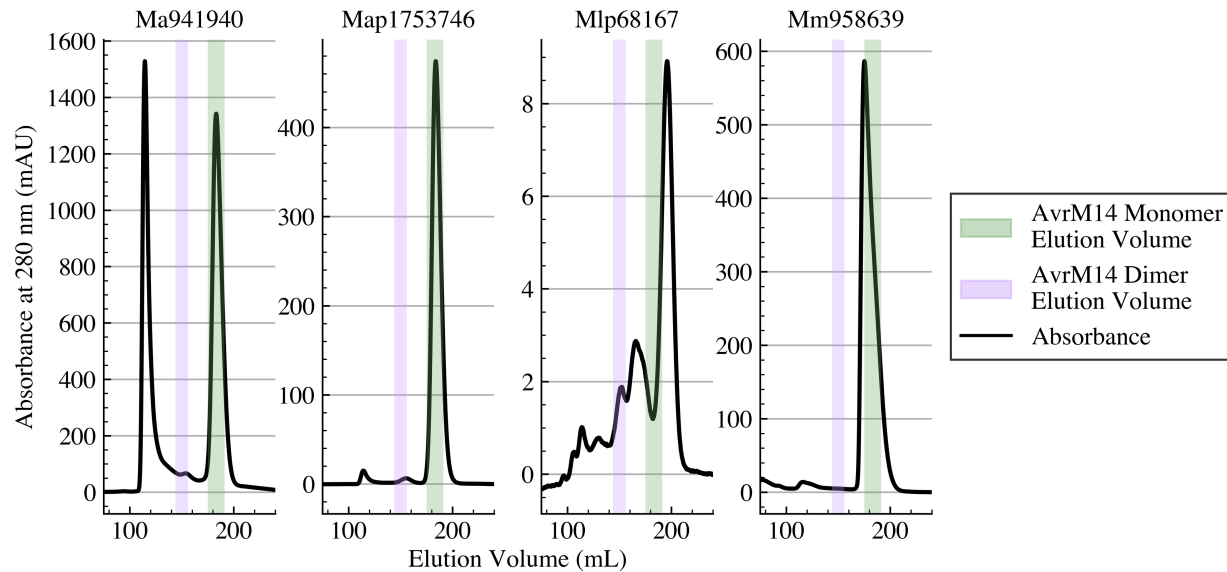


Fig. S10 The average expression level (\pm SD) in transcripts per million for AvrM14 genes in each of the RNA-Sequencing datasets.

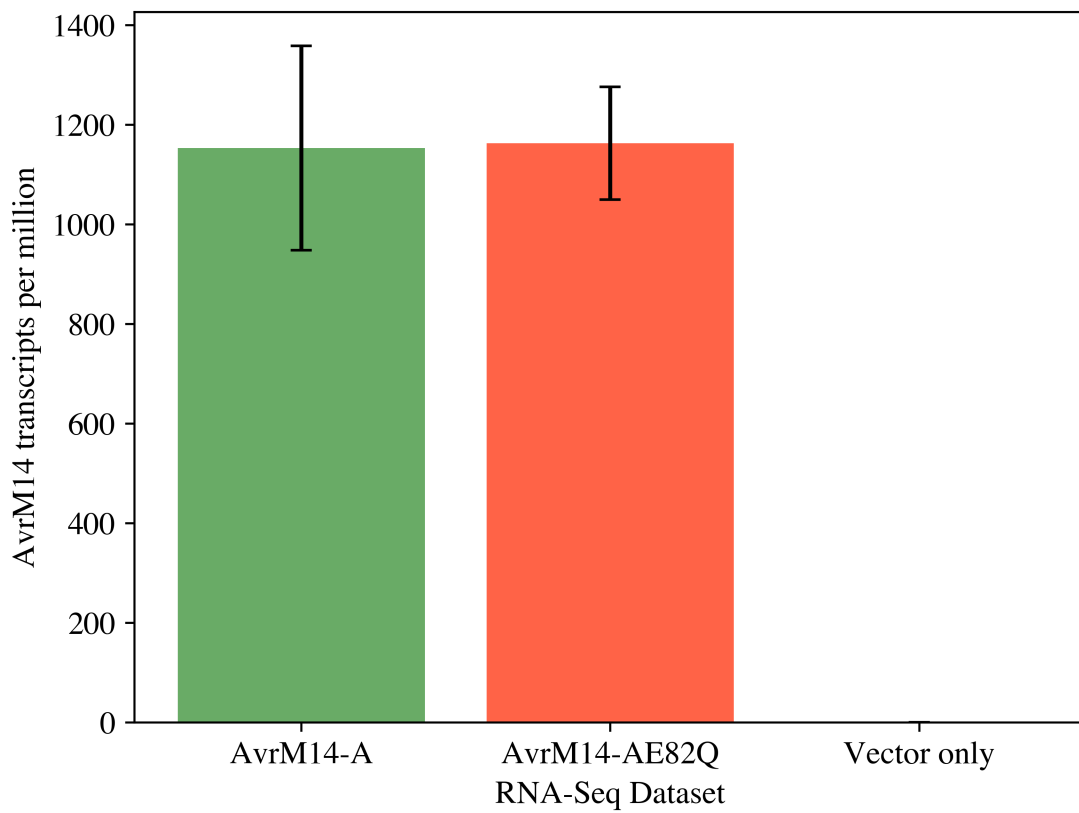


Fig. S11 Co-expression of AvrM14 wild-type and mutant proteins with M1 in tobacco. *Nicotiana tabacum* leaf sections were co-agroinfiltrated with a construct to express M1 and an AvrM14-A or AvrM14-B protein variant. The label on each leaf section indicates the AvrM14 protein being expressed as per the table below the images (e.g., the leaf section labelled with A-3 is expressing M1 and AvrM14-A^{E69K}, whereas the leaf section labelled with B-8 is expressing M1 and AvrM14-B^{E137Q/R142H}). The images shown are a representative result from between 4 to 15 replicates for each construct.



Label	Protein co-infiltrated with M1
A-1 / B-1	AvrM14-A / AvrM14-B
A-2 / B-2	AvrM14-A ^{K27E} / AvrM14-B ^{E27K}
A-3 / B-3	AvrM14-A ^{E69K} / AvrM14-B ^{K69E}
A-4 / B-4	AvrM14-A ^{K95Q} / AvrM14-B ^{Q95K}
A-5 / B-5	AvrM14-A ^{T108P} / AvrM14-B ^{P108T}
A-6 / B-6	AvrM14-A ^{Q137E} / AvrM14-B ^{E137Q}
A-7 / B-7	AvrM14-A ^{H142R} / AvrM14-B ^{R142H}
A-8 / B-8	AvrM14-A ^{Q137E/H142R} / AvrM14-B ^{E137Q/R142H}
A-9 / B-9	AvrM14-A ^{K95Q/H142R} / AvrM14-B ^{Q95K/R142H}
A-10 / B-10	AvrM14-A ^{E69K/T108P} / AvrM14-B ^{K69E/P108T}
A-11 / B-11	AvrM14-A ^{K95Q/T108P} / AvrM14-B ^{Q95K/P108T}

Fig. S12 Expression of wild-type and mutant AvrM14 proteins in *M1* and *M4* flax. Bison x M1 (Williston Brown) or M4 (Victory 'A') flax (*Linum usitatissimum*) lines were agroinfiltrated with a construct encoding either a wild-type (WT) or mutant AvrM14 protein. Multiple leaves from two or three independent plants were infiltrated with each construct. The agroinfiltrated leaves were photographed between 5 to 7 days post-infiltration to assess the cell-death response. Plants agroinfiltrated at the same time under identical conditions have been grouped together. Each group includes plants expressing WT AvrM14-A and AvrM14-B for comparison to the mutant constructs in the same group. The flax line being infiltrated is indicated at the top of each group; plants infiltrated with AvrM14-A variants are on the left and plants infiltrated with AvrM14-B variants are on the right. Whether the protein being expressed is WT or the identity of the residue/s mutated is listed on the far left of each group of images. For a summary of these results please see Supplementary Table 6.

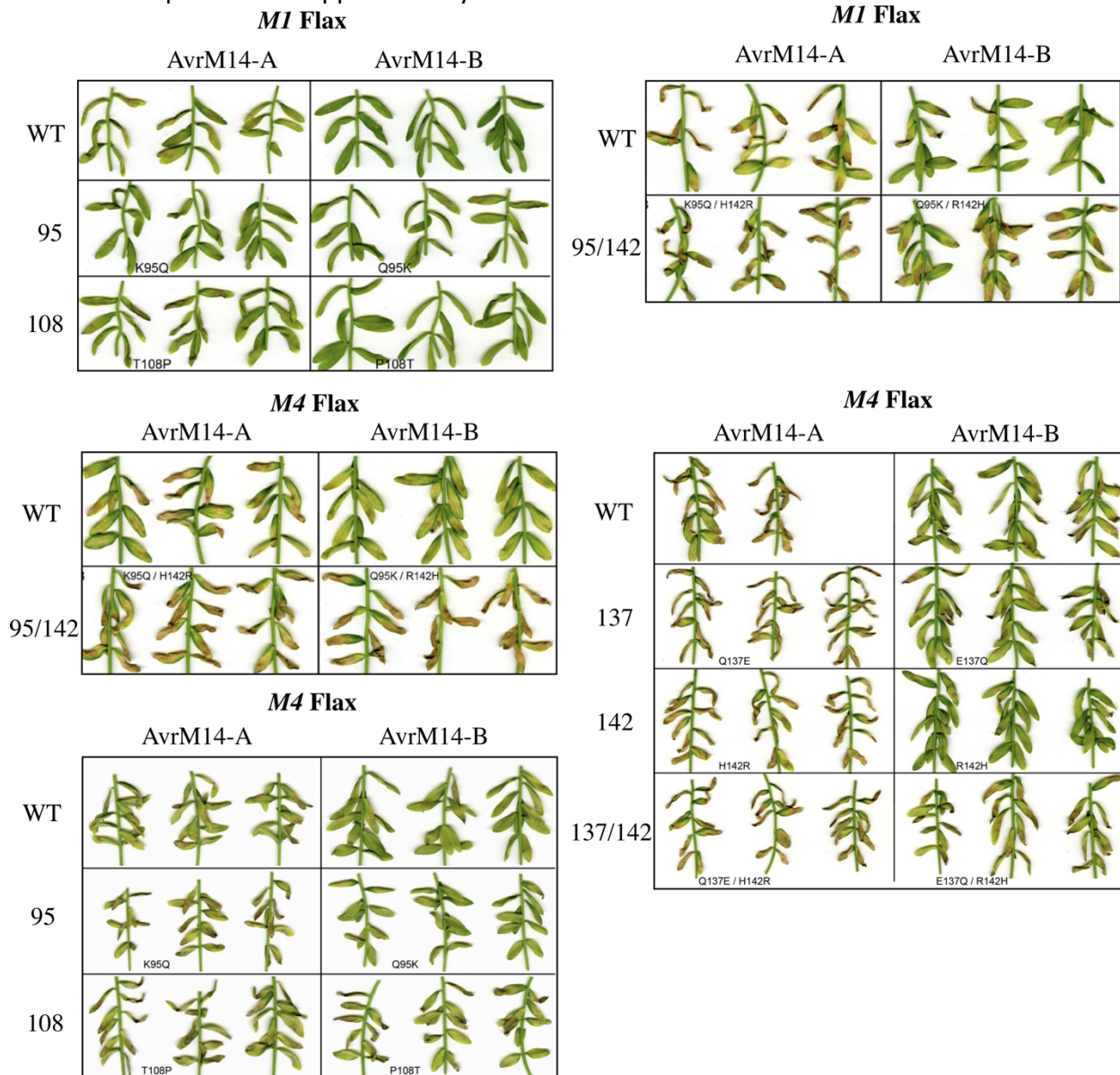


Table S1 DNA and protein sequences used in this study (see table S1.csv).

Table S2 Crystallography data collection and structure refinement statistics.

Protein	AvrM14-A		AvrM14-B Monomer	AvrM14-B Homodimer
	Bromide soak (SAD)	Native (MR)	Native (MR)	Native (MR)
Data collection				
Detector	ADSC-QUANTUM 315R	ADSC-QUANTUM 315R	Dectris Eiger X 16M	Dectris Eiger X 16M
Wavelength (Å)	0.9197	0.9537	0.9537	0.9537
Space group	P 21 21 21	P 21 21 21	P 61 2 2	P 41 21 2
a, b, c (Å)	38.645 63.241 167.195	37.645 166.842 62.911	80.059 80.059 293.949	79.663 79.663 201.317
α, β, γ (°)	90 90 90	90 90 90	90 90 120	90 90 90
Resolution (Å)	41.81 - 2.25 (2.33-2.25)	41.71 - 2.30 (2.38 - 2.30)	44.84 - 1.76 (1.82 - 1.76)	35.63 - 1.84 (1.90 - 1.84)
Total no. of reflections	383680 (32940)	108010 (10816)	1298084 (128096)	630813 (60186)
No. of unique reflections	20265 (1811)	18412 (1793)	56341 (5485)	57219 (5572)
Completeness (%)	99.9 (98.9)	99.8 (100)	99.9 (99.0)	99.5 (96.4)
Multiplicity	18.9 (18.2)	5.9 (6.0)	23.0 (23.4)	11.0 (10.8)
Anomalous completeness	99.8 (97.9)	-	-	-
Anomalous multiplicity	10.2 (9.6)	-	-	-
Mean I / s(I)	21.7 (4.3)	10.5 (2.4)	31.9 (4.2)	16.3 (0.8)
Rmerge (%)	0.125 (0.798)	0.160 (0.804)	0.068 (0.763)	0.089 (2.867)
Rmeas (%) ^c	0.128 (0.821)	0.175 (0.879)	0.070 (0.779)	0.0929 (3.008)
Rpim (%) ^d	0.029 (0.19)	0.070 (0.349)	0.015 (0.159)	0.028 (0.895)
CC _{1/2} ^b	0.99 (0.94)	0.99 (0.72)	1 (0.94)	1 (0.48)
Matthews coefficient (Å ³ Da ⁻¹) ^e	1.98	1.98	4.09	4.80
Phasing statistics determined by Crank2e				
No. of sites identified	24	-	-	-
Over all figure of merit (FOM)	0.286	-	-	-
FOM after density modification	0.649	-	-	-
Refinement				
Resolution range (Å)		41.71 - 2.30 (2.38 - 2.30)	44.84 - 1.76 (1.82 - 1.76)	35.63 - 1.84 (1.90 - 1.84)
R _{work} (%) ^g		18.3 (22.5)	17.7 (28.3)	19.0 (32.5)

$R_{\text{free}} (\%)^{\text{h}}$		25.15 (31.15)	20.14 (34.90)	22.14 (37.76)
No. of non-H atoms				
Total		3326	2438	2286
- Protein		3193	2162	2145
- Ligand		-	25	15
- Water		108	251	126
Average B -factor (\AA^2)		37.5	31.8	48.37
R.m.s.d. from ideal geometry				
Bond lengths (\AA)		0.008	0.009	0.010
Bond angles ($^{\circ}$)		0.982	0.990	0.960
Ramachandran plot, residues in (%) ⁱ				
Favoured regions		98.7	98.8	99.6
Additionally allowed regions		1.3	1.2	0.4
Outlier regions		0	0	0

Table S3 The substrates and secondary enzymes used in the phosphate sensing fluorophore-based hydrolysis assays with recombinant AvrM14-A.

Group	Substrate/s	Secondary enzyme
1	ADP-ribose GDP-glucose GDP-mannose	APase
2	CDP-choline CDP-glycerol TDP-glucose UDP-acetylglucosamine UDP-glucose	APase
3	Ap ₃ A Ap ₄ A Ap ₅ A Ap ₄ G	APase
4	Ap ₄ U Ap ₄ dT Ap ₅ G	APase
5	Gp ₂ G Gp ₃ G Gp ₅ G m ⁷ Gp ₃ C	APase
6	FAD Deamino-NAD ⁺ NAD ⁺ NADH	APase
7	N6-Me-ATP N1-Me-ATP dATP dADP ATP ADP 8-oxo-dATP 2'O-Me-ATP	PPase
8	N4-Me-dCTP CDP 5-OH-dCTP 5-MeOH-dCTP 5-Me-dCTP 2'O-Me-CTP	PPase
9	p ₄ G N1-Me-GTP dGTP dGDP GTP GDP 8-oxo-dGTP 8-oxo-GTP 3'-dGTP 2'O-Me-GTP	PPase
10	UTP UDP 5-Me-UTP 5-MeOH-UTP 2'O-Me-UTP	PPase
11	XTP TTP TDP ITP dITP	PPase
Ungrouped	ADP-glucose	APase
Ungrouped	GDP-fucose	APase
Ungrouped	UDP-galactose	APase
Ungrouped	UDP-glucuronic acid	APase
Ungrouped	m ⁷ Gp ₅ G	APase
Ungrouped	Ap ₆ A	APase
Ungrouped	CTP	PPase
Ungrouped	dCDP	PPase
Ungrouped	dUTP	PPase
Ungrouped	dCTP	PPase
Ungrouped	DHUTP	PPase

Table S4 The average read counts with standard deviations in TPM as determined by Salmon, the differential expression analysis output (log2fc and q-values) as determined by fishpond when comparing the AvrM14-A and vector only datasets, and the blast-2-go best hit for all transcripts (see table S4.csv).

Table S5 The average read counts with standard deviations in TPM as determined by Salmon, the differential expression analysis output (log2fc and q-values) as determined by fishpond when comparing the AvrM14-A and AvrM14-AE82Q datasets, and the blast-2-go best hit for all transcripts (see table S5.csv).

Table S6 Summary of the cell death results recorded during this study following the expression of various AvrM14 proteins in M1 flax (*Linum usitatissimum*), M4 flax, and tobacco (*Nicotiana tabacum*) co-expressing M1. The number represents the cell death response score following visual inspection of the leaves, whereby a higher score indicates increased cell death. Please see Fig 1, Fig 6, S3 Fig, S10 Fig, and S11 Fig for the original images. N/A values are listed if the protein/resistance protein combination was not tested in this study.

Mutation in AvrM14-A	M4 Flax	M1 Flax	M1 Tobacco	Mutation in AvrM14-B	M4 Flax	M1 Flax	M1 Tobacco
Wild-Type	3	2	2	Wild-Type	0	0	0
K95Q	3	0 - 1	0	Q95K	0	0 - 1	0 - 1
T108P	3	2	0 - 1	P108T	1	0	0
K95Q/T108P	0	0	0	Q95K/P108T	3	3	0 - 1
Q137E	3	N/A	2	E137Q	0	N/A	0
H142R	3	N/A	2	R142H	0	N/A	0 - 1
Q137E/H142R	3	N/A	1	E137Q/R142H	0 - 1	N/A	0 - 1
K95Q/H142R	4	3	0	Q95K/R142H	3	2	0 - 1
K27E	N/A	N/A	2	E27K	N/A	N/A	0
E69K	N/A	N/A	2	K69E	N/A	N/A	0
E69K/T108P	N/A	N/A	2	K69E/P108T	N/A	N/A	0
E82Q	4	3	2	E82Q	0	0	0

References

- Ashburner M, Ball CA, Blake JA, Botstein D, Butler H, Cherry JM, Davis AP, Dolinski K, Dwight SS, Eppig JT, et al. 2000.** Gene Ontology: tool for the unification of biology. The Gene Ontology Consortium. *Nature Genetics* **25**(1): 25-29.
- Consortium TGO. 2020.** The Gene Ontology resource: enriching a GOld mine. *Nucleic Acids Research* **49**(D1): D325-D334.
- Danecek P, Bonfield JK, Liddle J, Marshall J, Ohan V, Pollard MO, Whitwham A, Keane T, McCarthy SA, Davies RM, et al. 2021.** Twelve years of SAMtools and BCFtools. *GigaScience* **10**(2).
- Kim D, Paggi JM, Park C, Bennett C, Salzberg SL. 2019.** Graph-based genome alignment and genotyping with HISAT2 and HISAT-genotype. *Nature Biotechnology* **37**(8): 907-915.
- Love MI, Soneson C, Hickey PF, Johnson LK, Pierce NT, Shepherd L, Morgan M, Patro R. 2020.** Tximeta: Reference sequence checksums for provenance identification in RNA-seq. *PLOS Computational Biology* **16**(2): e1007664.
- Mi H, Ebert D, Muruganujan A, Mills C, Albou L-P, Mushayamaha T, Thomas PD. 2020.** PANTHER version 16: a revised family classification, tree-based classification tool, enhancer regions and extensive API. *Nucleic Acids Research* **49**(D1): D394-D403.
- Patro R, Duggal G, Love MI, Irizarry RA, Kingsford C. 2017.** Salmon provides fast and bias-aware quantification of transcript expression. *Nature Methods* **14**(4): 417-419.
- Pertea G, Pertea M. 2020.** GFF utilities: GffRead and GffCompare. *F1000Research* **9**(304).
- Pertea M, Pertea GM, Antonescu CM, Chang T-C, Mendell JT, Salzberg SL. 2015.** StringTie enables improved reconstruction of a transcriptome from RNA-seq reads. *Nature Biotechnology* **33**(3): 290-295.
- Studier FW. 2005.** Protein production by auto-induction in high-density shaking cultures. *Protein Expression and Purification* **41**(1): 207-234.
- Supek F, Bošnjak M, Škunca N, Šmuc T. 2011.** REVIGO summarizes and visualizes long lists of gene ontology terms. *PLOS ONE* **6**(7): e21800.
- Wang Z, Hobson N, Galindo L, Zhu S, Shi D, McDill J, Yang L, Hawkins S, Neutelings G, Datla R, et al. 2012.** The genome of flax (*Linum usitatissimum*) assembled de novo from short shotgun sequence reads. *The Plant journal : for cell and molecular biology* **72**(3): 461-473.
- Zhang Q, Shi Q, Shao M. 2021.** Scallop2 enables accurate assembly of multiple-end RNA-seq data. *bioRxiv [Preprint]*.
- Zhu A, Srivastava A, Ibrahim JG, Patro R, Love MI. 2019.** Nonparametric expression analysis using inferential replicate counts. *Nucleic Acids Research* **47**(18): e105-e105.

Chapter 3 A family of fungal effectors induce plant phosphate starvation responses by hydrolysing inositol pyrophosphates

In chapter 2, I established that AvrM14 and sequence-related effectors from the *Melampsora* genus are Nudix hydrolase enzymes. The effectors can remove the protective 5' cap from *in vitro* transcribed mRNA; notably, AvrM14 demonstrates remarkable substrate specificity, only hydrolysing capped mRNA and a molecule analogous to the 5' cap structure. I also report that AvrM14 hydrolase activity suppresses immune responses in both *N. benthamiana* and flax leaves. Overall, the results support a model whereby the *Melampsora* Nudix hydrolase effectors decap plant mRNA to suppress immune responses and ultimately promote the infection process. Following the AvrM14 study, I aimed to characterise the second identified family of predicted fungal Nudix hydrolase effectors.

Genome sequencing of *M. oryzae* in 2005 identified two identical copies of a putative Nudix effector called *MoNudix* (Dean *et al.*, 2005). Subsequent studies identified similar predicted Nudix effectors with approximately 40% amino acid sequence identity in *C. lentic*, *C. higginsianum*, *C. graminicola*, and *C. fructicola* (Bhaduria *et al.*, 2013, Crouch *et al.*, 2014). This chapter investigates the Nudix effectors from *Magnaporthe* and *Colletotrichum* genera. In this chapter, I use a combination of structural biology, enzymatic assays, and *in planta* experiments to characterise the *Magnaporthe* and *Colletotrichum* Nudix effectors. After a detailed analysis of the Nudix effectors in heterologous systems, we established a collaboration with Dr Ely Oliveira-Garcia at Louisiana State University to conduct experiments in the native *M. oryzae* system. Dr Oliveira-Garcia and his student Chenie Zamora used RNA interference to probe *MoNudix*'s contribution to rice blast disease symptoms, and live-cell imaging to assess *MoNudix*'s localisation during rice infection. Our collective research on the *Magnaporthe* and *Colletotrichum* Nudix effectors culminated in the preparation of a manuscript, completed in August 2023, which is presented in this chapter. For this manuscript, I wrote the initial draft and created all the figures, except Figure 4. See the statement of contribution for more details.

I presented my research on *MoNudix* at the International Society for Plant-Microbe Interactions 2023 Congress, Providence, Rhode Island in August. During my poster presentation I was approached by Florencia Casanova and Louisa Wirtz from Prof. Ulrich Schaffrath's group at

RWTH Aachen University, Germany. Florencia and Louisa informed me that the Schaffrath lab was involved in research concerning *MoNudix*. After the meeting we contacted Prof. Schaffrath and his research team, sharing our respective data sets. The Schaffrath lab had an unpublished manuscript, close to submission, which demonstrates that knocking out *MoNudix* in *M. oryzae* significantly reduces disease symptoms on multiple cultivars of rice and barley. They had also completed complementation experiments demonstrating that *MoNudix*'s hydrolase activity is essential for promoting disease. Collectively, our research was highly complementary, and we therefore decided to combine our manuscripts into a single manuscript. I wrote the initial draft of the combined manuscript and assembled all figures, except supplemental figure 1. The combined manuscript can be found as appendix 1 in this thesis, it is about to be submitted to a journal and has been made available on the preprint server bioRxiv (<https://doi.org/10.1101/2023.11.14.566975>).

References

- Bhaduria, V., S. Banniza, A. Vandenberg, G. Selvaraj and Y. Wei (2013). "Overexpression of a novel biotrophy-specific *Colletotrichum truncatum* effector, CtNUDIX, in hemibiotrophic fungal phytopathogens causes incompatibility with their host plants." *Eukaryot Cell* **12**(1): 2-11.
- Crouch, J., R. O'Connell, P. Gan, E. Buiate, M. F. Torres, L. Beirn, K. Shirasu and L. Vaillancourt (2014). "The genomics of *Colletotrichum*." *Genomics of plant-associated fungi: monocot pathogens*: 69-102.
- Dean, R. A., N. J. Talbot, D. J. Ebbot, M. L. Farman, T. K. Mitchell, M. J. Orbach, M. Thon, R. Kulkarni, J. R. Xu, H. Pan, N. D. Read, Y. H. Lee, I. Carbone, D. Brown, Y. Y. Oh, N. Donofrio, J. S. Jeong, D. M. Soanes, S. Djonovic, E. Kolomiets, C. Rehmeyer, W. Li, M. Harding, S. Kim, M. H. Lebrun, H. Bohnert, S. Coughlan, J. Butler, S. Calvo, L. J. Ma, R. Nicol, S. Purcell, C. Nusbaum, J. E. Galagan and B. W. Birren (2005). "The genome sequence of the rice blast fungus *Magnaporthe grisea*." *Nature* **434**(7036): 980-986.



Statement of Contribution

I declare that the research presented in this Thesis represents original work that I carried out during my candidature at the Australian National University, except for contributions to multi-author papers incorporated in the Thesis where my contributions are specified in this Statement of Contribution.

Title: A family of fungal effectors induce plant phosphate starvation responses by hydrolysing inositol pyrophosphates

Authors: Carl L. McCombe, Chenie S. Zamora, Shouvik Aditya, Julian R. Greenwood, Samuel de Paula, Eleanor England, Sascha Shang, Daniel J. Ericsson, Ely Oliveira-Garcia, Simon J. Williams

Publication outlet: Original manuscript (presented as Chapter 3) was going to be submitted to Cell Host and Microbe. With addition of new data from collaborators (see appendix 1) the manuscript was submitted to Science and is available on BioRxiv.

Current status of paper: Not Yet Submitted/Submitted/Under Revision/Accepted/Published

Contribution to paper: I generated ~85% of the data presented in this manuscript, generated all figures except Fig 4 and S6, and wrote the initial draft of the paper, which was subsequently edited and approved by all co-authors.

Data generated by others:

Figures 4 and S6 (Chenie S. Zamora and Ely Oliveira-Garcia)
Figures 2A and 2E (Shouvik Aditya)

Senior author or collaborating authors endorsement: 

Carl McCombe

Candidate – Print Name



13/11/2023

Signature

Date

Endorsed

Simon Williams

Primary Supervisor – Print Name



13/11/2023

Signature

Date

Title

A family of fungal effectors induce plant phosphate starvation responses by hydrolysing inositol pyrophosphates

Authors

Carl L. McCombe¹, Chenie S. Zamora², Shouvik Aditya¹, Julian R. Greenwood¹, Samuel de Paula², Eleanor England¹, Sascha Shang¹, Daniel J. Ericsson³, Ely Oliveira-Garcia^{2*}, Simon J. Williams^{1*}

¹ Plant Sciences Division, Research School of Biology, The Australian National University, Canberra, ACT, 2617, Australia

² Department of Plant Pathology and Crop Physiology, Louisiana State University Agricultural Center, Baton Rouge, LA, 70803, United States of America

³ ANSTO, Australian Synchrotron, Crystallography Beamline Group, Clayton, Victoria, 3168, Australia

*Correspondence: simon.williams@anu.edu.au or EOliveiraGarcia@agcenter.lsu.edu

Summary (<150 words)

Plant phosphate starvation response transcription factors (PHRs) play an essential role in maintaining phosphate homeostasis. Crucial links between plant PHRs and interactions with beneficial microbes, such as phosphate-providing arbuscular mycorrhizal fungi, are well established. In this study, we have identified a conserved effector family in pathogenic *Magnaporthe* and *Colletotrichum* fungi capable of activating PHRs *in planta*. We demonstrate that the effectors hydrolyse inositol pyrophosphates (PP-InsPs), which are used by plants to signal changes in phosphate availability and regulate PHR activity. In *M. oryzae*, the reduction of one PP-InsP hydrolase effector through RNA interference (RNAi) significantly diminishes virulence on rice, while simultaneously promoting reactive oxygen species (ROS) accumulation around the infection site. Altogether, our research elucidates a molecular mechanism whereby various pathogenic fungi directly target a conserved signalling molecule involved in phosphate homeostasis to disrupt plant defence, activate PHRs, and ultimately enhance disease progression.

Keywords

Phosphate starvation, Plant immunity, virulence effector, Nudix hydrolase, *Magnaporthe oryzae*

Introduction

Inositol pyrophosphates (PP-InsPs) are small molecules composed of a fully phosphorylated inositol ring with either one or two pyrophosphate moieties. PP-InsPs have the most concentrated array of phosphates in nature, resulting in a dense electronegative charge.¹ The intracellular concentration of PP-InsPs is linked to the availability of inorganic phosphate (Pi),^{2,3} and plants sense PP-InsP levels to control phosphate starvation responses (PSRs).²⁻⁶ Within eukaryotic cells, the electronegative PP-InsPs bind to basic surface clusters on SPX protein domains (named after yeast SYG1, Pho81, and human XPR1) to facilitate Pi sensing.² SPX domains are found in various proteins involved in eukaryotic phosphate homoeostasis and as single-domain proteins.⁷⁻¹⁴ In plants, single-domain SPX proteins act as PP-InsP-dependent repressors of the phosphate starvation response transcription factors (PHRs);^{4,15} PHRs complete extensive transcriptional reprogramming during phosphate starvation.¹⁶⁻¹⁸ When phosphate is abundant, PHRs are held in an inactive state by PP-InsP-bound SPX proteins.^{4,11,13-15} During phosphate starvation, PP-InsP levels decrease and PHRs are released by SPX proteins, resulting in the transcription of target genes. Notably, these target genes typically contain PHR binding sequences (P1BSs) (GnATATnC) within their promoter region.^{16,17}

Symbiosis with arbuscular mycorrhizal fungi (AMF) enables c. 80% of land plants to access more phosphate and other mineral nutrients from the environment in exchange for carbon.¹⁹ In soil with high levels of accessible phosphate, plants suppress AMF symbiosis, potentially to conserve carbon.²⁰⁻²⁸ Likewise, interactions between *Arabidopsis thaliana* and phosphate-providing endophyte *Colletotrichum tofieldiae* are regulated by plant phosphate status.²⁹⁻³¹ Recent research indicates that the regulation of AMF symbiosis is primarily mediated by PHRs.^{32,33} PHR transcriptional activity also represses certain plant defence responses, possibly to help facilitate interactions with beneficial microbes and/or prevent defence-mediated suppression of phosphate transport.³⁴⁻³⁶ One mechanism by which PHRs can influence plant immune function and promote root colonisation by phosphate providing microbiota, is by activating the expression of rapid alkalinisation factor (RALF) genes that possess the P1BS element within their promoter.³⁵ The receptor kinase FERONIA senses RALF peptides, which results in reduced assembly of the immune receptor complex composed of flagellin sensing 2 (FLS2) and BRASSINOSTEROID INSENSITIVE 1-associated receptor kinase 1 (BAK1).³⁷ Consequently, under phosphate-starved conditions, *A. thaliana* plants demonstrate compromised immune signalling pathways.³⁵

To facilitate infection, pathogenic microbes can secrete proteins known as effectors to manipulate the host plant. Effectors often suppress plant immune responses. Increasing evidence suggests that plant pathogens may specifically target PSRs to promote disease.³⁸ SAP11 is an effector from a parasitic phytoplasma capable of inducing PSRs and suppressing defense in transgenic *A. thaliana*,³⁹ potentially via PHR activation.³⁸ Likewise, infection with *Candidatus liberibacter asiaticus* bacteria induces PSR symptoms in the host *Citrus sinensis*.⁴⁰ Another effector, XopH, from *Xanthomonas campestris* pv. *Vesicatoria*, reduces plant PP-InsP levels by dephosphorylating inositol hexakisphosphate (InsP6), although it remains unknown if XopH induces PSRs.⁴¹ In addition to the suppression of plant immunity, pathogens may benefit from the increase in bioavailable intracellular phosphate resulting from the activation of PSRs.³⁸ For example, excessive phosphate supply renders rice plants more susceptible to *Magnaporthe oryzae*.⁴²

Nucleoside diphosphate linked to moiety-X (Nudix) hydrolase domains have been predicted in effectors from fungal, oomycete and bacterial plant pathogens.⁴³⁻⁴⁸ Nudix hydrolases share a consensus sequence called the Nudix box (GX₅EX₇REUXEEGU, where U represents a hydrophobic amino acid and X is any amino acid). Typically, Nudix hydrolases catalyse the hydrolysis of nucleoside diphosphate-containing compounds.⁴⁹ However, a subset of Nudix hydrolases can also hydrolyse diphosphate bonds in compounds without a nucleoside, including PP-InsPs.⁵⁰⁻⁵³ In this study, we identify a conserved group of Nudix hydrolase effectors from economically important pathogenic fungi, including *Magnaporthe oryzae*, the causative agent of rice blast disease, and multiple *Colletotrichum* species responsible for anthracnose disease on a wide variety of plants. Through a combination of experimental and computational structural biology, *in vitro* enzymatic assays, and *in planta* analysis, we establish that Nudix hydrolase effectors from *M. oryzae* and *Colletotrichum spp.* possess a conserved basic PP-InsP binding site, exhibit PP-InsP hydrolysis activity, and employ their hydrolase activity to induce PSRs and suppress immune-activated reactive oxygen species (ROS) production in plants. Additionally, our results indicate that an *M. oryzae* PP-InsP hydrolase effector is secreted into the cytoplasm of host rice cells during infection, and we demonstrate that this effector suppresses host immune responses and significantly contributes to the virulence of *M. oryzae*.

Results

Putative Nudix effectors are widespread in *Magnaporthe* and *Colletotrichum* pathogenic fungi

Recently, we demonstrated that Nudix effectors from pathogenic fungi in the *Melampsora* genus exhibit mRNA decapping activity.⁴⁶ Within fungi, the plant pathogens *C. lenthis* (previously *C. truncatum*), *M. oryzae*, and *C. higginsianum* also have predicted Nudix effectors.^{44,54,55} While the biochemical activity of these remains unknown, studies suggest they play a role in pathogen virulence. In *Colletotrichum*, Bhaduria *et al.*, (2013) suggested that *CtNudix*, a Nudix effector from *C. lenthis*, is important for the transition to necrotrophic growth,⁴⁴ and multiple putative Nudix effectors are specifically and highly upregulated during the biotrophic growth phase of *C. higginsianum*.⁵⁵ More recently, Yan *et al.*, (2023) reported that two identical Nudix effector genes from *M. oryzae* (MGG_14156 and MGG_14344, referred to here as *MoNudix*) were consistently among the top ten upregulated predicted effectors at 48 to 96 hours post inoculation (hpi) in three independent infection experiments involving two different rice cultivars.⁵⁴

Sequence analysis indicates that the *Magnaporthe* and *Colletotrichum* Nudix effectors are more closely related to each other than to the mRNA decapping *Melampsora* effectors, and resemble a distinct effector family (Figure 1A). We investigated the prevalence of the *Colletotrichum* and *Magnaporthe* Nudix hydrolase effector family in pathogenic and non-pathogenic fungi. Previous studies have reported sequence-related Nudix effectors in *C. higginsianum*, *C. graminicola*, *C. fructicola*, *C. orbiculare*, *C. lenthis*, and *M. oryzae*.^{44,56} To further explore the Nudix effector family, we searched NCBI databases (see ‘Methods’ for detailed information) to identify similar putative Nudix effectors. Our search recovered Nudix effectors (with a Nudix domain and a predicted signal peptide) across *Magnaporthe*, *Colletotrichum* and *Ceratocystis* genera (Figure 1A, Table S1). Notably, all predicted Nudix effector genes belong to pathogenic species, while no predicted Nudix effectors were identified in *C. tofieldiae*, a closely related genome-sequenced endophytic species.³⁰ Collectively, the fungi that possess predicted Nudix effectors infect a diverse range of monocot and dicot plant species (Table S1), suggesting that any shared target/s of the Nudix effectors may be widely conserved in land plants.

Magnaporthe and *Colletotrichum* Nudix effectors inhibit the ROS burst and specifically hydrolyse PP-InsPs

Previously characterised Nudix hydrolase effectors from plant pathogens, including Avr3b from *Phytophthora sojae*, RipN from *Ralstonia solanacearum*, and AvrM14 from *Melampsora lini*, can use hydrolase activity to inhibit plant immune signalling.^{43,45,46} To investigate whether Nudix effectors from *Magnaporthe* and *Colletotrichum* can also disrupt plant immune signalling through hydrolase activity, we utilised Agrobacterium-mediated transformation of *N. benthamiana* to transiently express *MoNudix*, and a Nudix effector from *C. higginsianum* (*ChNudix*), as well as mutant proteins where a conserved Nudix box glutamate (E) typically essential for hydrolase activity, was substituted to glutamine (Q) (*MoNudix*^{E79Q} and *ChNudix*^{E78Q}). Our results clearly demonstrate that the expression of *MoNudix* and *ChNudix*, but not the catalytic mutants (E-to-Q), significantly impairs the production of ROS in *N. benthamiana* leaf tissue upon exposure to either flg-22 or chitin (Figure 1B). Western blot analysis of soluble protein extracts from *N. benthamiana* confirms the expression and accumulation of all effector proteins (Figure S1).

To understand how the Nudix hydrolase activity of the *Magnaporthe* and *Colletotrichum* effectors interfere with flg-22 and chitin responses, we sought to identify the substrate/s hydrolysed by the effectors. For initial substrate screening, we utilised recombinant *MoNudix* effector protein produced in *E. coli* and purified to homogeneity (Figure S2). We screened multiple common substrates of Nudix hydrolases, including those identified as substrates (ADP-ribose, NADH, and mRNA caps) of the previously characterised Nudix effectors (Avr3b, RipN, and AvrM14).^{43,45,46} *MoNudix* did not efficiently hydrolyse any Nudix hydrolase substrates tested (Figure S3A and S3B), suggesting that the *Magnaporthe* and *Colletotrichum* Nudix effector family are functionally distinct from previous studied Nudix hydrolase effectors. Interestingly, the *Magnaporthe*, *Colletotrichum*, and *Ceratocystis* Nudix effectors share a conserved glycine at position +1 in the Nudix box (Figure S4A), which has been demonstrated to be important for the enzymatic activity of a human PP-InsP hydrolase, *HsDIPP1*.^{57,58} Furthermore, we utilised AlphaFold⁵⁹ to model the protein structures of the Nudix effector family, and the predicted structures exhibit similarity to *HsDIPP1* (Figure S4B). The prediction of structural similarity between *MoNudix* and *HsDIPP1* is consistent with recent publications that reported AlphaFold models for *M. oryzae* effectors.^{54,60}

To determine if *MoNudix* can hydrolyse PP-InsPs *in vitro*, we first synthesised 5-PP-InsP₅ using inositol hexakisphosphate (InsP₆) and an *Entamoeba histolytica* InsP₆ kinase (*EhIP6KA*).⁶¹ 5-PP-InsP₅ is one of the PP-InsPs produced in plants, and is involved in the

regulation of the PSR in a PHR-dependent manner.⁶ We then incubated the 5-PP-InsP₅ with purified recombinant *MoNudix* protein and utilised polyacrylamide gel electrophoresis to separate the inositol polyphosphate species. This assay demonstrates that *MoNudix* converts 5-PP-InsP₅ into InsP₆ (Figure 1C). Importantly, like ROS suppression, the enzymatic activity requires the Nudix box, as the glutamate to glutamine substitution (*MoNudix*^{E79Q}) abolishes 5-PP-InsP₅ hydrolysis (Figure 1C). To establish if this enzymatic activity is conserved in the extended Nudix effector family, we also evaluated whether *ChNudix* and a second *M. oryzae* effector (*MoNudix2*) (purified to homogeneity (Figure S2)), could hydrolyse 5-PP-InsP₅. Like *MoNudix*, *ChNudix* and *MoNudix2* both effectively hydrolyse 5-PP-InsP₅ *in vitro* using their Nudix box (Figure 1D and 1E). In contrast to the *Magnaporthe* and *Colletotrichum* Nudix effectors, the *M. lini* Nudix effector AvrM14-A cannot hydrolyse 5-PP-InsP₅ in our assay system, and neither can *AtNudx7*, a Nudix hydrolase with broad substrate specificity that negatively regulates plant immunity in *A. thaliana*⁶² (Figure S3C). Overall, our *in vitro* enzymatic assays demonstrate that the *Magnaporthe* and *Colletotrichum* Nudix effectors are PP-InsP hydrolases (Figure 1F).

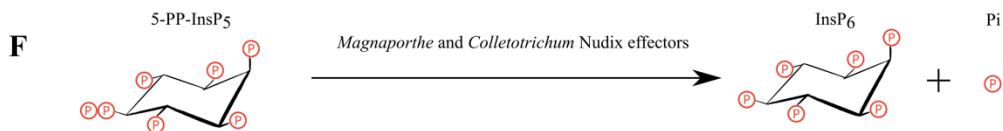
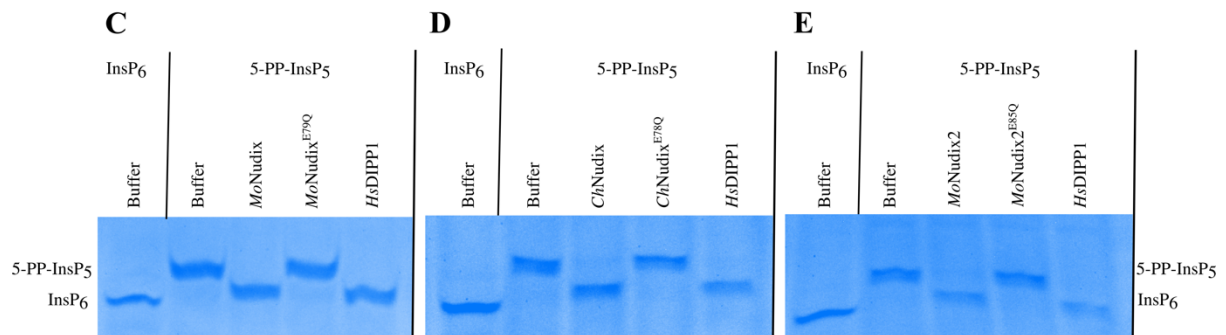
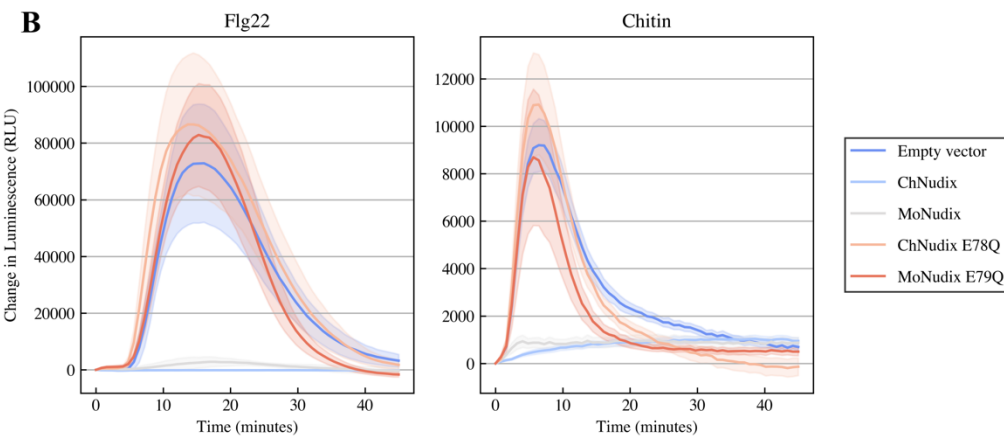
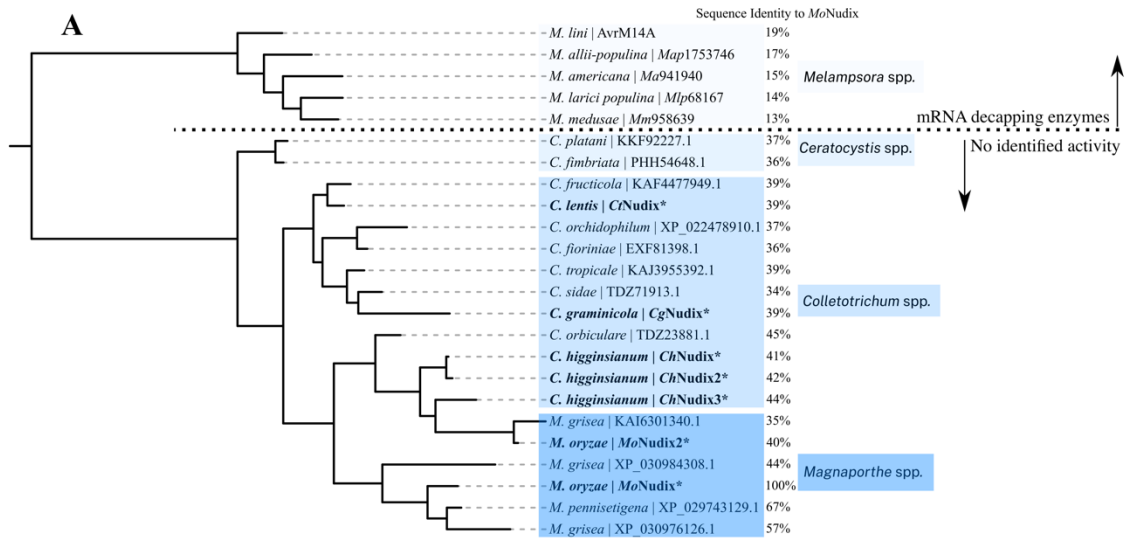


Figure 1: Nudix effectors from *Magnaporthe* and *Colletotrichum* pathogenic fungi hydrolyse inositol pyrophosphates and their hydrolase activity suppresses the flg-22- and chitin-triggered ROS burst in *Nicotiana benthamiana*. (A) A maximum-likelihood phylogeny estimated with PhyML⁶³ and visualised with iTOL,⁶⁴ using the protein sequences of select Nudix hydrolase effectors from pathogenic fungi. Each leaf is labelled with the species and protein names, those in bold and indicated with an * are analysed in this study (amino acid sequences in Table S1). The percentage next to each label indicates amino-acid sequence identity to *MoNudix*. The black dotted line separates effectors with no identified enzymatic activity from those previously characterised as mRNA decapping enzymes.⁴⁶ (B) *N. benthamiana* leaves were infiltrated with *Agrobacterium tumefaciens* (GV3101) harbouring either an empty vector or constructs encoding *MoNudix*, *ChNudix*, *MoNudix*^{E79Q}, or *ChNudix*^{E78Q} proteins with 3xHA N-terminal tags expressed under the 35 S promoter from the cauliflower mosaic virus. At 3 days post-infiltration (dpi), leaf tissue was exposed to 100 nM flg-22 (left) or 5 µg ml⁻¹ chitin (right) and ROS production was recorded as relative luminescence units over time. Results are mean (solid line) ± SEM (shaded area) where n = 8. (C), (D), and (E) Purified recombinant protein (*MoNudix*, *MoNudix*^{E79Q}, *HsDIPP1*, *ChNudix*, *ChNudix*^{E78Q}, *MoNudix2*, and *MoNudix2*^{E85Q}) at a concentration of 5 µM or protein storage buffer was incubated with either inositol hexakisphosphate (InsP₆) or an inositol pyrophosphate (5-PP-InsP₅) (indicated along the top of the gel) for 60 minutes at 37 °C. The reaction products were separated using a polyacrylamide gel and visualised by staining with toluidine blue. The downwards shift of the band in the *MoNudix*, *HsDIPP1*, *ChNudix*, and *MoNudix2* lanes when compared to the other 5-PP-InsP₅ treatments, indicates that these proteins convert 5-PP-InsP₅ to InsP₆ (as depicted in (F)).

A conserved, positively charged, binding site in the *Magnaporthe* and *Colletotrichum* Nudix effectors is required for 5-PP-InsP₅ hydrolysis

To enhance our understanding of *MoNudix* as a PP-InsP hydrolase, we sought to determine the protein's structure as a ligand bound complex. Access to sufficient PP-InsP for co-crystallisation was not possible. We instead performed co-crystallisation of *MoNudix* in saturating concentrations of InsP₆ (the product of PP-InsP hydrolysis), which has a disassociation constant (Kd) of 6.02 ± 1.36 mM with *MoNudix* (Figure 2A), calculated using micro-scale thermophoresis (MST).

The crystal structure of *MoNudix*, determined at a resolution of 1.6 Å (PDB ID: 8SXS), revealed a characteristic Nudix fold that shares a highly similar overall structure (TM score = 0.77) with *HsDIPP1*,⁵⁸ despite low sequence identity (c. 25%) (Figure 2B). While InsP₆ was required for crystallisation of *MoNudix*, the unambiguous placement of InsP₆ within the electron density maps was not possible, likely due to ligand occupancy. To interrogate the PP-InsP binding site and identify amino acids involved in substrate binding, we superimposed the structure of *MoNudix* with the 5-PP-InsP₅ bound *HsDIPP1* structure (PDB ID: 6wo7)⁵⁸ (Figure 2C). Analogous to *HsDIPP1*, the predicted PP-InsP binding site in *MoNudix* is characterised by basic amino acids (lysines and arginines), creating a positively charged putative binding cleft located adjacent to the negatively charged Nudix active site (Figure 2C and 2D). We targeted two lysine amino acids (K53 and K142), predicted to be involved in PP-InsP interactions, and substituted them with glutamate (*MoNudix*^{KKEE}). Using MST, we demonstrate that purified *MoNudix*^{KKEE} (Figure S2) exhibits a 70-fold reduction in InsP₆ binding affinity (Figure 2A and 2E). Moreover, *MoNudix*^{KKEE} is unable to hydrolyse 5-PP-InsP₅ *in vitro* (Figure 2F).

To identify conserved structural elements across the *Magnaporthe*, *Colletotrichum* and *Ceratocystis* Nudix effector family, we employed ConSurf⁶⁵ to independently identify homologous sequences and map sequence conservation onto the *MoNudix* protein surface (Figure 2G). The proposed 5-PP-InsP₅ binding site, including the basic amino acids (required for substrate binding) and the Nudix box, exhibits high conservation (Figure 2G, Figure S4A). The conservation of the PP-InsP binding site, and enzymatic activity in *ChNudix* and *MoNudix2* (Figure 1C), suggests that PP-InsP hydrolase activity is likely conserved across the sequence-related *Magnaporthe*, *Colletotrichum*, and *Ceratocystis* Nudix effector family.

The crystal structure also reveals a single disulphide bond in the *MoNudix* protein, which serves to anchor the Nudix helix to a β -sheet, potentially providing additional structural stability (Figure S4C). Analogous disulphide bonded cysteines have not been reported previously in Nudix hydrolase enzymes and are a conserved and unique feature of this fungal PP-InsP effector family (Figure S4A).

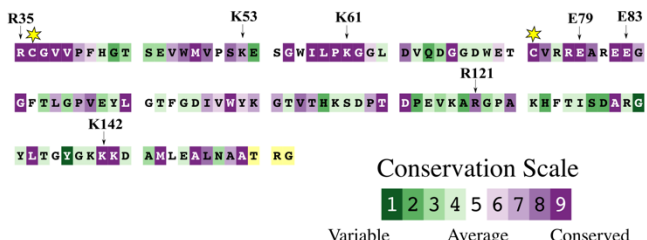
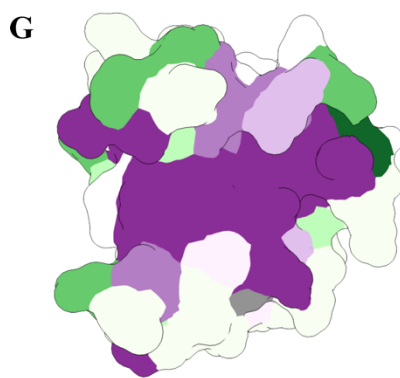
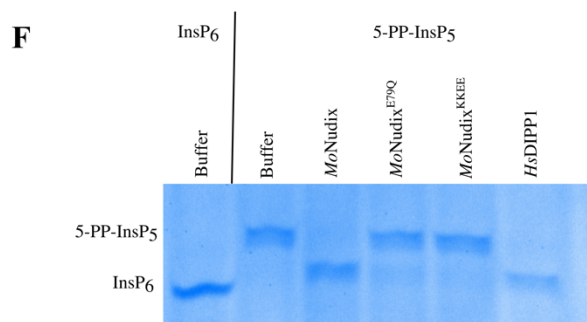
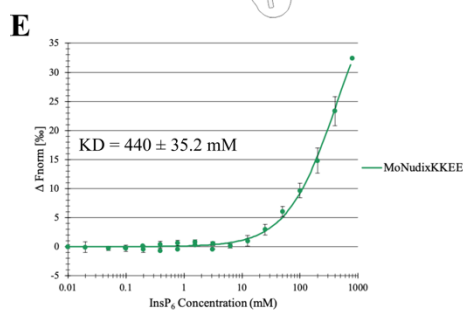
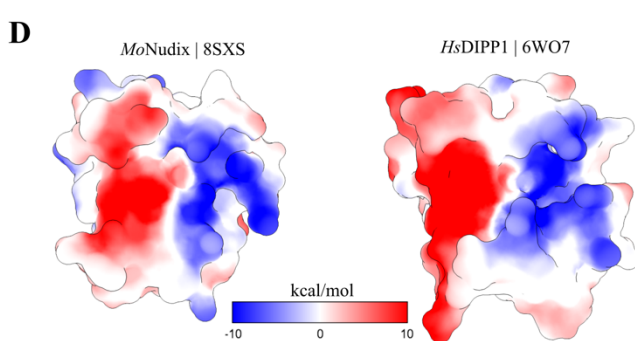
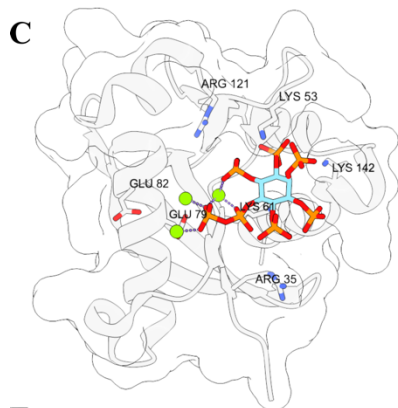
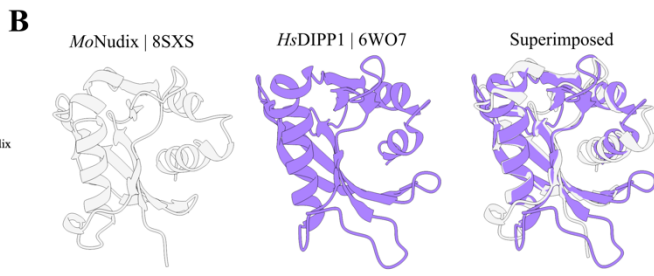
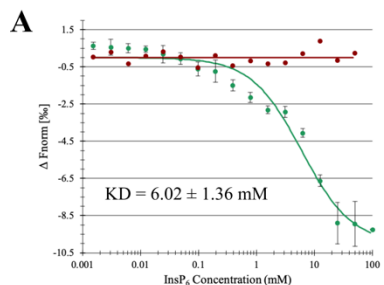


Figure 2: The crystal structure of *MoNudix* highlights a conserved, highly charged, binding site involved in inositol polyphosphate binding and hydrolysis. (A) and (E) Normalized microscale thermophoresis (MST) binding curves of *MoNudix* plus a protein storage buffer control (A) and *MoNudix*^{KKEE} (E) in the presence of InsP₆. The binding curve yields a Kd of 6.02 ± 1.32 mM for *MoNudix* and a Kd of 440 ± 35.2 mM for *MoNudix*^{KKEE}. Protein concentrations were kept constant while the InsP₆ concentration varied. (B) Ribbon diagrams of *MoNudix* (PDB ID: 8SXS) (grey) and *HsDIPP1* (PDB ID: 6WO7)⁵⁸ (purple) crystal structures superimposed to demonstrate their striking structural similarity (TM score = 0.77) despite low levels of sequence identity (25%). (C) A ribbon diagram of *MoNudix* with an overlaid transparent surface model with Mg²⁺ and 5-PP-InsP₅ docked into the structure via structural alignment with *HsDIPP1* (PDB ID: 6WO7). The amino acids potentially important for Mg²⁺ and 5-PP-InsP₅ binding are labelled and shown as stick models. (D) Analogous to *HsDIPP1*, the *MoNudix* structure demonstrates a large positively charged site adjacent to the negatively charged Nudix hydrolase active site region. Surface electrostatic potential was calculated in ChimeraX⁶⁶ and is displayed in kcal/mol. (F) Purified recombinant protein (*MoNudix*, *MoNudix*^{E79Q}, *MoNudix*^{KKEE}, or *HsDIPP1*) at a concentration of 5 μ M or protein storage buffer was incubated with either inositol hexakisphosphate (InsP₆) or an inositol pyrophosphate (5-PP-InsP₅) (indicated along the top of the gel) for 60 minutes at 37 °C. The reaction products were separated using a polyacrylamide gel and visualised by staining with toluidine blue. (G) *MoNudix* with the protein surface coloured according to amino acid conservation across homologous effectors as determined by ConSurf.⁶⁵ The N-terminus of the crystal structure is truncated to remove three non-native amino acids resulting from the purification process. Next to the structure is the sequence of the *MoNudix* protein used to determine the crystal structure, with residue colouring indicating conservation. The amino acids potentially important for PP-InsP binding and hydrolysis are indicated with arrows. The two conserved, disulphide-bonded cysteines are indicated with yellow stars.

Magnaporthe and *Colletotrichum* Nudix effectors induce phosphate starvation responses in *N. benthamiana*

PP-InsPs play a crucial role in controlling the activation of PHRs by regulating their interaction with SPX proteins, thereby preventing PHRs from binding to DNA (Figure 3A).^{2,4,15,67} A reduction in intracellular PP-InsP concentration, as occurs when phosphate is limited, leads to the release and activation of PHRs, resulting in the transcription of phosphate starvation-induced (PSI) genes.³ If the *Magnaporthe* and *Colletotrichum* Nudix effectors hydrolyse PP-InsPs within plant cells, we predicted that the transcription of PSI genes will increase even under phosphate sufficient conditions (Figure 3A). To investigate if the Nudix effectors activate PHRs in plants, we expressed *MoNudix*, *ChNudix*, and the mutated proteins with compromised enzymatic activity (*MoNudix*^{E79Q} and *ChNudix*^{E78Q}) in *N. benthamiana* leaf tissue. We first analysed the mRNA levels of two genes (*NbSPX1* and *NbPEPC1*, primer sequences in Table S2) that are homologous to well-characterised *A. thaliana* PSI genes^{68,69} and contain multiple P1BS elements in their promoter region (Figure 3B, Table S3). The expression of *MoNudix* and *ChNudix* significantly increased the abundance of both *NbSPX1* and *NbPEPC1* mRNA, when compared to the expression of *MoNudix*^{E79Q} and *ChNudix*^{E78Q} (Figure 3C). Recently, Tang *et al.*, (2022) reported that *AtPHR1* activates the expression of immunomodulatory RALF genes during phosphate starvation in *A. thaliana*. These RALF genes are characterised by a site-1 protease (S1P) cleavage site and a P1BS element within their promoter region.³⁵ S1P-processed RALF peptides negatively regulate plant immunity and suppress the immune-activated ROS burst.³⁷ We identified two potential *N. benthamiana* RALF genes homologous to the immune-suppressing *AtRALF23* and *AtRALF33*,³⁷ both with a S1P cleavage site and a P1BS element within their 3 kb promoter (Figure S5A, Table S3). Using qPCR, we demonstrate that the enzymatic activity of *ChNudix* significantly increases the mRNA abundance of both identified RALF genes (Figure S5B). The enzymatic activity of *MoNudix* significantly increases the mRNA abundance of one of the two RALF genes (Figure S5B), however, the increase for the second RALF gene was deemed insignificant by statistical testing (Figure S5B). Collectively, the qPCR results indicate that the hydrolase activity of *MoNudix* and *ChNudix* elevates the expression of PSI genes in *N. benthamiana* leaf tissue, consistent with the hydrolysis of PP-InsPs *in planta* by the *Magnaporthe* and *Colletotrichum* Nudix effectors.

To investigate this further, we developed a rapid *in planta* screening method to monitor PHR activation. In our system, the visible RUBY reporter gene is controlled by a promoter with multiple P1BS elements. RUBY converts tyrosine to red betalain, which can be visually

observed and quantified by extracting the betalain from plant tissue.⁷⁰ Therefore, in the assay, betalain production indicates activation of *N. benthamiana* PHRs. We utilised both a synthetic promoter sequence (PSI:RUBY) (Figure 3D, Table S3) and the promoter region from *NbPECP1* (PECP1:RUBY) (Table S3). When the PSI:RUBY or PECP1:RUBY gene alone is agroinfiltrated, no betalain production is observed (Figure 3E and 3F, Figure S5C and S5D). However, when co-transformed with the negative control genes, AvrM14-A, Nanoluciferase and the E-to-Q mutant Nudix proteins under the control of the 35S promoter, a low level of betalain production is detected (Figure 3E and 3F, Figure S5C and S5D). This suggests that overexpression of any gene using our system leads to a minor PHR activation in *N. benthamiana* leaf tissue, possibly due to excessive mRNA production depleting intracellular phosphate stores. Despite this, we demonstrate that co-transformation with six of the seven wild-type Nudix effectors significantly increases betalain production compared to the expression of the corresponding Nudix box (E-to-Q) mutant proteins and the negative controls (Figure 3E and 3F, Figure S5C and S5D). Additionally, we demonstrate that the *MoNudix*^{KKEE} mutation significantly (adjusted p-value ≤ 0.001) reduces betalain production compared to the wild-type protein (Figure 3E and F), which is consistent with the reduced InsP₆ binding and 5-PP-InsP₅ hydrolysis observed *in vitro*. Western blot analysis confirms the production of all tested effectors (Figure S1). Overall, our results demonstrate that the hydrolase activity of the *Magnaporthe* and *Colletotrichum* Nudix effector family increases the expression of genes controlled by *N. benthamiana* PHRs. These findings support the role of these effectors as PP-InsP hydrolases capable of inducing PSRs in plants.

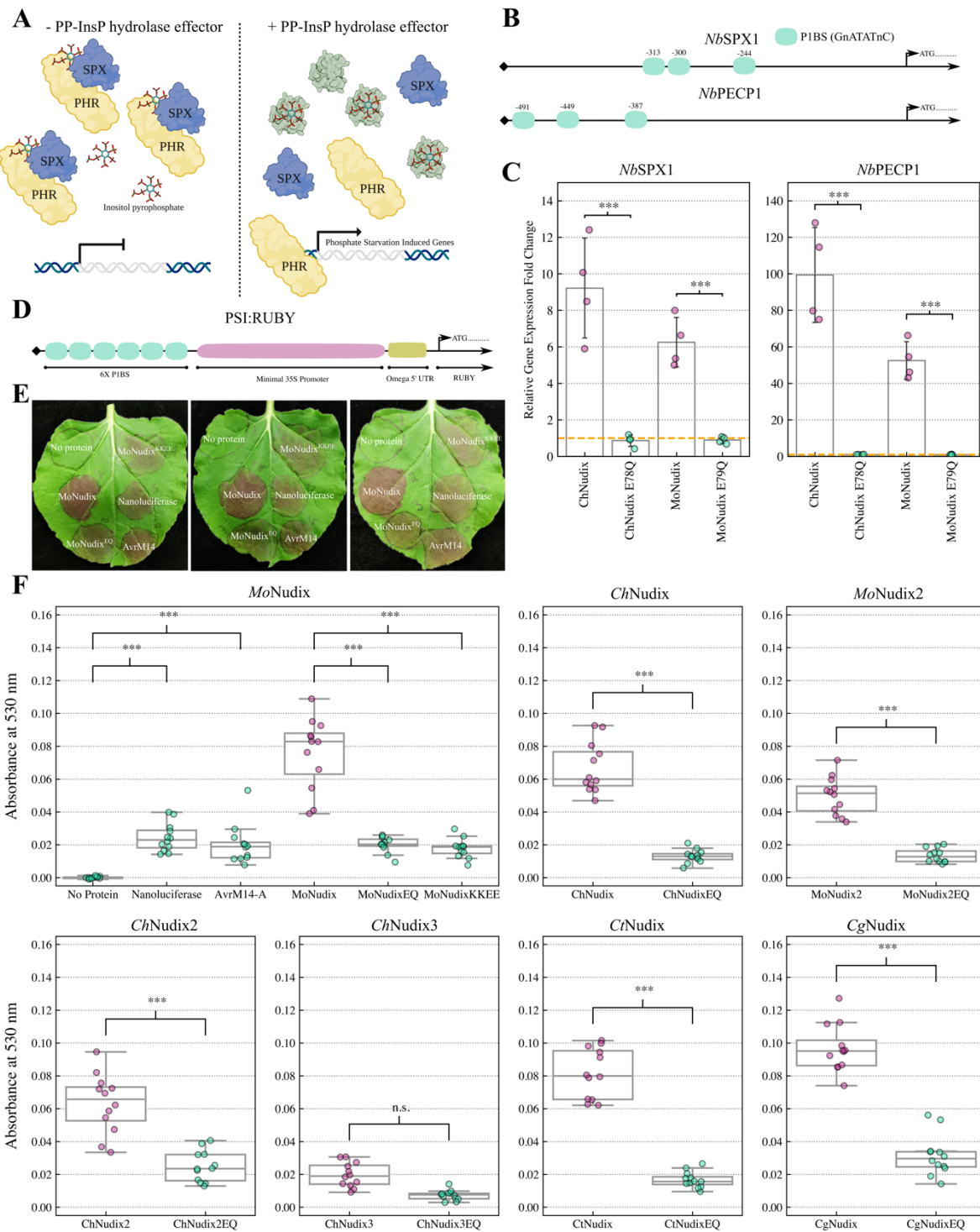


Figure 3: The *Magnaporthe* and *Colletotrichum* Nudix hydrolase effectors induce phosphate starvation responses in *Nicotiana benthamiana*. (A) A model for how a PP-InsP hydrolysing effector would activate the expression of phosphate starvation induced genes in plants by releasing PHRs from SPX proteins. (B) A schematic of the 500 base pairs upstream of the *NbSPX1* and *NbPECP1* start codons with the P1BS elements indicated. (C) RT-qPCR was completed on RNA extracted from *N. benthamiana* leaf tissue expressing either *MoNudix*, *ChNudix*, *MoNudix*^{E79Q}, *ChNudix*^{E78Q}, or leaf tissue transformed with an empty vector control. Values represent mean \pm SD across four biological replicates with individual data points shown as dots; *** p-value ≤ 0.001 (independent samples t-test). The relative gene expression fold change was calculated using the $2^{-\Delta\Delta Ct}$ method via comparison to the vector-only control treatment. The geometric mean of two reference genes was used for normalisation (*NbEF1a* and *NbUbe35*). The yellow dotted line indicates the relative expression level in the vector-only control treatment. (D) A schematic of the PSI:RUBY promoter and 5' UTR. The synthetic gene contains six P1BS elements in the promoter, a minimal 35 S sequence, and the Omega 5' UTR sequence from the Tobacco Mosaic Virus. Only the start of the RUBY CDS is depicted. Not to scale. (E) Representative leaf images demonstrating production of the red betalain pigment in leaf tissue co-transformed with the PSI:RUBY promoter/reporter and a Nudix effector or nanoluciferase (as labelled). (F) The absorbance at 530 nm of extracts from *N. benthamiana* leaf tissue co-transformed with the PSI:RUBY promoter/reporter with wild-type Nudix effectors and their corresponding mutant proteins (as labelled). There were 12 biological replicates for each treatment, as indicated by the dots overlaying the boxplots. In the boxplots, the horizontal line in the middle of the box represents the median value, and the box represents the interquartile range (IQR). To determine whether there was a significant difference between the treatments, a one-way ANOVA was completed followed by Tukey's post-hoc test; *** adjusted p-value ≤ 0.001 ; ** adjusted p-value ≤ 0.01 ; n.s. (not significant) adjusted p-value > 0.05 .

MoNudix promotes rice blast disease and inhibits rice immune responses

Both *MoNudix* and *ChNudix* use hydrolase activity to suppress the flg-22- and chitin-induced ROS burst in *N. benthamiana*. To further investigate the role of the PP-InsP hydrolase effectors in pathogen virulence and host immune suppression, we silenced *MoNudix* in *M. oryzae* using RNAi. We created two independent *M. oryzae* RNAi strains (RNAiNudix-1 and RNAiNudix-2), with a ~80% reduction in *MoNudix* gene expression in infected rice leaf sheaths at 28 hours post-inoculation (hpi) (Figure S6). Silencing of *MoNudix* resulted in a reduction of *M. oryzae* infection in whole plant spray inoculation assays (Figure 4A and 4B), indicating that the effector contributes to the virulence of the pathogen. Consistent with our experiments in *N. benthamiana*, silencing of *MoNudix* caused the accumulation of ROS in infected rice cells (Figure 4C and 4D), which coincided with restricted disease progression (Figure 4E).

Furthermore, confocal microscopy revealed that RNAiNudix-1 and RNAiNudix-2 strains triggered visible whole-cell and/or cell wall fluorescence in an average of 20 and 19%, respectively, of the host cells decorated by a single appressorium, as compared with only ~5% of those attacked by a single wild-type appressorium (Figures 4F and 4G). This result suggests that during infection the *MoNudix* effectors reduce the production of autofluorescent phenolic cell-wall components like lignin, that are induced by defense signalling. Collectively, our data demonstrate that *MoNudix* promotes the virulence of *M. oryzae* and the progression of rice blast disease, likely by suppressing rice defence responses.

Live-cell imaging studies have demonstrated that *M. oryzae* effectors are either delivered to the apoplast, the gaps between the fungal cell wall and host plasma membrane, or can be targeted to the host cell cytoplasm during infection.^{71,72} PP-InsPs are intracellular signalling molecules, therefore we hypothesise that *MoNudix* would function within the plant cell during infection. In the *M. oryzae*-rice pathosystem, cytoplasmic effectors are specifically localised within the biotrophic interfacial complex (BIC), which leads to the internalization of the effectors into the plant cell cytoplasm.⁷³⁻⁷⁶ Localization assays using *M. oryzae* strains expressing *MoNudix*:mRFP demonstrate that the Nudix hydrolase effector accumulates in BICs (Figure 4H), indicating that it functions as a cytoplasmic effector within the host plant cell. This localization pattern is consistent with sequence-based predictions⁷⁷ and with the predicted cytoplasmic localisation of plant Nudix hydrolases.^{78,79}

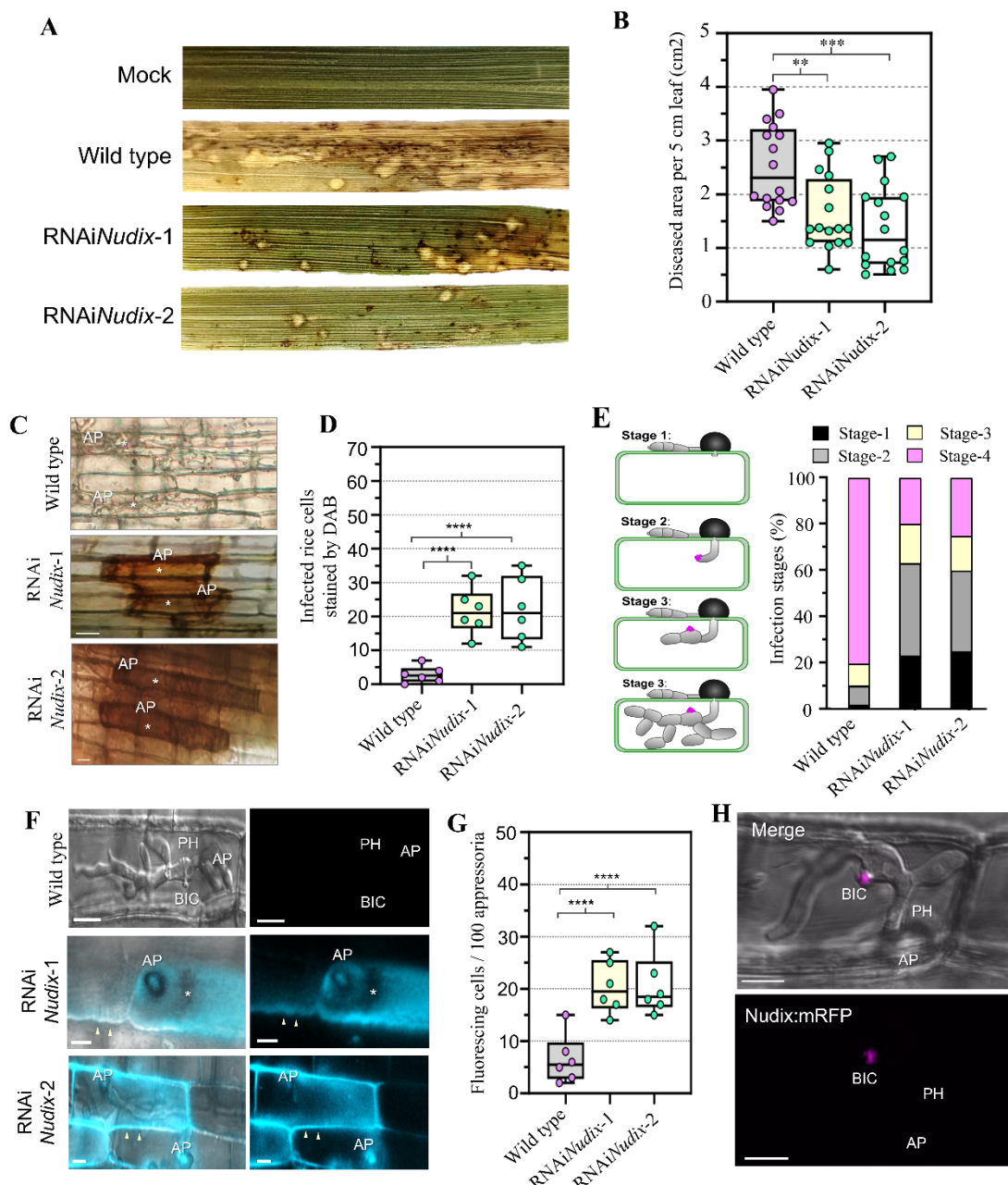


Figure 4: Silencing of *MoNudix* in *M. oryzae* indicates an important role in pathogen virulence and host immune suppression. (A) Whole plant spray inoculation assays with *M. oryzae* demonstrates that silencing *MoNudix* results in fewer, smaller lesions when compared to the wild-type control. (B) Quantification of the diseased area caused by wild type, RNAiNudix-1, and RNAiNudix-2 *M. oryzae* in 5 cm leaf segments of rice. Box and whisker plots with individual data points are shown; **P=0.0018, ***P=0.0002; n = 9 rice plants per replication. (C) DAB staining of penetrated plant cells at 32 hpi (hours-post inoculation). White asterisks

indicate infected rice cells. Scale bars = 10 μ m. (D) Percentages of infected cells stained by DAB. For each of the six replicates three sets of 100 cells were measured. ***P < 0.0001. (E) Quantification of four infection stages suggest a reduction of fungal virulence and colonization rate. For three replicates 100 infection sites were counted each. (F) Both wild-type and RNAi strains differentiated melanized appressoria (labelled AP) and invaded intact rice leaves, but the RNAi strains caused whole-cell (white asterisks) or cell wall fluorescence (white arrowheads) in rice under UV light, indicative of increased phenolic compound production and deposition in the cell wall. Scale bars = 10 μ m. (G) Quantification of fluorescing rice cells decorated with single appressoria of the wild-type or *Nudix*RNAi strains. For each of the six replicates three sets of 100 cells were measured. ***P < 0.0001. (H) *Nudix*:mRFP accumulates in BICs, which likely leads to its translocation into the rice cell cytoplasm. Images taken at 28 hpi. Image (top: merged bright field and mRFP fluorescence; bottom: mRFP fluorescence) shown as projections of confocal optical sections. Scale bars = 10 μ m.

Discussion

To monitor intracellular phosphate status, plant cells sense the level of PP-InsPs. In response to a lack of PP-InsPs, plants initiate a PSR that is predominantly mediated by the PHR family of transcription factors. In this study, we have identified a conserved family of PSR-inducing PP-InsP hydrolase effectors in *Magnaporthe* and *Colletotrichum* pathogenic fungi. Additionally, we demonstrate that the silencing of one PP-InsP hydrolase effector in *M. oryzae* significantly impairs the progression of rice blast disease.

Phosphate starvation and plant-microbe interactions

Plant phosphate status plays a critical role in establishing symbiosis with mycorrhizal fungi,^{32,33} and in regulating interactions between *A. thaliana* and the root endophyte *Colletotrichum tofieldiae*.²⁹⁻³¹ Phosphate starvation negatively regulates some plant immune responses, possibly to facilitate symbiosis with beneficial soil microbes,^{34,35} and/or to prevent immune-related suppression of Pi transport.³⁶ Our findings indicate that pathogenic *Magnaporthe* and *Colletotrichum* species employ PP-InsP hydrolase effectors which manipulate plant phosphate sensing mechanisms and inhibit immune responses. We demonstrate that the PP-InsP hydrolase effectors inhibit defence-related ROS production both during the infection process and when expressed in *N. benthamiana*. Suppression of ROS may occur due to the activation of PHRs. In *A. thaliana*, *AtPHR1* negatively regulates immune responses triggered by flg-22,³⁴ potentially via the increased production of RALF peptides.³⁵ Immunomodulatory RALFs are perceived by the receptor kinase FERONIA, which acts as a scaffolding protein to regulate immune receptor complex formation.³⁷ In support of PHR-activated RALF/FERONIA-mediated ROS suppression, we observe an increase in the expression of two *N. benthamiana* RALF genes with a P1BS element in their 3kb promoter region, facilitated by the enzymatic activity of the effectors. Tang *et al.*, (2022) reported 17 RALF genes in rice with at least one P1BS element in their 2 kb promoter region.³⁵ Further investigation is required to determine whether these rice RALFs act as negative-regulators of plant immunity, if their expression is controlled by PHRs, and if the PP-InsP hydrolase effectors from *M. oryzae* promote their production to inhibit immune signalling and enhance infection. The suppression of innate immune responses such as ROS production, may explain the significant contribution *MoNudix* makes to the severity of rice blast disease observed in our infection assays. Additionally, the increase in bioavailable intracellular phosphate that occurs during a PSR could enhance pathogen growth. Supporting this hypothesis, transcriptomic analysis suggests that *C.*

fructicola is starved of phosphate during initial biotrophic growth,⁸⁰ and infection assays indicate that excessive phosphate supply promotes *M. oryzae* virulence on rice.⁴²

Other roles of PP-InsPs in plants

While PP-InsPs play a critical role in regulating PHRs, they also possess other important signalling roles in plants cells, which could contribute to the virulence function of PP-InsP hydrolase effectors. PP-InsPs are involved in signalling by the phytohormones auxin and jasmonate. The jasmonate receptor complex consisting of CORONATINE INSENSITIVE 1 (COI1) and a JASMONATE ZIM DOMAIN (JAZ) protein, requires a PP-InsP co-factor to detect the bioactive form of jasmonate, JA-Ile ((3R,7S)-jasmonoyl-L-isoleucine).^{81,82} Similarly, the auxin receptor complex consisting of TRANSPORT INHIBITOR RESPONSE1 (TIR1), ARABIDOPSIS SKP1 HOMOLOG 1 (ASK1), and an AUXIN RESISTANT/INDOLE-3-ACETIC ACID-INDUCIBLE (Aux/IAA) transcriptional repressor also requires a PP-InsP co-factor.^{83,84} By manipulating intracellular PP-InsP levels, the *Magnaporthe* and *Colletotrichum* effectors may influence jasmonate and auxin signalling pathways, both of which have been identified as likely targets of previously studied effectors.⁸⁵⁻⁹⁰

While our results indicate that these effectors hydrolyse PP-InsPs both *in vitro* and *in planta*, further research is required to isolate which of the various functions of PP-InsPs are important for the virulence of pathogenic *Magnaporthe* and *Colletotrichum* fungi. Identifying if the effectors preferentially hydrolyse a specific PP-InsP isomer/s *in planta* may provide further insight into their virulence function.

Which PP-InsP isomer is hydrolysed by the *Magnaporthe* and *Colletotrichum* effectors *in planta*?

The presence of at least four distinct PP-InsP compounds in plants, 1/3-PP-InsP₅, 5-PP-InsP₅, 4/6-PP-InsP₅, and 1/3,5-PP-InsP₄ (commonly referred to as InsP₈), is supported by experimental evidence.⁶ However, in our study, we exclusively examined the ability of the *Magnaporthe* and *Colletotrichum* effectors to hydrolyse 5-PP-InsP₅. This limitation is primarily due to the commercial unavailability of PP-InsPs. Nevertheless, our *in planta* findings demonstrate the ability of these effectors to activate PHRs, strongly suggesting that at least 5-PP-InsP₅ and/or InsP₈ are hydrolysed by the effectors. InsP₈ mediates SPX binding to PHRs,^{3,4} and its levels are likely dependent on the availability of 5-PP-InsP₅.⁶ Consistently, plants unable to synthesise 5-PP-InsP₅ and InsP₈ demonstrate a PHR-dependent constitutive

PSR.^{3,5,6,91} Therefore, the hydrolysis of either compound by the effectors would explain the observed PHR activation. The structure of *MoNudix* indicates that the binding site can accommodate either 5-PP-InsP₅ or InsP₈. Intriguingly, we predict that the additional phosphate moiety in InsP₈ would interact with the highly conserved arginine-35 residue and may enhance binding affinity, suggesting a potential preference for InsP₈ over 5-PP-InsP₅. To precisely identify the targeted PP-InsP/s, future studies could use the recently developed capillary electrophoresis coupled to electrospray ionization mass spectrometry (CE-ESI-MS) method to analyse PP-InsP extracts from plant tissue expressing the effectors.⁹²

A model for the biological function of the PP-InsP hydrolase effector family

Our live-cell imaging results demonstrate that RFP-tagged *MoNudix* localises to the BIC during infection. BIC localisation suggests that the *MoNudix* effector is translocated into the host cytoplasm and does not function as an apoplastic effector.^{72,73,93} This contrasts with a previous study on the sequence-related *CtNudix*,⁴⁴ which suggested that the effector would function in the apoplast, as expression of the effector in *N. tabacum* with a signal peptide results in cell death. The decision of Bhadauria *et al.*, (2013) to produce the effector with a signal peptide was not informed by protein tracking during infection and therefore the cell death phenotype when the effector is secreted in *N. tabacum* is potentially unrelated to its virulence function during infection.

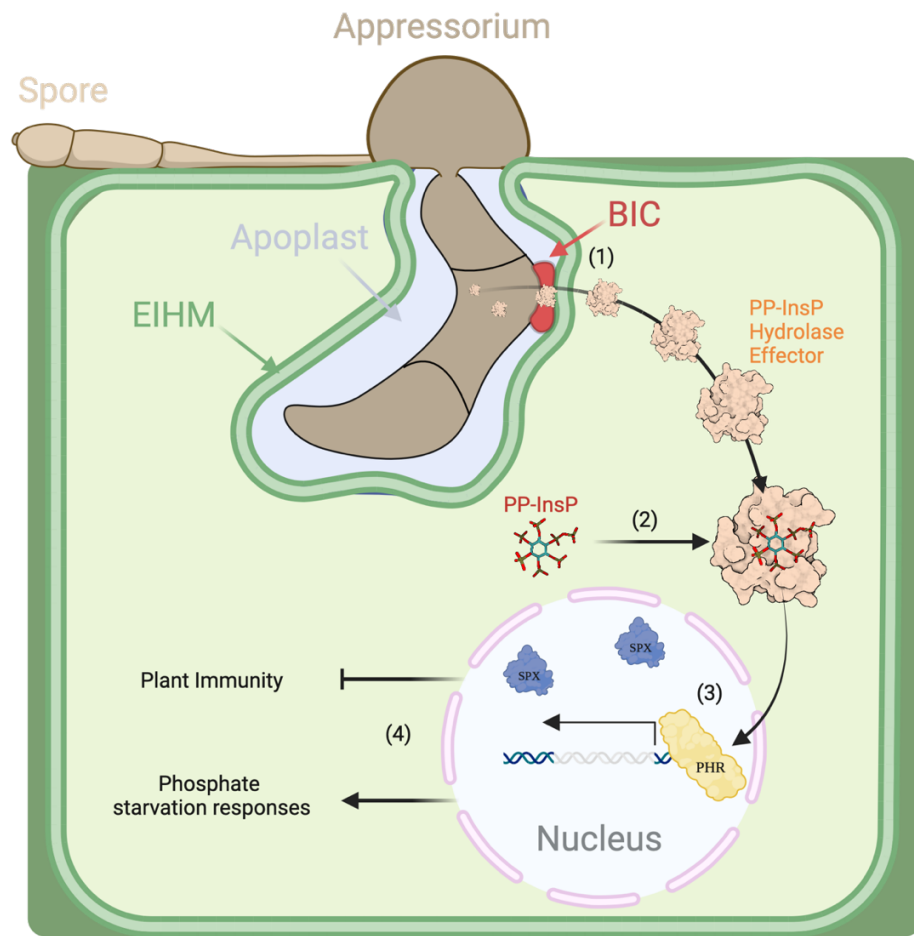


Figure 5: A model for the virulence function of the *Magnaporthe* and *Colletotrichum* Nudix hydrolase effectors. (1) The effectors are secreted from the invading fungus into the host plant cell cytoplasm. (2) The effectors act as enzymes, hydrolysing the pyrophosphate bonds on inositol pyrophosphate signalling molecules. (3) The loss of inositol pyrophosphates prevents SPX-mediated inhibition of PHRs, resulting in the transcription of phosphate starvation inducible genes. (4) Phosphate starvation responses are activated, including those that suppress plant immune responses.

On the basis of our data, we propose a model by which the *Magnaporthe* and *Colletotrichum* Nudix effectors, including *CtNudix*, are translocated into their respective host plant cells (Figure 5). Once inside, the effectors function as PP-InsP hydrolase enzymes, reducing the availability of plant PP-InsPs and subsequently activating PHRs (Figure 5). This induces a plethora of transcriptional changes, some resulting in the suppression of immune responses like ROS production and lignin deposition (Figure 5). Ultimately, the immune suppression promotes disease progression.

Acknowledgments

We thank the Plant Services Team at the Australian National University for providing *N. benthamiana* seedlings, and all the Williams lab members for helpful discussion. This work was supported by funding from the ANU Future Scheme (35665). SJW was supported by an ARC Future Fellowship (FT200100135). EO-G was supported by Louisiana Board of Regents grant #LEQSF (2022-24)-RD-A-01. CLM was supported by the Australian Government Research Training Programme (RTP) Stipend Scholarship and the Australian Institute of Nuclear Science and Engineering (AINSE) Ltd. Postgraduate Research Award (PGRA). The authors acknowledge the use of the ANU crystallisation facility. The authors also acknowledge the use of the Australian Synchrotron MX facility and thank the staff for their support. This research was undertaken in part using the MX2 beamline at the Australian Synchrotron, part of ANSTO, and made use of the Australian Cancer Research Foundation (ACRF) detector.

Figures 3A and 5 were created with BioRender.com.

Author contributions

C.L.M, J.R.G, E.O-G, and S.J.W designed the experiments. C.L.M, C.S.Z., S.A, S.d.P, E.E, and S.S performed the experiments. C.L.M, C.S.Z, S.A, J.R.G, D.J.E, E.O-G, and S.J.W analysed the data. C.L.M wrote the manuscript with input from all authors.

Declaration of interests

The authors declare no competing interests.

Methods

Resource availability

Further information and requests for resources and reagents should be directed to and will be fulfilled by the lead contact, Simon J. Williams (simon.williams@anu.edu.au).

Materials availability

All requests for the plasmids and purified proteins should be directed to and will be fulfilled by the lead contact, Simon J. Williams (simon.williams@anu.edu.au).

Data and code availability

- Atomic coordinates and structure factor amplitudes for *MoNudix* have been deposited in the Protein Data Bank (PDB) under accession code 8SXS. The diffraction images have been uploaded to proteindiffraction.org.
- This paper does not report original code.
- Any additional information required to reanalyse the data reported in this paper is available from the lead contact upon request.

Experimental model and subject details

Nicotiana benthamiana

Nicotiana benthamiana plants were grown in a growth room at 25 °C under a 16-hour/8-hour light/dark photoperiod. Fully expanded leaves from 5-week-old plants were used for *Agrobacterium*-mediated transient gene expression for qPCR and RUBY promoter/reporter assays.

Oryza sativa

Rice (*O. sativa*) plants for both whole plant spray inoculation and detached leaf sheath assays were grown in Bacto Top Soil (Michigan Peat Co., Houston, Texas) in a Caron 7301-50 Plant Growth Chamber with equal numbers of fluorescent lamps (Philips ED37, 400 W). At rice seedling height, ~1 m from the bulbs, light ranged in intensity from 600 to 1,200 $\mu\text{mol m}^{-2} \text{s}^{-1}$. Plants were grown at ~70% relative humidity under a daily cycle of 12 h of light at 28°C and 12 h of darkness at 24°C. At 2 weeks, plants are fertilized with Jack's Professional Peat Lite 20-10-20 Fertilizer (#77860; JR Peters, Inc.; Allentown, PA). Whole plant infection assays were performed by spray inoculation of 2–3-week-old rice plants as previously described.⁷²

Fungal strains

Fungal strains (*M. oryzae*) were stored on dried filter papers at -20°C and cultured on rice bran agar plates⁹⁴ at 25°C for up to 2 weeks under continuous light in Percival Scientific (Model

CU-36L5) tissue culture incubators equipped with one half fluorescent lights (FT20T12/cw, 20W) and one-half black lights (FT20T12/BL, 20W).

Bacterial strains

E. coli NEB® 5-alpha and *Agrobacterium tumefaciens* strain GV3101 were grown in LB media with 220 rpm shaking at 37 °C and 28 °C, respectively. Appropriate antibiotic concentrations when used for *E. coli* and *Agrobacterium tumefaciens* growth were ampicillin 100 µg/mL, kanamycin 50 µg/mL, spectinomycin 50 µg/mL, gentamycin 25 µg/mL and rifampicin 50 µg/mL.

For protein expression in Shuffle® T7 express *E. coli* the growth conditions were terrific broth (TB) media at 30 °C with 50 µg/mL kanamycin. For protein expression in *E. coli* BL21 (DE3) the growth conditions were ZYM-5052 media⁹⁵ at 37 °C with 50 µg/mL kanamycin.

Method details

Plasmid construction

All effector gene sequences had their predicted signal peptide⁹⁶ removed, were codon optimised for *E. coli* and ordered from Integrated DNA technologies, Inc IDT® as double-stranded DNA fragments. The DNA fragments were cloned into either a modified pOPIN plasmid⁹⁷ with a T7 promoter and a 6xHIS 3C protease site N-terminal tag⁹⁷ if used for protein expression in *E. coli*, or a level 1 MoClo plasmid⁹⁸ along with a 35 S promoter, Omega 5' UTR translational enhancer, 3xHA N-terminal tag, and octopine synthase terminator if used for expression in *N. benthamiana*. All level 1 MoClo genes were subsequently inserted into the level 2 acceptor plasmid pICSL4723 before transformation into *Agrobacterium tumefaciens* (GV3101).

The RUBY polyprotein gene sequence⁹⁹, and all gene promoter sequences used in this study (listed in Table S3) were ordered from Integrated DNA technologies, Inc IDT® as double-stranded DNA fragments and cloned into level 0 MoClo plasmids⁹⁸, before being used to create level 1 and level 2 plasmids. *Entamoeba histolytica* IP6KA and *Homo sapiens* DIPP1 were ordered as *E. coli*-codon optimised double-stranded DNA fragments and cloned into the modified pOPIN⁹⁷ plasmid with a T7 promoter and a 6xHIS 3C protease site N-terminal tag. All gene sequences had any BbsI and BsaI cleavage sites removed without altering protein sequence to enable GoldenGate assembly.

Protein expression and purification

AvrM14-A, *At*Nudx7, and *At*Nudx7^{E154Q} proteins were purified previously.⁴⁶ *Eh*IP6KA and *Hs*DIPP1 were expressed in *E. coli* BL21 (DE3) cells using ZYM-5052 autoinduction media.⁹⁵

Cells were grown by continuous shaking at 37 °C until the OD_{600nm} reached 0.6 – 0.8. The temperature was then dropped to 18 °C and cells were incubated with shaking for another 18 hours before harvesting via centrifugation.

MoNudix, *MoNudix2*, and *ChNudix* proteins (wild-type and mutants) were expressed in *E. coli* Shuffle® cells grown in Terrific Broth. Cells were grown by continuous shaking at 30 °C until the OD_{600nm} reached 0.6 – 0.8. The temperature was then dropped to 16 °C, IPTG was added to a final concentration of 200 μM, and incubation with shaking continued for another 18 hours before harvesting via centrifugation.

Following centrifugation, all cell pellets were resuspended in lysis buffer (50 mM HEPES pH 8.0 (*MoNudix*, *MoNudix*^{E79Q}, *MoNudix*^{KKKE}), pH 7.5 (*MoNudix2*, *MoNudix2*^{EQ} *ChNudix*, *ChNudix*^{E78Q}), or pH 7.0 (*HsDIPP1*, *EhIP6KA*), 150 mM NaCl, 1 mM PMSF, 1 μg ml⁻¹ DNase, and 1 mM DTT (DTT only included for *EhIP6KA* and *HsDIPP1*)). All cells were lysed using sonication and cellular debris pelleted by centrifugation. The resulting supernatant was applied to a 5 mL HisTrap FF crude column (Cytiva, Marlborough, Massachusetts). To remove loosely bound proteins, the column was washed with the lysis buffer without PMSF or DNase containing 30 mM imidazole. The remaining bound proteins were eluted with a continuous gradient of imidazole from 30 mM to 250 mM over 10 minutes, using an Äkta pure chromatography system. Fractions were analysed by Coomassie-stained SDS-PAGE and fractions containing the protein of interest were pooled, dialysed to remove the imidazole, and incubated with recombinant 6xHis-tagged 3C protease overnight at 4 °C (except *EhIP6KA*, which was stored following dialysis without 3C protease incubation). The protein of interest was separated from any uncleaved protein, the fusion tag, and 3C protease by immobilized metal affinity chromatography and purified further by size-exclusion chromatography (SEC) using either a HiLoad 16/600 Superdex® 75 pg or a HiLoad 26/600 Superdex® 75 pg column pre-equilibrated in buffer (10 mM HEPES (pH same as in corresponding lysis buffer), and 150 mM NaCl). After SEC, fractions containing the protein of interest were identified using SDS-PAGE and concentrated using Amicon® Ultra Centrifugal filters (Merck, Darmstadt, Germany) before storage at -80 °C. The sequences of all purified proteins used in this study are listed in Table S4.

Putative Nudix hydrolase effector identification

To identify putative Nudix hydrolase effectors homologous to *MoNudix*, the NCBI protein database¹⁰⁰ was searched using blastp with the protein sequence of *MoNudix* (default parameters; word size = 5, expect threshold = 0.05). Any identified hits without a predicted signal peptide or Nudix hydrolase domain were filtered out by screening the sequences using

SignalP6.0⁹⁶ and InterProScan.¹⁰¹ To reduce the length of the list while retaining sequence diversity, if two or more sequences shared > 95% sequence identity, only one sequence was selected at random to remain in the list presented in Table S1.

PhyML⁶³ (version 3.3) was used to estimate a maximum-likelihood phylogeny with selected protein sequences from this list, the resulting phylogeny was visualised using iTOL⁶⁴ (version 6.7.6).

Agroinfiltrations

Agrobacterium tumefaciens (GV3101) with the desired plasmid was suspended in infiltration buffer (10 mM MES pH 5.6, 10 mM MgCl₂ and 200 μM acetosyringone) to an optical density at 600 nm (OD_{600nm}) of 0.5 (for PSI:RUBY co-infiltrations) or 1.0 (for qPCR and the ROS burst assay). For co-infiltrations, *Agrobacterium tumefaciens* (GV3101) with a PSI:RUBY promoter/reporter plasmid was added to the infiltration buffer to an OD_{600nm} of 0.5. The final combined OD_{600nm} was 1.0 for all infiltrations. All cultures were incubated in the dark at 28 °C with 220 rpm shaking for 2 to 3 hours before syringe-infiltration into *N. benthamiana* leaves. Infiltrated plants were kept in the same growing conditions as before infiltration.

ROS burst assays

Measurement of ROS was completed as described previously with some minor modifications.¹⁰² In brief, *N. benthamiana* leaf discs (4 mm diameter) were floated on water overnight in a 96-well plate. The water was replaced with an elicitor solution (200 μM luminol, 20 μg ml⁻¹ horseradish peroxidase and 100 nM flg-22 or 5 μg ml⁻¹ chitin), and luminescence was measured over time using a Tecan Infinite® M Plex (Tecan, Männedorf, Switzerland) plate reader at room temperature.

Immunoblot analysis

N. benthamiana leaf tissue was frozen in liquid nitrogen and ground into a fine powder. Soluble protein was extracted by adding an equal volume of lysis buffer (50 mM HEPES (pH 7.5), 1 mM EDTA, 2% PVPP, 5 mM DTT, 1 mM PMSF). The samples were mixed by rotating at 4 °C for 2 minutes, prior to centrifugation at 4 °C for 15 minutes at 17 000 xg and the supernatant was collected. Approximately 20 μg of each protein solution was separated on two 15% SDS-PAGE gels. The first gel was stained with Coomassie blue to assess protein loading across samples, while proteins from the second gel were transferred onto a 0.22 μM nitrocellulose membrane. Blots were probed with HRP-conjugated mouse anti HA-tag (1:2000 dilution) either from ABclonal (Woburn, Massachusetts) or Roche (Basel, Switzerland). Pierce™ ECL substrate (Thermo Fisher Scientific, Waltham, Massachusetts) was added to the immunoblots and chemiluminescence detected using a ChemiDoc imager (Bio-Rad, Hercules, California).

General substrate screening and mRNA decapping assays

The phosphomolybdate Nudix hydrolase enzyme assays and the mRNA decapping assays were performed as described previously.⁴⁶

Inositol pyrophosphate hydrolysis assays

To assess inositol pyrophosphohydrolase activity 5-PP-InsP₅ was first synthesised in a 500 µL reaction volume following previously described methods¹⁰³ using the purified *EhIP6KA* protein. The resulting 5-PP-InsP₅ was purified using the previously described gel electrophoresis-based method.¹⁰⁴ Purified 5-PP-InsP₅ was incubated with 5 µM recombinant protein in 50 mM Tri-HCl pH 8.0, 5 mM MgCl₂ at 37 °C for 60 minutes. After incubation the reaction products were separated and visualised using previously described methods¹⁰⁵ with minor modifications (we utilised a smaller gel (8.3 x 7.3 x 0.1 cm) and ran the gel at 300V for approximately 5 hours, until the dye front was 2/3 of the way through the gel).

Protein crystallisation and structure determination

Crystallisation screening with purified *MoNudix* protein (residues 35 to 156) was conducted using a Mosquito robot (STP LabTech, Melbourn, UK) in a 96-well plate format using sparse matrix screens. The sitting drop vapour-diffusion method of crystallization was used and drops consisting of 100 nL 30 mg/mL *MoNudix* containing 18 mM InsP₆ (Merck, Darmstadt, Germany) combined with 100 nL reservoir solution were equilibrated against 100 µL reservoir solution. The reservoir solution resulting in the *MoNudix* crystals analysed in the study was 200 mM Potassium thiocyanate with 20% PEG3350 (from the SG1™ Screen (Molecular Dimensions, Newmarket, United Kingdom)). To create the cryoprotectant 80 µL of the reservoir solution was combined with 10 µL of glycerol and 10 µL of ethylene glycol. The crystal was transferred to the cryoprotectant before flash cooling in liquid nitrogen. Diffraction datasets were collected on the MX2 beamline at the Australian Synchrotron.¹⁰⁶ The highest resolution dataset allowed by the beamline geometry was selected for processing in XDS, and then scaled using AIMLESS in the CCP4 suite.^{107,108} The *MoNudix* crystal structure was determined using maximum-likelihood molecular replacement (MR) with Phaser in Phenix.^{109,110} The MR search model was an AlphaFold⁵⁹ model of the *MoNudix* sequence used for crystallisation (sequence in Table S4). For all datasets automated model building and initial refinement was completed using Phenix AutoBuild.¹¹¹ Subsequent model building was carried out manually in Coot¹¹² in-between rounds of automated refinement using Phenix Refine¹¹³. Analysis of the final structures was performed with Coot¹¹², ChimeraX⁶⁶, and ConSurf⁶⁵ (default parameters were used for analysis). Map coordinates and structure files have been deposited in the Protein Data Bank under ID 8SXS, summary statistics are listed in Table S5.

Micro-scale Thermophoresis

MST experiments were performed on a Monolith.NT115 instrument (NanoTemper Technologies, Munich, Germany) at 25 °C. MoNudix and MoNudix^{KKEE} were labelled with Alexa Flour 647 succinimidyl ester (Thermo Fisher Scientific) and used at a final concentration of 50 nM. In brief, 20 µM of the protein solution was incubated with 2-fold molar excess of the fluorophore for 2 hours in the dark at room temperature, and the free dye was subsequently removed using a PD-10 desalting column (Cytiva). A stock solution of InsP₆ was serially diluted in buffer (10 mM HEPES pH 8.0, 150 mM NaCl), mixed 1:1 with the labelled protein and loaded into standard capillaries (NanoTemper Technologies). MST measurements were recorded using 20 % LED power and 20 to 80 % MST power and analysed using MO. Affinity Analysis software 2.2.7 (NanoTemper Technologies).

RNA Extractions and RT-qPCR

At 3 days post-infiltration (dpi) approx. 100 mg of *N. benthamiana* leaf tissue was collected from each infiltration site and frozen in liquid nitrogen. For RNA extraction and purification, the Monarch® Total RNA Miniprep Kit (NEB, Ipswich, Massachusetts) was used following the recommended protocol for plant tissue, with tissue lysis achieved by grinding the plant tissue into a fine powder while frozen in liquid nitrogen.

cDNA synthesis from the purified RNA was achieved using the LunaScript® RT SuperMix Kit (NEB). qRT-PCR was performed using the Luna® Universal qPCR Master Mix (NEB) on a ViiA 7 PCR System (Applied Biosystems, Waltham, Massachusetts), with primers listed in Table S2. Relative expression levels were calculated using the 2^{-ΔΔCt} method,¹¹⁴ accounting for the PCR efficiency of each primer,¹¹⁵ and normalised to the geometric mean¹¹⁶ of the internal controls, *NbUbe35*, and *NbEIF1a*.

Betalain extraction and measurement

We used a modified version of a previous betalain extraction method.⁹⁹ In brief, at 3 dpi six 4 mm leaf disks were excised from the infiltrated area, incubated for 30 minutes with 30 rpm rotation in 1 mL 50% methanol, and then 200 µL from each solution was transferred into a transparent 96-well plate and absorbance at 530 nm was measured. All values were zeroed using the absorbance measurement of 50% methanol alone.

Live-cell imaging of Nudix:mRFP *M. oryzae* and the RNAi strains *in planta*

Rice leaf sheath inoculations were performed as described¹¹⁷ with the following modification. We used sheath pieces that were thinner trimmed sheaths (~3 cell layers thick). Susceptible rice variety YT-16 was used unless otherwise mentioned. Briefly, 7-cm long leaf sheath pieces from 3-week-old plants were placed in a sealable Pyrex glass moist chamber. Leaf sheath

sections were placed on inverted 8-well PCR tube strips to avoid contact with wet paper and to hold the epidermal cells directly above the mid-vein horizontally flat for the uniform distribution of inoculum in trimmed leaf sheath pieces.⁷⁶ A spore suspension (104 spores/ml in sterile 0.25% gelatin, Cat. #G-6650, Sigma-Aldrich) was prepared from 10-day-old cultures and injected into one end of the sheath using a 100-ml pipette. Each segment was trimmed at 18 to 30 hours post inoculation (hpi), and imaged immediately by laser confocal microscopy. Biological replicates were independent experiments performed with fungal cultures fresh out of frozen storage and with new rice plants. All conclusions are supported by at least 3 biological reps, with each replication including observation of ~100 infection sites. Confocal imaging was performed with a Leica SP8 confocal microscope system using two water immersion objectives, C-Apochromat 40x/1.2 WCorr. and C-Apochromat 63x/1.2 WCorr. Excitation/emission wavelengths were 543 nm/560–615 nm for mRFP, and were 358 nm/461 nm for cell wall fluorescence. Image acquisition and processing were done using Leica LAS X 2020 software. For ROS analysis, rice leaves inoculated with conidium suspensions (3x10⁵ spores/mL) of the wild-type and RNAi strains were stained with DAB at 32 hpi (hours-post inoculation).

ROS detection *in planta*

Host-derived ROS was observed by staining with DAB (Sigma-Aldrich) as described previously.¹¹⁸ Rice leaves inoculated with RNAi and wild type strains at 30 hpi were incubated in 1mg/mL DAB solution, pH 3.8, at room temperature for 8 hours and destained with ethanol:acetic acid solution (94:4, v/v) for 1 hour.¹¹⁹

Generation of RNAi strains in *M. oryzae*.

The RNAi cassette from plasmid pRedi¹²⁰ was used to generate an RNAi construct targeting *MoNudix* transcripts. The 312-bp sense and antisense fragments were amplified from genomic DNA of *M. oryzae*, using the primers RNAi(Nudix1)-fw and RNAi(Nudix1)-Rv, and RNAi(Nudix1)i-fw and RNAi(Nudix1)i-Rv, respectively (sequences listed in Table S2). The sense and antisense fragments were used to replace the XhoI-SnaBI and BglII-ApaI fragments of pRedi and were thus separated by 135 bp of the intron of the *M. oryzae* Cut2 gene (National Center for Biotechnology Information: XM_365241.1), existing in pRedi, as a linker.¹²⁰ Plasmid inserts were subsequently sequenced to verify sequence accuracy. The resulting 6.0-kb RNAi construct was excised from pRedi by DraI digestion, purified by gel elution, and transformed into conidial protoplasts of *M. oryzae*, and single spore isolates were generated.¹¹⁷ Knockdown of the target genes was confirmed by qRT-PCR¹²¹ at 28 hours post inoculation. At

this point, rice plants showing satisfactory reduction of the transcription levels were used in our standard conidial spray inoculation and leaf sheath assays.

Statistics for *M. oryzae* experiments

All experiments were performed with at least 3 biological replications, which are independent experiments with fungal cultures directly growing out from frozen storage and different rice plantings. Biological replications included at least two technical repeats (independent assays with the same biological materials) for further confirming reproducibility of the data. The sample sizes, number of biological replicates, and the statistical tests used in each experiment are specified in the figure legends. Data were analysed using an unpaired two-tailed Student's t-test. $P < 0.05$ was considered significant and exact values are shown where appropriate. All statistical analysis was performed using R Statistical Software (version 4.1.2) and Prism9 (GraphPad). Dot plots were routinely used to show individual data points and generated using Prism9 (GraphPad). Bar graphs show the mean \pm s.e.m. (unless stated otherwise) and were generated using Prism9 (GraphPad). Analysis of datasets are represented by box-and-whisker plots that show the 25th and 75th percentiles, the median indicated by a horizontal line, and the minimum and maximum values indicated by the ends of the whiskers.

Supplemental information

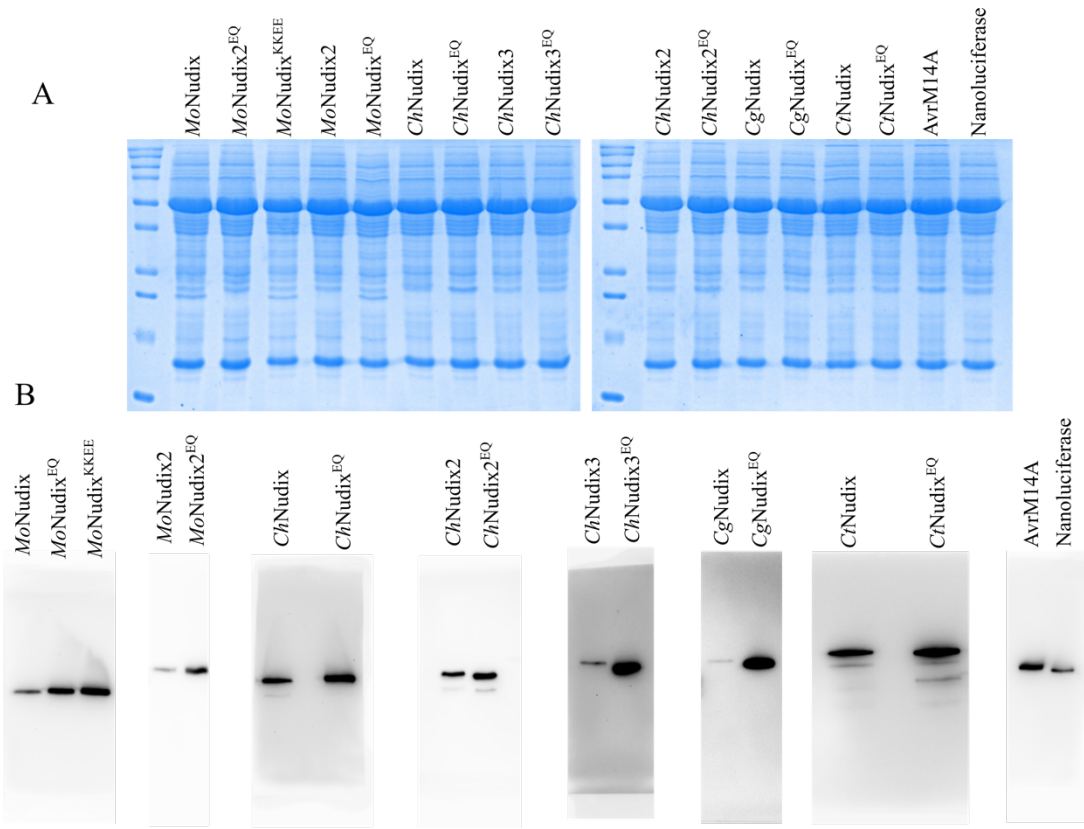


Figure S1: Western blots of soluble protein extracts demonstrates production of all effector proteins in *N. benthamiana* leaves. Related to Figure 1 and Figure 3. (A) Coomassie-stained SDS-PAGE protein gels demonstrate equivalent total protein amounts in the soluble *N. benthamiana* protein extracts from the agroinfiltrated plant tissue used for western blotting. The effector that should be present in each sample is indicated along the top of the gel; the first lane of both gels contains the Precision Plus Protein Dual Color Standards (Biorad, Hercules, California) (B) Total protein extracts from *N. benthamiana* leaf tissue agroinfiltrated with a construct to express a HA-tagged effector, as labelled along the top of each blot, were analysed by western blotting. Blots were probed with mouse anti-HA HRP-conjugated antibodies.

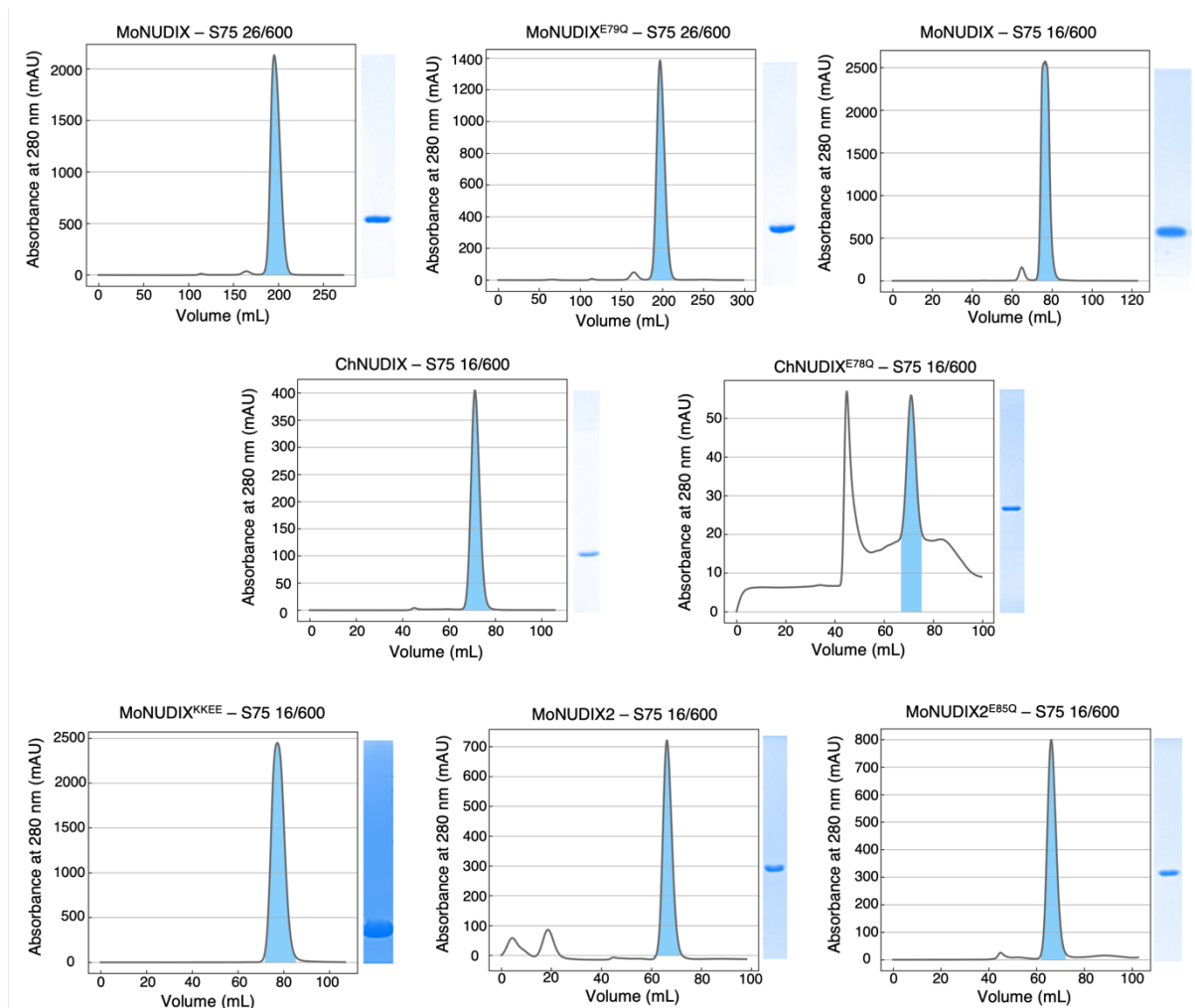


Figure S2: All effector proteins used in enzymatic assays were purified to homogeneity. Related to Figure 1, Figure 2, and Figure S3. Size exclusion chromatography (SEC) profiles for all effector proteins purified in this study. The label at the top of each profile indicates the protein and the Highload Superdex column (Cytiva) used in the purification process. The area under the peak shaded blue indicates the volume collected for each effector. Alongside each profile is a Coomassie-stained SDS-PAGE gel demonstrating the purity of the final protein sample collected following SEC.

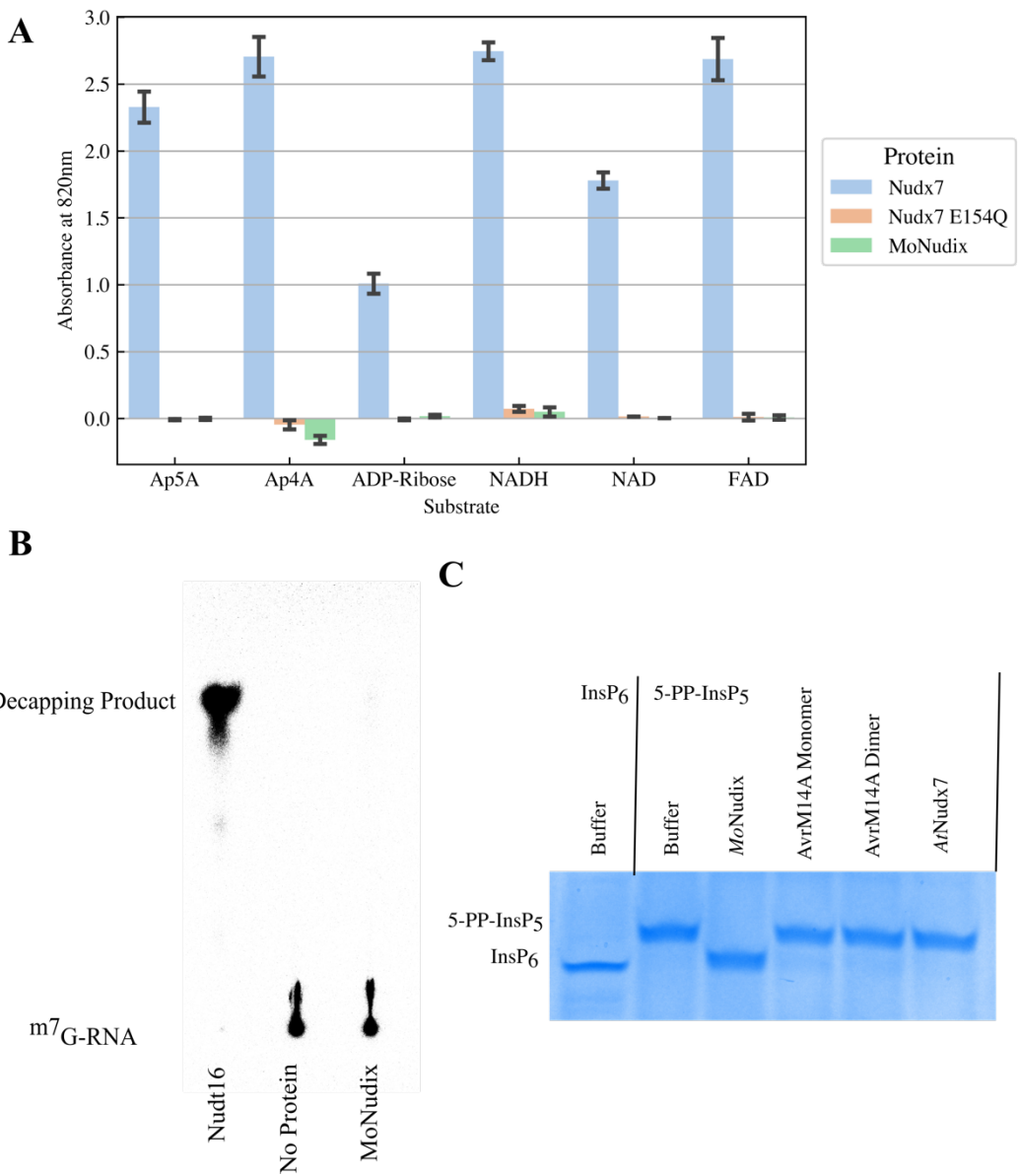


Figure S3: *MoNudix* does not effectively hydrolyse the substrates hydrolysed by previously characterised Nudix effectors *in vitro*. Related to Figure 1. (A) Purified recombinant proteins (*AtNudx7*, *AtNudx7^{E154Q}*, and *MoNudix*) were incubated with 2 mM of the indicated substrate at 37 °C for 30 minutes. Substrate hydrolysis was detected via the production of a blue-coloured phosphomolybdate complex that absorbs light with a wavelength of 820 nm. Results are presented as mean absorbance ± standard deviation (n = 3). A buffer only control without any Nudix hydrolase protein was used to blank the spectrophotometer before measurement. *AtNUDX7* and *AtNUDX7^{E154Q}* were used as positive and negative controls, respectively. (B) Recombinant proteins (*HsNudt16*, a known mRNA decapping enzyme,¹²² and *MoNudix*) were incubated with ^{m7}Gp₃₂pp-RNA and the reaction products analysed by thin-layer chromatography (TLC). Capped RNA remains at the origin of the TLC plate, whereas decapping products migrate up the plate. (C) Purified recombinant protein (*MoNudix*, *AvrM14-A* monomer, *AvrM14-A* homodimer, *AtNudx7*) at a concentration of 5 μM or protein storage buffer was incubated with either inositol hexakisphosphate (InsP₆) or an inositol pyrophosphate (5-PP-InsP₅) (indicated along the top of the gel) for 60 minutes at 37 °C. The reaction products were separated using a polyacrylamide gel and visualised by staining

with toluidine blue. The downwards shift of the band in the *MoNudix* lane when compared to the other 5-PP-InsP₅ treatments, indicates that *MoNudix* converts 5-PP-InsP₅ to InsP₆.

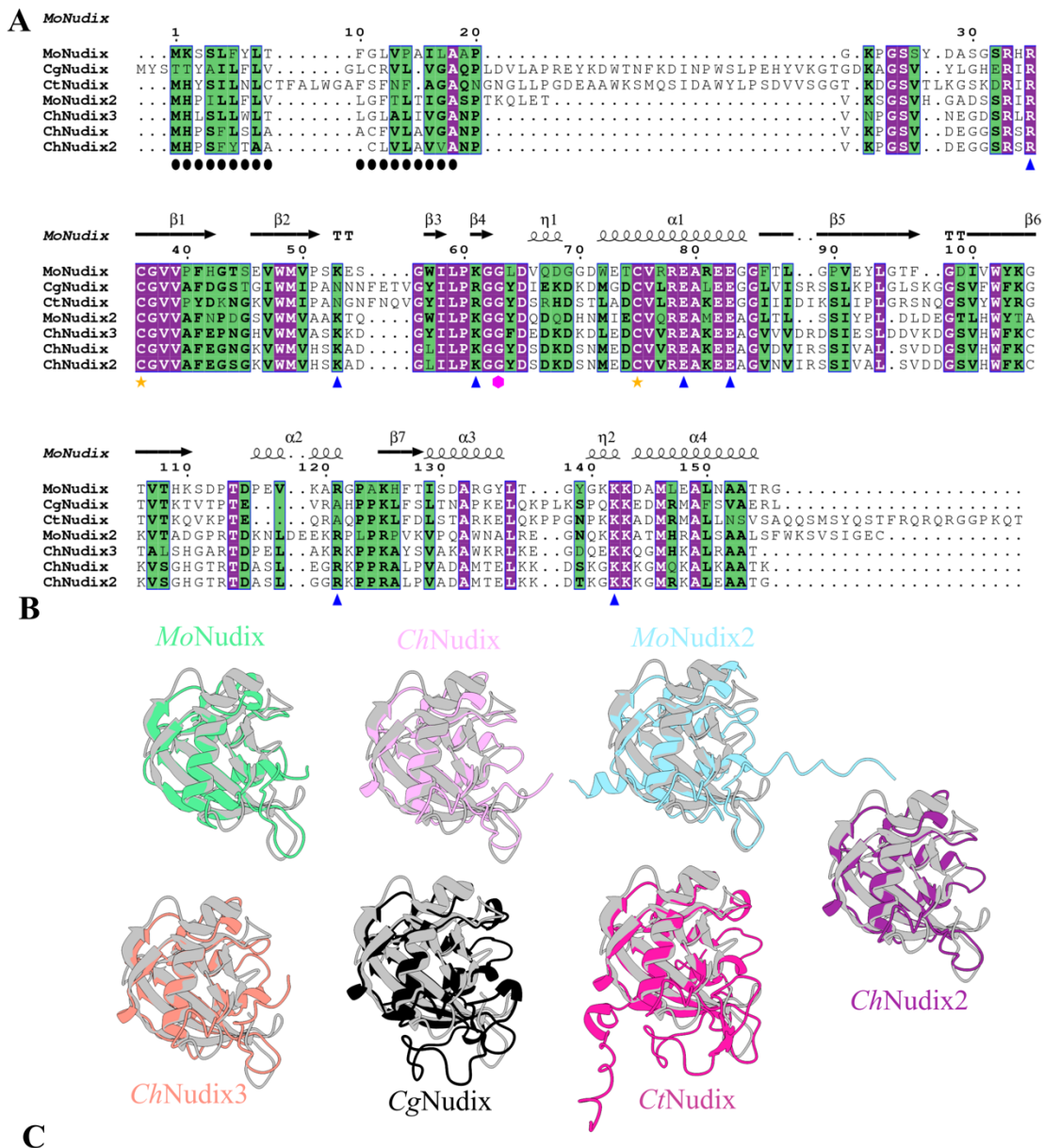


Figure S4: MoNudix and homologous effectors exhibit structural similarity to *HsDIPP1* and conservation of disulphide bonded cysteines as well as the predicted signal peptide and amino acids likely involved in PP-InsP binding and hydrolysis. Related to Figure 2.

(A) Sequence alignment (produced using ESPript 3.0¹²³) of the *Magnaporthe* and *Colletotrichum* Nudix effectors analysed in this study. Residues with 100% conservation are

coloured purple, conserved substitutions are coloured green, non-conserved residues are white. The predicted signal peptide region from *MoNudix* is indicated by black circles, the cysteines involved in disulphide bond formation are indicated by stars, the conserved glycine at position +1 in the Nudix box by a pink hexagon, and the amino acids likely involved in PP-InsP binding and hydrolysis in *MoNudix* are indicated by blue triangles. Above the sequence alignment is the secondary structure of *MoNudix* (black arrows indicating β -strands, squiggles indicating helices, and the TT symbol indicating β -turns. (B) Ribbon diagrams of predicted AlphaFold structures of *Magnaporthe* and *Colletotrichum* Nudix effectors, aligned with *HsDIPP1* (6WO7) in grey. (C) A ribbon diagram of *MoNudix* (PDB ID: 8SX5) with the disulphide bond show as a stick model. Inset is a zoomed view of the disulphide bond with the electron density maps displayed as a transparent blue surface contoured at a rmsd of 1.5 Å and amino acid side chains displayed as stick models, demonstrating the clear covalent bond between the cysteines.

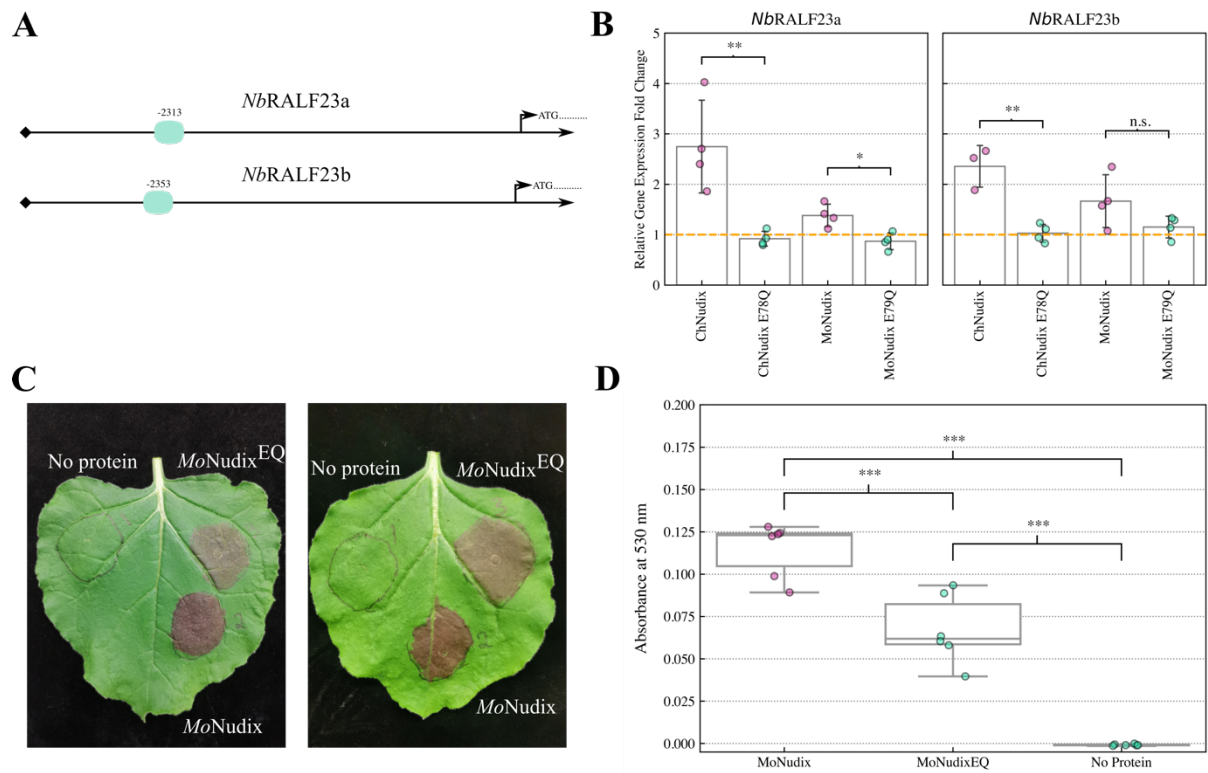


Figure S5: The enzymatic activity of the *Magnaporthe* and *Colletotrichum* Nudix hydrolase effectors induce phosphate starvation responses in *Nicotiana benthamiana*. Related to Figure 3. (A) A diagram of the 3 kb region upstream of two *N. benthamiana* RALF genes with all P1BS elements indicated by a green circle. (B) RT-qPCR was completed on RNA extracted from *N. benthamiana* leaf tissue expressing either MoNudix, ChNudix, MoNudix^{E79Q}, ChNudix^{E78Q}, or leaf tissue transformed with an empty vector control. Values represent mean \pm SD across three or four biological replicates with all individual data points shown as dots; *** p-value ≤ 0.001 (independent samples t-test). The relative gene expression fold change was calculated using the $2-\Delta\Delta Ct$ method via comparison to the vector-only control treatment. The geometric mean of two reference genes was used for normalisation (*NbeIF1a* and *NbUbe35*). The yellow dotted line indicates the relative expression level in the vector-only control treatment. (C) Representative leaf images demonstrating production of the red betalain pigment in leaf tissue co-transformed with the PEPC:RUBY promoter/reporter gene and a Nudix effector, or no effector, as labelled. (D) The absorbance at 530 nm of extracts from *N. benthamiana* leaf tissue co-transformed with the PEPC:RUBY promoter/reporter with the wild-type MoNudix effector, the corresponding Nudix box mutant protein, or no effector (as indicated). There were 6 biological replicates for each treatment, as indicated by the dots on top overlaying the boxplots. In the boxplots, the horizontal line in the middle of the box represents the median value, the box represents the interquartile range (IQR), and the whiskers extend to 1.5 x IQR. To determine whether there was a significant difference between the treatments, a one-way ANOVA was completed followed by Tukey's post-hoc test; *** adjusted p-value ≤ 0.001 .

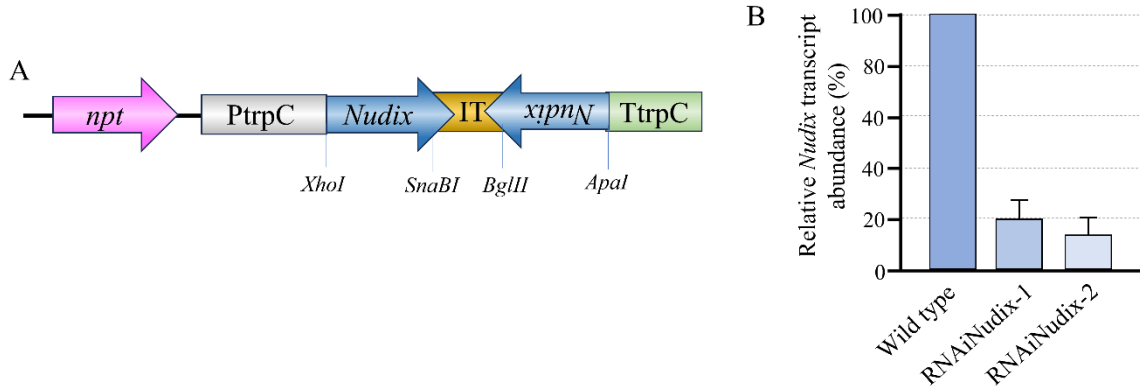


Figure S6: Silencing of *MoNudix* in *Magnaporthe oryzae*. Related to Figure 3. (A) RNAi cassette transformed into *M. oryzae*. Consisting of the TrpC promoter (PtrpC) from *A. nidulans*, followed by 300-bp of the sense and antisense of *MoNudix* sequence (*Nudix*) separated by the Intron2 from the Cutinase2 of *M. oryzae* (IT), followed by the TrpC terminator (TtrpC). The neomycin phosphotransferase (npt) resistance cassette was used as a resistance marker. Not to scale. (B) Relative transcript abundance of *M. oryzae* *MoNudix* in infected leaf sheaths at 28 hpi. Three biological replications with 9 infected leaf sheaths each were evaluated. Error bars indicate standard deviations.

Table S1: The names, species, host plant, protein sequences, and accession IDs of identified *Magnaporthe*, *Colletotrichum*, and *Ceratocystis* Nudix effectors. Related to Figure 1.

Table S2: Primer sequences used throughout this study. Related to Figure 3, Figure 4, Figure S5 and Figure S6.

Table S3: Promoter sequences discussed in this study. Related to Figure 3 and Figure S5.

Table S4: Sequences of the purified proteins used in this study. Related to Figure 1, Figure 2, Figure S2, and Figure S3.

Table S5: Crystallography data collection and structure refinement statistics for 8SXS. Related to Figure 2 and Figure S4.

Supplementary tables provided as .xls file.

References

1. Shears, S.B. (2018). Intimate connections: Inositol pyrophosphates at the interface of metabolic regulation and cell signaling. *J Cell Physiol* *233*, 1897-1912. 10.1002/jcp.26017.
2. Wild, R., Gerasimaite, R., Jung, J.Y., Truffault, V., Pavlovic, I., Schmidt, A., Saiardi, A., Jessen, H.J., Poirier, Y., Hothorn, M., and Mayer, A. (2016). Control of eukaryotic phosphate homeostasis by inositol polyphosphate sensor domains. *Science* *352*, 986-990. 10.1126/science.aad9858.
3. Dong, J., Ma, G., Sui, L., Wei, M., Satheesh, V., Zhang, R., Ge, S., Li, J., Zhang, T.E., Wittwer, C., et al. (2019). Inositol Pyrophosphate InsP(8) Acts as an Intracellular Phosphate Signal in *Arabidopsis*. *Mol Plant* *12*, 1463-1473. 10.1016/j.molp.2019.08.002.
4. Ried, M.K., Wild, R., Zhu, J., Pipercevic, J., Sturm, K., Broger, L., Harmel, R.K., Abriata, L.A., Hothorn, L.A., Fiedler, D., et al. (2021). Inositol pyrophosphates promote the interaction of SPX domains with the coiled-coil motif of PHR transcription factors to regulate plant phosphate homeostasis. *Nat Commun* *12*, 384. 10.1038/s41467-020-20681-4.
5. Zhu, J., Lau, K., Puschmann, R., Harmel, R.K., Zhang, Y., Pries, V., Gaugler, P., Broger, L., Dutta, A.K., Jessen, H.J., et al. (2019). Two bifunctional inositol pyrophosphate kinases/phosphatases control plant phosphate homeostasis. *Elife* *8*. 10.7554/eLife.43582.
6. Riemer, E., Qiu, D., Laha, D., Harmel, R.K., Gaugler, P., Gaugler, V., Frei, M., Hajirezaei, M.R., Laha, N.P., Krusenbaum, L., et al. (2021). ITPK1 is an InsP(6)/ADP phosphotransferase that controls phosphate signaling in *Arabidopsis*. *Mol Plant* *14*, 1864-1880. 10.1016/j.molp.2021.07.011.
7. Secco, D., Wang, C., Arpat, B.A., Wang, Z., Poirier, Y., Tyerman, S.D., Wu, P., Shou, H., and Whelan, J. (2012). The emerging importance of the SPX domain-containing proteins in phosphate homeostasis. *New Phytol* *193*, 842-851. 10.1111/j.1469-8137.2011.04002.x.
8. Luan, M., Zhao, F., Sun, G., Xu, M., Fu, A., Lan, W., and Luan, S. (2022). A SPX domain vacuolar transporter links phosphate sensing to homeostasis in *Arabidopsis*. *Mol Plant* *15*, 1590-1601. 10.1016/j.molp.2022.09.005.
9. Pipercevic, J., Kohl, B., Gerasimaite, R., Comte-Miserez, V., Hostachy, S., Müntener, T., Agustoni, E., Jessen, H.J., Fiedler, D., Mayer, A., and Hiller, S. (2023). Inositol pyrophosphates activate the vacuolar transport chaperone complex in yeast by disrupting a homotypic SPX domain interaction. *Nat Commun* *14*, 2645. 10.1038/s41467-023-38315-w.
10. Li, X., Gu, C., Hostachy, S., Sahu, S., Wittwer, C., Jessen, H.J., Fiedler, D., Wang, H., and Shears, S.B. (2020). Control of XPR1-dependent cellular phosphate efflux by InsP(8) is an exemplar for functionally-exclusive inositol pyrophosphate signaling. *Proc Natl Acad Sci U S A* *117*, 3568-3574. 10.1073/pnas.1908830117.

11. Puga, M.I., Mateos, I., Charukesi, R., Wang, Z., Franco-Zorrilla, J.M., de Lorenzo, L., Irigoyen, M.L., Masiero, S., Bustos, R., Rodríguez, J., et al. (2014). SPX1 is a phosphate-dependent inhibitor of Phosphate Starvation Response 1 in Arabidopsis. *Proc Natl Acad Sci U S A* *111*, 14947-14952. 10.1073/pnas.1404654111.
12. Liu, F., Wang, Z., Ren, H., Shen, C., Li, Y., Ling, H.Q., Wu, C., Lian, X., and Wu, P. (2010). OsSPX1 suppresses the function of OsPHR2 in the regulation of expression of OsPT2 and phosphate homeostasis in shoots of rice. *Plant J* *62*, 508-517. 10.1111/j.1365-313X.2010.04170.x.
13. Wang, Z., Ruan, W., Shi, J., Zhang, L., Xiang, D., Yang, C., Li, C., Wu, Z., Liu, Y., Yu, Y., et al. (2014). Rice SPX1 and SPX2 inhibit phosphate starvation responses through interacting with PHR2 in a phosphate-dependent manner. *Proc Natl Acad Sci U S A* *111*, 14953-14958. 10.1073/pnas.1404680111.
14. Lv, Q., Zhong, Y., Wang, Y., Wang, Z., Zhang, L., Shi, J., Wu, Z., Liu, Y., Mao, C., Yi, K., and Wu, P. (2014). SPX4 Negatively Regulates Phosphate Signaling and Homeostasis through Its Interaction with PHR2 in Rice. *Plant Cell* *26*, 1586-1597. 10.1105/tpc.114.123208.
15. Guan, Z., Zhang, Q., Zhang, Z., Zuo, J., Chen, J., Liu, R., Savarin, J., Broger, L., Cheng, P., Wang, Q., et al. (2022). Mechanistic insights into the regulation of plant phosphate homeostasis by the rice SPX2 - PHR2 complex. *Nat Commun* *13*, 1581. 10.1038/s41467-022-29275-8.
16. Bustos, R., Castrillo, G., Linhares, F., Puga, M.I., Rubio, V., Pérez-Pérez, J., Solano, R., Leyva, A., and Paz-Ares, J. (2010). A central regulatory system largely controls transcriptional activation and repression responses to phosphate starvation in Arabidopsis. *PLoS Genet* *6*, e1001102. 10.1371/journal.pgen.1001102.
17. Rubio, V., Linhares, F., Solano, R., Martín, A.C., Iglesias, J., Leyva, A., and Paz-Ares, J. (2001). A conserved MYB transcription factor involved in phosphate starvation signaling both in vascular plants and in unicellular algae. *Genes Dev* *15*, 2122-2133. 10.1101/gad.204401.
18. Zhou, J., Jiao, F., Wu, Z., Li, Y., Wang, X., He, X., Zhong, W., and Wu, P. (2008). OsPHR2 is involved in phosphate-starvation signaling and excessive phosphate accumulation in shoots of plants. *Plant Physiol* *146*, 1673-1686. 10.1104/pp.107.111443.
19. Smith, S.E., Jakobsen, I., Grønlund, M., and Smith, F.A. (2011). Roles of arbuscular mycorrhizas in plant phosphorus nutrition: interactions between pathways of phosphorus uptake in arbuscular mycorrhizal roots have important implications for understanding and manipulating plant phosphorus acquisition. *Plant Physiol* *156*, 1050-1057. 10.1104/pp.111.174581.
20. Breuillin, F., Schramm, J., Hajirezaei, M., Ahkami, A., Favre, P., Druege, U., Hause, B., Bucher, M., Kretzschmar, T., Bossolini, E., et al. (2010). Phosphate systemically inhibits development of arbuscular mycorrhiza in Petunia hybrida and represses genes involved in mycorrhizal functioning. *Plant J* *64*, 1002-1017. 10.1111/j.1365-313X.2010.04385.x.

21. Balzergue, C., Puech-Pagès, V., Bécard, G., and Rochange, S.F. (2011). The regulation of arbuscular mycorrhizal symbiosis by phosphate in pea involves early and systemic signalling events. *J Exp Bot* 62, 1049-1060. 10.1093/jxb/erq335.
22. Menge, J.A., Steirle, D., Bagyaraj, D.J., Johnson, E.L.V., and Leonard, R.T. (1978). Phosphorus concentrations in plants responsible for inhibition of mycorrhizal infection. *New Phytologist* 80, 575-578. 10.1111/j.1469-8137.1978.tb01589.x.
23. Jasper, D.A., Robson, A.D., and Abbott, L.K. (1979). Phosphorus and the formation of vesicular-arbuscular mycorrhizas. *Soil Biology and Biochemistry* 11, 501-505. 10.1016/0038-0717(79)90009-9.
24. Thomson, B.D., Robson, A.D., and Abbott, L.K. (1986). Effects of phosphorus on the formation of mycorrhizas by *Gigaspora calospora* and *Glomus fasciculatum* in relation to root carbohydrates. *New Phytologist* 103, 751-765. 10.1111/j.1469-8137.1986.tb00850.x.
25. Amijee, F., Tinker, P.B., and Sibley, D.P. (1989). The development of endomycorrhizal root systems. *New Phytologist* 111, 435-446. 10.1111/j.1469-8137.1989.tb00706.x.
26. Nagy, R., Drissner, D., Amrhein, N., Jakobsen, I., and Bucher, M. (2009). Mycorrhizal phosphate uptake pathway in tomato is phosphorus-repressible and transcriptionally regulated. *New Phytol* 181, 950-959. 10.1111/j.1469-8137.2008.02721.x.
27. Amijee, B.F., Sibley, D.P., and Lane, P.W. (1993). The susceptibility of roots to infection by an arbuscular mycorrhizal fungus in relation to age and phosphorus supply. *New Phytologist* 125, 581-586. 10.1111/j.1469-8137.1993.tb03906.x.
28. Bruce, A., Smith, S.E., and Tester, M. (1994). The development of mycorrhizal infection in cucumber: effects of P supply on root growth, formation of entry points and growth of infection units. *New Phytologist* 127, 507-514. 10.1111/j.1469-8137.1994.tb03968.x.
29. Hiruma, K., Gerlach, N., Sacristán, S., Nakano, R.T., Hacquard, S., Kracher, B., Neumann, U., Ramírez, D., Bucher, M., O'Connell, R.J., and Schulze-Lefert, P. (2016). Root Endophyte *Colletotrichum tofieldiae* Confers Plant Fitness Benefits that Are Phosphate Status Dependent. *Cell* 165, 464-474. 10.1016/j.cell.2016.02.028.
30. Hacquard, S., Kracher, B., Hiruma, K., Münch, P.C., Garrido-Oter, R., Thon, M.R., Weimann, A., Damm, U., Dallery, J.F., Hainaut, M., et al. (2016). Survival trade-offs in plant roots during colonization by closely related beneficial and pathogenic fungi. *Nat Commun* 7, 11362. 10.1038/ncomms11362.
31. Frerigmann, H., Piotrowski, M., Lemke, R., Bednarek, P., and Schulze-Lefert, P. (2021). A Network of Phosphate Starvation and Immune-Related Signaling and Metabolic Pathways Controls the Interaction between *Arabidopsis thaliana* and the Beneficial Fungus *Colletotrichum tofieldiae*. *Mol Plant Microbe Interact* 34, 560-570. 10.1094/mpmi-08-20-0233-r.

32. Shi, J., Zhao, B., Zheng, S., Zhang, X., Wang, X., Dong, W., Xie, Q., Wang, G., Xiao, Y., Chen, F., et al. (2021). A phosphate starvation response-centered network regulates mycorrhizal symbiosis. *Cell* *184*, 5527-5540.e5518. 10.1016/j.cell.2021.09.030.
33. Das, D., Paries, M., Hobecker, K., Gigl, M., Dawid, C., Lam, H.M., Zhang, J., Chen, M., and Gutjahr, C. (2022). PHOSPHATE STARVATION RESPONSE transcription factors enable arbuscular mycorrhiza symbiosis. *Nat Commun* *13*, 477. 10.1038/s41467-022-27976-8.
34. Castrillo, G., Teixeira, P.J., Paredes, S.H., Law, T.F., de Lorenzo, L., Feltcher, M.E., Finkel, O.M., Breakfield, N.W., Mieczkowski, P., Jones, C.D., et al. (2017). Root microbiota drive direct integration of phosphate stress and immunity. *Nature* *543*, 513-518. 10.1038/nature21417.
35. Tang, J., Wu, D., Li, X., Wang, L., Xu, L., Zhang, Y., Xu, F., Liu, H., Xie, Q., Dai, S., et al. (2022). Plant immunity suppression via PHR1-RALF-FERONIA shapes the root microbiome to alleviate phosphate starvation. *EMBO J* *41*, e109102. 10.15252/embj.2021109102.
36. Dindas, J., DeFalco, T.A., Yu, G., Zhang, L., David, P., Bjornson, M., Thibaud, M.C., Custódio, V., Castrillo, G., Nussaume, L., et al. (2022). Direct inhibition of phosphate transport by immune signaling in *Arabidopsis*. *Curr Biol* *32*, 488-495.e485. 10.1016/j.cub.2021.11.063.
37. Stegmann, M., Monaghan, J., Smakowska-Luzan, E., Rovenich, H., Lehner, A., Holton, N., Belkhadir, Y., and Zipfel, C. (2017). The receptor kinase FER is a RALF-regulated scaffold controlling plant immune signaling. *Science* *355*, 287-289. 10.1126/science.aal2541.
38. Paries, M., and Gutjahr, C. (2023). The good, the bad, and the phosphate: regulation of beneficial and detrimental plant-microbe interactions by the plant phosphate status. *New Phytol* *239*, 29-46. 10.1111/nph.18933.
39. Lu, Y.-T., Li, M.-Y., Cheng, K.-T., Tan, C.M., Su, L.-W., Lin, W.-Y., Shih, H.-T., Chiou, T.-J., and Yang, J.-Y. (2014). Transgenic Plants That Express the Phytoplasma Effector SAP11 Show Altered Phosphate Starvation and Defense Responses. *Plant Physiology* *164*, 1456-1469. 10.1104/pp.113.229740.
40. Zhao, H., Sun, R., Albrecht, U., Padmanabhan, C., Wang, A., Coffey, M.D., Girke, T., Wang, Z., Close, T.J., Roose, M., et al. (2013). Small RNA profiling reveals phosphorus deficiency as a contributing factor in symptom expression for citrus huanglongbing disease. *Mol Plant* *6*, 301-310. 10.1093/mp/sst002.
41. Blüher, D., Laha, D., Thieme, S., Hofer, A., Eschen-Lippold, L., Masch, A., Balcke, G., Pavlovic, I., Nagel, O., Schonsky, A., et al. (2017). A 1-phytase type III effector interferes with plant hormone signaling. *Nat Commun* *8*, 2159. 10.1038/s41467-017-02195-8.
42. Campos-Soriano, L., Bundó, M., Bach-Pages, M., Chiang, S.F., Chiou, T.J., and San Segundo, B. (2020). Phosphate excess increases susceptibility to pathogen infection in rice. *Mol Plant Pathol* *21*, 555-570. 10.1111/mpp.12916.

43. Dong, S., Yin, W., Kong, G., Yang, X., Qutob, D., Chen, Q., Kale, S.D., Sui, Y., Zhang, Z., Dou, D., et al. (2011). Phytophthora sojae avirulence effector Avr3b is a secreted NADH and ADP-ribose pyrophosphorylase that modulates plant immunity. *PLoS Pathog* 7, e1002353. 10.1371/journal.ppat.1002353.
44. Bhaduria, V., Banniza, S., Vandenberg, A., Selvaraj, G., and Wei, Y. (2013). Overexpression of a novel biotrophy-specific *Colletotrichum truncatum* effector, CtNUDIX, in hemibiotrophic fungal phytopathogens causes incompatibility with their host plants. *Eukaryot Cell* 12, 2-11. 10.1128/ec.00192-12.
45. Sun, Y., Li, P., Shen, D., Wei, Q., He, J., and Lu, Y. (2019). The *Ralstonia solanacearum* effector RipN suppresses plant PAMP-triggered immunity, localizes to the endoplasmic reticulum and nucleus, and alters the NADH/NAD(+) ratio in *Arabidopsis*. *Mol Plant Pathol* 20, 533-546. 10.1111/mpp.12773.
46. McCombe, C.L., Catanzariti, A.-M., Greenwood, J.R., Desai, A.M., Outram, M.A., Yu, D.S., Ericsson, D.J., Brenner, S.E., Dodds, P.N., Kobe, B., et al. (2023). A rust-fungus Nudix hydrolase effector decaps mRNA in vitro and interferes with plant immune pathways. *New Phytologist*. 10.1111/nph.18727.
47. Dong, S., and Wang, Y. (2016). Nudix Effectors: A Common Weapon in the Arsenal of Plant Pathogens. *PLoS Pathog* 12, e1005704. 10.1371/journal.ppat.1005704.
48. Kong, G., Zhao, Y., Jing, M., Huang, J., Yang, J., Xia, Y., Kong, L., Ye, W., Xiong, Q., Qiao, Y., et al. (2015). The Activation of Phytophthora Effector Avr3b by Plant Cyclophilin is Required for the Nudix Hydrolase Activity of Avr3b. *PLoS Pathog* 11, e1005139. 10.1371/journal.ppat.1005139.
49. McLennan, A.G. (2006). The Nudix hydrolase superfamily. *Cell Mol Life Sci* 63, 123-143. 10.1007/s00018-005-5386-7.
50. Safrany, S.T., Caffrey, J.J., Yang, X., Bembeneck, M.E., Moyer, M.B., Burkhart, W.A., and Shears, S.B. (1998). A novel context for the 'MutT' module, a guardian of cell integrity, in a diphosphoinositol polyphosphate phosphohydrolase. *Embo j* 17, 6599-6607. 10.1093/emboj/17.22.6599.
51. Safrany, S.T., Ingram, S.W., Cartwright, J.L., Falck, J.R., McLennan, A.G., Barnes, L.D., and Shears, S.B. (1999). The diadenosine hexaphosphate hydrolases from *Schizosaccharomyces pombe* and *Saccharomyces cerevisiae* are homologues of the human diphosphoinositol polyphosphate phosphohydrolase. Overlapping substrate specificities in a MutT-type protein. *J Biol Chem* 274, 21735-21740. 10.1074/jbc.274.31.21735.
52. Caffrey, J.J., Safrany, S.T., Yang, X., and Shears, S.B. (2000). Discovery of molecular and catalytic diversity among human diphosphoinositol-polyphosphate phosphohydrolases. An expanding Nudt family. *J Biol Chem* 275, 12730-12736. 10.1074/jbc.275.17.12730.
53. Hua, L.V., Hidaka, K., Pesesse, X., Barnes, L.D., and Shears, S.B. (2003). Paralogous murine Nudt10 and Nudt11 genes have differential expression patterns but encode

- identical proteins that are physiologically competent diphosphoinositol polyphosphate phosphohydrolases. *Biochem J* 373, 81-89. 10.1042/bj20030142.
54. Yan, X., Tang, B., Ryder, L.S., MacLean, D., Were, V.M., Eseola, A.B., Cruz-Mireles, N., Ma, W., Foster, A.J., Osés-Ruiz, M., and Talbot, N.J. (2023). The transcriptional landscape of plant infection by the rice blast fungus *Magnaporthe oryzae* reveals distinct families of temporally co-regulated and structurally conserved effectors. *The Plant Cell*. 10.1093/plcell/koad036.
55. O'Connell, R.J., Thon, M.R., Hacquard, S., Amyotte, S.G., Kleemann, J., Torres, M.F., Damm, U., Buiate, E.A., Epstein, L., Alkan, N., et al. (2012). Lifestyle transitions in plant pathogenic *Colletotrichum* fungi deciphered by genome and transcriptome analyses. *Nat Genet* 44, 1060-1065. 10.1038/ng.2372.
56. Crouch, J., O'Connell, R., Gan, P., Buiate, E., Torres, M.F., Beirn, L., Shirasu, K., and Vaillancourt, L. (2014). The genomics of *Colletotrichum*. Genomics of plant-associated fungi: monocot pathogens, 69-102.
57. Yang, X., Safrany, S.T., and Shears, S.B. (1999). Site-directed mutagenesis of diphosphoinositol polyphosphate phosphohydrolase, a dual specificity NUDT enzyme that attacks diadenosine polyphosphates and diphosphoinositol polyphosphates. *J Biol Chem* 274, 35434-35440. 10.1074/jbc.274.50.35434.
58. Zong, G., Jork, N., Hostachy, S., Fiedler, D., Jessen, H.J., Shears, S.B., and Wang, H. (2021). New structural insights reveal an expanded reaction cycle for inositol pyrophosphate hydrolysis by human DIPP1. *Faseb j* 35, e21275. 10.1096/fj.202001489R.
59. Jumper, J., Evans, R., Pritzel, A., Green, T., Figurnov, M., Ronneberger, O., Tunyasuvunakool, K., Bates, R., Žídek, A., Potapenko, A., et al. (2021). Highly accurate protein structure prediction with AlphaFold. *Nature* 596, 583-589. 10.1038/s41586-021-03819-2.
60. Seong, K., and Krasileva, K.V. (2023). Prediction of effector protein structures from fungal phytopathogens enables evolutionary analyses. *Nat Microbiol* 8, 174-187. 10.1038/s41564-022-01287-6.
61. Wang, H., DeRose, E.F., London, R.E., and Shears, S.B. (2014). IP6K structure and the molecular determinants of catalytic specificity in an inositol phosphate kinase family. *Nat Commun* 5, 4178. 10.1038/ncomms5178.
62. Ge, X., Li, G.J., Wang, S.B., Zhu, H., Zhu, T., Wang, X., and Xia, Y. (2007). AtNUDT7, a negative regulator of basal immunity in *Arabidopsis*, modulates two distinct defense response pathways and is involved in maintaining redox homeostasis. *Plant Physiol* 145, 204-215. 10.1104/pp.107.103374.
63. Guindon, S., Dufayard, J.F., Lefort, V., Anisimova, M., Hordijk, W., and Gascuel, O. (2010). New algorithms and methods to estimate maximum-likelihood phylogenies: assessing the performance of PhyML 3.0. *Syst Biol* 59, 307-321. 10.1093/sysbio/syq010.

64. Letunic, I., and Bork, P. (2021). Interactive Tree Of Life (iTOL) v5: an online tool for phylogenetic tree display and annotation. *Nucleic Acids Res* 49, W293-w296. 10.1093/nar/gkab301.
65. Yariv, B., Yariv, E., Kessel, A., Masrati, G., Chorin, A.B., Martz, E., Mayrose, I., Pupko, T., and Ben-Tal, N. (2023). Using evolutionary data to make sense of macromolecules with a "face-lifted" ConSurf. *Protein Sci* 32, e4582. 10.1002/pro.4582.
66. Pettersen, E.F., Goddard, T.D., Huang, C.C., Meng, E.C., Couch, G.S., Croll, T.I., Morris, J.H., and Ferrin, T.E. (2021). UCSF ChimeraX: Structure visualization for researchers, educators, and developers. *Protein Sci* 30, 70-82. 10.1002/pro.3943.
67. Qi, W., Manfield, I.W., Muench, S.P., and Baker, A. (2017). AtSPX1 affects the AtPHR1-DNA-binding equilibrium by binding monomeric AtPHR1 in solution. *Biochem J* 474, 3675-3687. 10.1042/bcj20170522.
68. Hanchi, M., Thibaud, M.C., Légeret, B., Kuwata, K., Pochon, N., Beisson, F., Cao, A., Cuyas, L., David, P., Doerner, P., et al. (2018). The Phosphate Fast-Responsive Genes PECP1 and PPspase1 Affect Phosphocholine and Phosphoethanolamine Content. *Plant Physiol* 176, 2943-2962. 10.1104/pp.17.01246.
69. Duan, K., Yi, K., Dang, L., Huang, H., Wu, W., and Wu, P. (2008). Characterization of a sub-family of *Arabidopsis* genes with the SPX domain reveals their diverse functions in plant tolerance to phosphorus starvation. *Plant J* 54, 965-975. 10.1111/j.1365-313X.2008.03460.x.
70. He, Y., Zhang, T., Sun, H., Zhan, H., and Zhao, Y. (2020). A reporter for noninvasively monitoring gene expression and plant transformation. *Hortic Res* 7, 152. 10.1038/s41438-020-00390-1.
71. Mosquera, G., Giraldo, M.C., Khang, C.H., Coughlan, S., and Valent, B. (2009). Interaction transcriptome analysis identifies *Magnaporthe oryzae* BAS1-4 as Biotrophy-associated secreted proteins in rice blast disease. *Plant Cell* 21, 1273-1290. 10.1105/tpc.107.055228.
72. Oliveira-Garcia, E., Tamang, T.M., Park, J., Dalby, M., Martin-Urdiroz, M., Rodriguez Herrero, C., Vu, A.H., Park, S., Talbot, N.J., and Valent, B. (2023). Clathrin-mediated endocytosis facilitates the internalization of *Magnaporthe oryzae* effectors into rice cells. *Plant Cell* 35, 2527-2551. 10.1093/plcell/koad094.
73. Khang, C.H., Berruyer, R., Giraldo, M.C., Kankanala, P., Park, S.Y., Czymbek, K., Kang, S., and Valent, B. (2010). Translocation of *Magnaporthe oryzae* effectors into rice cells and their subsequent cell-to-cell movement. *The Plant Cell* 22, 1388-1403. 10.1105/tpc.109.069666.
74. Giraldo, M.C., and Valent, B. (2013). Filamentous plant pathogen effectors in action. *Nat Rev Microbiol* 11, 800-814. 10.1038/nrmicro3119.
75. Oliveira-Garcia, E., and Valent, B. (2015). How eukaryotic filamentous pathogens evade plant recognition. *Curr Opin Microbiol* 26, 92-101. 10.1016/j.mib.2015.06.012.

76. Oliveira-Garcia, E., and Valent, B. (2021). Characterizing the Secretion Systems of *Magnaporthe oryzae*. *Methods Mol Biol* *2356*, 69-77. 10.1007/978-1-0716-1613-0_5.
77. Sperschneider, J., and Dodds, P.N. (2022). EffectorP 3.0: Prediction of Apoplastic and Cytoplasmic Effectors in Fungi and Oomycetes. *Mol Plant Microbe Interact* *35*, 146-156. 10.1094/mpmi-08-21-0201-r.
78. Ogawa, T., Ueda, Y., Yoshimura, K., and Shigeoka, S. (2005). Comprehensive analysis of cytosolic Nudix hydrolases in *Arabidopsis thaliana*. *J Biol Chem* *280*, 25277-25283. 10.1074/jbc.M503536200.
79. Ogawa, T., Yoshimura, K., Miyake, H., Ishikawa, K., Ito, D., Tanabe, N., and Shigeoka, S. (2008). Molecular characterization of organelle-type Nudix hydrolases in *Arabidopsis*. *Plant Physiol* *148*, 1412-1424. 10.1104/pp.108.128413.
80. Liang, X., Shang, S., Dong, Q., Wang, B., Zhang, R., Gleason, M.L., and Sun, G. (2018). Transcriptomic analysis reveals candidate genes regulating development and host interactions of *Colletotrichum franticola*. *BMC Genomics* *19*, 557. 10.1186/s12864-018-4934-0.
81. Sheard, L.B., Tan, X., Mao, H., Withers, J., Ben-Nissan, G., Hinds, T.R., Kobayashi, Y., Hsu, F.F., Sharon, M., Browse, J., et al. (2010). Jasmonate perception by inositol-phosphate-potentiated COI1-JAZ co-receptor. *Nature* *468*, 400-405. 10.1038/nature09430.
82. Laha, D., Parvin, N., Dynowski, M., Johnen, P., Mao, H., Bitters, S.T., Zheng, N., and Schaaf, G. (2016). Inositol Polyphosphate Binding Specificity of the Jasmonate Receptor Complex. *Plant Physiol* *171*, 2364-2370. 10.1104/pp.16.00694.
83. Tan, X., Calderon-Villalobos, L.I., Sharon, M., Zheng, C., Robinson, C.V., Estelle, M., and Zheng, N. (2007). Mechanism of auxin perception by the TIR1 ubiquitin ligase. *Nature* *446*, 640-645. 10.1038/nature05731.
84. Laha, N.P., Giehl, R.F.H., Riemer, E., Qiu, D., Pullagurla, N.J., Schneider, R., Dhir, Y.W., Yadav, R., Mihiret, Y.E., Gaugler, P., et al. (2022). INOSITOL (1,3,4) TRIPHOSPHATE 5/6 KINASE1-dependent inositol polyphosphates regulate auxin responses in *Arabidopsis*. *Plant Physiol* *190*, 2722-2738. 10.1093/plphys/kiac425.
85. Zhao, Y., Yang, B., Xu, H., Wu, J., Xu, Z., and Wang, Y. (2022). The Phytophthora effector Avh94 manipulates host jasmonic acid signaling to promote infection. *J Integr Plant Biol* *64*, 2199-2210. 10.1111/jipb.13358.
86. Plett, J.M., Daguerre, Y., Wittulsky, S., Vayssières, A., Deveau, A., Melton, S.J., Kohler, A., Morrell-Falvey, J.L., Brun, A., Veneault-Fourrey, C., and Martin, F. (2014). Effector MiSSP7 of the mutualistic fungus *Laccaria bicolor* stabilizes the *Populus JAZ6* protein and represses jasmonic acid (JA) responsive genes. *Proc Natl Acad Sci U S A* *111*, 8299-8304. 10.1073/pnas.1322671111.
87. Gimenez-Ibanez, S., Boter, M., Fernández-Barbero, G., Chini, A., Rathjen, J.P., and Solano, R. (2014). The bacterial effector HopX1 targets JAZ transcriptional repressors to activate jasmonate signaling and promote infection in *Arabidopsis*. *PLoS Biol* *12*, e1001792. 10.1371/journal.pbio.1001792.

88. Bindics, J., Khan, M., Uhse, S., Kogelmann, B., Baggely, L., Reumann, D., Ingole, K.D., Stirnberg, A., Rybecky, A., Darino, M., et al. (2022). Many ways to TOPLESS - manipulation of plant auxin signalling by a cluster of fungal effectors. *New Phytol* **236**, 1455-1470. 10.1111/nph.18315.
89. Chen, Z., Agnew, J.L., Cohen, J.D., He, P., Shan, L., Sheen, J., and Kunkel, B.N. (2007). *Pseudomonas syringae* type III effector AvrRpt2 alters *Arabidopsis thaliana* auxin physiology. *Proc Natl Acad Sci U S A* **104**, 20131-20136. 10.1073/pnas.0704901104.
90. Evangelisti, E., Govetto, B., Minet-Kebdani, N., Kuhn, M.L., Attard, A., Ponchet, M., Panabières, F., and Gourgues, M. (2013). The *Phytophthora parasitica* RXLR effector penetration-specific effector 1 favours *Arabidopsis thaliana* infection by interfering with auxin physiology. *New Phytol* **199**, 476-489. 10.1111/nph.12270.
91. Kuo, H.F., Hsu, Y.Y., Lin, W.C., Chen, K.Y., Munnik, T., Brearley, C.A., and Chiou, T.J. (2018). *Arabidopsis* inositol phosphate kinases IPK1 and ITPK1 constitute a metabolic pathway in maintaining phosphate homeostasis. *Plant J.* 10.1111/tpj.13974.
92. Qiu, D., Wilson, M.S., Eisenbeis, V.B., Harmel, R.K., Riemer, E., Haas, T.M., Wittwer, C., Jork, N., Gu, C., Shears, S.B., et al. (2020). Analysis of inositol phosphate metabolism by capillary electrophoresis electrospray ionization mass spectrometry. *Nat Commun* **11**, 6035. 10.1038/s41467-020-19928-x.
93. Zhang, S., and Xu, J.R. (2014). Effectors and effector delivery in *Magnaporthe oryzae*. *PLoS Pathog* **10**, e1003826. 10.1371/journal.ppat.1003826.
94. Oliveira-Garcia, E., and Valent, B. (2021). Characterizing the Secretion Systems of *Magnaporthe oryzae**Magnaporthe oryzae*. In *Magnaporthe oryzae: Methods and Protocols*, S. Jacob, ed. (Springer US), pp. 69-77. 10.1007/978-1-0716-1613-0_5.
95. Studier, F.W. (2005). Protein production by auto-induction in high density shaking cultures. *Protein Expr Purif* **41**, 207-234. 10.1016/j.pep.2005.01.016.
96. Teufel, F., Almagro Armenteros, J.J., Johansen, A.R., Gíslason, M.H., Pihl, S.I., Tsirigos, K.D., Winther, O., Brunak, S., von Heijne, G., and Nielsen, H. (2022). SignalP 6.0 predicts all five types of signal peptides using protein language models. *Nat Biotechnol* **40**, 1023-1025. 10.1038/s41587-021-01156-3.
97. Bentham, A.R., Youles, M., Mendel, M.N., Varden, F.A., Concepcion, J.C.D.I., and Banfield, M.J. (2021). pOPIN-GG: A resource for modular assembly in protein expression vectors. *bioRxiv*, 2021.2008.2010.455798. 10.1101/2021.08.10.455798.
98. Weber, E., Engler, C., Gruetzner, R., Werner, S., and Marillonnet, S. (2011). A modular cloning system for standardized assembly of multigene constructs. *PLoS One* **6**, e16765. 10.1371/journal.pone.0016765.
99. Chen, J., Luo, M., Hands, P., Rolland, V., Zhang, J., Li, Z., Outram, M., Dodds, P., and Ayliffe, M. (2023). A split GAL4 RUBY assay for visual in planta detection of protein–protein interactions. *The Plant Journal*. 10.1111/tpj.16234.

100. Sayers, E.W., Bolton, E.E., Brister, J.R., Canese, K., Chan, J., Comeau, D.C., Connor, R., Funk, K., Kelly, C., Kim, S., et al. (2022). Database resources of the national center for biotechnology information. *Nucleic Acids Res* 50, D20-d26. 10.1093/nar/gkab1112.
101. Blum, M., Chang, H.Y., Chuguransky, S., Grego, T., Kandasamy, S., Mitchell, A., Nuka, G., Paysan-Lafosse, T., Qureshi, M., Raj, S., et al. (2021). The InterPro protein families and domains database: 20 years on. *Nucleic Acids Res* 49, D344-d354. 10.1093/nar/gkaa977.
102. Heese, A., Hann, D.R., Gimenez-Ibanez, S., Jones, A.M., He, K., Li, J., Schroeder, J.I., Peck, S.C., and Rathjen, J.P. (2007). The receptor-like kinase SERK3/BAK1 is a central regulator of innate immunity in plants. *Proc Natl Acad Sci U S A* 104, 12217-12222. 10.1073/pnas.0705306104.
103. Puschmann, R., Harmel, R.K., and Fiedler, D. (2019). Scalable Chemoenzymatic Synthesis of Inositol Pyrophosphates. *Biochemistry* 58, 3927-3932. 10.1021/acs.biochem.9b00587.
104. Loss, O., Azevedo, C., Sziogyarto, Z., Bosch, D., and Saiardi, A. (2011). Preparation of quality inositol pyrophosphates. *J Vis Exp*, e3027. 10.3791/3027.
105. Losito, O., Sziogyarto, Z., Resnick, A.C., and Saiardi, A. (2009). Inositol pyrophosphates and their unique metabolic complexity: analysis by gel electrophoresis. *PLoS One* 4, e5580. 10.1371/journal.pone.0005580.
106. Aragão, D., Aishima, J., Cherukuvada, H., Clarken, R., Clift, M., Cowieson, N.P., Ericsson, D.J., Gee, C.L., Macedo, S., and Mudie, N. (2018). MX2: a high-flux undulator microfocus beamline serving both the chemical and macromolecular crystallography communities at the Australian Synchrotron. *Journal of synchrotron radiation* 25, 885-891.
107. Kabsch, W. (2010). XDS. *Acta Crystallogr D Biol Crystallogr* 66, 125-132. 10.1107/S0907444909047337.
108. Evans, P.R., and Murshudov, G.N. (2013). How good are my data and what is the resolution? *Acta Crystallogr D Biol Crystallogr* 69, 1204-1214. 10.1107/S0907444913000061.
109. McCoy, A.J., Grosse-Kunstleve, R.W., Adams, P.D., Winn, M.D., Storoni, L.C., and Read, R.J. (2007). Phaser crystallographic software. *J Appl Crystallogr* 40, 658-674. 10.1107/s0021889807021206.
110. Liebschner, D., Afonine, P.V., Baker, M.L., Bunkóczki, G., Chen, V.B., Croll, T.I., Hintze, B., Hung, L.W., Jain, S., McCoy, A.J., et al. (2019). Macromolecular structure determination using X-rays, neutrons and electrons: recent developments in Phenix. *Acta Crystallogr D Struct Biol* 75, 861-877. 10.1107/s2059798319011471.
111. Terwilliger, T.C., Grosse-Kunstleve, R.W., Afonine, P.V., Moriarty, N.W., Zwart, P.H., Hung, L.W., Read, R.J., and Adams, P.D. (2008). Iterative model building, structure refinement and density modification with the PHENIX AutoBuild wizard. *Acta Crystallogr D Biol Crystallogr* 64, 61-69. 10.1107/s090744490705024x.

112. Emsley, P., Lohkamp, B., Scott, W.G., and Cowtan, K. (2010). Features and development of Coot. *Acta Crystallogr D Biol Crystallogr* 66, 486-501. 10.1107/s0907444910007493.
113. Afonine, P.V., Grosse-Kunstleve, R.W., Echols, N., Headd, J.J., Moriarty, N.W., Mustyakimov, M., Terwilliger, T.C., Urzhumtsev, A., Zwart, P.H., and Adams, P.D. (2012). Towards automated crystallographic structure refinement with phenix.refine. *Acta Crystallogr D Biol Crystallogr* 68, 352-367. 10.1107/s0907444912001308.
114. Livak, K.J., and Schmittgen, T.D. (2001). Analysis of relative gene expression data using real-time quantitative PCR and the 2(-Delta Delta C(T)) Method. *Methods* 25, 402-408. 10.1006/meth.2001.1262.
115. Rao, X., Huang, X., Zhou, Z., and Lin, X. (2013). An improvement of the 2^Δ(-delta CT) method for quantitative real-time polymerase chain reaction data analysis. *Biostat Bioinforma Biomath* 3, 71-85.
116. Vandesompele, J., De Preter, K., Pattyn, F., Poppe, B., Van Roy, N., De Paepe, A., and Speleman, F. (2002). Accurate normalization of real-time quantitative RT-PCR data by geometric averaging of multiple internal control genes. *Genome Biol* 3, Research0034. 10.1186/gb-2002-3-7-research0034.
117. Kankanala, P., Czymbek, K., and Valent, B. (2007). Roles for rice membrane dynamics and plasmodesmata during biotrophic invasion by the blast fungus. *The Plant Cell* 19, 706-724. 10.1105/tpc.106.046300.
118. Ding, S.L., Liu, W., Iliuk, A., Ribot, C., Vallet, J., Tao, A., Wang, Y., Lebrun, M.H., and Xu, J.R. (2010). The tig1 histone deacetylase complex regulates infectious growth in the rice blast fungus *Magnaporthe oryzae*. *Plant Cell* 22, 2495-2508. 10.1105/tpc.110.074302.
119. Chen, X.L., Shi, T., Yang, J., Shi, W., Gao, X., Chen, D., Xu, X., Xu, J.R., Talbot, N.J., and Peng, Y.L. (2014). N-glycosylation of effector proteins by an α-1,3-mannosyltransferase is required for the rice blast fungus to evade host innate immunity. *Plant Cell* 26, 1360-1376. 10.1105/tpc.114.123588.
120. Janus, D., Hoff, B., Hofmann, E., and Kück, U. (2007). An efficient fungal RNA-silencing system using the DsRed reporter gene. *Appl Environ Microbiol* 73, 962-970. 10.1128/aem.02127-06.
121. Che Omar, S., Bentley, M.A., Morieri, G., Preston, G.M., and Gurr, S.J. (2016). Validation of Reference Genes for Robust qRT-PCR Gene Expression Analysis in the Rice Blast Fungus *Magnaporthe oryzae*. *PLoS One* 11, e0160637. 10.1371/journal.pone.0160637.
122. Li, Y., Song, M., and Kiledjian, M. (2011). Differential utilization of decapping enzymes in mammalian mRNA decay pathways. *Rna* 17, 419-428. 10.1261/rna.2439811.
123. Robert, X., and Gouet, P. (2014). Deciphering key features in protein structures with the new ENDscript server. *Nucleic Acids Res* 42, W320-324. 10.1093/nar/gku316.

Chapter 4 Discussion, conclusions, and future perspectives

4.1 Summary of key findings

Nudix hydrolase effectors are widespread in phytopathogens, with examples in plant infecting bacteria, oomycetes and fungi (Dong and Wang 2016). The conservation of the Nudix motif has led to suggestions that effectors within this class may have similar functions during infection. Often, researchers have compared Nudix effectors to *A. thaliana*'s Nudx7, a known negative regulator of plant immunity, speculating that these effectors may mimic Nudx7 to suppress immunity and promote infection.

In this thesis, I establish that the Nudix hydrolase effectors from phytopathogenic fungi, including species from *Melampsora*, *Colletotrichum* and *Magnaporthe* genera, target substrates distinct from those hydrolysed by Nudx7 and the Nudix effectors from bacteria and oomycetes. Notably, the fungal effectors exhibit greater substrate specificity than previously characterised Nudix effectors and can be divided into two sequence-related groups with differing substrate specificity. Despite hydrolysing different substrates, both groups of fungal Nudix effectors can suppress plant immune responses.

In chapter 2, I determined that AvrM14 from *M. lini* is a highly specific Nudix hydrolase enzyme capable of removing the protective 5' cap from mRNA transcripts. Intriguingly, AvrM14 homodimerisation alters the pyrophosphate bond hydrolysed by the enzyme, suggesting the monomer and homodimer possess unique modes of substrate binding. I determined that four homologues of AvrM14 from other *Melampsora* species also decap mRNA, establishing the conservation of enzymatic activity throughout the evolution of this effector family. AvrM14 expression in flax results in M1-triggered HR suppression and alters the abundance of certain circadian-rhythm associated mRNA transcripts. Collectively, the findings from chapter 2 support a model where the *Melampsora* spp. Nudix hydrolase effectors promote infection by decapping plant mRNA to suppress immune responses.

Chapter 3 focuses on characterising *MoNudix* from *M. oryzae*. Unlike AvrM14, *MoNudix* displayed no mRNA decapping activity *in vitro*. However, *MoNudix* and sequence-related effectors from *Colletotrichum* spp. effectively hydrolysed PP-InsPs. Despite low sequence similarity, *MoNudix*'s crystal structure closely resembled DIPP1, a well-characterised PP-InsP hydrolase from *Homo sapiens*. When expressed in *N. benthamiana*, the Nudix hydrolase activity of *MoNudix* and homologous effectors induced phosphate starvation responses, consistent with reduced PP-InsP levels. The starvation responses coincided with ROS burst

suppression in *N. benthamiana* leaves. I confirmed the critical role of two binding site lysines via mutagenesis to glutamate, which reduced InsP₆ binding affinity, PP-InsP hydrolase activity, and phosphate starvation induction when expressed in *N. benthamiana*. Our collaborators then determined that *MoNudix* is important for *M. oryzae* virulence on rice by reducing its gene expression using RNAi. Additionally, their live-cell imaging of *M. oryzae* expressing mRFP-tagged *MoNudix* indicates that the effector functions within rice cells during infection.

4.2 Enzymatic effectors from pathogenic fungi

Only a few fungal effectors have demonstrated enzymatic activity. Of the enzymatic effectors studied to date, most are plant cell-wall degrading/modifying enzymes, including cellulases, glucanases, hemicellulases, xylanases, and pectin lyases (reviewed in (Kubicek *et al.*, 2014)). Another class of enzymatic fungal effectors are chitinases; these are conserved in diverse pathogenic fungi and typically function by degrading chitin oligomers to evade detection by plant chitin receptors (Mart Nez-Cruz *et al.*, 2021). I demonstrate that for AvrM14 and *MoNudix*, enzymatic activity is essential for the suppression of the MAMP-triggered ROS burst. This contrasts with chitinase effectors, where enzymatic activity is not always required to suppress immunity; non-catalytic chitinase-like effectors retain chitin-binding properties and can block chitin recognition (Fiorin *et al.*, 2018).

The chitin and plant cell-wall targeting effectors act in the apoplast, whereas previous research on AvrM14 (Anderson *et al.*, 2016), and the data presented on *MoNudix* localisation in Chapter 3 and appendix 1, indicates that fungal Nudix effectors function within the host cell cytoplasm. There exist only a few examples of cytosolic fungal effectors with enzymatic activity (reviewed in (He *et al.*, 2020)). Two effectors from the pathogenic fungi *Ustilago maydis* and *Verticillium dahliae* possess chorismate mutase and isochorismate mutase activity (Djamei *et al.*, 2011, Liu *et al.*, 2014). The substrates of both enzymes are important for the synthesis of salicylic acid (SA) and accordingly, the effectors influence SA metabolism in their host plants. The Nudix hydrolase effectors, as well as the chorismate and isochorismate mutases, were originally predicted to be enzymes by identifying conserved amino acid sequence motifs. In contrast, the chitinase effectors were predicted from computational protein structure modelling (Mart Nez-Cruz *et al.*, 2021).

Recently, Seong and Krasileva (2021) utilised computational protein structure modelling and identified multiple effectors with predicted similarity to a diverse range of enzymes (Seong and Krasileva 2021). Some of these lack amino acids essential for catalysis, suggesting that

they may contribute to pathogenicity through non-enzymatic means, such as sequestration of target molecules (Seong and Krasileva 2021). I anticipate that the rapid advances in protein structure prediction will accelerate the identification of fungal effectors with enzymatic activity, leading to a greater understanding of fungal pathogenesis in plants.

4.3 Substrate selectivity mechanisms in Nudix hydrolases

The Nudix motif provides a versatile scaffold which facilitates the hydrolysis of various compounds with a pyrophosphate. This motif typically forms a loop-helix-loop structure, where amino acids within the conserved sequence enable pyrophosphate binding mediated by divalent cations. The Nudix motif does not interact other regions of the substrate; Nudix hydrolase substrate specificity therefore arises from structural features outside of the Nudix motif.

In a limited subset of Nudix hydrolases, conserved amino acid sequence motifs external to the Nudix box refine substrate specificity. For example, NAD⁺/NADH and NAD-capped RNA targeting Nudix hydrolases from evolutionary diverse organisms, including *E. coli*, *S. cerevisiae*, and *H. sapiens*, all possess an SQXWPXP(X)S motif on the C-terminal side of the Nudix box (Dunn *et al.*, 1999). Structural analysis of nicotinamide-bound NudC from *E. coli* revealed that the conserved tryptophan forms a π - π stacking interaction with the nicotinamide sugar ring and the final serine is involved in hydrogen bonding with a phosphate (Höfer *et al.*, 2016, Zhang *et al.*, 2016). Π -stacking via aromatic amino acids is a common mechanism utilised by Nudix hydrolases that bind to substrates with ring structures (Wakamatsu *et al.*, 2008, Svensson *et al.*, 2011, Tang *et al.*, 2015, Sharma *et al.*, 2020), notably both AvrM14 and *MoNudix* lack aromatic amino acids in and around the substrate binding site and demonstrate no conserved sequence motifs external to the Nudix box.

NudC's conserved tryptophan is at the beginning of a loop region that overhangs the substrate binding site (Höfer *et al.*, 2016, Zhang *et al.*, 2016). A meta-analysis of substrate-bound Nudix hydrolase structures demonstrates that amino acids within this loop are regularly involved in substrate interactions, and therefore often play a role in substrate selectivity (Srouji *et al.*, 2017). Srouji *et al.*, (2017) named this the X-loop, as it often binds to the X-moiety in Nudix (**N**ucleoside **d**iphosphate linked to moiety-**X**) substrates. The crystal structures from chapter 2 demonstrate that the AvrM14-A X-loop is from proline-103 to valine-111 (PGSKDTQRV), with the threonine replaced by proline in AvrM14-B. It is unlikely that the X-loop plays a critical role in AvrM14 substrate binding, as this region demonstrates no discernible

conservation across AvrM14 homologs which all retain mRNA decapping activity. Similarly, the X-loop from *MoNudix* and homologs is unlikely to contribute to PP-InsP binding. The *MoNudix* crystal structure demonstrates a very short X-loop (FGDI), which does not overhang the binding site, and the distance between the X-loop and the putative PP-InsP binding site likely prevents any interactions. This contrasts with *HsDIPP1*, where the X-loop overhangs the binding site and an arginine in this loop interacts with a phosphate on the inositol ring (Zong *et al.*, 2021).

Without functional X-loops the Nudix effectors must rely on other structural features to achieve substrate selectivity. My attempts to co-crystallise AvrM14 with the mRNA cap analogue molecule ${}^m7\text{Gp}_5\text{G}$ to understand substrate binding were unsuccessful. Mugridge *et al.*, (2016) characterised Dcp2 mRNA-cap binding via co-crystallisation with ${}^m7\text{Gp}_s\text{ppp}_s{}^m7\text{G}$. Unlike ${}^m7\text{Gp}_5\text{G}$, this molecule is not hydrolysed during Dcp2 crystallisation, however, producing it requires specialised chemical synthesis and therefore it was not utilised in my study (Mugridge *et al.*, 2016). In the absence of a substrate bound structure or notable similarity to previously studied Nudix hydrolases, the amino acids involved in AvrM14 substrate specificity remain enigmatic. For *MoNudix*, I attempted co-crystallisation with InsP₆, the predicted product of 5-PP-InsP₅ hydrolysis. Chapter 3 demonstrates that InsP₆ binds to *MoNudix*, and it was required for *MoNudix* crystallisation; however, InsP₆ could not be unambiguously placed in the electron density maps. Despite this, the structural similarity between *MoNudix* and *HsDIPP1* enabled the identification of putative substrate binding amino acids. The importance of two lysines was confirmed for InsP₆ binding, 5-PP-InsP₅ hydrolysis, and the induction of phosphate starvation in *N. benthamiana*.

Overall, my findings indicate that while the X-loop can be a determinant of substrate specificity, its involvement in substrate binding is not an absolute requirement. As the enzymatic activity of more sequence diverse Nudix hydrolases like AvrM14 and *MoNudix* are characterised, our ability to predict substrate specificity from sequence will likely improve.

4.4 Evidence for RNA decapping influencing plant immune signalling

The characterisation of AvrM14 presented in chapter 2 is the first evidence for an effector from a plant pathogen acting as an mRNA decapping enzyme. Decapping facilitates mRNA decay from the 5' end by exoribonucleases, suggesting that AvrM14 may accelerate host mRNA decay. AvrM14 is analogous to the mRNA decapping Nudix hydrolases encoded by certain

mammalian viruses which can promote mRNA decay in the host cell (Parrish and Moss 2007, Parrish *et al.*, 2007, Quintas *et al.*, 2017).

In addition to AvrM14, the effector PST02549 from *Puccinia striiformis* f. sp. *tritici* may also target mRNA decapping pathways to promote pathogen virulence. PST02549 localises to processing bodies (P-bodies) (Petre *et al.*, 2016), which are ribonucleoprotein particles containing non-translating mRNAs along with various proteins involved in mRNA metabolism, including mRNA decapping proteins (Sheth and Parker 2003). Furthermore, the enhancer of mRNA decapping protein (EDC) 4 from *N. benthamiana* was identified as a potential interactor of PST02549 (Petre *et al.*, 2016). EDC4 regulates the activity and specificity of the mRNA decapping Nudix hydrolase Dcp2 (Chang *et al.*, 2014, Charenton *et al.*, 2016, Valkov *et al.*, 2016, Mugridge *et al.*, 2018, He *et al.*, 2022), suggesting that PST02549 may influence host mRNA decapping during infection.

mRNA decay pathways may be an effective target for effector proteins due to their involvement in modulating plant immune responses. During PTI, the *A. thaliana* decapping activator PAT1 is phosphorylated by mitogen-activated protein kinase 4 (MPK4) and accumulates in P-bodies (Roux *et al.*, 2015), indicating that immune signalling alters PAT1 activity. Like EDC4, PAT1 can influence mRNA decapping activity and specificity (He *et al.*, 2018, He *et al.*, 2022), and the loss of PAT1 in *A. thaliana* leads to the constitutive activation of some EDS1-dependant defence responses (Roux *et al.*, 2015). mRNA decapping and decay can also regulate plant immunity by controlling NLR transcript levels (Gloggnitzer *et al.*, 2014, Jung *et al.*, 2020), and by promoting the decay of negative regulators of plant immunity during PTI (Yu *et al.*, 2019). Mounting evidence indicates that mRNA decapping is important for the proper function of the plant immune system; further study is required to determine how fungal effectors like AvrM14 and PST02549 may exploit these pathways.

4.5 The influence of phosphate homeostasis on plant-microbe interactions

The precise regulation of phosphate levels is vital for all living organisms, but it is especially crucial for plants due to the often-limited bioavailability of phosphorus in soil. In plant cells, PP-InsPs signal phosphate availability through binding to SPX domains which inhibit PHRs, the master transcriptional regulators of phosphate starvation responses. The enzymes VIH1 and VIH2 are dual-function proteins with PP-InsP synthase and hydrolase domains; these are crucial for integrating phosphate availability with the regulation of PP-InsP concentration in plants (Zhu *et al.*, 2019), where phosphate inhibits the phosphatase activity of VIH1/2, while ATP levels, which are decreased during phosphate starvation, regulate the kinase activity (Zhu

et al., 2019). Altering the kinetics of the kinase and phosphatase VIH1/2 domains depending on phosphate levels, ensures PP-InsP concentration accurately reflects phosphate status. My results indicate that PP-InsP hydrolysis by *MoNudix* and homologous *Colletotrichum* effectors uncouples PP-InsP levels from phosphate availability, preventing accurate phosphate sensing and initiating starvation responses.

These Nudix effectors are particularly intriguing in the context of recent research into the regulation of plant interactions with mycorrhizal fungi; multiple independent research groups have demonstrated that the infection of monocot and dicot plants with phosphate-providing mycorrhizal fungi is dependent on the PP-InsP/PHR/SPX signalling pathway (Shi *et al.*, 2021, Wang *et al.*, 2021, Das *et al.*, 2022, Liao *et al.*, 2022). My results therefore suggest that pathogenic *Magnaporthe* and *Colletotrichum* fungi use PP-InsP hydrolysing Nudix effectors to hijack a highly conserved plant signalling pathway that functions in the promotion of beneficial plant-fungal interactions.

A notable difference between the results presented in chapter 3 and previous studies on phosphate signalling in plant microbe-interactions, is that in our experiments the activation of phosphate starvation was localised. Our findings demonstrate that localised PP-InsP depletion is sufficient for PHR activation and provide further support for the essential role of PP-InsPs in plant phosphate homeostasis. Future studies could utilise localised Nudix effector expression to determine if phosphate starvation in one area of the plant is communicated to other areas with sufficient phosphate, for example by the transport of PSI miRNAs as previously suggested (Loreti and Perata 2022). The ability of the Nudix effectors to activate PSRs likely provides considerable benefits to the pathogen. The reason for this is two-fold. First, the induction of phosphate starvation suppresses plant immune responses (Castrillo *et al.*, 2017, Tang *et al.*, 2022). Second, high concentrations of phosphate, as is expected to occur in plant tissue with sufficient phosphate supply undergoing a PSR, can promote fungal infection (Campos-Soriano *et al.*, 2020).

Another difference between the work described in chapter 3 and most studies of phosphate-regulated plant-microbe interactions, is that our experiments were conducted using leaf and not root tissue. The main reason for this is that rice blast is primarily a foliar pathogen, although it can infect via roots (Sesma and Osbourn 2004). Our results suggest that like findings in roots, phosphate starvation inhibits immune responses in leaves. While there are differences in gene expression changes in rice roots and shoots during phosphate starvation, comprehensive RNA-Sequencing experiments indicate that the overall changes to cellular function are similar (Secco

et al., 2013). The integration of immune signalling and phosphate status is likely important for regulating interactions with beneficial root microbes; potentially immune suppression in leaves during phosphate starvation also benefits plants by conserving resources, as immune responses are energetically costly (Huot *et al.*, 2014).

In addition to my findings, previous research suggests that other pathogens may benefit from inducing phosphate starvation during plant infection (reviewed in (Paries and Gutjahr 2023)). Prior to this thesis, research into the function of bacterial effector XopH provided evidence for phosphate sensing manipulation by a plant pathogen. Like the *Magnaporthe* and *Colletotrichum* Nudix effectors, XopH likely reduces the intracellular concentrations of PP-InsPs in host plant cells during infection (Blüher *et al.*, 2017). XopH achieves this by dephosphorylating InsP₆. While the authors noted changes to ethylene and jasmonate signalling in plants expressing XopH, they did not monitor PSRs. Our results suggest that XopH likely activates PSRs, in addition to causing the reported changes in hormone signalling. As more effectors are characterised, I anticipate the identification of further mechanisms by which pathogens exploit phosphate signalling pathways in plants.

4.6 Are Nudix effectors critical pathogenicity factors in *Colletotrichum*?

Characterised *Colletotrichum* species are predominantly plant pathogens. *Colletotrichum tofieldiae* is a notable exception, it promotes *A. thaliana* growth in low-phosphate environments by transferring phosphate to the plant (Hiruma *et al.*, 2016). *C. tofieldiae* and *A. thaliana* interactions fluctuate between beneficial, benign, or parasitic, and are influenced by a variety of factors including phosphate availability, plant indole glucosinolate levels, and the production of fungal secondary metabolites (Hacquard *et al.*, 2016, Hiruma *et al.*, 2016, Frerigmann *et al.*, 2021, Hiruma *et al.*, 2023). I was unable to identify Nudix effectors in *C. tofieldiae*, and their absence is likely required to ensure *C. tofieldiae* growth remains appropriately regulated by plant phosphate status.

In contrast, *C. higginsianum*, a pathogen of *A. thaliana* and other Brassicaceae, has four putative Nudix effector genes. Two copies of *ChNudix* and one of *ChNudix2* are located on a mini-chromosome, chromosome 11, while *ChNudix3* is on chromosome 9 (Dallery *et al.*, 2017). All Nudix effectors are produced early in plant infection (O'connell *et al.*, 2012). *C. higginsianum* mutants lacking chromosome 11 display normal vegetative growth and can successfully penetrate host plant cells but demonstrate inhibited disease progression, similar to the phenotypes observed in Chapter 3 when *MoNudix* was silenced in *M. oryzae* (Plaumann *et*

al., 2018). Given that chromosome 11 has only eight predicted effectors (Dallery *et al.*, 2017), it is likely that *ChNudix* and *ChNudix2* are critical to the pathogenicity of *C. higginsianum*. Hiruma *et al.*, (2023) sequenced the genome of *C. higginsianum* KHC, a non-pathogenic strain isolated from *Scopolia japonica*. This strain maintains *ChNudix3* but has lost *ChNudix2* and both copies of *ChNudix*. Hiruma *et al.*, (2023) did not include a detailed analysis of the KHC genome; however, my examination of the available data suggests that strain KHC lacks chromosome 11, further indicating that this chromosome's genes are non-essential for fungal growth and certain plant interactions but are critical for pathogenicity.

Chapter 3 identified *ChNudix3* as the only *Magnaporthe/Colletotrichum* Nudix effector unable to trigger PHR activity in *N. benthamiana*. This observation suggests that *ChNudix3* would not compensate for the absence of the other Nudix effectors in *C. higginsianum* strains without chromosome 11. While this thesis did not investigate the molecular basis for *ChNudix3*'s lack of activity, a plausible explanation may be the substitution of a potentially critical lysine amino acid. This lysine is conserved in all other examined *Magnaporthe* and *Colletotrichum* Nudix effectors (Figure 1A). The lysine may act analogously to arginine 10 in *HsDIPP1*, which is also found in a flexible loop region immediately prior to the first β -sheet and binds to the top of 5-PP-InsP₅ (Figure 1B) (Zong *et al.*, 2021).

The curious loss of active Nudix effectors in non-pathogenic *C. higginsianum* and *C. tofieldiae*, coupled with the regulation of *C. tofieldiae*-*A. thaliana* interactions by phosphate status, hints to the Nudix effectors having a key role in determining the fate of plant/*Colletotrichum* interactions.

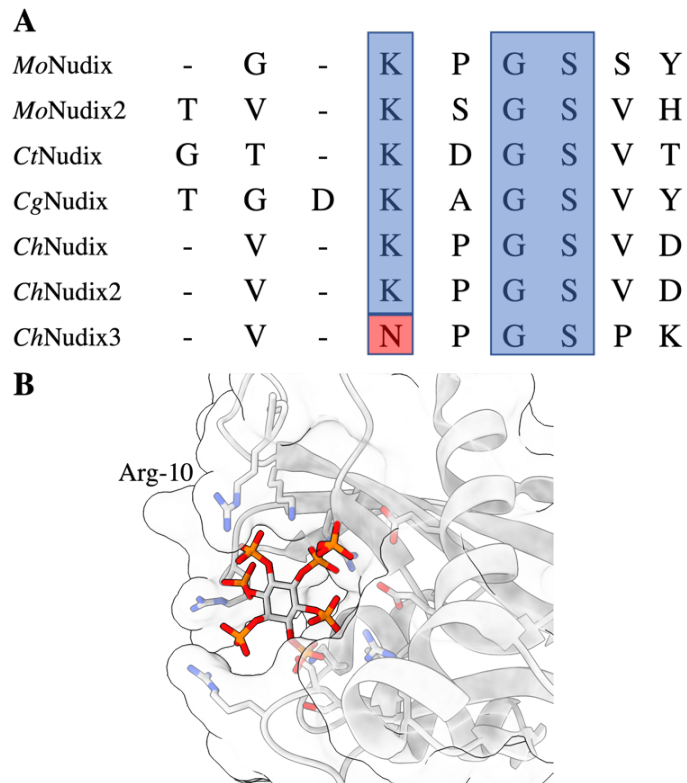


Figure 1: (A) A lysine conserved in all other tested Nudix effectors is substituted with an asparagine in *ChNudix3*. The protein sequences of the Nudix effectors were aligned using MUSCLE (Edgar 2004), with the region surrounding the lysine shown. Conserved amino acids are indicated in blue and the substituted asparagine in red. (B) The conserved lysine may act like arginine 10 from *HsDIPP1*, which is involved in 5-PP-InsP₅ binding (PDB ID: 6WO7).

4.7 Links between phosphate status and mRNA decay

AvrM14 and *MoNudix* exhibit no discernible sequence conservation outside of the Nudix motif and hydrolyse distinct substrates. However, the pathways they influence are interconnected in humans, and potentially in other organisms. This is demonstrated by studies on *HsDIPP1* and its yeast orthologue *Ddp1*, which function as both PP-InsP hydrolase and mRNA decapping enzymes (Safrany *et al.*, 1998, Safrany *et al.*, 1999, Song *et al.*, 2013, Grudzien-Nogalska *et al.*, 2016). Research by Sahu *et al.*, (2020) indicates that PP-InsPs can modulate the mRNA decapping activity of *HsDIPP1* in human cells, likely due to competition for the *HsDIPP1* active site (Sahu *et al.*, 2020). Similarly, an African Swine Fever virus Nudix hydrolase can hydrolyse both PP-InsPs and mRNA caps, and InsP₆ can inhibit its decapping activity *in vitro* (Yang *et al.*, 2022). The benefits of PP-InsP-mediated mRNA decapping regulation are unknown, but this may represent an additional mechanism to align gene expression with phosphate availability. Whether plants possess mRNA decapping enzymes that can be inhibited

by PP-InsPs, and hence if *MoNudix* promotes mRNA decapping via PP-InsP hydrolysis, remains to be determined.

4.8 Targeting Nudix effectors to achieve disease resistance

This study provides insights into fungal Nudix effectors that could inform the creation of novel R-proteins and strategies to neutralise Nudix effectors to enhance plant disease resistance. For example, Chapter 2 identifies the amino acids that enable AvrM14-B to escape M1 and M4 recognition and could therefore inform the engineering of M1 to recognise AvrM14-B. However, I propose that future research efforts should prioritise *MoNudix*, as *M. oryzae* represents a greater threat than *M. lini* to global food security (Dean *et al.*, 2012). *MoNudix* is also a promising candidate for the development of novel resistance strategies, as it is highly expressed early during infection (Yan *et al.*, 2023), and the results in Chapter 3 indicates that *MoNudix* makes a significant contribution to the virulence of the rice blast pathogen.

Recently, Kourelis *et al.*, (2023) described the engineering of plant NLRs to recognise fluorescent proteins (FP) via swapping the integrated domain in a rice CC-NLR with a nanobody that binds to the FP (Kourelis *et al.*, 2023). Nanobodies are generated by the adaptive immune system of camelids and cartilaginous fish, they are small (~15kDa) and generally very stable proteins that bind to target antigens with high affinity. *MoNudix* is straightforward to express and purify to homogeneity using an *E. coli* system, with a yield of ~10 mg of purified protein per L of bacteria culture. *MoNudix* is also exceptionally stable in solution, for example in chapter 3 *MoNudix* was concentrated to 30 mg/mL for protein crystallisation. The highly stable, easy to purify nature of *MoNudix* would enable efficient nanobody identification and optimisation, as nanobody production methods typically require >1 mg of stable, properly folded, and highly pure protein (Pardon *et al.*, 2014). Future studies should identify nanobody binders for *MoNudix*, integrate these into the system described by Kourelis *et al.*, (2023), and generate immune receptors able to recognise *MoNudix* and confer rice blast disease resistance. To reduce the virulence of rice blast, another strategy could involve creating compounds that inhibit the enzymatic activity of the *MoNudix* effector. In appendix 1, our collaborators demonstrate that enzymatic activity is required for *MoNudix* to promote *M. oryzae* virulence. Nudix hydrolases are suitable candidates for enzyme-inhibitor design (Michel *et al.*, 2020). For example, *H. sapiens* Nudt1 plays a key role in maintaining cancer cell viability, and multiple small-molecule inhibitors of this enzyme have been developed (Gad *et al.*, 2014, Huber *et al.*, 2014, Warpman Berglund *et al.*, 2016). Likewise, inhibitors of *H. sapiens* Nudt5 and Nudt15

have been developed that bind to the active site of their targeted enzymes with low-nanomolar affinity (Page *et al.*, 2018, Zhang *et al.*, 2020). All inhibitors for Nudt1 and Nudt15 are specific to the targeted enzyme and do not inhibit other *H. sapiens* Nudix hydrolases (Gad *et al.*, 2014, Huber *et al.*, 2014, Warpman Berglund *et al.*, 2016, Zhang *et al.*, 2020). Furthermore, no identified plant Nudix hydrolases hydrolyse PP-InsPs, it is therefore unlikely that a *MoNudix* inhibitor would interfere with the function of a plant Nudix hydrolase. Collectively, the studies with *H. sapiens* Nudix hydrolases demonstrate the potential to generate targeted small-molecule inhibitors for *MoNudix*.

However, the use of *MoNudix* small-molecule inhibitors poses a multitude of challenges, including applying the inhibitor at the correct time during the infection process, ensuring the inhibitor is taken up by the plant cell, and making enough of the inhibitor for spraying large cropping areas. Instead, the use of a protein-based inhibitor may be more feasible. A protein/peptide could be genetically encoded, eliminating the challenges described above for chemical inhibitors. Recent advances in the *de novo* design of protein binding proteins (Cao *et al.*, 2022, Bennett *et al.*, 2023, Watson *et al.*, 2023), may enable the generation of peptide/protein inhibitors for important effectors like *MoNudix* and achieve disease resistance without requiring the engineering of immunity receptors. This approach is analogous to previously identified protein-based effector inhibition systems functioning in diverse cross-kingdom interactions. For example, plant chitinases and proteinases are inhibited by fungal effectors predicted to bind to and obstruct the active site of the plant enzymes (Homma *et al.*, 2023). Another example is the toxic NAD⁺ glycohydrolase secreted by *Mycobacterium tuberculosis* during human infection, which can be inhibited by another *M. tuberculosis* protein to prevent self-poisoning (Sun *et al.*, 2015) (Figure 2). We are currently investigating both the nanobody and *de novo* protein binder strategies to target *MoNudix* and achieve rice blast disease resistance.

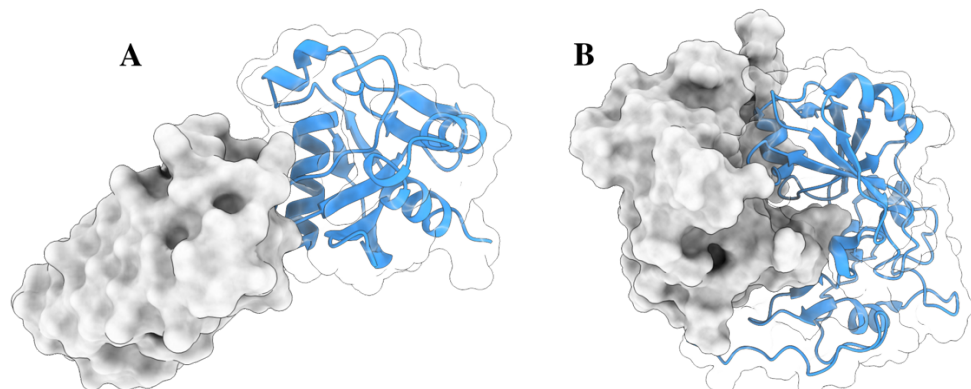


Figure 2: Enzymatic effectors could be inhibited by protein binders that obstruct the active site. (A) The crystal structure of *MoNudix* (transparent surface with ribbon diagram) bound to a computationally designed theoretical protein binder (solid surface). (B) The co-crystal structure of the *Mycobacterium tuberculosis* tuberculosis necrotizing toxin (TNT) (transparent surface with ribbon diagram) bound to its corresponding *M. tuberculosis* protein inhibitor (solid surface) (PDB ID: 4QLP).

4.9 Conclusion

This thesis has demonstrated that the predicted Nudix hydrolase effectors from phytopathogenic fungi are enzymes, characterised their substrate specificity, and identified their potential functions during pathogenesis. The work lays the foundation for further characterisation of plant mRNA decapping and PP-InsP signalling mechanisms, as well as the development of disease resistance mechanisms targeting Nudix effectors.

4.10 References

- Anderson, C., M. A. Khan, A.-M. Catanzariti, C. A. Jack, A. Nemri, G. J. Lawrence, N. M. Upadhyaya, A. R. Hardham, J. G. Ellis, P. N. Dodds and D. A. Jones (2016). "Genome analysis and avirulence gene cloning using a high-density RADseq linkage map of the flax rust fungus, *Melampsora lini*." *BMC genomics* **17**(1): 667-667.
- Bennett, N. R., B. Coventry, I. Goreshnik, B. Huang, A. Allen, D. Vafeados, Y. P. Peng, J. Dauparas, M. Baek, L. Stewart, F. DiMaio, S. De Munck, S. N. Savvides and D. Baker (2023). "Improving de novo protein binder design with deep learning." *Nat Commun* **14**(1): 2625.
- Blüher, D., D. Laha, S. Thieme, A. Hofer, L. Eschen-Lippold, A. Masch, G. Balcke, I. Pavlovic, O. Nagel, A. Schonsky, R. Hinkelmann, J. Wörner, N. Parvin, R. Greiner, S. Weber, A. Tissier, M. Schutkowski, J. Lee, H. Jessen, G. Schaaf and U. Bonas (2017). "A 1-phytase type III effector interferes with plant hormone signaling." *Nature Communications* **8**(1): 2159.
- Campos-Soriano, L., M. Bundó, M. Bach-Pages, S. F. Chiang, T. J. Chiou and B. San Segundo (2020). "Phosphate excess increases susceptibility to pathogen infection in rice." *Mol Plant Pathol* **21**(4): 555-570.
- Cao, L., B. Coventry, I. Goreshnik, B. Huang, W. Sheffler, J. S. Park, K. M. Jude, I. Marković, R. U. Kadam, K. H. G. Verschueren, K. Verstraete, S. T. R. Walsh, N. Bennett, A. Phal, A. Yang, L. Kozodoy, M. DeWitt, L. Picton, L. Miller, E. M. Strauch, N. D. DeBouver, A. Pires, A. K. Bera, S. Halabiya, B. Hammerson, W. Yang, S. Bernard, L. Stewart, I. A. Wilson, H. Ruohola-Baker, J. Schlessinger, S. Lee, S. N. Savvides, K. C. Garcia and D. Baker (2022). "Design of protein-binding proteins from the target structure alone." *Nature* **605**(7910): 551-560.
- Castrillo, G., P. J. Teixeira, S. H. Paredes, T. F. Law, L. de Lorenzo, M. E. Feltcher, O. M. Finkel, N. W. Breakfield, P. Mieczkowski, C. D. Jones, J. Paz-Ares and J. L. Dangl (2017). "Root microbiota drive direct integration of phosphate stress and immunity." *Nature* **543**(7646): 513-518.
- Chang, C. T., N. Bercovich, B. Loh, S. Jonas and E. Izaurralde (2014). "The activation of the decapping enzyme DCP2 by DCP1 occurs on the EDC4 scaffold and involves a conserved loop in DCP1." *Nucleic Acids Res* **42**(8): 5217-5233.
- Charenton, C., V. Taverniti, C. Gaudon-Plesse, R. Back, B. Séraphin and M. Graille (2016). "Structure of the active form of Dcp1-Dcp2 decapping enzyme bound to m(7)GDP and its Edc3 activator." *Nat Struct Mol Biol* **23**(11): 982-986.
- Dallery, J. F., N. Lapalu, A. Zampounis, S. Pigné, I. Luyten, J. Amselem, A. H. J. Wittenberg, S. Zhou, M. V. de Queiroz, G. P. Robin, A. Auger, M. Hainaut, B. Henrissat, K. T. Kim, Y. H. Lee, O. Lespinet, D. C. Schwartz, M. R. Thon and R. J. O'Connell (2017). "Gapless genome assembly of *Colletotrichum higginsianum* reveals chromosome structure and association of transposable elements with secondary metabolite gene clusters." *BMC Genomics* **18**(1): 667.
- Das, D., M. Paries, K. Hobecker, M. Gigl, C. Dawid, H. M. Lam, J. Zhang, M. Chen and C. Gutjahr (2022). "PHOSPHATE STARVATION RESPONSE transcription factors enable arbuscular mycorrhiza symbiosis." *Nat Commun* **13**(1): 477.
- Dean, R., J. A. Van Kan, Z. A. Pretorius, K. E. Hammond-Kosack, A. Di Pietro, P. D. Spanu, J. J. Rudd, M. Dickman, R. Kahmann, J. Ellis and G. D. Foster (2012). "The Top 10 fungal pathogens in molecular plant pathology." *Mol Plant Pathol* **13**(4): 414-430.
- Djamei, A., K. Schipper, F. Rabe, A. Ghosh, V. Vincon, J. Kahnt, S. Osorio, T. Tohge, A. R. Fernie, I. Feussner, K. Feussner, P. Meinicke, Y. D. Stierhof, H. Schwarz, B. Macek, M. Mann and R. Kahmann (2011). "Metabolic priming by a secreted fungal effector." *Nature* **478**(7369): 395-398.
- Dong, S. and Y. Wang (2016). "Nudix effectors: a common weapon in the arsenal of plant pathogens." *PLoS pathogens* **12**(8): e1005704-e1005704.
- Dunn, C. A., S. F. O'Handley, D. N. Frick and M. J. Bessman (1999). "Studies on the ADP-ribose pyrophosphatase subfamily of the nudix hydrolases and tentative identification of *trgB*, a gene associated with tellurite resistance." *J Biol Chem* **274**(45): 32318-32324.
- Edgar, R. C. (2004). "MUSCLE: multiple sequence alignment with high accuracy and high throughput." *Nucleic Acids Res* **32**(5): 1792-1797.
- Fiorin, G. L., A. Sánchez-Vallet, D. P. T. Thomazella, P. F. V. do Prado, L. C. do Nascimento, A. V. O. Figueira, B. Thomma, G. A. G. Pereira and P. Teixeira (2018). "Suppression of Plant Immunity by Fungal Chitinase-like Effectors." *Curr Biol* **28**(18): 3023-3030.e3025.
- Frerigmann, H., M. Piotrowski, R. Lemke, P. Bednarek and P. Schulze-Lefert (2021). "A Network of Phosphate Starvation and Immune-Related Signaling and Metabolic Pathways Controls the Interaction between *Arabidopsis thaliana* and the Beneficial Fungus *Colletotrichum tofieldiae*." *Mol Plant Microbe Interact* **34**(5): 560-570.
- Gad, H., T. Koolmeister, A. S. Jemth, S. Eshtad, S. A. Jacques, C. E. Ström, L. M. Svensson, N. Schultz, T. Lundbäck, B. O. Einarsson, A. Saleh, C. Göktürk, P. Baranczewski, R. Svensson, R. P. Berntsson, R. Gustafsson, K. Strömberg, K. Sanjiv, M. C. Jacques-Cordonnier, M. Desroses, A. L. Gustavsson, R. Olofsson, F. Johansson, E. J. Homan, O. Loseva, L. Bräutigam, L. Johansson, A. Höglund, A. Hagenkort, T. Pham, M. Altun, F. Z. Gaugaz, S. Vikingsson, B. Evers, M. Henriksson, K. S. Vallin, O. A. Wallner, L. G. Hammarström, E. Wiita, I. Almlöf, C. Kalderén, H. Axelsson, T. Djureinovic, J. C. Puigvert, M. Häggblad, F. Jeppsson, U. Martens, C. Lundin, B. Lundgren, I. Granelli, A. J. Jensen, P. Artursson, J. A. Nilsson, P. Stenmark, M. Scobie, U. W. Berglund and T. Helleday (2014). "MTH1 inhibition eradicates cancer by preventing sanitation of the dNTP pool." *Nature* **508**(7495): 215-221.

Gloggnitzer, J., S. Akimcheva, A. Srinivasan, B. Kusenda, N. Riehs, H. Stampfl, J. Bautor, B. Dekrout, C. Jonak, J. M. Jiménez-Gómez, J. E. Parker and K. Riha (2014). "Nonsense-mediated mRNA decay modulates immune receptor levels to regulate plant antibacterial defense." *Cell host microbe* **16**(3): 376-390.

Grudzien-Nogalska, E., X. Jiao, M. G. Song, R. P. Hart and M. Kiledjian (2016). "Nudt3 is an mRNA decapping enzyme that modulates cell migration." *Rna* **22**(5): 773-781.

Hacquard, S., B. Kracher, K. Hiruma, P. C. Münch, R. Garrido-Oter, M. R. Thon, A. Weimann, U. Damm, J. F. Dallery, M. Hainaut, B. Henrissat, O. Lepinet, S. Sacristán, E. Ver Loren van Themaat, E. Kemen, A. C. McHardy, P. Schulze-Lefert and R. J. O'Connell (2016). "Survival trade-offs in plant roots during colonization by closely related beneficial and pathogenic fungi." *Nat Commun* **7**: 11362.

He, F., A. Celik, C. Wu and A. Jacobson (2018). "General decapping activators target different subsets of inefficiently translated mRNAs." *eLife* **7**: e34409.

He, F., C. Wu and A. Jacobson (2022). "Dcp2 C-terminal cis-binding elements control selective targeting of the decapping enzyme by forming distinct decapping complexes." *eLife* **11**: e74410.

He, Q., H. McLellan, P. C. Boevink and P. R. J. Birch (2020). "All Roads Lead to Susceptibility: The Many Modes of Action of Fungal and Oomycete Intracellular Effectors." *Plant Commun* **1**(4): 100050.

Hiruma, K., S. Aoki, J. Takino, T. Higa, Y. D. Utami, A. Shiina, M. Okamoto, M. Nakamura, N. Kawamura, Y. Ohmori, R. Sugita, K. Tanoi, T. Sato, H. Oikawa, A. Minami, W. Iwasaki and Y. Saijo (2023). "A fungal sesquiterpene biosynthesis gene cluster critical for mutualist-pathogen transition in *Colletotrichum tofieldiae*." *Nat Commun* **14**(1): 5288.

Hiruma, K., N. Gerlach, S. Sacristán, R. T. Nakano, S. Hacquard, B. Kracher, U. Neumann, D. Ramírez, M. Bucher, R. J. O'Connell and P. Schulze-Lefert (2016). "Root Endophyte *Colletotrichum tofieldiae* Confers Plant Fitness Benefits that Are Phosphate Status Dependent." *Cell* **165**(2): 464-474.

Höfer, K., S. Li, F. Abele, J. Frindert, J. Schlotthauer, J. Gräwenhoff, J. Du, D. J. Patel and A. Jäschke (2016). "Structure and function of the bacterial decapping enzyme NudC." *Nat Chem Biol* **12**(9): 730-734.

Homma, F., J. Huang and R. A. L. van der Hoorn (2023). "AlphaFold-Multimer predicts cross-kingdom interactions at the plant-pathogen interface." *Nature Communications* **14**(1): 6040.

Huber, K. V., E. Salah, B. Radic, M. Gridling, J. M. Elkins, A. Stukalov, A. S. Jemth, C. Göktürk, K. Sanjiv, K. Strömberg, T. Pham, U. W. Berglund, J. Colinge, K. L. Bennett, J. I. Loizou, T. Helleday, S. Knapp and G. Superti-Furga (2014). "Stereospecific targeting of MTH1 by (S)-crizotinib as an anticancer strategy." *Nature* **508**(7495): 222-227.

Huot, B., J. Yao, B. L. Montgomery and S. Y. He (2014). "Growth-defense tradeoffs in plants: a balancing act to optimize fitness." *Mol Plant* **7**(8): 1267-1287.

Jung, H. W., G. K. Panigrahi, G. Y. Jung, Y. J. Lee, K. H. Shin, A. Sahoo, E. S. Choi, E. Lee, K. Man Kim, S. H. Yang, J.-S. Jeon, S. C. Lee and S. H. Kim (2020). "Pathogen-Associated Molecular Pattern-Triggered Immunity Involves Proteolytic Degradation of Core Nonsense-Mediated mRNA Decay Factors During the Early Defense Response[OPEN]." *The Plant Cell* **32**(4): 1081-1101.

Kourelis, J., C. Marchal, A. Posbeykian, A. Harant and S. Kamoun (2023). "NLR immune receptor-nanobody fusions confer plant disease resistance." *Science* **379**(6635): 934-939.

Kubicek, C. P., T. L. Starr and N. L. Glass (2014). "Plant cell wall-degrading enzymes and their secretion in plant-pathogenic fungi." *Ann Rev Phytopathol* **52**: 427-451.

Liao, D., C. Sun, H. Liang, Y. Wang, X. Bian, C. Dong, X. Niu, M. Yang, G. Xu, A. Chen and S. Wu (2022). "SISPX1-SIPHR complexes mediate the suppression of arbuscular mycorrhizal symbiosis by phosphate repletion in tomato." *Plant Cell* **34**(10): 4045-4065.

Liu, T., T. Song, X. Zhang, H. Yuan, L. Su, W. Li, J. Xu, S. Liu, L. Chen, T. Chen, M. Zhang, L. Gu, B. Zhang and D. Dou (2014). "Unconventionally secreted effectors of two filamentous pathogens target plant salicylate biosynthesis." *Nat Commun* **5**: 4686.

Loreti, E. and P. Perata (2022). "Mobile plant microRNAs allow communication within and between organisms." *New Phytol* **235**(6): 2176-2182.

Mart Nez-Cruz, J. S., D. Romero, J. S. Hierrezuelo, M. Thon, A. de Vicente and P. R.-G. A. A (2021). "Effectors with chitinase activity (EWCAs), a family of conserved, secreted fungal chitinases that suppress chitin-triggered immunity." *Plant Cell* **33**(4): 1319-1340.

Michel, M., E. J. Homan, E. Wiita, K. Pedersen, I. Almlöf, A. L. Gustavsson, T. Lundbäck, T. Helleday and U. Warpman Berglund (2020). "In silico Druggability Assessment of the NUDIX Hydrolase Protein Family as a Workflow for Target Prioritization." *Front Chem* **8**: 443.

Mugridge, J. S., R. W. Tibble, M. Ziemniak, J. Jemielity and J. D. Gross (2018). "Structure of the activated Edc1-Dcp1-Dcp2-Edc3 mRNA decapping complex with substrate analog poised for catalysis." *Nat Commun* **9**(1): 1152.

Mugridge, J. S., M. Ziemniak, J. Jemielity and J. D. Gross (2016). "Structural basis of mRNA-cap recognition by Dcp1-Dcp2." *Nat Struct Mol Biol* **23**(11): 987-994.

O'Connell, R. J., M. R. Thon, S. Hacquard, S. G. Amyotte, J. Kleemann, M. F. Torres, U. Damm, E. A. Buiate, L. Epstein, N. Alkan, J. Altmüller, L. Alvarado-Balderrama, C. A. Bauser, C. Becker, B. W. Birren, Z. Chen, J. Choi, J. A. Crouch, J. P. Duvick, M. A. Farman, P. Gan, D. Heiman, B. Henrissat, R. J. Howard, M. Kabbage, C. Koch, B. Kracher, Y. Kubo, A. D. Law, M. H. Lebrun, Y. H. Lee, I. Miyara, N. Moore, U. Neumann, K. Nordström, D. G. Panaccione, R. Panstruga, M. Place, R. H. Proctor, D. Prusky, G. Rech, R. Reinhardt, J. A. Rollins, S. Rounseley, C. L. Schardl, D. C. Schwartz, N. Shenoy, K. Shirasu, U. R. Sikkakolli, K. Stüber, S. A. Sukno, J. A. Sweigard, Y. Takano, H. Takahara, F. Trail, H. C. van der Does, L. M. Voll, I. Will, S. Young, Q. Zeng, J. Zhang, S. Zhou, M. B. Dickman, P. Schulze-Lefert, E. Ver Loren van Themaat, L. J. Ma and L. J. Vaillancourt (2012). "Lifestyle transitions in plant pathogenic Colletotrichum fungi deciphered by genome and transcriptome analyses." *Nat Genet* **44**(9): 1060-1065.

Page, B. D. G., N. C. K. Valerie, R. H. G. Wright, O. Wallner, R. Isaksson, M. Carter, S. G. Rudd, O. Loseva, A. S. Jemth, I. Almlöf, J. Font-Mateu, S. Llona-Minguez, P. Baranczewski, F. Jeppsson, E. Homan, H. Almqvist, H. Axelsson, S. Regmi, A. L. Gustavsson, T. Lundbäck, M. Scobie, K. Strömbärg, P. Stenmark, M. Beato and T. Helleday (2018). "Targeted NUDT5 inhibitors block hormone signaling in breast cancer cells." *Nat Commun* **9**(1): 250.

Pardon, E., T. Laeremans, S. Triest, S. G. Rasmussen, A. Wohlköning, A. Ruf, S. Muyldermans, W. G. Hol, B. K. Kobilka and J. Steyaert (2014). "A general protocol for the generation of Nanobodies for structural biology." *Nat Protoc* **9**(3): 674-693.

Paries, M. and C. Gutjahr (2023). "The good, the bad, and the phosphate: regulation of beneficial and detrimental plant-microbe interactions by the plant phosphate status." *New Phytol* **239**(1): 29-46.

Parrish, S. and B. Moss (2007). "Characterization of a second vaccinia virus mRNA-decapping enzyme conserved in poxviruses." *Journal of virology* **81**(23): 12973-12978.

Parrish, S., W. Resch and B. Moss (2007). "Vaccinia virus D10 protein has mRNA decapping activity, providing a mechanism for control of host and viral gene expression." *Proceedings of the National Academy of Sciences* **104**(7): 2139-2144.

Petre, B., D. G. Saunders, J. Sklenar, C. Lorrain, K. V. Krasileva, J. Win, S. Duplessis and S. Kamoun (2016). "Heterologous Expression Screens in Nicotiana benthamiana Identify a Candidate Effector of the Wheat Yellow Rust Pathogen that Associates with Processing Bodies." *PLoS One* **11**(2): e0149035.

Plaumann, P. L., J. Schmidpeter, M. Dahl, L. Taher and C. Koch (2018). "A Dispensable Chromosome Is Required for Virulence in the Hemibiotrophic Plant Pathogen Colletotrichum higginsianum." *Front Microbiol* **9**: 1005.

Quintas, A., D. Pérez-Núñez, E. G. Sánchez, M. L. Nogal, M. W. Hentze, A. Castelló and Y. Revilla (2017). "Characterization of the African swine fever virus decapping enzyme during infection." *Journal of virology* **91**(24).

Roux, M. E., M. W. Rasmussen, K. Palma, S. Lolle, M. Regué Á, G. Bethke, J. Glazebrook, W. Zhang, L. Sieburth, M. R. Larsen, J. Mundy and M. Petersen (2015). "The mRNA decay factor PAT1 functions in a pathway including MAP kinase 4 and immune receptor SUMM2." *Embo J* **34**(5): 593-608.

Safrany, S. T., J. J. Caffrey, X. Yang, M. E. Bembenek, M. B. Moyer, W. A. Burkhardt and S. B. Shears (1998). "A novel context for the 'MutT' module, a guardian of cell integrity, in a diphosphoinositol polyphosphate phosphohydrolase." *The EMBO Journal* **17**(22): 6599-6607.

Safrany, S. T., S. W. Ingram, J. L. Cartwright, J. R. Falck, A. G. McLennan, L. D. Barnes and S. B. Shears (1999). "The diadenosine hexaphosphate hydrolases from Schizosaccharomyces pombe and Saccharomyces cerevisiae are homologues of the human diphosphoinositol polyphosphate phosphohydrolase: overlapping substrate specificities in a MutT-type protein." *Journal of biological chemistry* **274**(31): 21735-21740.

Sahu, S., Z. Wang, X. Jiao, C. Gu, N. Jork, C. Wittwer, X. Li, S. Hostachy, D. Fiedler, H. Wang, H. J. Jessen, M. Kiledjian and S. B. Shears (2020). "InsP7 is a small-molecule regulator of NUDT3-mediated mRNA decapping and processing-body dynamics." *Proceedings of the National Academy of Sciences* **117**(32): 19245-19253.

Secco, D., M. Jabnoune, H. Walker, H. Shou, P. Wu, Y. Poirier and J. Whelan (2013). "Spatio-temporal transcript profiling of rice roots and shoots in response to phosphate starvation and recovery." *Plant Cell* **25**(11): 4285-4304.

Seong, K. and K. V. Krasileva (2021). "Computational Structural Genomics Unravels Common Folds and Novel Families in the Secretome of Fungal Phytopathogen Magnaporthe oryzae." *Mol Plant Microbe Interact* **34**(11): 1267-1280.

Sesma, A. and A. E. Osbourn (2004). "The rice leaf blast pathogen undergoes developmental processes typical of root-infecting fungi." *Nature* **431**(7008): 582-586.

Sharma, S., E. Grudzien-Nogalska, K. Hamilton, X. Jiao, J. Yang, L. Tong and M. Kiledjian (2020). "Mammalian Nudix proteins cleave nucleotide metabolite caps on RNAs." *Nucleic Acids Res* **48**(12): 6788-6798.

Sheth, U. and R. Parker (2003). "Decapping and decay of messenger RNA occur in cytoplasmic processing bodies." *Science* **300**(5620): 805-808.

Shi, J., B. Zhao, S. Zheng, X. Zhang, X. Wang, W. Dong, Q. Xie, G. Wang, Y. Xiao, F. Chen, N. Yu and E. Wang (2021). "A phosphate starvation response-centered network regulates mycorrhizal symbiosis." *Cell* **184**(22): 5527-5540.e5518.

Song, M.-G., S. Bail and M. Kiledjian (2013). "Multiple Nudix family proteins possess mRNA decapping activity." *RNA* **19**(3): 390-399.

Srouji, J. R., A. Xu, A. Park, J. F. Kirsch and S. E. Brenner (2017). "The evolution of function within the Nudix homology clan." *Proteins: structure, function, and bioinformatics* **85**(5): 775-811.

Sun, J., A. Siroy, R. K. Lokareddy, A. Speer, K. S. Doornbos, G. Cingolani and M. Niederweis (2015). "The tuberculosis necrotizing toxin kills macrophages by hydrolyzing NAD." *Nat Struct Mol Biol* **22**(9): 672-678.

Svensson, L. M., A. S. Jemth, M. Desroses, O. Loseva, T. Helleday, M. Högbom and P. Stenmark (2011). "Crystal structure of human MTH1 and the 8-oxo-dGMP product complex." *FEBS Lett* **585**(16): 2617-2621.

Tang, J., D. Wu, X. Li, L. Wang, L. Xu, Y. Zhang, F. Xu, H. Liu, Q. Xie, S. Dai, D. Coleman-Derr, S. Zhu and F. Yu (2022). "Plant immunity suppression via PHR1-RALF-FERONIA shapes the root microbiome to alleviate phosphate starvation." *Embo J* **41**(6): e109102.

Tang, Q., C. Liu, C. Zhong and J. Ding (2015). "Crystal Structures of *Arabidopsis thaliana* Nudix Hydrolase NUDT7 Reveal a Previously Unobserved Conformation." *Molecular plant* **8**(10): 1557-1559.

Valkov, E., S. Muthukumar, C.-T. Chang, S. Jonas, O. Weichenrieder and E. Izaurrealde (2016). "Structure of the Dcp2–Dcp1 mRNA-decapping complex in the activated conformation." *Nature Structural & Molecular Biology* **23**(6): 574-579.

Wakamatsu, T., N. Nakagawa, S. Kuramitsu and R. Masui (2008). "Structural basis for different substrate specificities of two ADP-ribose pyrophosphatases from *Thermus thermophilus* HB8." *J Bacteriol* **190**(3): 1108-1117.

Wang, P., R. Snijders, W. Kohlen, J. Liu, T. Bisseling and E. Limpens (2021). "Medicago SPX1 and SPX3 regulate phosphate homeostasis, mycorrhizal colonization, and arbuscule degradation." *Plant Cell* **33**(11): 3470-3486.

Warpman Berglund, U., K. Sanjiv, H. Gad, C. Kalderén, T. Koolmeister, T. Pham, C. Gokturk, R. Jafari, G. Maddalo, B. Seashore-Ludlow, A. Chernobrovkin, A. Manoilov, I. S. Pateras, A. Rasti, A. S. Jemth, I. Almlöf, O. Loseva, T. Visnes, B. O. Einarsdóttir, F. Z. Gaugaz, A. Saleh, B. Platzack, O. A. Wallner, K. S. Vallin, M. Henriksson, P. Wakchaure, S. Borhade, P. Herr, Y. Kallberg, P. Baranczewski, E. J. Homan, E. Wiita, V. Nagpal, T. Meijer, N. Schipper, S. G. Rudd, L. Bräutigam, A. Lindqvist, A. Filppula, T. C. Lee, P. Artursson, J. A. Nilsson, V. G. Gorgoulis, J. Lehtipö, R. A. Zubarev, M. Scobie and T. Helleday (2016). "Validation and development of MTH1 inhibitors for treatment of cancer." *Ann Oncol* **27**(12): 2275-2283.

Watson, J. L., D. Juergens, N. R. Bennett, B. L. Trippe, J. Yim, H. E. Eisenach, W. Ahern, A. J. Borst, R. J. Ragotte, L. F. Milles, B. I. M. Wicky, N. Hanikel, S. J. Pellock, A. Courbet, W. Sheffler, J. Wang, P. Venkatesh, I. Sappington, S. V. Torres, A. Lauko, V. De Bortoli, E. Mathieu, S. Ovchinnikov, R. Barzilay, T. S. Jaakkola, F. DiMaio, M. Baek and D. Baker (2023). "De novo design of protein structure and function with RFdiffusion." *Nature* **620**(7976): 1089-1100.

Yan, X., B. Tang, L. S. Ryder, D. MacLean, V. M. Were, A. B. Eseola, N. Cruz-Mireles, W. Ma, A. J. Foster, M. Osés-Ruiz and N. J. Talbot (2023). "The transcriptional landscape of plant infection by the rice blast fungus *Magnaporthe oryzae* reveals distinct families of temporally co-regulated and structurally conserved effectors." *The Plant Cell* **35**(5): 1360-1385.

Yang, Y., C. Zhang, X. Li, L. Li, Y. Chen, X. Yang, Y. Zhao, C. Chen, W. Wang, Z. Zhong, C. Yang, Z. Huang and D. Su (2022). "Structural Insight into Molecular Inhibitory Mechanism of InsP(6) on African Swine Fever Virus mRNA-Decapping Enzyme g5Rp." *J Virol* **96**(10): e0190521.

Yu, X., B. Li, G.-J. Jiang, S. Jiang, D. Jiang, J.-C. Jiang, S.-H. Wu, L. Shan and P. He (2019). "Orchestration of processing body dynamics and mRNA decay in *Arabidopsis* immunity." *Cell reports* **28**(8): 2194-2205.e2196.

Zhang, D., Y. Liu, Q. Wang, Z. Guan, J. Wang, J. Liu, T. Zou and P. Yin (2016). "Structural basis of prokaryotic NAD-RNA decapping by NudC." *Cell Res* **26**(9): 1062-1066.

Zhang, S. M., M. Desroses, A. Hagenkort, N. C. K. Valerie, D. Rehling, M. Carter, O. Wallner, T. Koolmeister, A. Throup, A. S. Jemth, I. Almlöf, O. Loseva, T. Lundbäck, H. Axelsson, S. Regmi, A. Sarno, A. Krämer, L. Pudelko, L. Bräutigam, A. Rasti, M. Göttmann, E. Wiita, J. Kutzner, T. Schaller, C. Kalderén, A. Cázares-Körner, B. D. G. Page, R. Krimpenfort, S. Eshstad, M. Altun, S. G. Rudd, S. Knapp, M. Scobie, E. J. Homan, U. W. Berglund, P. Stenmark and T. Helleday (2020). "Development of a chemical probe against NUDT15." *Nat Chem Biol* **16**(10): 1120-1128.

Zhu, J., K. Lau, R. Puschmann, R. K. Harmel, Y. Zhang, V. Pries, P. Gaugler, L. Broger, A. K. Dutta, H. J. Jessen, G. Schaaf, A. R. Fernie, L. A. Hothorn, D. Fiedler and M. Hothorn (2019). "Two bifunctional inositol pyrophosphate kinases/phosphatases control plant phosphate homeostasis." *Elife* **8**.

Zong, G., N. Jork, S. Hostachy, D. Fiedler, H. J. Jessen, S. B. Shears and H. Wang (2021). "New structural insights reveal an expanded reaction cycle for inositol pyrophosphate hydrolysis by human DIPP1." *Faseb J* **35**(2): e21275.

Appendix 1

This manuscript is available on bioRxiv <https://doi.org/10.1101/2023.11.14.566975>. It includes most of the results described in chapter 3, as well as additional research completed by Alex Wegner, Florencia Casanova, Louisa Wirtz, and Ulrich Schaffrath.

Title: Plant pathogenic fungi hijack phosphate starvation signaling with conserved enzymatic effectors

Authors: Carl L. McCombe^{1†}, Alex Wegner^{2†}, Chenie S. Zamora³, Florencia Casanova², Shouvik Aditya¹, Julian R. Greenwood¹, Louisa Wirtz², Samuel de Paula³, Eleanor England¹, Sascha Shang¹, Daniel J. Ericsson⁴, Ely Oliveira-Garcia^{3*}, Simon J. Williams^{1*}, Ulrich Schaffrath^{2*}

Affiliations:

¹Research School of Biology, The Australian National University; Canberra, 2617, Australia.

²Department of Plant Physiology, RWTH Aachen University; Aachen, 52056, Germany.

³Department of Plant Pathology and Crop Physiology, Louisiana State University Agricultural Center; Baton Rouge, 70803, United States of America.

⁴ANSTO, Australian Synchrotron, Crystallography Beamline Group; Melbourne, 3168, Australia.

*Corresponding author. Email: schaffrath@bio3.rwth-aachen.de (U.S.); simon.williams@anu.edu.au (S.J.W.); EOliveiraGarcia@agcenter.lsu.edu (E.O.-G.)

† These authors contributed equally to this work.

Abstract: Phosphate availability modulates plant immune function and regulates interactions with beneficial, phosphate-providing, microbes. Here, we describe the hijacking of plant phosphate sensing by a family of Nudix hydrolase effectors from pathogenic *Magnaporthe oryzae* and *Colletotrichum* fungi. Structural and enzymatic analyses of the Nudix effector family demonstrate that they selectively hydrolyze inositol pyrophosphates, a molecule used by plants to monitor phosphate status and regulate starvation responses. In *M. oryzae*, gene deletion and complementation experiments reveal that the enzymatic activity of a Nudix effector significantly contributes to pathogen virulence. Further, we show that this conserved effector family induces phosphate starvation signaling in plants. Our study elucidates a molecular mechanism, utilized by multiple phytopathogenic fungi, that manipulates the highly conserved plant phosphate sensing pathway to exacerbate disease.

One-Sentence Summary: A family of conserved enzyme effectors from pathogenic fungi manipulate plant phosphate sensing to promote infection.

Main Text: Plant-microbe interactions range from beneficial to parasitic. Balancing the recruitment and support of symbiotic microbes, while maintaining the ability to defend against pathogens, is a major driver of plant evolution (1). The symbiosis between plants and arbuscular mycorrhizal fungi (AMF) predates the development of roots (2) and was likely instrumental in enabling land colonization by plants (3). Today, approximately 71% of vascular plants recruit AMF to access more phosphate and other mineral nutrients from the environment (4). In contrast to AMF, pathogenic fungi steal nutrients and constrain plant growth. Fungal diseases of important calorie crops threaten global food security by reducing crop yield (5). For example, *Magnaporthe oryzae* causes blast disease in major cereal crops including rice, wheat, and barley (6), resulting in annual food losses that could sustain hundreds of millions of people (7). Both symbiotic and pathogenic fungi secrete small proteins, called effectors, to optimize the host environment and support colonization.

Plant-AMF symbiosis is tightly regulated by the phosphate status of the plant (8). In eukaryotic cells, inositol pyrophosphates (PP-InsPs) signal phosphate availability through binding to SPX domains (9). When phosphate in plant cells is abundant, PP-InsP-bound SPX-domain proteins inhibit phosphate starvation response transcription factors (PHRs), thereby suppressing the expression of starvation induced genes (10-13). PHRs are conserved throughout land plants and green algae (14), and the regulation of plant-AMF symbiosis in both monocots and dicots is dependent on the PP-InsP/SPX/PHR signaling pathway (15-18). PHR activation also stimulates the expression of immune-suppressing genes and thereby inhibits the responsiveness of the plant immune system (19,20), indicating that plants prioritize symbiosis over defense during nutrient starvation. It is unknown whether any pathogenic fungi exploit the ancient and conserved phosphate-sensing pathway to promote plant infection. In this study, we demonstrate that a conserved family of Nudix (Nucleoside-diphosphate linked to moiety-X) hydrolase effectors secreted by pathogenic fungi hydrolyze PP-InsPs. This function mimics phosphate depletion and hijacks the plant PHR signaling pathway. Gene deletion and complementation of *M. oryzae* Nudix effectors indicate that PP-InsP hydrolysis is essential for full virulence of the pathogen.

A conserved Nudix hydrolase effector family promotes blast disease

Pathogenic *Magnaporthe* and *Colletotrichum* fungi possess effectors with putative Nudix hydrolase activity (Fig. 1A and table S1) (21). There are three predicted Nudix effector genes in *M. oryzae* (table S1) (22); two of these, named *MoNUDIX*, are identical in sequence and are highly upregulated during infection (23). To examine the role of Nudix effectors in cereal blast disease, we first utilized RNA interference (RNAi) to simultaneously lower the expression of both identical *MoNUDIX* genes (fig. S1, A and B). Silencing of *MoNUDIX* reduced blast disease symptoms in whole rice plant spray inoculation assays (fig. S1C). Furthermore, we report that silencing *MoNUDIX* enhances reactive oxygen species (ROS) accumulation, slows disease progression, and increases cell-wall autofluorescence (fig. S1, D to G). Collectively, the results indicate that *MoNUDIX* is important for *M. oryzae* virulence and host immune suppression. To corroborate the RNAi results and further characterize the Nudix effectors, we generated *MoNUDIX* deletion and complementation mutants in *M. oryzae* utilizing CRISPR/Cas9 genome editing (fig. S2). The

deletion of both identical *MoNUDIX* gene copies (*M. oryzae*^{ΔΔ*MoNUDIX*}) resulted in a drastic reduction in rice blast lesion size (Fig. 1, B and C). To assess whether the contribution of *MoNUDIX* to blast virulence was specific to rice infection, we also performed infection assays with barley and again observed significantly reduced lesion size with *M. oryzae*^{ΔΔ*MoNUDIX*} (Fig. 1, D and E). Our results were consistent across multiple rice and barley cultivars (Fig. 1, B and C, fig. S3, A and B), and microscopy analysis demonstrates a clear reduction in the growth of *M. oryzae*^{ΔΔ*MoNUDIX*} running hyphae during infection (fig. S3C). The two identical *MoNUDIX* genes likely function redundantly, as single deletion mutants exhibit only slight reductions in disease symptoms when compared to wild-type *M. oryzae* (fig. S4, A and B). *M. oryzae*^{ΔΔ*MoNUDIX*} displays normal vegetative growth, abiotic stress tolerance, conidia germination, appressorium formation, and infection following leaf wounding, which bypasses the requirement for an appressorium-mediated penetration (fig. S4, C to F). Collectively, our data indicate that *MoNUDIX* is important specifically for appressorium-mediated plant infection, this is consistent with the previously reported timing of Nudix effector gene induction during the late biotrophic growth stage of *M. oryzae*, *C. lenthis*, and *C. higginsianum* (21,23,24).

Nudix hydrolases possess a conserved sequence motif, GX₅EX₇REUXEEXGU, where U represents a hydrophobic amino acid and X is any amino acid (25). The first glutamate and arginine form a stabilizing salt bridge, while the remaining glutamates often bind divalent metal co-factors essential for enzymatic activity. To investigate the importance of *MoNUDIX* Nudix hydrolase activity, *M. oryzae*^{ΔΔ*MoNUDIX*} was complemented with either the wild-type effector, or effectors with various substitution mutations in the Nudix sequence motif. The expression of wild-type *MoNUDIX* successfully rescued the virulence of *M. oryzae*^{ΔΔ*MoNUDIX*}, whereas expression of the mutant effector genes did not (Fig. 1, D to F). These data demonstrate that the Nudix motif and therefore hydrolytic activity is essential for the promotion of blast disease by *MoNUDIX*.

***Magnaporthe* and *Colletotrichum* Nudix effectors are diphosphoinositol polyphosphate phosphohydrolases**

Nudix hydrolases typically hydrolyze pyrophosphate bonds in molecules with a nucleoside diphosphate. To characterize the enzymatic activity and substrate specificity of the Nudix effectors, we determined the crystal structure of *MoNUDIX*. Structural similarity searches revealed that *Homo sapiens* diphosphoinositol polyphosphate phosphohydrolase 1 (*HsDIPP1*) is remarkably similar to *MoNUDIX* in both overall structure and surface charge properties (Fig. 2A). *HsDIPP1*, a well-characterized Nudix hydrolase, hydrolyzes diadenosine polyphosphates (Ap_nAs) (26), the protective 5' mRNA cap (27), and PP-InsPs (28). Substrate screening with purified *MoNUDIX* protein demonstrated Nudix motif-dependent hydrolysis of 5-PP-InsP₅ (Fig. 2B), while no activity was detected with Ap_nAs, mRNA caps, or other common substrates of Nudix hydrolases (fig. S5, A and B). Our results demonstrate that *MoNUDIX* is a selective diphosphoinositol polyphosphate phosphohydrolase *in vitro*. To understand the mode of PP-InsP binding to *MoNUDIX*, we modelled 5-PP-InsP₅ into the *MoNUDIX* crystal structure via alignment with substrate bound *HsDIPP1* (29) (Fig. 2C). We identified basic amino acids likely required for PP-InsP binding (Fig. 2C); to confirm their involvement two lysines were mutated to glutamate

(MoNUDIX^{KKKE}). The MoNUDIX^{KKKE} protein demonstrated an approximately 70-fold reduction in inositol hexakisphosphate (InsP₆) binding affinity as measured by micro-scale thermophoresis (fig. S5C) and was unable to hydrolyze 5-PP-InsP₅ (Fig. 2D). The predicted PP-InsP binding site, including the basic amino acids, are conserved throughout the *Magnaporthe* and *Colletotrichum* Nudix effector family (Fig. 2, E and F), suggesting the conservation of substrate selectivity and enzymatic activity. To test this, we purified two homologs of MoNUDIX, one from *C. higginsianum* (ChNUDIX) and a second predicted *M. oryzae* Nudix effector (MoNUDIX2). Both ChNUDIX and MoNUDIX2 hydrolyze 5-PP-InsP₅ and this activity is dependent on a Nudix motif glutamate (Fig. 2G). Conversely, AvrM14, a sequence-unrelated mRNA decapping Nudix hydrolase effector from the fungus *Melampsora lini* (30), does not hydrolyze 5-PP-InsP₅ (fig S5D). All Nudix effectors used throughout this study were purified to homogeneity prior to *in vitro* characterization (fig. S6). Overall, structural analysis and enzymatic assays reveal that the *Magnaporthe* and *Colletotrichum* Nudix effectors are diphosphoinositol polyphosphate phosphohydrolases.

MoNUDIX localizes in the host cell cytoplasm during plant infection

Magnaporthe oryzae effectors can function within the host plant cell, or in the apoplastic space between the fungal cell wall and plant plasma membrane. The proteins involved in PP-InsP metabolism and signaling are intracellular. We therefore hypothesized that the Nudix effector family would function within the host plant cell during infection. We sought to identify the localization of MoNUDIX during plant infection using live-cell imaging techniques. First, we transformed *M. oryzae* with mRFP-tagged MoNUDIX controlled by the native promoter and determined that the effector co-localizes with the known cytoplasmic effector *MoPwl2* in the biotrophic interfacial complex (BIC) (Fig. 3A). Using the native promoter was required for BIC localization, constitutive expression of MoNUDIX resulted in localization throughout the fungal hyphae (fig. S7). The BIC is the site of cytoplasmic effector translocation from the fungus into the host cell (31, 32), therefore our data suggest that MoNUDIX is a cytoplasmic effector. Treatment with brefeldin A (BFA), a potent inhibitor of Golgi trafficking (33), prevents the secretion of apoplastic but not cytoplasmic *M. oryzae* effectors (32). We demonstrate that the BIC localization of MoNUDIX is not influenced by BFA treatment, further indicating that MoNUDIX functions as a cytoplasmic effector (Fig. 3B). For concentration of cytoplasmic fluorescence and verification of MoNUDIX localization in the host cell cytoplasm, we utilized a gentle plasmolysis procedure. The MoNUDIX:mRFP signal is clearly observed in the host plant cell protoplasts following treatment with KNO₃ (Fig. 3C). Overall, our results demonstrate that MoNUDIX localizes within the host cell cytoplasm during plant infection.

The Nudix effector family activates plant phosphate starvation responses

A reduction in intracellular PP-InsP concentration, as occurs when phosphate is limited, leads to the activation of PHRs and phosphate starvation responses (PSRs). The depletion of PP-InsPs due to hydrolysis by the Nudix effectors should mimic localized phosphate starvation (fig. S8A). To determine if the Nudix effectors activate PHRs and PSRs in plants, we transiently expressed MoNUDIX, ChNUDIX, and mutated proteins without enzymatic activity (MoNUDIX^{E79Q} and

ChNUDIX^{E78Q}) in *Nicotiana benthamiana*. We selected two phosphate starvation induced (PSI) genes, *NbSPX1* and *NbPECP1*, for gene expression analysis (34, 35). Both *NbSPX1* and *NbPECP1* have multiple PHR1-binding sequence (P1BS) elements in their promoter regions (fig. S8B). MoNUDIX and ChNUDIX significantly increased the abundance of *NbSPX1* and *NbPECP1* mRNA, when compared to MoNUDIX^{E79Q}, ChNUDIX^{E78Q}, and a no effector protein control (Fig. 4A). To investigate this further, we developed a rapid *in planta* screening method to monitor PHR activation. In our system, the RUBY reporter gene is controlled by a synthetic promoter with multiple P1BS elements, we named the promoter/reporter construct PSI:RUBY (fig. S8C). This system allowed us to screen six Nudix effector family members along with their corresponding Nudix motif mutants and other negative controls (nanoluciferase and AvrM14). We report that all six Nudix effectors significantly increase the expression of the RUBY reporter when compared to the corresponding Nudix motif mutant proteins and the negative controls (Fig. 4, B and C). Additionally, MoNUDIX^{KKEE} expression results in reduced RUBY expression when compared to wild-type MoNUDIX, consistent with the reduced InsP₆ binding and a lack of 5-PP-InsP₅ hydrolysis observed *in vitro* (Fig. 4, B and C). We also observe similar results when swapping the synthetic P1BS promoter with the 1 kb promoter region from *NbPECP1* (fig. S8, D and E). For all proteins, accumulation in *N. benthamiana* leaf tissue was detected via immunoblotting (fig. S8F). Collectively, our data demonstrate that the enzymatic activity of the Nudix effectors activates PHRs and PSI gene expression in *N. benthamiana*.

To determine if MoNUDIX induces PSRs during rice infection, we compared the mRNA levels of two PSI rice genes (*OsSPX1* and *OsIPS2*) in two different rice cultivars throughout the infection process with either wild-type *M. oryzae* or *M. oryzae* ^{ΔΔMoNUDIX}. At 72 hours post inoculation the expression of both *OsSPX1* and *OsIPS2* is significantly upregulated in rice infected with wild-type MoNUDIX when compared to *M. oryzae* ^{ΔΔMoNUDIX}, suggesting that MoNUDIX promotes the expression of PSI genes in rice (Fig. 4D).

In *A. thaliana*, phosphate starvation induces the expression of immunosuppressant rapid alkalinization factor (RALF) genes with P1BS elements in their promoter region (for example *AtRALF23*) (20, 36). This reduces reactive oxygen species (ROS) production triggered by immune elicitors (20, 36). Similarly, in *N. benthamiana* the enzymatic activity of the Nudix effectors induces the expression of an *AtRALF23* homolog (designated *NbRALF23*) and prevents the immune-activated ROS burst (Fig. 4, E and F). Overall, our results demonstrate that the diphosphoinositol polyphosphate phosphohydrolase effectors can activate phosphate starvation responses, which likely results in the suppression of plant immunity.

Discussion and conclusion

Phosphate is an essential but often limiting nutrient for plant growth, with phosphate-starved plants actively recruiting soil microbes to improve phosphate acquisition. Plant phosphate status is important for the regulation of multiple plant-microbe interactions (37-42). Here, we describe the molecular basis for phosphate status manipulation by pathogenic fungi. Our findings provide direct evidence for the hijacking of symbiosis-facilitating mechanisms by pathogenic fungi to promote disease.

The deletion of *MoNUDIX* genes in *M. oryzae* resulted in impaired plant colonization and fungal growth. The infection phenotype of *M. oryzae*^{ΔΔMoNUDIX} is analogous to phr2-mutant rice inoculated with AMF (17) and suggests that PHR-activation can enhance both beneficial and pathogenic infection in rice. Like AMF, *Colletotrichum tofieldiae* promotes host plant growth by providing phosphate under starvation conditions (38). We were unable to identify Nudix effectors in *C. tofieldiae*, and their absence may be required to ensure *C. tofieldiae* growth remains appropriately regulated by plant phosphate status. Conversely, multiple pathogenic *Colletotrichum* species have Nudix effectors that we demonstrate activate starvation responses. Three *C. higginsianum* Nudix effectors (two copies of *ChNUDIX*, one copy of *ChNUDIX2*) are clustered together on a mini-chromosome (chromosome 11) and are highly upregulated early in plant infection (24). Similar to *M. oryzae*^{ΔΔMoNUDIX}, *C. higginsianum* mutants lacking chromosome 11 display normal vegetative growth and can successfully penetrate host plant cells but demonstrate inhibited disease progression (43). There are only 8 predicted effector genes on chromosome 11 (44), and therefore it is likely that Nudix effectors are also important for the pathogenicity of *C. higginsianum*.

In addition to their central role in phosphate homeostasis, PP-InsPs are co-factors for the receptors sensing the phytohormones auxin and jasmonate (45-48). Phosphate status and jasmonate signaling are intricately linked in plants. For example, jasmonate treatment stimulates PP-InsP synthesis (49), and PHR-activation enhances jasmonate production and signaling (50, 51). By manipulating intracellular PP-InsP levels, the Nudix effectors may influence jasmonate and auxin signaling in their host plants in addition to inducing starvation responses.

Based on our data, we propose the following model describing the function of the *Magnaporthe* and *Colletotrichum* Nudix hydrolase effector family (Fig. 5). First, the effectors are translocated into their respective host plant cells. Once inside, they function as PP-InsP hydrolase enzymes, effectively uncoupling PHR activation from intracellular phosphate availability. This induces a plethora of transcriptional changes to promote phosphate acquisition and suppress immune responses, ultimately promoting disease.

References and Notes

1. P. M. Delaux, S. Schornack, Plant evolution driven by interactions with symbiotic and pathogenic microbes. *Science* **371**, 934-939 (2021).
2. M. C. Brundrett, Coevolution of roots and mycorrhizas of land plants. *New Phytol.* **154**, 275-304 (2002).
3. M. Parniske, Arbuscular mycorrhiza: the mother of plant root endosymbioses. *Nat. Rev. Microbiol.* **6**, 763-775 (2008).
4. M. C. Brundrett, L. Tedersoo, Evolutionary history of mycorrhizal symbioses and global host plant diversity. *New Phytol.* **220**, 1108-1115 (2018).
5. E. Stukenbrock, S. Gurr, Address the growing urgency of fungal disease in crops. *Nature* **617**, 31-34 (2023).
6. N. J. Talbot, On the trail of a cereal killer: Exploring the biology of Magnaporthe grisea. *Annu Rev Microbiol.* **57**, 177-202 (2003).
7. M. C. Fisher, D. A. Henk, C. J. Briggs, J. S. Brownstein, L. C. Madoff, S. L. McCraw, S. J. Gurr, Emerging fungal threats to animal, plant and ecosystem health. *Nature* **484**, 186-194 (2012).
8. L. M. Müller, M. J. Harrison, Phytohormones, miRNAs, and peptide signals integrate plant phosphorus status with arbuscular mycorrhizal symbiosis. *Curr. Opin. Plant Biol.* **50**, 132-139 (2019).
9. R. Wild, R. Gerasimaite, J.-Y. Jung, V. Truffault, I. Pavlovic, A. Schmidt, A. Saiardi, H. J. Jessen, Y. Poirier, M. Hothorn, A. Mayer, Control of eukaryotic phosphate homeostasis by inositol polyphosphate sensor domains. *Science* **352**, 986-990 (2016).
10. M. K. Ried, R. Wild, J. Zhu, J. Pipercevic, K. Sturm, L. Broger, R. K. Harmel, L. A. Abriata, L. A. Hothorn, D. Fiedler, S. Hiller, M. Hothorn, Inositol pyrophosphates promote the interaction of SPX domains with the coiled-coil motif of PHR transcription factors to regulate plant phosphate homeostasis. *Nat. Commun.* **12**, 384 (2021).
11. Z. Guan, Q. Zhang, Z. Zhang, J. Zuo, J. Chen, R. Liu, J. Savarin, L. Broger, P. Cheng, Q. Wang, K. Pei, D. Zhang, T. Zou, J. Yan, P. Yin, M. Hothorn, Z. Liu, Mechanistic insights into the regulation of plant phosphate homeostasis by the rice SPX2 - PHR2 complex. *Nat. Commun.* **13**, 1581 (2022).
12. J. Dong, G. Ma, L. Sui, M. Wei, V. Satheesh, R. Zhang, S. Ge, J. Li, T. E. Zhang, C. Wittwer, H. J. Jessen, H. Zhang, G. Y. An, D. Y. Chao, D. Liu, M. Lei, Inositol Pyrophosphate InsP₈ Acts as an Intracellular Phosphate Signal in Arabidopsis. *Mol. Plant* **12**, 1463-1473 (2019).
13. J. Zhu, K. Lau, R. Puschmann, R. K. Harmel, Y. Zhang, V. Pries, P. Gaugler, L. Broger, A. K. Dutta, H. J. Jessen, G. Schaaf, A. R. Fernie, L. A. Hothorn, D. Fiedler, M. Hothorn, Two bifunctional inositol pyrophosphate kinases/phosphatases control plant phosphate homeostasis. *eLife* **8**, e43582 (2019).
14. V. Rubio, F. Linhares, R. Solano, A. C. Martín, J. Iglesias, A. Leyva, J. Paz-Ares, A conserved MYB transcription factor involved in phosphate starvation signaling both in vascular plants and in unicellular algae. *Genes Dev.* **15**, 2122-2133 (2001).
15. P. Wang, R. Snijders, W. Kohlen, J. Liu, T. Bisseling, E. Limpens, Medicago SPX1 and SPX3 regulate phosphate homeostasis, mycorrhizal colonization, and arbuscule degradation. *Plant Cell* **33**, 3470-3486 (2021).
16. D. Liao, C. Sun, H. Liang, Y. Wang, X. Bian, C. Dong, X. Niu, M. Yang, G. Xu, A. Chen, S. Wu, S1SPX1-S1PHR complexes mediate the suppression of arbuscular mycorrhizal symbiosis by phosphate repletion in tomato. *Plant Cell* **34**, 4045-4065 (2022).
17. D. Das, M. Paries, K. Hobbecker, M. Gigl, C. Dawid, H. M. Lam, J. Zhang, M. Chen, C. Gutjahr, PHOSPHATE STARVATION RESPONSE transcription factors enable arbuscular mycorrhiza symbiosis. *Nat. Commun.* **13**, 477 (2022).
18. J. Shi, B. Zhao, S. Zheng, X. Zhang, X. Wang, W. Dong, Q. Xie, G. Wang, Y. Xiao, F. Chen, N. Yu, E. Wang, A phosphate starvation response-centered network regulates mycorrhizal symbiosis. *Cell* **184**, 5527-5540 e5518 (2021).
19. G. Castrillo, P. J. Teixeira, S. H. Paredes, T. F. Law, L. de Lorenzo, M. E. Feltcher, O. M. Finkel, N. W. Breakfield, P. Mieczkowski, C. D. Jones, J. Paz-Ares, J. L. Dangl, Root microbiota drive direct integration of phosphate stress and immunity. *Nature* **543**, 513-518 (2017).
20. J. Tang, D. Wu, X. Li, L. Wang, L. Xu, Y. Zhang, F. Xu, H. Liu, Q. Xie, S. Dai, D. Coleman-Derr, S. Zhu, F. Yu, Plant immunity suppression via PHR1-RALF-FERONIA shapes the root microbiome to alleviate phosphate starvation. *EMBO J.* **41**, e109102 (2022).
21. V. Bhadauria, S. Banniza, A. Vandenberg, G. Selvaraj, Y. Wei, Overexpression of a novel biotrophy-specific *Colletotrichum truncatum* effector, CtNUDIX, in hemibiotrophic fungal phytopathogens causes incompatibility with their host plants. *Eukaryot Cell* **12**, 2-11 (2013).

22. R. A. Dean, N. J. Talbot, D. J. Ebbole, M. L. Farman, T. K. Mitchell, M. J. Orbach, M. Thon, R. Kulkarni, J. R. Xu, H. Pan, N. D. Read, Y. H. Lee, I. Carbone, D. Brown, Y. Y. Oh, N. Donofrio, J. S. Jeong, D. M. Soanes, S. Djonovic, E. Kolomiets, C. Rehmeyer, W. Li, M. Harding, S. Kim, M. H. Lebrun, H. Bohnert, S. Coughlan, J. Butler, S. Calvo, L. J. Ma, R. Nicol, S. Purcell, C. Nusbaum, J. E. Galagan, B. W. Birren, The genome sequence of the rice blast fungus *Magnaporthe grisea*. *Nature* **434**, 980-986 (2005).
23. X. Yan, B. Tang, L. S. Ryder, D. MacLean, V. M. Were, A. B. Eseola, N. Cruz-Mireles, W. Ma, A. J. Foster, M. Osés-Ruiz, N. J. Talbot, The transcriptional landscape of plant infection by the rice blast fungus *Magnaporthe oryzae* reveals distinct families of temporally co-regulated and structurally conserved effectors. *Plant Cell* **35**, 1360-1385 (2023).
24. R. J. O'Connell, M. R. Thon, S. Hacquard, S. G. Amyotte, J. Kleemann, M. F. Torres, U. Damm, E. A. Buiate, L. Epstein, N. Alkan, J. Altmüller, L. Alvarado-Balderrama, C. A. Bauser, C. Becker, B. W. Birren, Z. Chen, J. Choi, J. A. Crouch, J. P. Duvick, M. A. Farman, P. Gan, D. Heiman, B. Henrissat, R. J. Howard, M. Kabbage, C. Koch, B. Kracher, Y. Kubo, A. D. Law, M. H. Lebrun, Y. H. Lee, I. Miyara, N. Moore, U. Neumann, K. Nordström, D. G. Panaccione, R. Panstruga, M. Place, R. H. Proctor, D. Prusky, G. Rech, R. Reinhardt, J. A. Rollins, S. Rounseley, C. L. Schardl, D. C. Schwartz, N. Shenoy, K. Shirasu, U. R. Sikhhakolli, K. Stüber, S. A. Sukno, J. A. Sweigard, Y. Takano, H. Takahara, F. Trail, H. C. van der Does, L. M. Voll, I. Will, S. Young, Q. Zeng, J. Zhang, S. Zhou, M. B. Dickman, P. Schulze-Lefert, E. Ver Loren van Themaat, L. J. Ma, L. J. Vaillancourt, Lifestyle transitions in plant pathogenic *Colletotrichum* fungi deciphered by genome and transcriptome analyses. *Nat Genet* **44**, 1060-1065 (2012).
25. A. G. McLennan, The Nudix hydrolase superfamily. *Cell. Mol. Life Sci.* **63**, 123-143 (2006).
26. S. T. Safrany, S. W. Ingram, J. L. Cartwright, J. R. Falck, A. G. McLennan, L. D. Barnes, S. B. Shears, The diadenosine hexaphosphate hydrolases from *Schizosaccharomyces pombe* and *Saccharomyces cerevisiae* are homologues of the human diphosphoinositol polyphosphate phosphohydrolase: overlapping substrate specificities in a MutT-type protein. *J. Biol. Chem.* **274**, 21735-21740 (1999).
27. E. Grudzien-Nogalska, X. Jiao, M. G. Song, R. P. Hart, M. Kiledjian, Nudt3 is an mRNA decapping enzyme that modulates cell migration. *RNA* **22**, 773-781 (2016).
28. S. T. Safrany, J. J. Caffrey, X. Yang, M. E. Bembeneck, M. B. Moyer, W. A. Burkhardt, S. B. Shears, A novel context for the 'MutT' module, a guardian of cell integrity, in a diphosphoinositol polyphosphate phosphohydrolase. *EMBO J.* **17**, 6599-6607 (1998).
29. G. Zong, N. Jork, S. Hostachy, D. Fiedler, H. J. Jessen, S. B. Shears, H. Wang, New structural insights reveal an expanded reaction cycle for inositol pyrophosphate hydrolysis by human DIPP1. *FASEB J.* **35**, e21275 (2021).
30. C. L. McCombe, A. M. Catanzariti, J. R. Greenwood, A. M. Desai, M. A. Outram, D. S. Yu, D. J. Ericsson, S. E. Brenner, P. N. Dodds, B. Kobe, D. A. Jones, S. J. Williams, A rust-fungus Nudix hydrolase effector decaps mRNA *in vitro* and interferes with plant immune pathways. *New Phytol.* **239**, 222-239 (2023).
31. C. H. Khang, R. Berruyer, M. C. Giraldo, P. Kankanala, S. Y. Park, K. Czymmek, S. Kang, B. Valent, Translocation of *Magnaporthe oryzae* effectors into rice cells and their subsequent cell-to-cell movement. *Plant Cell* **22**, 1388-1403 (2010).
32. M. C. Giraldo, Y. F. Dagdas, Y. K. Gupta, T. A. Mentlak, M. Yi, A. L. Martinez-Rocha, H. Saitoh, R. Terauchi, N. J. Talbot, B. Valent, Two distinct secretion systems facilitate tissue invasion by the rice blast fungus *Magnaporthe oryzae*. *Nat. Commun.* **4**, 1996 (2013).
33. P. Chardin, F. McCormick, Brefeldin A: the advantage of being uncompetitive. *Cell* **97**, 153-155 (1999).
34. K. Duan, K. Yi, L. Dang, H. Huang, W. Wu, P. Wu, Characterization of a sub-family of *Arabidopsis* genes with the SPX domain reveals their diverse functions in plant tolerance to phosphorus starvation. *Plant J.* **54**, 965-975 (2008).
35. A. E. Angkawijaya, Y. Nakamura, *Arabidopsis* PECP1 and PS2 are phosphate starvation-inducible phosphocholine phosphatases. *Biochem. Biophys. Res. Commun.* **494**, 397-401 (2017).
36. M. Stegmann, J. Monaghan, E. Smakowska-Luzan, H. Rovenich, A. Lehner, N. Holton, Y. Belkhadir, C. Zipfel, The receptor kinase FER is a RALF-regulated scaffold controlling plant immune signaling. *Science* **355**, 287-289 (2017).
37. M. Paries, C. Gutjahr, The good, the bad, and the phosphate: regulation of beneficial and detrimental plant-microbe interactions by the plant phosphate status. *New Phytol.* **239**, 29-46 (2023).
38. K. Hiruma, N. Gerlach, S. Sacristán, R. T. Nakano, S. Hacquard, B. Kracher, U. Neumann, D. Ramírez, M. Bucher, R. J. O'Connell, P. Schulze-Lefert, Root Endophyte *Colletotrichum tofieldiae* Confers Plant Fitness Benefits that Are Phosphate Status Dependent. *Cell* **165**, 464-474 (2016).
39. S. Hacquard, B. Kracher, K. Hiruma, P. C. Münch, R. Garrido-Oter, M. R. Thon, A. Weimann, U. Damm, J. F. Dallery, M. Hainaut, B. Henrissat, O. Lespinet, S. Sacristán, E. Ver Loren van Themaat, E. Kemen, A.

- C. McHardy, P. Schulze-Lefert, R. J. O'Connell, Survival trade-offs in plant roots during colonization by closely related beneficial and pathogenic fungi. *Nat. Commun.* **7**, 11362 (2016).
40. I. Fabiańska, N. Gerlach, J. Almario, M. Bucher, Plant-mediated effects of soil phosphorus on the root-associated fungal microbiota in *Arabidopsis thaliana*. *New Phytol.* **221**, 2123-2137 (2019).
 41. O. M. Finkel, I. Salas-González, G. Castrillo, S. Spaepen, T. F. Law, P. Teixeira, C. D. Jones, J. L. Dangl, The effects of soil phosphorus content on plant microbiota are driven by the plant phosphate starvation response. *PLoS Biol.* **17**, e3000534 (2019).
 42. R. J. Morcillo, S. K. Singh, D. He, G. An, J. I. Vílchez, K. Tang, F. Yuan, Y. Sun, C. Shao, S. Zhang, Y. Yang, X. Liu, Y. Dang, W. Wang, J. Gao, W. Huang, M. Lei, C. P. Song, J. K. Zhu, A. P. Macho, P. W. Paré, H. Zhang, Rhizobacterium-derived diacetlyl modulates plant immunity in a phosphate-dependent manner. *EMBO J.* **39**, e102602 (2020).
 43. P. L. Plaumann, J. Schmidpeter, M. Dahl, L. Taher, C. Koch, A Dispensable Chromosome Is Required for Virulence in the Hemibiotrophic Plant Pathogen *Colletotrichum higginsianum*. *Front Microbiol* **9**, 1005 (2018).
 44. J. F. Dallery, N. Lapalu, A. Zampounis, S. Pigné, I. Luyten, J. Amselem, A. H. J. Wittenberg, S. Zhou, M. V. de Queiroz, G. P. Robin, A. Auger, M. Hainaut, B. Henrissat, K. T. Kim, Y. H. Lee, O. Lespinet, D. C. Schwartz, M. R. Thon, R. J. O'Connell, Gapless genome assembly of *Colletotrichum higginsianum* reveals chromosome structure and association of transposable elements with secondary metabolite gene clusters. *BMC Genomics* **18**, 667 (2017).
 45. L. B. Sheard, X. Tan, H. Mao, J. Withers, G. Ben-Nissan, T. R. Hinds, Y. Kobayashi, F. F. Hsu, M. Sharon, J. Browse, S. Y. He, J. Rizo, G. A. Howe, N. Zheng, Jasmonate perception by inositol-phosphate-potentiated COI1-JAZ co-receptor. *Nature* **468**, 400-405 (2010).
 46. D. Laha, N. Parvin, M. Dynowski, P. Johnen, H. Mao, S. T. Bitters, N. Zheng, G. Schaaf, Inositol Polyphosphate Binding Specificity of the Jasmonate Receptor Complex. *Plant Physiol.* **171**, 2364-2370 (2016).
 47. X. Tan, L. I. Calderon-Villalobos, M. Sharon, C. Zheng, C. V. Robinson, M. Estelle, N. Zheng, Mechanism of auxin perception by the TIR1 ubiquitin ligase. *Nature* **446**, 640-645 (2007).
 48. N. P. Laha, R. F. H. Giehl, E. Riemer, D. Qiu, N. J. Pullagurla, R. Schneider, Y. W. Dhir, R. Yadav, Y. E. Mihiret, P. Gaugler, V. Gaugler, H. Mao, N. Zheng, N. von Wirén, A. Saiardi, S. Bhattacharjee, H. J. Jessen, D. Laha, G. Schaaf, INOSITOL (1,3,4) TRIPHOSPHATE 5/6 KINASE1-dependent inositol polyphosphates regulate auxin responses in *Arabidopsis*. *Plant Physiol.* **190**, 2722-2738 (2022).
 49. D. Laha, P. Johnen, C. Azevedo, M. Dynowski, M. Weiß, S. Capolicchio, H. Mao, T. Iven, M. Steenbergen, M. Freyer, P. Gaugler, M. K. de Campos, N. Zheng, I. Feussner, H. J. Jessen, S. C. Van Wees, A. Saiardi, G. Schaaf, VIH2 Regulates the Synthesis of Inositol Pyrophosphate InsP8 and Jasmonate-Dependent Defenses in *Arabidopsis*. *Plant Cell* **27**, 1082-1097 (2015).
 50. G. A. Khan, E. Vogiatzaki, G. Glauser, Y. Poirier, Phosphate Deficiency Induces the Jasmonate Pathway and Enhances Resistance to Insect Herbivory. *Plant Physiol.* **171**, 632-644 (2016).
 51. K. He, J. Du, X. Han, H. Li, M. Kui, J. Zhang, Z. Huang, Q. Fu, Y. Jiang, Y. Hu, PHOSPHATE STARVATION RESPONSE1 (PHR1) interacts with JASMONATE ZIM-DOMAIN (JAZ) and MYC2 to modulate phosphate deficiency-induced jasmonate signaling in *Arabidopsis*. *Plant Cell* **35**, 2132-2156 (2023).
 52. E. Oliveira-Garcia, T. M. Tamang, J. Park, M. Dalby, M. Martin-Urdiroz, C. Rodriguez Herrero, A. H. Vu, S. Park, N. J. Talbot, B. Valent, Clathrin-mediated endocytosis facilitates the internalization of Magnaporthe oryzae effectors into rice cells. *Plant Cell* **35**, 2527-2551 (2023).
 53. A. Wegner, F. Casanova, M. Loehrer, A. Jordine, S. Bohnert, X. Liu, Z. Zhang, U. Schaffrath, Gene deletion and constitutive expression of the pectate lyase gene 1 (MoPL1) lead to diminished virulence of Magnaporthe oryzae. *J. Microbiol.* **60**, 79-88 (2022).
 54. F. Teufel, J. J. Almagro Armenteros, A. R. Johansen, M. H. Gíslason, S. I. Pihl, K. D. Tsirigos, O. Winther, S. Brunak, G. von Heijne, H. Nielsen, SignalP 6.0 predicts all five types of signal peptides using protein language models. *Nat. Biotechnol.* **40**, 1023-1025 (2022).
 55. A. R. Bentham, M. Youles, M. N. Mendel, F. A. Varden, J. C. D. I. Concepcion, M. J. Banfield, pOPIN-GG: A resource for modular assembly in protein expression vectors. *bioRxiv*, 2021.2008.2010.455798 [Preprint] (2021). <https://doi.org/10.1101/2021.08.10.455798>.
 56. E. Weber, C. Engler, R. Gruetzner, S. Werner, S. Marillonnet, A modular cloning system for standardized assembly of multigene constructs. *PLoS One* **6**, e16765 (2011).
 57. F. W. Studier, Protein production by auto-induction in high density shaking cultures. *Protein Expr. Purif.* **41**, 207-234 (2005).

58. E. W. Sayers, E. E. Bolton, J. R. Brister, K. Canese, J. Chan, D. C. Comeau, C. M. Farrell, M. Feldgarden, A. M. Fine, K. Funk, E. Hatcher, S. Kannan, C. Kelly, S. Kim, W. Klimke, M. J. Landrum, S. Lathrop, Z. Lu, T. L. Madden, A. Malheiro, A. Marchler-Bauer, T. D. Murphy, L. Phan, S. Pujar, S. H. Rangwala, V. A. Schneider, T. Tse, J. Wang, J. Ye, B. W. Trawick, K. D. Pruitt, S. T. Sherry, Database resources of the national center for biotechnology information in 2023. *Nucleic Acids Res.* **51**, D29-D38 (2023).
59. M. Blum, H. Y. Chang, S. Chuguransky, T. Grego, S. Kandasamy, A. Mitchell, G. Nuka, T. Paysan-Lafosse, M. Qureshi, S. Raj, L. Richardson, G. A. Salazar, L. Williams, P. Bork, A. Bridge, J. Gough, D. H. Haft, I. Letunic, A. Marchler-Bauer, H. Mi, D. A. Natale, M. Necci, C. A. Orengo, A. P. Pandurangan, C. Rivoire, C. J. A. Sigrist, I. Sillitoe, N. Thanki, P. D. Thomas, S. C. E. Tosatto, C. H. Wu, A. Bateman, R. D. Finn, The InterPro protein families and domains database: 20 years on. *Nucleic Acids Res.* **49**, D344-D354 (2021).
60. S. Guindon, J. F. Dufayard, V. Lefort, M. Anisimova, W. Hordijk, O. Gascuel, New algorithms and methods to estimate maximum-likelihood phylogenies: assessing the performance of PhyML 3.0. *Syst. Biol.* **59**, 307-321 (2010).
61. I. Letunic, P. Bork, Interactive Tree Of Life (iTOL) v5: an online tool for phylogenetic tree display and annotation. *Nucleic Acids Res.* **49**, W293-W296 (2021).
62. A. Heese, D. R. Hann, S. Gimenez-Ibanez, A. M. E. Jones, K. He, J. Li, J. I. Schroeder, S. C. Peck, J. P. Rathjen, The receptor-like kinase SERK3/BAK1 is a central regulator of innate immunity in plants. *Proc. Natl. Acad. Sci. U S A* **104**, 12217-12222 (2007).
63. R. Puschmann, R. K. Harmel, D. Fiedler, Scalable Chemoenzymatic Synthesis of Inositol Pyrophosphates. *Biochemistry* **58**, 3927-3932 (2019).
64. O. Loss, C. Azevedo, Z. Szijgyarto, D. Bosch, A. Saiardi, Preparation of quality inositol pyrophosphates. *JoVE* **55**, e3027 (2011).
65. D. Aragão, J. Aishima, H. Cherukuvada, R. Clarken, M. Clift, N. P. Cowieson, D. J. Ericsson, C. L. Gee, S. Macedo, N. Mudie, MX2: a high-flux undulator microfocus beamline serving both the chemical and macromolecular crystallography communities at the Australian Synchrotron. *Journal of synchrotron radiation* **25**, 885-891 (2018).
66. W. Kabsch, XDS. *Acta Crystallogr. D Biol. Crystallogr.* **66**, 125-132 (2010).
67. P. R. Evans, G. N. Murshudov, How good are my data and what is the resolution? *Acta Crystallogr. D Biol. Crystallogr.* **69**, 1204-1214 (2013).
68. D. Liebschner, P. V. Afonine, M. L. Baker, G. Bunkóczki, V. B. Chen, T. I. Croll, B. Hintze, L.-W. Hung, S. Jain, A. J. McCoy, Macromolecular structure determination using X-rays, neutrons and electrons: recent developments in Phenix. *Acta Crystallogr. D Struct. Biol.* **75**, 861-877 (2019).
69. J. Jumper, R. Evans, A. Pritzel, T. Green, M. Figurnov, O. Ronneberger, K. Tunyasuvunakool, R. Bates, A. Žídek, A. Potapenko, A. Bridgland, C. Meyer, S. A. A. Kohl, A. J. Ballard, A. Cowie, B. Romera-Paredes, S. Nikolov, R. Jain, J. Adler, T. Back, S. Petersen, D. Reiman, E. Clancy, M. Zielinski, M. Steinegger, M. Pacholska, T. Berghammer, S. Bodenstein, D. Silver, O. Vinyals, A. W. Senior, K. Kavukcuoglu, P. Kohli, D. Hassabis, Highly accurate protein structure prediction with AlphaFold. *Nature* **596**, 583-589 (2021).
70. T. C. Terwilliger, R. W. Grosse-Kunstleve, P. V. Afonine, N. W. Moriarty, P. H. Zwart, L.-W. Hung, R. J. Read, P. D. Adams, Iterative model building, structure refinement and density modification with the PHENIX AutoBuild wizard. *Acta Crystallogr. D Biol. Crystallogr.* **64**, 61-69 (2008).
71. A. Casanál, B. Lohkamp, P. Emsley, Current developments in Coot for macromolecular model building of Electron Cryo-microscopy and Crystallographic Data. *Protein Sci.* **29**, 1069-1078 (2020).
72. P. V. Afonine, R. W. Grosse-Kunstleve, N. Echols, J. J. Headd, N. W. Moriarty, M. Mustyakimov, T. C. Terwilliger, A. Urzhumtsev, P. H. Zwart, P. D. Adams, Towards automated crystallographic structure refinement with phenix. refine. *Acta Crystallogr. D Biol. Crystallogr.* **68**, 352-367 (2012).
73. E. F. Pettersen, T. D. Goddard, C. C. Huang, E. C. Meng, G. S. Couch, T. I. Croll, J. H. Morris, T. E. Ferrin, UCSF ChimeraX: Structure visualization for researchers, educators, and developers. *Protein Sci.* **30**, 70-82 (2021).
74. B. Yariv, E. Yariv, A. Kessel, G. Maserati, A. B. Chorin, E. Martz, I. Mayrose, T. Pupko, N. Ben-Tal, Using evolutionary data to make sense of macromolecules with a "face-lifted" ConSurf. *Protein Sci.* **32**, e4582 (2023).
75. J. Vandesompele, K. De Preter, F. Pattyn, B. Poppe, N. Van Roy, A. De Paepe, F. Speleman, Accurate normalization of real-time quantitative RT-PCR data by geometric averaging of multiple internal control genes. *Genome Biol.* **3**, research0034 (2002).

76. M. A. Pombo, R. N. Ramos, Y. Zheng, Z. Fei, G. B. Martin, H. G. Rosli, Transcriptome-based identification and validation of reference genes for plant-bacteria interaction studies using *Nicotiana benthamiana*. *Sci. Rep.* **9**, 1632 (2019).
77. J. Chen, M. Luo, P. Hands, V. Rolland, J. Zhang, Z. Li, M. Outram, P. Dodds, M. Ayliffe, A split GAL4 RUBY assay for visual in planta detection of protein-protein interactions. *Plant J.* **114**, 1209-1226 (2023).
78. D. Janus, B. Hoff, E. Hofmann, U. Kück, An efficient fungal RNA-silencing system using the DsRed reporter gene. *Appl. Environ. Microbiol.* **73**, 962-970 (2007).
79. P. Kankanala, K. Czymmek, B. Valent, Roles for rice membrane dynamics and plasmodesmata during biotrophic invasion by the blast fungus. *Plant Cell* **19**, 706-724 (2007).
80. S. Che Omar, M. A. Bentley, G. Morieri, G. M. Preston, S. J. Gurr, Validation of Reference Genes for Robust qRT-PCR Gene Expression Analysis in the Rice Blast Fungus *Magnaporthe oryzae*. *PLoS One* **11**, e0160637 (2016).
81. S. L. Ding, W. Liu, A. Iliuk, C. Ribot, J. Vallet, A. Tao, Y. Wang, M. H. Lebrun, J. R. Xu, The tig1 histone deacetylase complex regulates infectious growth in the rice blast fungus *Magnaporthe oryzae*. *Plant Cell* **22**, 2495-2508 (2010).
82. E. Oliveira-Garcia, B. Valent, Characterizing the Secretion Systems of *Magnaporthe oryzae*. *Methods Mol Biol* **2356**, 69-77 (2021).
83. X. L. Chen, T. Shi, J. Yang, W. Shi, X. Gao, D. Chen, X. Xu, J. R. Xu, N. J. Talbot, Y. L. Peng, N-glycosylation of effector proteins by an α -1,3-mannosyltransferase is required for the rice blast fungus to evade host innate immunity. *Plant Cell* **26**, 1360-1376 (2014).
84. A. Wegner, L. Wirtz, T. Leisen, M. Hahn, U. Schaffrath, Fenhexamid - an efficient and inexpensive fungicide for selection of *Magnaporthe oryzae* transformants. *European Journal of Plant Pathology* **162**, 697-707 (2022).
85. T. Leisen, F. Bietz, J. Werner, A. Wegner, U. Schaffrath, D. Scheuring, F. Willmund, A. Mosbach, G. Scalliet, M. Hahn, CRISPR/Cas with ribonucleoprotein complexes and transiently selected telomere vectors allows highly efficient marker-free and multiple genome editing in *Botrytis cinerea*. *PLoS Pathog* **16**, e1008326 (2020).
86. A. J. Foster, M. Martin-Urdiroz, X. Yan, H. S. Wright, D. M. Soanes, N. J. Talbot, CRISPR-Cas9 ribonucleoprotein-mediated co-editing and counterselection in the rice blast fungus. *Scientific Reports* **8**, 14355 (2018).
87. P. Virtanen, R. Gommers, T. E. Oliphant, M. Haberland, T. Reddy, D. Cournapeau, E. Burovski, P. Peterson, W. Weckesser, J. Bright, S. J. van der Walt, M. Brett, J. Wilson, K. J. Millman, N. Mayorov, A. R. J. Nelson, E. Jones, R. Kern, E. Larson, C. J. Carey, İ. Polat, Y. Feng, E. W. Moore, J. VanderPlas, D. Laxalde, J. Perktold, R. Cimrman, I. Henriksen, E. A. Quintero, C. R. Harris, A. M. Archibald, A. H. Ribeiro, F. Pedregosa, P. van Mulbregt, SciPy 1.0: fundamental algorithms for scientific computing in Python. *Nat Methods* **17**, 261-272 (2020).
88. M.-G. Song, Y. Li, M. Kiledjian, Multiple mRNA decapping enzymes in mammalian cells. *Molecular cell* **40**, 423-432 (2010).

Acknowledgments: We thank the Plant Services Team at the Australian National University for providing *N. benthamiana* seedlings, and all the Williams lab members for helpful discussion. The authors acknowledge the use of the ANU crystallization facility. The authors also acknowledge the use of the Australian Synchrotron MX facility and thank the staff for their support. This research was undertaken in part using the MX2 beamline at the Australian Synchrotron, part of ANSTO, and made use of the Australian Cancer Research Foundation (ACRF) detector. Fig. 5 and S8A were created with BioRender.com.

Funding:

Australian Institute of Nuclear Science and Engineering Ltd. Postgraduate Research Award (CLM)

Australian Government Research Training Programme Stipend (CLM)

ANU Future Scheme 35665 (SJW)

ARC Future Fellowship FT200100135 (SJW)

Louisiana Board of Regents grant #LEQSF (2022-24)-RD-A-01 (EOG)

RWTH Aachen University scholarships for Doctoral Students (AW, FC, LW)

Funded by the Deutsche Forschungsgemeinschaft (DFG, German Research Foundation) – 410278620 (US, AW)

Author contributions:

Conceptualization: CLM, AW, SJW, US

Methodology: CLM, AW, SA, JRG, EOG, SJW, US

Investigation: CLM, AW, CSZ, FC, SA, JRG, LW, SdP, EE, SS, EOG

Formal Analysis: CLM, AW, CSZ, FC, SA, DJE, EOG, SJW

Visualization: CLM, AW, CSZ, FC, SA, EOG

Funding acquisition: EOG, SJW, US

Project administration: CLM, AW, SJW, US

Supervision: CLM, AW, EOG, SJW, US

Writing – original draft: CLM, AW

Writing – review & editing: CLM, AW, FC, SA, JRG, LW, SS, EE, DJE, EOG, SJW, US

Competing interests: Authors declare that they have no competing interests.

Data and materials availability: Where possible all materials generated in this study will be made available upon request to the corresponding authors. The data that support the MoNUDIX protein structure described in this study are openly available under accession 8SXS at the PDB. All other data are available in the main text or supplementary materials.

Supplementary Materials

Materials and Methods

Figs. S1 to S8

Tables S1 to S6

References (52–88)

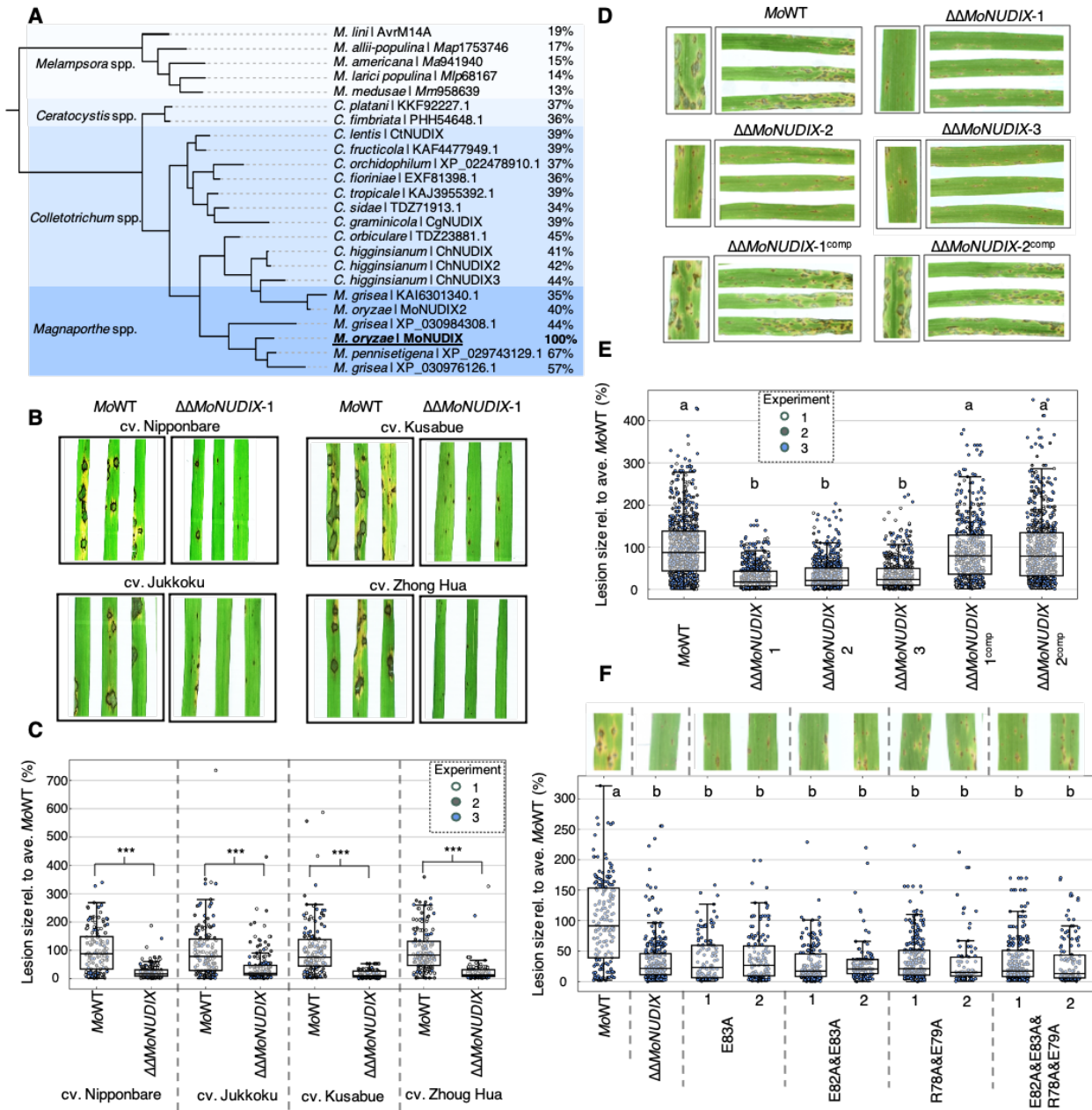


Fig. 1. MoNUDIX is important for *Magnaporthe oryzae* virulence on rice and barley.
(A) A phylogeny indicating the evolutionary relationships between Nudix hydrolase effectors from pathogenic fungi, the percentage value indicates amino acid sequence identity with MoNUDIX.
(B) Rice cultivars Nipponbare, Jukkoku, Kusabue and Zhong Hua were spray inoculated with *M. oryzae* isolate Guy11 (*MoWT*) and *MoNUDIX* double gene deletion mutant $\Delta\Delta\text{MoNUDIX-1}$. Leaves were photographed six days post inoculation (dpi). **(C)** Boxplots summarize the results of three independent experiments, with the size of approximately 50 lesions measured across 5 rice leaves per treatment. Asterisks indicate treatments on the same cultivar with significantly different lesion sizes (Mann-Whitney U test, $P < 0.001$). **(D)** The barley cultivar Ingrid was inoculated with *MoWT*, $\Delta\Delta\text{MoNUDIX-1}$, $\Delta\Delta\text{MoNUDIX-2}$, $\Delta\Delta\text{MoNUDIX-3}$, and *MoNUDIX* complementation mutants ($\Delta\Delta\text{MoNUDIX-1}^{\text{comp}}$ and $\Delta\Delta\text{MoNUDIX-2}^{\text{comp}}$). Leaves were photographed seven dpi. **(E)**

Boxplots summarize the results of three independent experiments with approximately 150 lesions measured across 10 barley leaves per treatment. Letters depict significant differences between treatments (Kruskal-Wallis H test, Dunn's post-hoc test, $P < 0.01$). (F) The barley cultivar Ingrid was inoculated with *MoWT*, $\Delta\Delta MoNUDIX-1$, and $\Delta\Delta MoNUDIX-1$ complemented with MoNUDIX variants harboring substitution mutations in the Nudix box motif. Two independent complementation lines were tested for each variant. Example images at seven dpi are displayed. Boxplots summarize the results, the size of approximately 150 lesions were measured across 10 barley leaves. Letters depict significant differences between treatments (Kruskal-Wallis H test, Dunn's post-hoc test, $P < 0.01$).

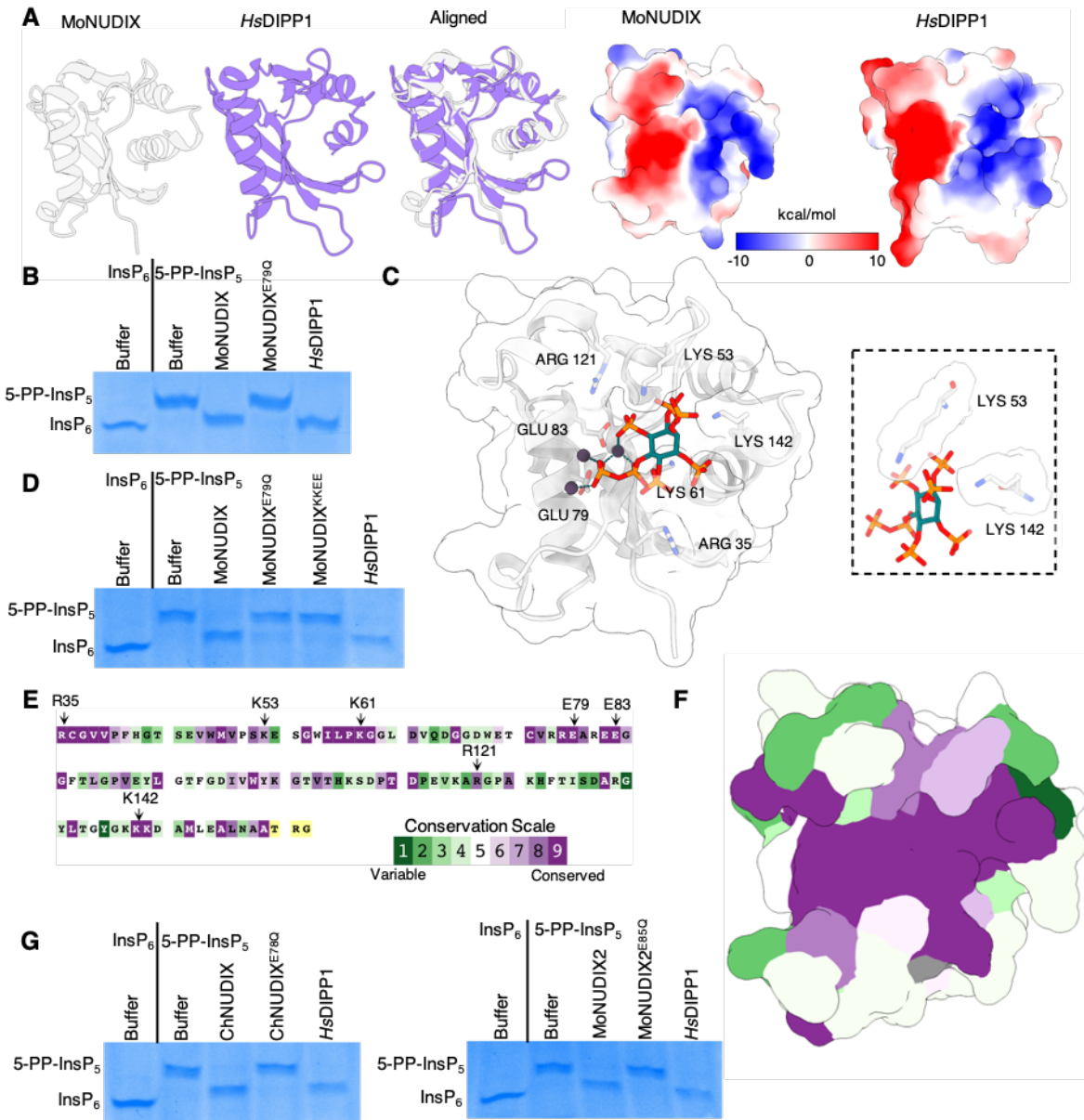


Fig. 2. *Magnaporthe* and *Colletotrichum* Nudix effectors are diphosphoinositol polyphosphate phosphohydrolases.

(A) MoNUDIX and *Homo sapiens* DIPP1 (PDB: 6WO7) (26) crystal structures superimposed to demonstrate their structural similarity despite low levels of sequence identity (25%). (Right) Both MoNUDIX and *Hs*DIPP1 demonstrate similar surface charge properties at the putative active site. (B) Purified MoNUDIX, MoNUDIX^{E79Q}, and *Hs*DIPP1 were incubated with 5-PP-*In*sP₅. Buffer alone was incubated with both *In*sP₆ and 5-PP-*In*sP₅. The reaction products were separated using a polyacrylamide gel and stained with toluidine blue. (C) MoNUDIX with Mg²⁺ and 5-PP-*In*sP₅ docked into the crystal structure via alignment with *Hs*DIPP1 (PDB: 6WO7). The amino acids potentially important for Mg²⁺ and 5-PP-*In*sP₅ binding are labelled. In the box are the two lysine amino acids selected for mutagenesis. (D) Inositol pyrophosphate hydrolysis assays demonstrate the importance of lysine 53 and 142. (E) The sequence of MoNUDIX used to determine the crystal

structure, with colouring indicating amino acid conservation across homologous effectors. The amino acids labelled in **(C)** are indicated with arrows. **(F)** MoNUDIX with the protein surface coloured according to amino acid conservation across homologous effectors, demonstrating high conservation of the putative substrate binding site. **(G)** Inositol pyrophosphate hydrolysis assays with MoNUDIX homologs ChNUDIX and MoNUDIX2 demonstrates Nudix motif-dependent hydrolysis of 5-PP-InsP₅.

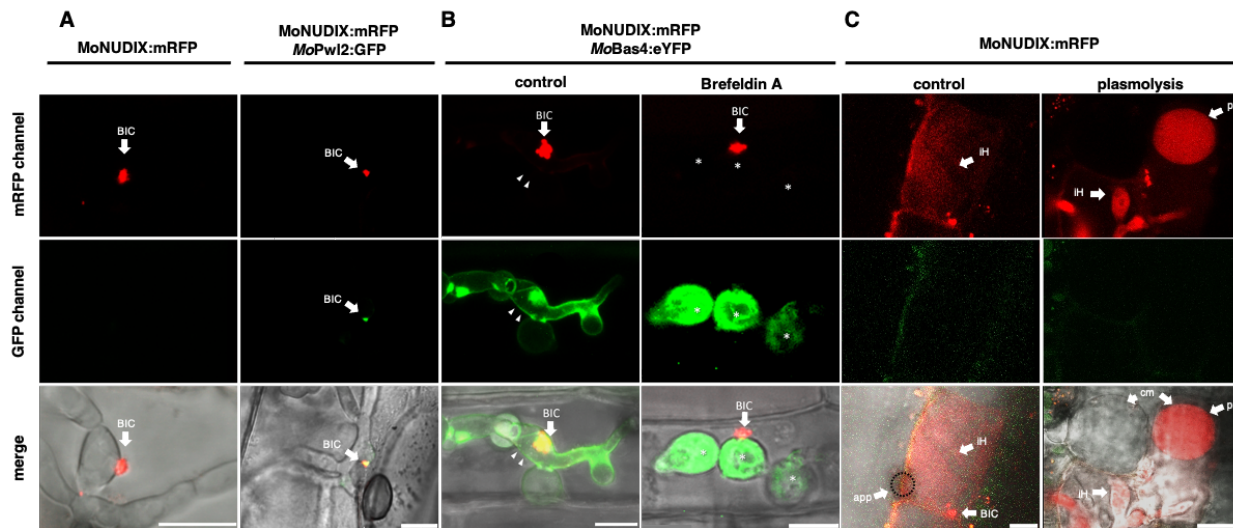


Fig. 3. MoNUDIX localizes to the biotrophic interfacial complex and is secreted into the host cytoplasm during infection.

Confocal laser-scanning microscopy images of barley and rice leaves infected with *Magnaporthe oryzae* expressing fluorescent protein-tagged effectors. (A) (Left) Barley leaves were inoculated with *M. oryzae* expressing MoNUDIX:mRFP. At 48 hours post inoculation (hpi), punctual accumulation of the mRFP fusion protein in the fungal hyphae was observed in the first infected cell, consistent with BIC localization. (Right) The cytoplasmic effector MoPwl2 (27) was co-expressed as a GFP-fusion protein demonstrating co-localization of MoNUDIX:mRFP and MoPwl2:GFP. (B) Rice leaves were inoculated with *M. oryzae* expressing MoNUDIX:mRFP and MoBas4:eYFP. MoBas4:eYFP (green) shows apoplastic localization outlining the invasive hypha (arrowheads). In the presence of BFA, MoBas4:eYFP (green) is retained in the fungal ER (asterisks), but MoNUDIX:mRFP remains BIC-localized (arrow), imaged with the same transformant at 3 h after exposure to BFA. (C) Secretion of MoNUDIX into the rice cell cytoplasm. Rice leaves were inoculated with *M. oryzae* expressing MoNUDIX:mRFP and analyzed 48 hpi. For concentration of the intracellular mRFP signal we used plasmolysis with 0.5 M KNO₃ prior to imaging; BIC: biotrophic interfacial complex; iH: invasive hyphae; p: rice protoplast after plasmolysis; i: infected cell; cm: cell membrane of protoplast. Scale bar: 10 μ m.

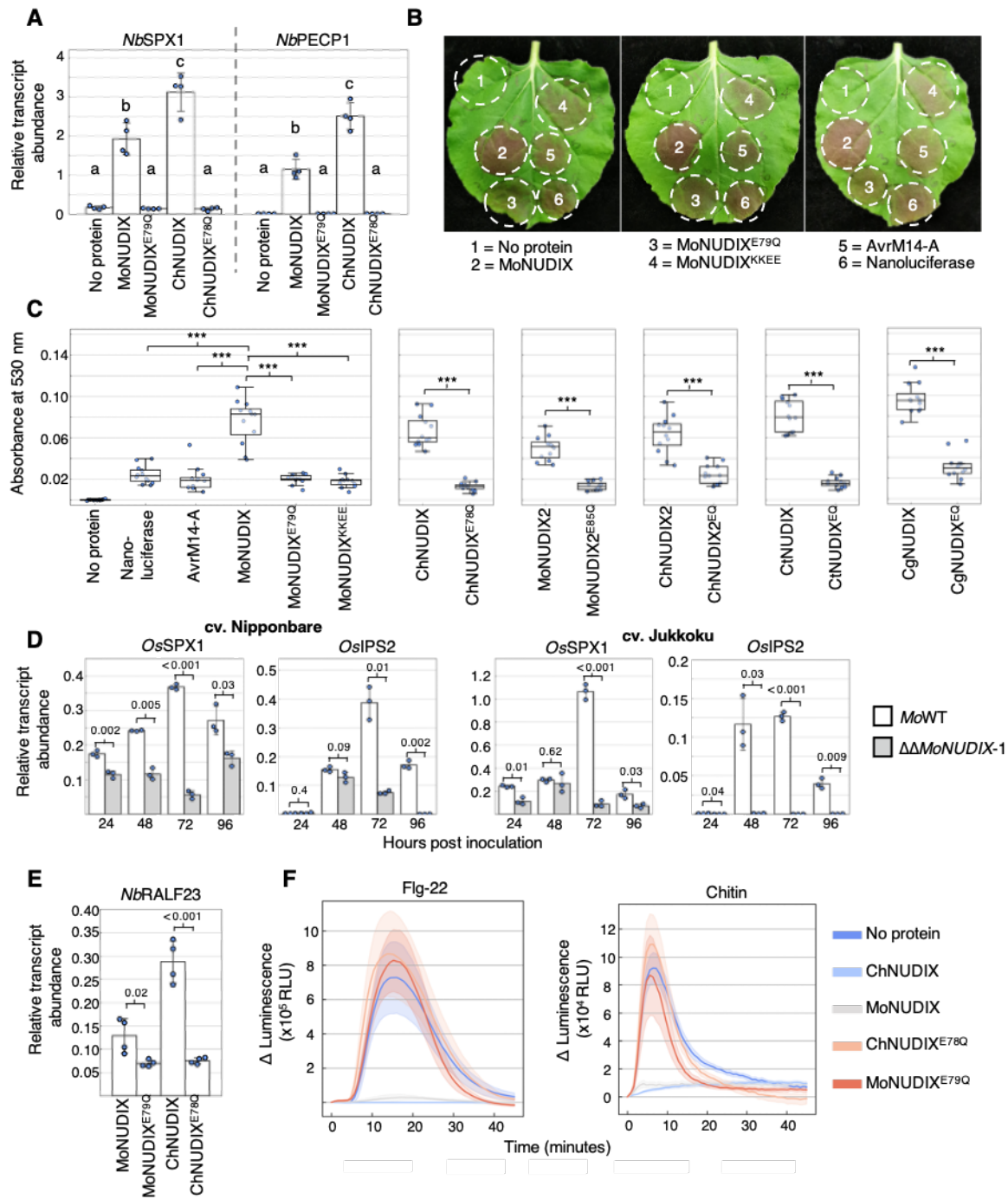


Fig. 4. The Nudix effector family activates plant phosphate starvation responses.

(A) The transcript abundance of *NbSPX1* and *NbPECP1* in *N. benthamiana* expressing Nudix effectors, or leaves transformed with an empty vector control (no protein). Values are mean expression \pm SD ($n = 4$) relative to the reference genes, letters indicate significantly different groups (one-way ANOVA, Tukey's HSD, $P < 0.001$). (B) Visible RUBY production in leaves co-transformed with PSI:RUBY and Nudix effectors or controls. (C) The absorbance of extracts from leaves co-transformed with PSI:RUBY and Nudix effectors or controls ($n = 12$), asterisks indicate

significant differences between treatments (one-way ANOVA, Tukey's HSD, *** P <0.001). **(D)** Rice cultivars Nipponbare and Jukkoku were inoculated with *M. oryzae* isolate Guy11 (*MoWT*) and *M. oryzae*^{ΔΔ*MoNUDIX-1*}. *OsSPX1* and *OsIPS2* transcript abundance was calculated relative to *OsACTIN* at four timepoints throughout the infection process, values are mean ± SD (n = 3), significant differences between *MoWT* and $\Delta\Delta MoNUDIX-1$ treatments were identified by an independent samples t test, p-values are listed. **(E)** The expression of *NbRALF23* in *N. benthamiana* leaves expressing Nudix proteins (as labelled). Values are mean ± SD (n=4) relative to the reference genes, with p-values from an independent samples t-test displayed. **(F)** Reactive oxygen species production in *N. benthamiana* expressing Nudix effectors, or leaves transformed with an empty vector control (no protein), following exposure to flg-22 (left) or chitin (right). Values are mean (solid line) ± SEM (shaded area) (n = 8).

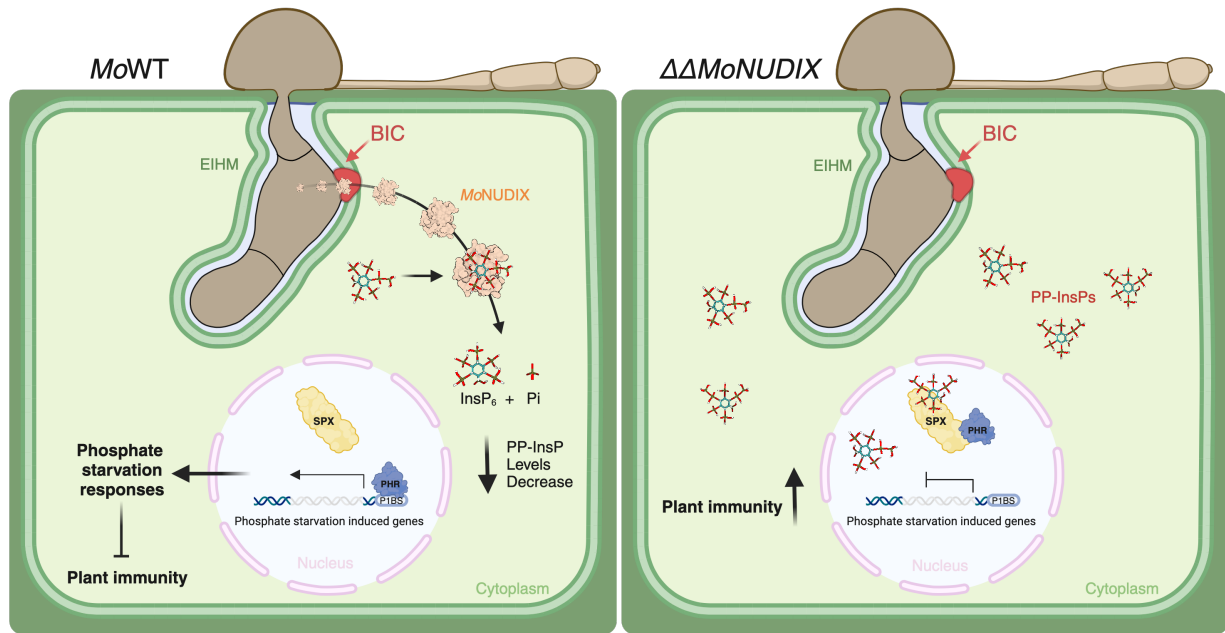


Fig. 5. A model for the virulence function of the *Magnaporthe* and *Colletotrichum* Nudix hydrolase effectors. (Left) In wild-type *M. oryzae* (MoWT) MoNUDIX is secreted from the invading fungus into the host cell cytoplasm. MoNUDIX functions as an enzyme, hydrolyzing inositol pyrophosphate (PP-InsP) signaling molecules into inositol hexakisphosphate (InsP₆) and phosphate (Pi). The decrease in PP-InsP concentration prevents SPX-mediated inhibition of PHRs, resulting in the transcription of phosphate starvation inducible genes. Phosphate starvation responses are therefore activated, including those which suppress plant immune responses. (Right) Without MoNUDIX, the ability of *M. oryzae*^{ΔΔMoNUDIX} to stimulate PP-InsP hydrolysis is compromised. Available PP-InsPs are detected by SPX domains, resulting in the binding of SPX domains to PHRs. This prevents PHRs from binding to the P1BS elements in phosphate starvation induced genes. In the absence of phosphate starvation signaling, plant immune responses are prioritized.

Supplementary Materials for

Plant pathogenic fungi hijack phosphate starvation signaling with conserved enzymatic effectors

Carl L. McCombe, Alex Wegner *et al.*

Corresponding authors: Ulrich Schaffrath, schaffrath@bio3.rwth-aachen.de; Simon Williams, simon.williams@anu.edu.au; Ely Oliveira-Garcia, EOliveiraGarcia@agcenter.lsu.edu

The PDF file includes:

Materials and Methods

Figs. S1 to S8

References 52 - 88

Other Supplementary Materials for this manuscript include the following:

Tables S1 to S6

Materials and Methods

Plant growth and *Magnaporthe oryzae* infection conditions

Nicotiana benthamiana plants were grown in a controlled environment at 25 °C under a 16-hour/8-hour light/dark photoperiod. Fully expanded leaves from 5-week-old plants were used in Agrobacterium-mediated transient gene expression experiments to generate qPCR, RUBY promoter/reporter and ROS burst assay results.

Rice (*O. sativa*) plants for RNAi and BFA-treatment protein localization experiments were grown in Baccto Top Soil (Michigan Peat Co., Houston, Texas) in a Caron 7301-50 Plant Growth Chamber with equal numbers of fluorescent lamps (Philips ED37, 400 W). At rice seedling height, ~1 m from the bulbs, light ranged in intensity from 600 to 1,200 $\mu\text{mol m}^{-2} \text{s}^{-1}$. Plants were grown at ~70 % relative humidity under a daily cycle of 12 h of light at 28 °C and 12 h of darkness at 24 °C. At 2 weeks, plants were fertilized with Jack's Professional Peat Lite 20-10-20 Fertilizer (#77860; JR Peters, Inc.; Allentown, PA). Whole plant infection assays for RNAi experiments were performed by spray inoculation of 2–3-week-old rice plants as previously described (52).

Rice and barley used for the plasmolysis localization experiments and for the characterization of infection phenotypes with *M. oryzae* *MoNUDIX* gene deletion and complementation mutants. Barley plants were cultivated in plant-growth chambers at a temperature of 18 °C, relative humidity of 60 %, and a 16/8 h light-dark cycle with a light intensity of 210 $\mu\text{mol/m}^2\text{s}$ in ED73-soil (Balster Einheitserdewerk GmbH, Germany), as previously described (53). After 7 days the primary leaves of the plants were inoculated with *M. oryzae* (10000 conidia mL^{-1}) using a compressed air atomizer. Subsequently, the plants were kept in the dark at 24 °C and 100 % relative humidity for 24 hours before being transferred to growth chamber conditions. Rice plants were cultivated in P-soil (Balster Einheitserdewerk GmbH, Germany) at 24 °C in a growth chamber with a 15/9 h light-dark cycle, 80 % relative humidity, and a light intensity of 300 $\mu\text{mol/m}^2\text{s}$. Rice plants were spray inoculated after 12 days with 20000 conidia mL^{-1} . Subsequently, the plants were kept in the dark at 24 °C and 100 % relative humidity for 24 hours before being transferred to growth chamber conditions. Infected rice leaves were evaluated at 5 dpi, barley leaves at 6 dpi. Images were captured using a Nikon D3500 camera. Disease symptoms were quantified by determining the size in pixels of each symptom using ImageJ software. All reported values in the manuscript are relative to the average lesion size for the wild-type *M. oryzae* isolate Guy11.

Fungal cultivation

For RNAi and BFA-treatment protein localization experiments, fungal strains (*M. oryzae*) were stored on dried filter papers at -20°C and cultured on rice bran agar plates at 25°C for up to 2 weeks under continuous light in Percival Scientific (Model CU-36L5) tissue culture incubators equipped with one half fluorescent lights (FT20T12/cw, 20W) and one-half black lights (FT20T12/BL, 20W).

For all other experiments, the original *M. oryzae* strain Guy11 (MoWT) was provided by Dr. D. Tharreau from CIRAD in Montpellier, France. Fungi were cultivated on oatmeal agar, which consisted of 20 g/L agar, 2 g/L yeast extract, 10 g/L starch, and 30 g/L oat flakes. Alternatively, they were grown on potato dextrose agar (PDA) at a temperature of 23 °C in the absence of light. Conidia were obtained as described in (53) by cultivating the fungi placed under fluorescent tubes emitting blacklight (310 to 360 nm) with a 16/8 h light/dark cycle and at a constant temperature of 26 °C for 7 days. The concentration of conidia was adjusted in a solution containing 1 g/L gelatin and 0.5 ml/L Tween 20.

Plasmid construction for gene expression in *E. coli* and *N. benthamiana*

All effector gene sequences had their signal peptide predicted using SignalP 6.0 (54) and removed, were codon optimised for *E. coli*, and ordered from Integrated DNA technologies, Inc IDT® as double-stranded DNA fragments. The DNA fragments were cloned into either a modified pOPIN plasmid (55) with a T7 promoter and a 6xHIS 3C protease site N-terminal tag if used for protein expression in *E. coli*, or a level 1 MoClo plasmid (56) along with a 35 S promoter, Omega 5' UTR translational enhancer, 3xHA N-terminal tag, and octopine synthase terminator if used for expression in *N. benthamiana*. The sequences of all proteins expressed in *E. coli* and *N. benthamiana* in this study are listed in **Table S2** and **Table S3**. All level 1 MoClo genes were subsequently inserted into the level 2 acceptor plasmid pICSL4723 before transformation into *Agrobacterium tumefaciens* (GV3101). The RUBY polyprotein gene sequence, and all gene promoter sequences used in this study (listed in **Table S4**) were ordered from Integrated DNA technologies, Inc IDT® as double-stranded DNA fragments and cloned into level 0 MoClo plasmids (56), before being used to create level 1 and level 2 plasmids. *Entamoeba histolytica* IP6KA and *Homo sapiens* DIPP1 were ordered as *E. coli*-codon optimised double-stranded DNA

fragments and cloned into the modified pOPIN (53) plasmid with a T7 promoter and a 6xHIS 3C protease site N-terminal tag. All gene sequences had any BbsI and BsaI cleavage sites removed without altering protein sequence to enable GoldenGate assembly.

Protein expression and purification

AvrM14-A, *HsNudt16*, *AtNudx7*, and *AtNudx7^{E154Q}* proteins were purified previously (30). *EhIP6KA* and *HsDIPP1* were expressed in *E. coli* BL21 (DE3) cells using ZYM-5052 autoinduction media (57). Cells were grown by continuous shaking at 37 °C until the OD_{600nm} reached 0.6 – 0.8. The temperature was then dropped to 18 °C and cells were incubated with shaking for another 18 hours before harvesting via centrifugation. MoNUDIX, MoNUDIX2, and ChNUDIX proteins (wild-type and mutants) were expressed in *E. coli* Shuffle® cells grown in Terrific Broth. Cells were grown by continuous shaking at 30 °C until the OD_{600nm} reached 0.6 – 0.8. The temperature was then dropped to 16 °C, IPTG was added to a final concentration of 200 μM, and incubation with shaking continued for another 18 hours before harvesting via centrifugation. Following centrifugation, all cell pellets were resuspended in lysis buffer (50 mM HEPES pH 8.0 (MoNUDIX, MoNUDIX^{E79Q}, MoNUDIX^{KKEE}), pH 7.5 (MoNUDIX2, MoNUDIX2^{EQ} ChNUDIX, ChNUDIX^{E78Q}), or pH 7.0 (*HsDIPP1*, *EhIP6KA*), 150 mM NaCl, 1 mM PMSF, 1 μg ml⁻¹ DNase, and 1 mM DTT (DTT only included for *EhIP6KA* and *HsDIPP1*)). All cells were lysed using sonication and cellular debris pelleted by centrifugation. The resulting supernatant was applied to a 5 mL HisTrap FF crude column (Cytiva, Marlborough, Massachusetts). To remove loosely bound proteins, the column was washed with the lysis buffer without PMSF or DNase containing 30 mM imidazole. The remaining bound proteins were eluted with a continuous gradient of imidazole from 30 mM to 250 mM over 10 minutes, using an Äkta pure chromatography system. Fractions were analysed by Coomassie-stained SDS-PAGE and fractions containing the protein of interest were pooled, dialysed to remove the imidazole, and incubated with recombinant 6xHis-tagged 3C protease overnight at 4 °C (except *EhIP6KA*, which was stored following dialysis without 3C protease incubation). The protein of interest was separated from any uncleaved protein, the fusion tag, and 3C protease by immobilized metal affinity chromatography and purified further by size-exclusion chromatography (SEC) using either a HiLoad 16/600 Superdex® 75 pg or a HiLoad 26/600 Superdex® 75 pg column pre-equilibrated in buffer (10 mM HEPES (pH same as in corresponding lysis buffer), and 150 mM NaCl). After

SEC, fractions containing the protein of interest were identified using SDS-PAGE and concentrated using Amicon® Ultra Centrifugal filters (Merck, Darmstadt, Germany) before storage at -80 °C.

Putative Nudix hydrolase effector identification and phylogenetic tree construction

To identify putative Nudix hydrolase effectors homologous to MoNUDIX, the NCBI protein database (58) was searched using blastp with the protein sequence of MoNUDIX (default parameters; word size = 5, expect threshold = 0.05). Any identified hits without a predicted signal peptide or Nudix hydrolase domain were filtered out by screening the sequences using SignalP6.0 (54) and InterProScan (59). To reduce the length of the list while retaining sequence diversity, if two or more sequences shared > 95% sequence identity, only one sequence was selected at random to remain in the list presented in **Table S1**. PhyML (60) (version 3.3) was used to estimate a maximum-likelihood phylogeny with selected protein sequences from this list, along with previously identified fungal Nudix effectors (30). The resulting phylogeny was visualized using iTOL (61) (version 6.7.6).

Transient gene expression via agrobacterium infiltration

Agrobacterium tumefaciens (GV3101) with the desired plasmid was suspended in infiltration buffer (10 mM MES pH 5.6, 10 mM MgCl₂ and 200 µM acetosyringone) to an optical density at 600 nm (OD_{600nm}) of 0.5 (for RUBY co-infiltrations) or 1.0 (for qPCR and the ROS burst assay). For co-infiltrations, *A. tumefaciens* (GV3101) with a RUBY promoter/reporter plasmid was added to the infiltration buffer to an OD_{600nm} of 0.5. The final combined OD_{600nm} was 1.0 for all infiltrations. All cultures were incubated in the dark at 28 °C with 220 rpm shaking for 2 to 3 hours before syringe-infiltration into *N. benthamiana* leaves. Infiltrated plants were kept in the same growing conditions as before infiltration.

ROS burst assay

Measurement of ROS was completed as described previously with some minor modifications (62). In brief, *N. benthamiana* leaf discs (4 mm diameter) were floated on water overnight in a 96-

well plate. The water was replaced with an elicitor solution (200 μ M luminol, 20 μ g mL $^{-1}$ horseradish peroxidase and 100 nM flg-22 or 5 μ g mL $^{-1}$ chitin), and luminescence was measured over time using a Tecan Infinite® M Plex (Tecan, Männedorf, Switzerland) plate reader at room temperature.

Immunoblot analysis

N. benthamiana leaf tissue was frozen in liquid nitrogen and ground into a fine powder. Soluble protein was extracted by adding an equal volume of lysis buffer (50 mM HEPES (pH 7.5), 1 mM EDTA, 2% PVPP, 5 mM DTT, 1 mM PMSF). The samples were mixed by rotating at 4°C for 2 minutes, prior to centrifugation at 4 °C for 15 minutes at 17 000 xg and the supernatant was collected. Approximately 20 μ g of each protein solution was separated on two 15% SDS-PAGE gels. The first gel was stained with Coomassie blue to assess protein loading across samples, while proteins from the second gel were transferred onto a 0.22 μ M nitrocellulose membrane. Blots were probed with HRP-conjugated mouse anti HA-tag (1:2000 dilution) either from ABclonal (Woburn, Massachusetts) or for the CtNUDIX effectors from Roche (Basel, Switzerland) due to low levels of CtNUDIX protein accumulation. Pierce™ ECL substrate (Thermo Fisher Scientific, Waltham, Massachusetts) was added to the immunoblots and chemiluminescence detected using a ChemiDoc imager (Bio-Rad, Hercules, California).

Nudix hydrolase enzyme assays

The phosphomolybdate Nudix hydrolase enzyme assays and the mRNA decapping assays were performed as described previously (30). To assess inositol pyrophosphohydrolase activity 5-PP-InsP₅ was first synthesized from InsP₆ (Merck, Darmstadt, Germany) in a 500 μ L reaction volume following previously described methods (63) using the purified *EhIP6KA* protein. The resulting 5-PP-InsP₅ was purified using the previously described gel electrophoresis-based method (64). Purified 5-PP-InsP₅ was incubated with 5 μ M recombinant protein in 50 mM Tri-HCl pH 8.0, 5 mM MgCl₂ at 37 °C for 60 minutes. After incubation the reaction products were separated and identified using previously described methods (64) with minor modifications, we utilized a smaller gel (8.3 x 7.3 x 0.1 cm) and ran the gel at 300V for approximately 5 hours, until the dye front was 2/3 of the way through the gel.

Protein crystal structure determination

Crystallization screening with purified MoNUDIX protein (amino acids 35 to 156) was conducted using a Mosquito robot (STP LabTech, Melbourn, UK) in a 96-well plate format using sparse matrix screens. The sitting drop vapor-diffusion method of crystallization was used and drops consisting of 100 nL 30 mg/mL MoNUDIX containing 18 mM InsP₆ combined with 100 nL reservoir solution were equilibrated against a 100 μ L reservoir solution. The reservoir solution resulting in the MoNUDIX crystals analyzed in the study was 200 mM Potassium thiocyanate with 20% PEG3350 from the SG1™ Screen (Molecular Dimensions, Newmarket, United Kingdom). To create the cryoprotectant 80 μ L of the reservoir solution was combined with 10 μ L of glycerol and 10 μ L of ethylene glycol. The crystal was transferred to the cryoprotectant before flash cooling in liquid nitrogen. Diffraction datasets were collected on the MX2 beamline at the Australian Synchrotron (65). The highest resolution dataset allowed by the beamline geometry was selected for processing in XDS, and then scaled using AIMLESS in the CCP4 suite (66, 67). The MoNUDIX crystal structure was determined using maximum-likelihood molecular replacement (MR) with Phaser in Phenix (68). The MR search model was an AlphaFold (69) model of the MoNUDIX sequence used for crystallization (sequence in **Table S2**). For all datasets automated model building and initial refinement was completed using Phenix AutoBuild (70). Subsequent model building was carried out manually in Coot (71) in-between rounds of automated refinement using Phenix Refine (72). Analysis of the final structures was performed with Coot (71), ChimeraX (73), and ConSurf (74) (default parameters were used for analysis). Data collection and refinement statistics are listed in **Table S5**. Map coordinates and structure files have been deposited in the Protein Data Bank under ID 8SXS.

Micro-scale thermophoresis (MST)

MST experiments were performed on a Monolith NT.115 instrument (NanoTemper Technologies, Munich, Germany) at 25 °C. MoNUDIX and MoNUDIX^{KKEE} were labelled with Alexa Flour 647 succinimidyl ester (Thermo Fisher Scientific) and used at a final concentration of 50 nM and 110 nM, respectively. In brief, 20 μ M of the protein solution was incubated with 2-fold molar excess of the fluorophore for 2 hours in the dark at room temperature, and the free dye was

subsequently removed using a PD-10 desalting column (Cytiva). A stock solution of InsP₆ was serially diluted in buffer (10 mM HEPES pH 8.0, 150 mM NaCl), mixed 1:1 with the labelled protein, and loaded into standard capillaries (NanoTemper Technologies). MST measurements were recorded using 20 % LED power and 20 to 80 % MST power and analyzed using MO. Affinity Analysis software 2.2.7 (NanoTemper Technologies).

RNA extractions and RT-qPCR

For *N. benthamiana* samples, at 3 days post-infiltration approx. 100 mg of leaf tissue was collected from each infiltration site and frozen in liquid nitrogen. For RNA extraction and purification, the Monarch® Total RNA Miniprep Kit (NEB, Ipswich, Massachusetts) was used following the recommended protocol for plant tissue, with tissue lysis achieved by grinding the plant tissue into a fine powder while frozen in liquid nitrogen. cDNA synthesis from the purified RNA was achieved using the LunaScript® RT SuperMix Kit (NEB). qRT-PCR was performed using the Luna® Universal qPCR Master Mix (NEB) on a ViiA 7 PCR System (Applied Biosystems, Waltham, Massachusetts), with primers listed in **Table S6**. Expression levels were calculated relative to the geometric mean (75) of the reference genes, *NbUbe35* (76), and *NbeIF1a*.

For *O. sativa* and *H. vulgare* samples, extraction of total RNA from plant tissue or fungal mycelium followed by cDNA synthesis was completed as described in (53). Primers used are listed in **Table S6** and marked with the suffix “qPCR”. For the determination of transcript abundance or gene copy number, the protocols were similar to (53).

Betalain extraction and measurement

We used a modified version of a previously described betalain extraction method from *N. benthamiana* leaves (77). In brief, at 3 dpi six 4 mm leaf disks were excised from the infiltrated area, incubated for 30 minutes with 30 rpm rotation in 1 mL 50% methanol, and then 200 µL from each solution was transferred into a transparent 96-well plate and absorbance at 530 nm was measured. All values were zeroed using the absorbance measurement of 50% methanol alone.

Generation of RNAi strains of *M. oryzae*

The RNAi cassette from plasmid pRedi (78) was used to generate an RNAi construct targeting *MoNUDIX* transcripts. The 312-bp sense and antisense fragments were amplified from genomic DNA of *M. oryzae*, using the primers RNAi(Nudix1)-fw and RNAi(Nudix1)-Rv, and RNAi(Nudix1)i-fw and RNAi(Nudix1)i-Rv, respectively (sequences listed in **Table S6**). The sense and antisense fragments were used to replace the XhoI-SnaBI and BglII-ApaI fragments of pRedi and were thus separated by 135 bp of the intron of the *M. oryzae* Cut2 gene (NCBI accession: XM_365241.1), existing in pRedi, as a linker (78). Plasmid inserts were subsequently sequenced to verify sequence accuracy. The resulting 6.0-kb RNAi construct was excised from pRedi by DraI digestion, purified by gel elution, and transformed into conidial protoplasts of *M. oryzae*, and single spore isolates were generated as described previously (79). Knockdown of the target genes was confirmed by qRT-PCR at 28 hours post inoculation using previously described methods (80). At this point, rice plants showing satisfactory reduction of the transcription levels were used in our standard conidial spray inoculation and leaf sheath assays.

Analysis of *MoNUDIX* RNAi infection phenotypes

Susceptible rice variety YT-16 was used for *MoNUDIX* RNAi experiments. Rice leaf sheath inoculations were performed as described (81) with the following modification. We used sheath pieces that were thinner trimmed sheaths (~3 cell layers thick). Briefly, 7-cm long leaf sheath pieces from 3-week-old plants were placed in a sealable Pyrex glass moist chamber. Leaf sheath sections were placed on inverted 8-well PCR tube strips to avoid contact with wet paper and to hold the epidermal cells directly above the mid-vein horizontally flat for the uniform distribution of inoculum in trimmed leaf sheath pieces (82). A spore suspension (10⁴ spores/mL in sterile 0.25% gelatin) was prepared from 10-day-old cultures and injected into one end of the sheath using a 100- μ L pipette. Each segment was trimmed at 18 to 30 hpi and imaged immediately by laser confocal microscopy. Biological replicates were independent experiments performed with fungal cultures fresh out of frozen storage and with new rice plants. All conclusions are supported by at least 3 biological replicates, with each replication including observation of ~100 infection sites. Confocal imaging was performed with a Leica SP8 confocal microscope system using two water immersion objectives, C-Apochromat 40x/1.2 WCorr. and C-Apochromat 63x/1.2WCorr. Excitation/emission wavelengths were 358 nm/461 nm for cell wall fluorescence. Image acquisition and processing were done using Leica LAS X 2020 software. For ROS analysis, rice

leaves inoculated with conidium suspensions (3×10^5 spores/mL) of the wild-type and RNAi strains were stained with DAB at 32 hpi as described previously (81, 83). The leaves inoculated with RNAi and wild type strains were incubated in 1 mg/mL DAB solution, pH 3.8, at room temperature for 8 hours and destained with ethanol:acetic acid solution (94:4, v/v) for 1 hour.

Deletion of *MoNUDIX*

Design of primers, gRNAs and the prediction of gene sequences was done using the *M. oryzae* 70-15 genome assembly MG8 (GCF_000002495.2) and ASM292509v1 of isolate Guy 11. All primers are listed in **Table S6**. For genome editing, protoplast transformation was performed as described in (84, 85). Deletion of the first *MoNUDIX* paralog was done using CRISPR/Cas9 mediated genome editing by replacing the coding sequence of *MoNUDIX* with a PCR product encoding a hygromycin resistance cassette (HygR). To enable homologous recombination, the HygR was flanked by 50 bp homologous regions as described by (86). The flanks were added by using primer MhNx_HygR F/R and plasmid pTK144 as a template for HygR. To exclude off-target effects, different gRNAs were used to generate three independent mutants. The mutants with a single *MoNUDIX* gene deletion were generated using gRNA-1 ($\Delta\Delta MoNUDIX\text{-M1}^1$ and -M2^1), gRNA2 ($\Delta\Delta MoNUDIX\text{-M3}^1$, -M4^1 , and -M5^1) and gRNA-3 ($\Delta\Delta MoNUDIX\text{-M6}^1$ and -M7^1), respectively. gRNA was generated with primers gRNA-1/-2/-3 similar to the procedure described in (85). PCR analysis was conducted to verify successful gene replacement through homologous recombination (HR). In all these mutants the second copy of the *MoNUDIX* gene was still present (fig. S2A). To generate double gene deletion mutants, three mutants with a single gene deletion were selected ($\Delta\Delta MoNUDIX\text{-M2}^1$, -M3^1 and -M6^1). The second gene replacement was conducted using either fenhexamid or nourseothricin resistance cassettes (FenR/NatR) flanked by 50 bp homologous sequences, generated with primers MhNx_pTel_F/R and pTelFen/Nat as a template, see (85). Protoplasts of the single-deletion mutants were transformed with the FenR/NatR encoding DNA-repair-template and Cas9-RNP. The $\Delta\Delta MoNUDIX\text{-1}$ mutant was generated using gRNA-2 and NatR, the $\Delta\Delta MoNUDIX\text{-2}$ mutant using gRNA-3 and FenR, and the $\Delta\Delta MoNUDIX\text{-3}$ mutant using gRNA-1 and FenR. Again, PCR analysis was performed to genotype resulting mutants and the absence of both Nudix genes was verified using the gene-specific primer pair MoNX_F1_F and MoNX_F1_R (fig. S2B). An additional PCR analysis with one primer located within the resistance cassette and the other outside the modified region (primers: SeqMoNX_F &

pTel_F) confirmed the integration of FenR or NatR at the second gene locus. Additionally, qPCR was performed to confirm the absence of *MoNUDIX* transcripts in $\Delta\Delta MoNUDIX-1/-2/-3$ (primers: qPCR MoNUDIX F/R and qPCR MoACTIN F/R).

Constitutive expression of *MoNUDIX*

Generation of mutants constitutively expressing *MoNUDIX:mRFP* was done as described in (53). The sequence of *MoNUDIX* was amplified with primers Nx_pTK Gib and Nx_pTK Gib-Stop and the gene sequence was inserted into the *BcuI/NotI* linearized vector pTK144 by Gibson assembly. The expression construct was amplified using primers pTK144_OE F/R. Transformants were selected using HygR and screened by PCR for the insertion of the construct. Additionally, qPCR was performed to confirm the accumulation of transcripts of *MoNUDIX:mRFP*.

Complementation of *MoNUDIX* deletion

To verify that the observed phenotypes correlate with the deletion of *MoNUDIX* and is not caused by off targets effects potentially introduced by CRISPR/Cas9, the *MoNUDIX* locus was amplified from the genome of *MoWT* with approximately 500 bp of downstream and 1000 bp of upstream UTR flanks (NXcompl_Gib F/R) and cloned into pTelFen linearized with *AscI* and *BamHI*. 15 μ g of the purified PCR product (generated with primers SeqMoNX_F /Nwcomp R) were used together with 1 μ g pTelNat or pTelFen to enable co-selection, and a Cas9-RNP, that targets the HygR (generated with primer gRNA_Hyg), for the co-transformation of protoplasts. Insertion of the DNA repair template into the original *MoNUDIX* locus, which was replaced by HygR, was verified by PCR using primers NW-KO-NX-F/MoNX-F1-R and NW-Comp F2/R2 (fig. S2C). Since ectopic insertion might occur, the copy number of the complemented *MoNUDIX* gene was determined by qPCR for the mutants $\Delta\Delta MoNUDIX-1/2^{comp}$, as described in (84), revealing two insertions for $\Delta\Delta MoNUDIX-1^{comp}$ and five insertions for mutant $\Delta\Delta MoNUDIX-2^{comp}$.

Site directed mutagenesis was performed to complement double gene-deletion mutants with potentially enzymatic inactive versions of the MoNUDIX protein. Therefore, codons encoding for amino acids within the Nudix box were replaced with alanine encoding codons (mutant 1: E83A, mutant 2: E82A&E83A, mutant 3: R78A&E79A and mutant 4: E82A&E83A&R78A&E79A). The primers used for site directed mutagenesis were: NxF-F1_mut F/R, NX78/79_F/R,

NXKombi78/79/82/83F/R, NXFLFMUT F/R, NX82/83F/R, and NX83F/R. Constructs were amplified with overlapping sequences, ligated with Gibson-Assembly and subsequently inserted into plasmid pTelFen to fuse the construct with FenR. The resulting plasmid containing Promotor^{NUDIX}:*MoNUDIX*^{mutant}:Terminator:FenR was linearized and introduced into the gene deletion mutant $\Delta\Delta MoNUDIX$ -1 by PEG-mediated protoplast transformation. Expression of each mutated *MoNUDIX* gene and the insertion copy number was verified by qPCR.

Co-expression of MoNUDIX:mRFP and Pwl2:GFP

For the mRFP in-locus tagging of *MoNUDIX*, 1000 bp of the promoter region, the Nudix encoding sequence with an artificial SNP in the gRNA1 target region, an mRFP encoding sequence and approx. 500 bp of the terminator sequence were amplified by PCR with overlapping primers and cloned by Gibson-Assembly into pTK144 (5UTR_NXiL_Gib F, NxILRsnp, NxILFsnP, NxILRtomRFP, NxILmRFPF, NxILmRFPR, 3UTRF, 3UTR_Gib R). The artificial SNP was designed not to change the amino acid sequence, but prevent the repair template from Cas9-RNP cleavage. The MoNUDIX:mRFP expression construct with the original promoter and terminator (*Promoter*^{NUDIX}:*NUDIX*^{SNP}:*mRFP*:*Terminator*^{NUDIX}) was amplified and together with Cas9-gRNA1-RNP used for co-transformation of *MoWT*. For selection, 1 μ g of pTelFen was used. Fen selected transformants were screened by PCR for the insertion of the construct into at least one original *MoNUDIX* locus (Nwcomp F/ MoNX-F1 R).

Pwl2:GFP was used as a BIC marker to check for co-accumulation. To express Pwl2:GFP under the control of the original promoter, the native locus of *PWL2*, including the 1000 bp native promoter and terminator region, was amplified by PCR from *M. oryzae* isolate Guy11. Additionally, a GFP encoding sequence was amplified from plasmid pSite4NB and fused to the *PWL2* construct by Gibson Assembly (primer used: PWL Promoter F, PWL R, PWL GFP F, PWL GFP R, PWL term F, PWL term R). The construct (*Promoter*^{PWL2}:*PWL2*:*GFP*:*Terminator*^{PWL2}) was inserted into pTelFen to fuse it with the fenhexamid resistance cassette and subsequently the linearized plasmid was used for the transformation of mutants expressing MoNUDIX:mRFP under the control of the original promoter. After selection of fenhexamid-resistant transformants, the insertion of the construct was verified by PCR. Mutants showing co-expression of MoNUDIX:mRFP and Pwl2:GFP-were then inoculated on barley cultivar Ingrid (40000 conidia ml^{-1}).

Live-cell imaging of plants infected with *M. oryzae*

Confocal laser scanning microscopy was conducted using a Leica TCS SP8 Spectral Confocal Microscope. Inoculated barley leaves were infiltrated with Phosphate Buffered Saline (PBS) pH 7.0 (8 g L⁻¹ NaCl, 0.2 g L⁻¹ KCL, 1.4 g L⁻¹ Na₂HPO₄, 0.27g L⁻¹ KH₂PO₄) by vacuum infiltration. For mRFP detection, the samples were excited with a wavelength of 561 nm and the emission was monitored at 580–620 nm. GFP-fluorescence was captured by exciting with 488 nm and emission was monitored at 500–530 nm. To confirm mRFP fluorescence and to distinguish it from plant tissue autofluorescence, lambda scans were performed. In addition, the GFP channel was used to distinguish autofluorescence from mRFP fluorescence. Plasmolysis of the rice cells was conducted by vacuum infiltration of leaves with 0.5 M KNO₃. Treatments with brefeldin A (BFA) (Invitrogen, Waltham, Massachusetts) were performed on infected rice sheath tissue at 25–28 hpi (2×10^4 spores/ml in 0.25% gelatin solution) using 50 µg ml⁻¹ BFA (0.1% DMSO) to inhibit specifically Golgi-dependent secretion of apoplastic effectors (32). Infected leaf sheaths treated with 0.1% DMSO were used as a control.

Leave samples used for WGA-AlexaFluor488 staining were cut into approximately 0.5 x 0.5 cm² tissue pieces and incubated in 1 M KOH for 1h at 37 °C. After the incubation, leaf samples were washed with PBS buffer pH 7.4 containing 0.1% TritonX. The leave samples were incubated in staining solution overnight (20 µg/ml WGA-AlexaFluor488, 50 µg/ml propidium iodide, 20 µg/ml BSA and 0.1% TritonX in PBS buffer pH 7.4). Before microscopy, the samples were washed with 1x PBS buffer pH 7.4.

Statistical analysis

Datasets with normal distributions were analysed using an independent-samples t-test (for pairs) or a one-way ANOVA with Tukey's post-hoc test for multiple comparisons. For other datasets, significance testing was completed using either a Mann-Whitney U test, when making pair-wise comparisons, or a Kruskal-Wallis H test with Dunn's post-hoc when making three or more comparisons simultaneously. The number of replicates for each experiment is stated in the appropriate figure caption. All statistical tests were completed using the 'stats' module in SciPy (87).

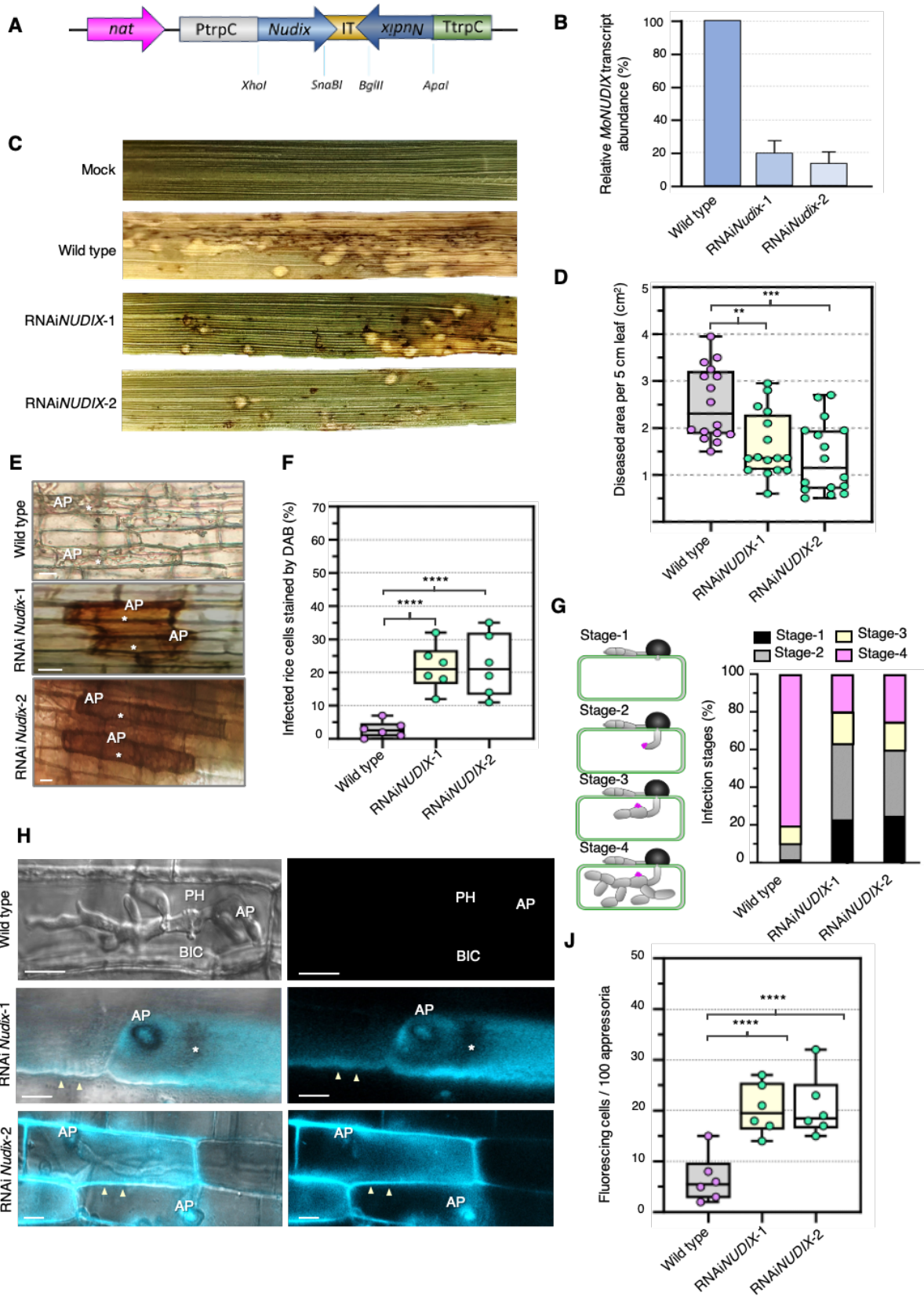


Fig. S1. Silencing of *MoNUDIX* in *M. oryzae* indicates an important role in pathogen virulence and host immune suppression. (A) The RNAi cassette transformed into *M. oryzae*. Consisting of the TrpC promoter (PtrpC) from *A. nidulans*, followed by 300-bp of the sense and antisense of *MoNUDIX* sequence (Nudix) separated by the Intron2 from the Cutinase2 of *M. oryzae* (IT), followed by the TrpC terminator (TtrpC). The neomycin phosphotransferase (npt) resistance cassette was used as a resistance marker. Not to scale. (B) Mean \pm SD (n = 3) relative transcript abundance of *MoNUDIX* in infected leaf sheaths at 28 hpi (hours-post inoculation) with either wild-type *M. oryzae* or the RNAi strains. (C) Whole plant spray inoculation assays demonstrates that silencing *MoNUDIX* results in fewer, smaller lesions. (D) Quantification of the diseased area caused by wild type, RNAiNudix-1, and RNAiNudix-2 *M. oryzae* in 5 cm leaf segments of rice. Box and whisker plots with individual data points are shown; independent samples t-test **P=0.0018, ***P=0.0002; n = 16. (E) DAB staining of penetrated plant cells at 32 hpi. White asterisks indicate infected rice cells, AP indicates appressoria. Scale bars = 10 μ m. (F) Percentages of infected cells stained by DAB. For each of the six replicates three sets of 100 cells were measured. ****P < 0.0001, independent samples t-test. (G) Quantification of four infection stages suggests a reduction of fungal virulence and colonization rate. For three replicates 100 infection sites were counted each. (H) Both wild-type and RNAi strains differentiated melanized appressoria (labelled AP) and invaded intact rice leaves, but the RNAi strains caused whole-cell (white asterisks) or cell wall fluorescence (white arrowheads) in rice under UV light, indicative of increased phenolic compound production and deposition in the cell wall. Scale bars = 10 μ m. (J) Quantification of fluorescing rice cells decorated with single appressoria of the wild-type or RNAi strains. For each of the six replicates three sets of 100 cells were measured. ****P < 0.0001, independent samples t-test.

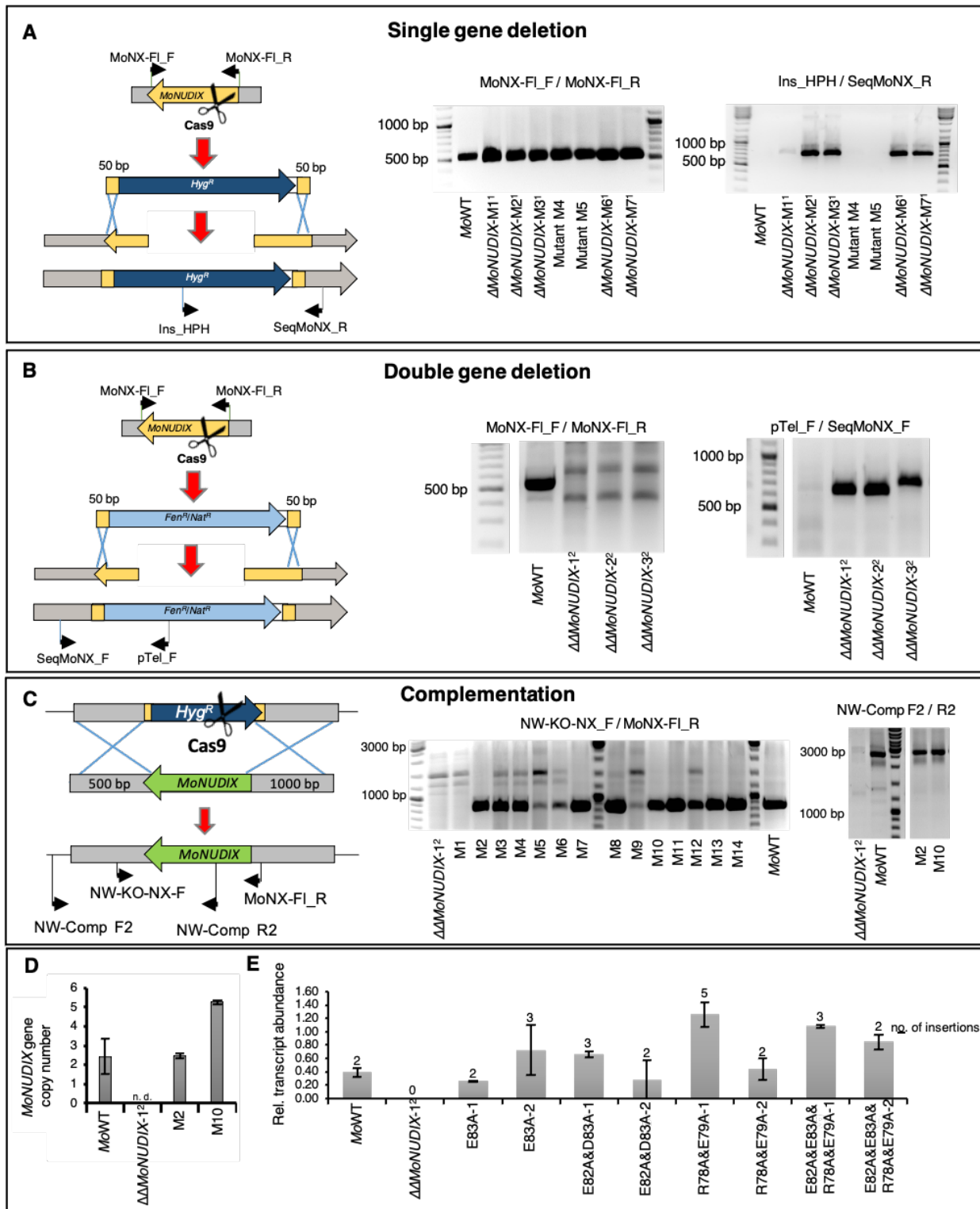


Fig. S2. Gene deletion and complementation of *MoNUDIX* in *M. oryzae*.

(A) Deletion of the first *MoNUDIX* allele was completed using CRISPR/Cas9 mediated genome editing via replacement with a hygromycin resistance encoding gene flanked by 50 bp homologous

regions. Mutants M1 and M2 were generated using gRNA-1, mutants M3, M4, and M5 using gRNA-2, and mutants M6 and M7 using gRNA-3. PCR analysis using primers Ins_HPH and SeqMoNx_R was conducted to verify successful gene replacement through homologous recombination (HR). The expected size of the PCR product after HR was 686 bp. In all mutants (M1 to M7) the parologue gene was detected by PCR, using the *MoNUDIX* specific primers MoNX-F1_F and MoNX-F1_R, resulting in a product of 530 bp. **(B)** Mutants M2, M3 and M6 with the single deletion were then taken to introduce the second deletion using the same approach as described in **(A)**. Again, PCR analysis was performed to genotype resulting mutants and the absence of both Nudix genes was determined using the gene-specific primer pair MoNX-F1_F and MoNX-F1_R. An additional PCR analysis with one primer located within the resistance cassette and the other outside the modified region (primers: SeqMoNX_F and pTel_F) confirmed the integration of FenR or NatR at the second gene locus. The expected size of the PCR product after HR was approximately 670 bp while it was approximately 150 bp larger in case of NHEJ. The $\Delta\Delta$ *MoNUDIX*-1 mutant was generated using gRNA-2 and NatR, the $\Delta\Delta$ *MoNUDIX*-2 mutant using gRNA-3 and FenR, and the $\Delta\Delta$ *MoNUDIX*-3 mutant using gRNA-1 and FenR. **(C)** For complementation, $\Delta\Delta$ *MoNUDIX*-1 and -2 gene deletion mutants were co-transformed with a CRISPR/Cas9-RNP, targeting the hygromycin resistance cassette, and with a DNA repair template encoding the sequence of the *MoNUDIX* locus. The plasmid pTEL-Fen was used for co-selection of $\Delta\Delta$ *MoNUDIX*-1 and pTEL-Nat for co-selection of $\Delta\Delta$ *MoNUDIX*-2 mutants. To promote homologous recombination into the target locus, 500 and 1000 bp homologous flanks were used. Insertion of the DNA repair template into the original *MoNUDIX* locus was determined by PCR with primers NW-KO-NX_F and MoNX-F1_R. If complementation was successful, a PCR product of approximately 840 bp was expected. PCR with primers NW-Comp F2 /R2 indicates an insertion of the DNA repair template into at least one *MoNUDIX* locus (PCR product size 2950 bp); mutants M1-M7 were generated from gene deletion mutant $\Delta\Delta$ *MoNUDIX*-1 and mutants M8-M14 from gene deletion mutant $\Delta\Delta$ *MoNUDIX*-2. **(D)** *MoNUDIX* gene copy number determined by qPCR for *MoWT*, $\Delta\Delta$ *MoNUDIX*-1 and M2/M10 ($\Delta\Delta$ *MoNUDIX*-1/2^{comp}). **(E)** To verify the expression of *MoNUDIX* in the complemented $\Delta\Delta$ *MoNUDIX* *M. oryzae* used for the infection experiments in Fig. 1F, transcript abundance of the mutated *MoNUDIX* genes was quantified by qPCR at 72 hpi. The *MoNUDIX* gene insertion number was calculated by qPCR as described in (84) and is indicated above each bar.

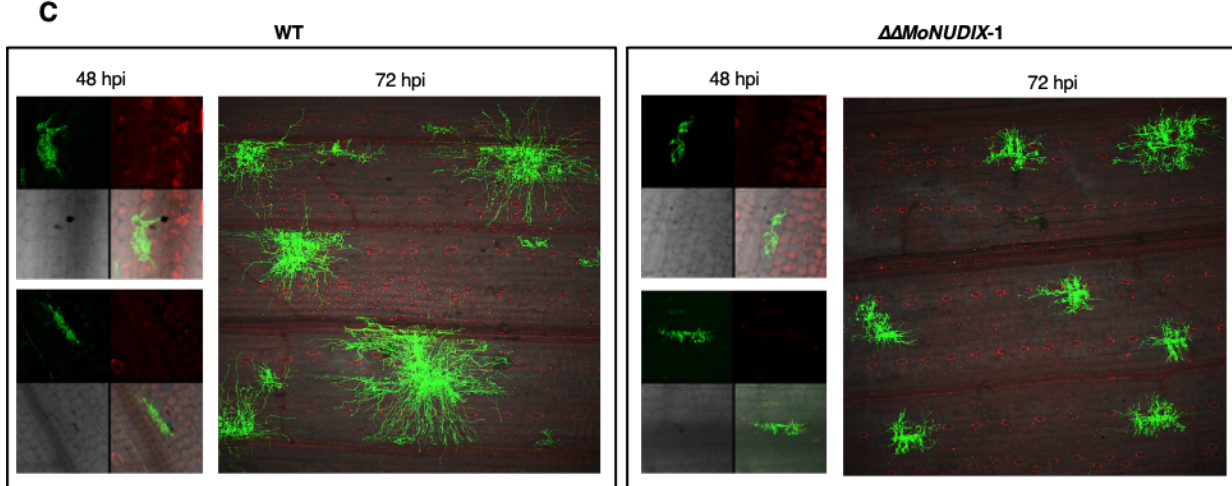
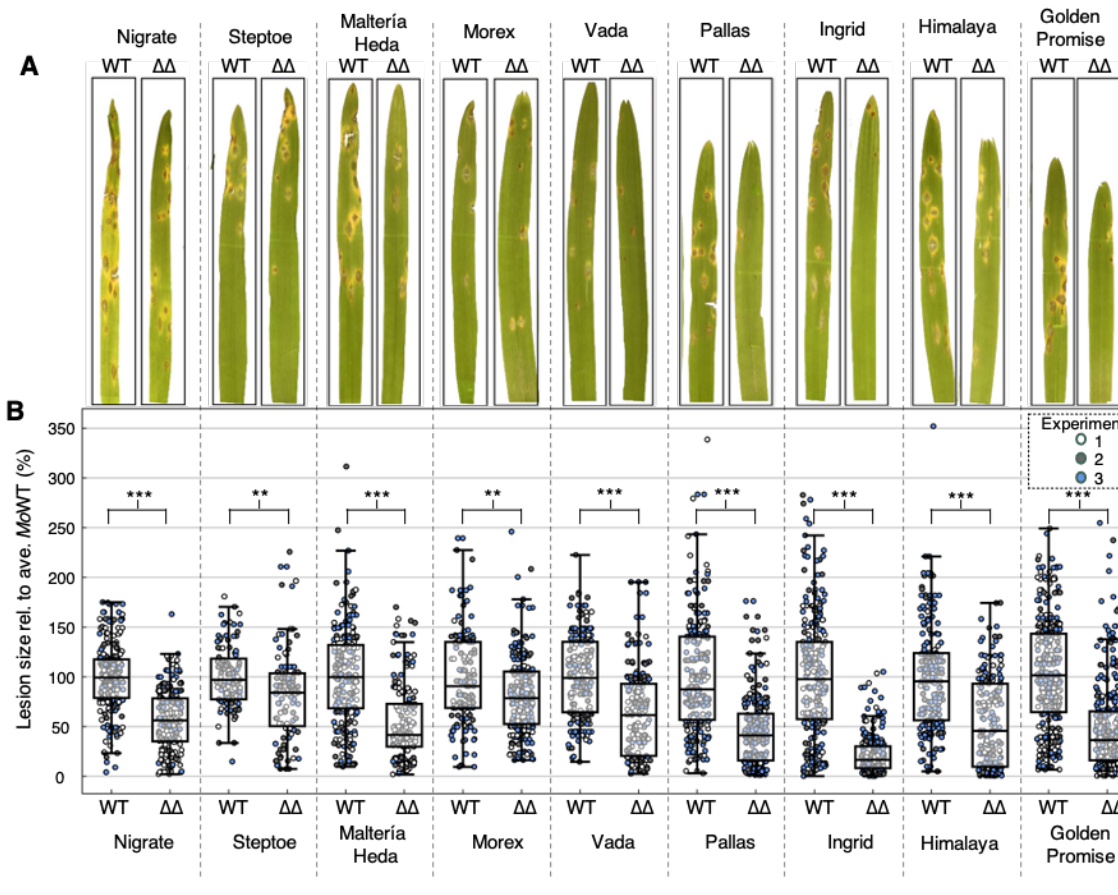


Fig. S3. *MoNUDIX* significantly contributes to the virulence of *M. oryzae* on multiple barley cultivars.

(A) Seven-day-old primary leaves of the barley cultivars Nigrate, Steptoe, Malteria Heda, Morex, Vada, Pallas, Ingrid, Himalaya, and Golden Promise were inoculated with conidia (10000 conidia mL^{-1}) of the *M. oryzae* wild-type isolate Guy11 (WT) and the *MoNUDIX* double gene deletion mutant $\Delta\Delta\text{MoNUDIX-1}$ ($\Delta\Delta$). Leaves were photographed seven days post inoculation. Representative pictures of leaves are shown for each interaction. **(B)** Blast lesion size was

determined in pixels and plotted as boxplots. To combine the results of the three independent experiments, the average lesion size of WT was set to 100 %, all other values were set relative to WT. Differences between WT and $\Delta\Delta$ are indicated with asterisks, as determined with the Mann-Whitney U test, **P < 0.005, ***P < 0.0005. (C) Conidia of WT and $\Delta\Delta$ *MoNUDIX-1* were inoculated on barley leaves of the cultivar Ingrid and fungal hypha were stained with wheat germ agglutinin (WGA) conjugated to Alexa® Fluor 488 at 48 and 72 hours post infection (hpi). To visualize plant cells, ethidium bromide was used. Confocal laser-scanning microscopy was carried out to show the progress of the infection on barley. Each infection site was recorded using different light excitations shown as a composite figure (48 hpi) or a merged image (72 hpi). For the 48 hpi composite figure: GFP-channel, 488 nm (top left), mRFP-channel, 561 nm (top right), bright field (bottom left) and merged channel (bottom right).

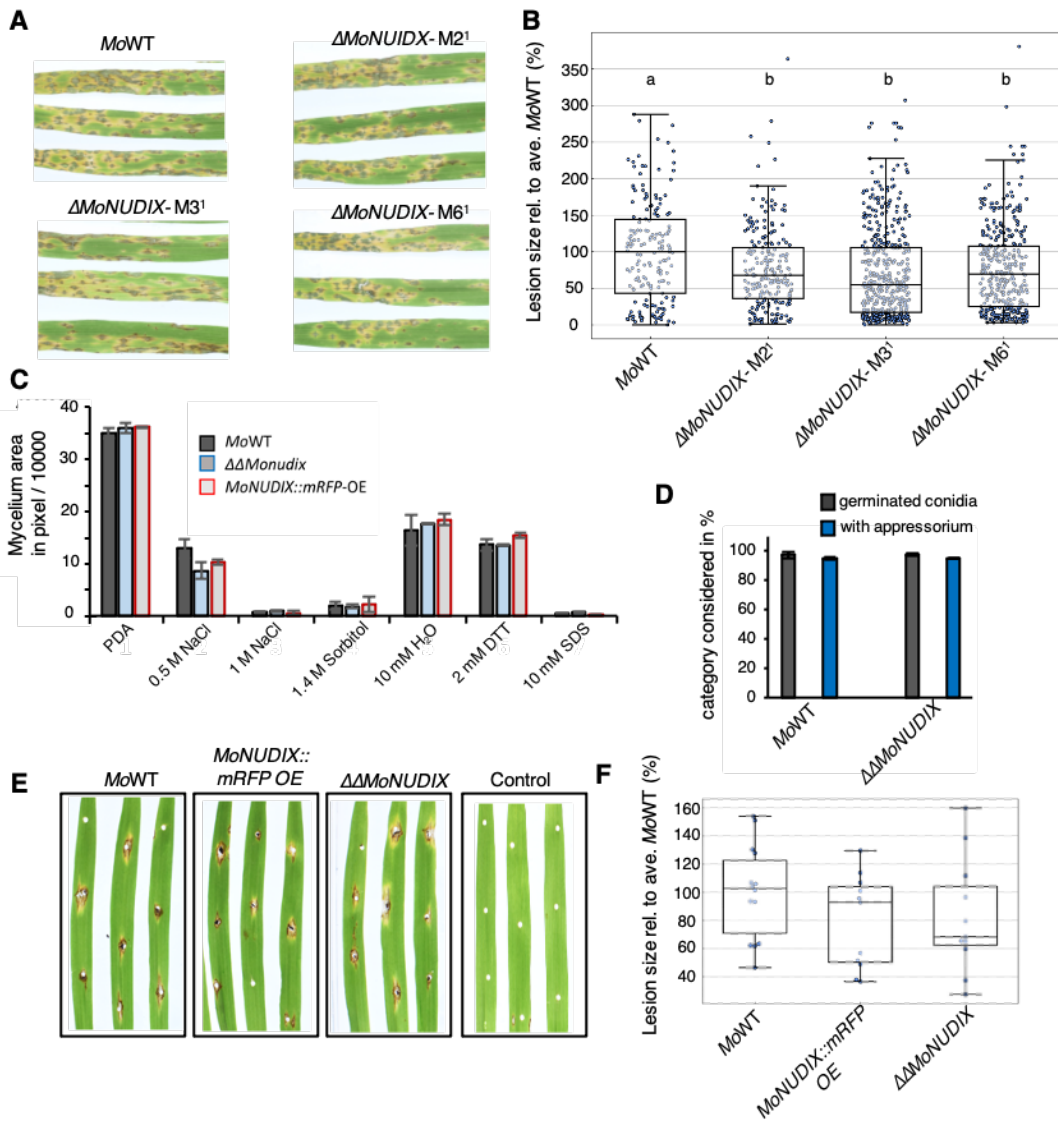


Fig. S4. Single *MoNUDIX* gene deletion results in a very minor reduction in lesion size, and double *MoNUDIX* gene deletion specifically effects *M. oryzae* growth during infection.

(A) To assess the impact of a single *MoNUDIX* gene deletion, wild-type *M. oryzae* (*MoWT*) and mutants $\Delta\text{MoNUDIX-M2}^1$, $\Delta\text{MoNUDIX-M3}^1$, $\Delta\text{MoNUDIX-M6}^1$ were spray inoculated on seven-day old barley leaves. Representative images of each interaction at seven days post inoculation are shown. (B) The size of ~ 200 lesions across 10 leaves were determined for each interaction using ImageJ and plotted in a box-plot diagram. Letters depict significant differences between treatments as determined with the Kruskal-Wallis H test followed by Dunn's post-hoc test ($P < 0.05$). (C) Comparison of vegetative mycelial growth of *MoWT*, a constitutively *MoNUDIX:mRFP* expressing mutant (*MoNUDIX:mRFP-OE*), and $\Delta\Delta\text{MoNUDIX-1}$. An agar block overgrown with mycelium was placed onto minimal agar with various additives to induce pH, osmotic or oxidative stress as described in (84). The mycelium grown at 25 °C in the dark was photographed after five days and evaluated using ImageJ. The mean value of the overgrown mycelium area in pixels and the

standard deviation of three technical replicates are plotted. The experiment was repeated with comparable results. (D) *In vitro* germination test and appressoria formation rate of conidia suspensions from *MoWT* and $\Delta\Delta MoNUDIX-1$ after 48 hours placed in a hemocytometer. (E) Seven-day-old primary leaves of the barley cultivar Ingrid were wounded with forceps. Vegetative mycelium of *MoWT*, *MoNUDIX:mRFP-OE*, and $\Delta\Delta MoNUDIX-1$ were placed on the injured leaf site. After seven days lesions were photographed, and representative pictures of infection sites are shown. Injured but not mycelium-inoculated leaves were used as a control. (F) The lesion size of each infection site was determined in pixels using image analysis software ImageJ and plotted in a box-plot diagram. No significant differences were detected between *MoWT* and $\Delta\Delta MoNUDIX-1$ or *MoNUDIX:mRFP-OE* (Mann-Whitney U test, $P > 0.05$).

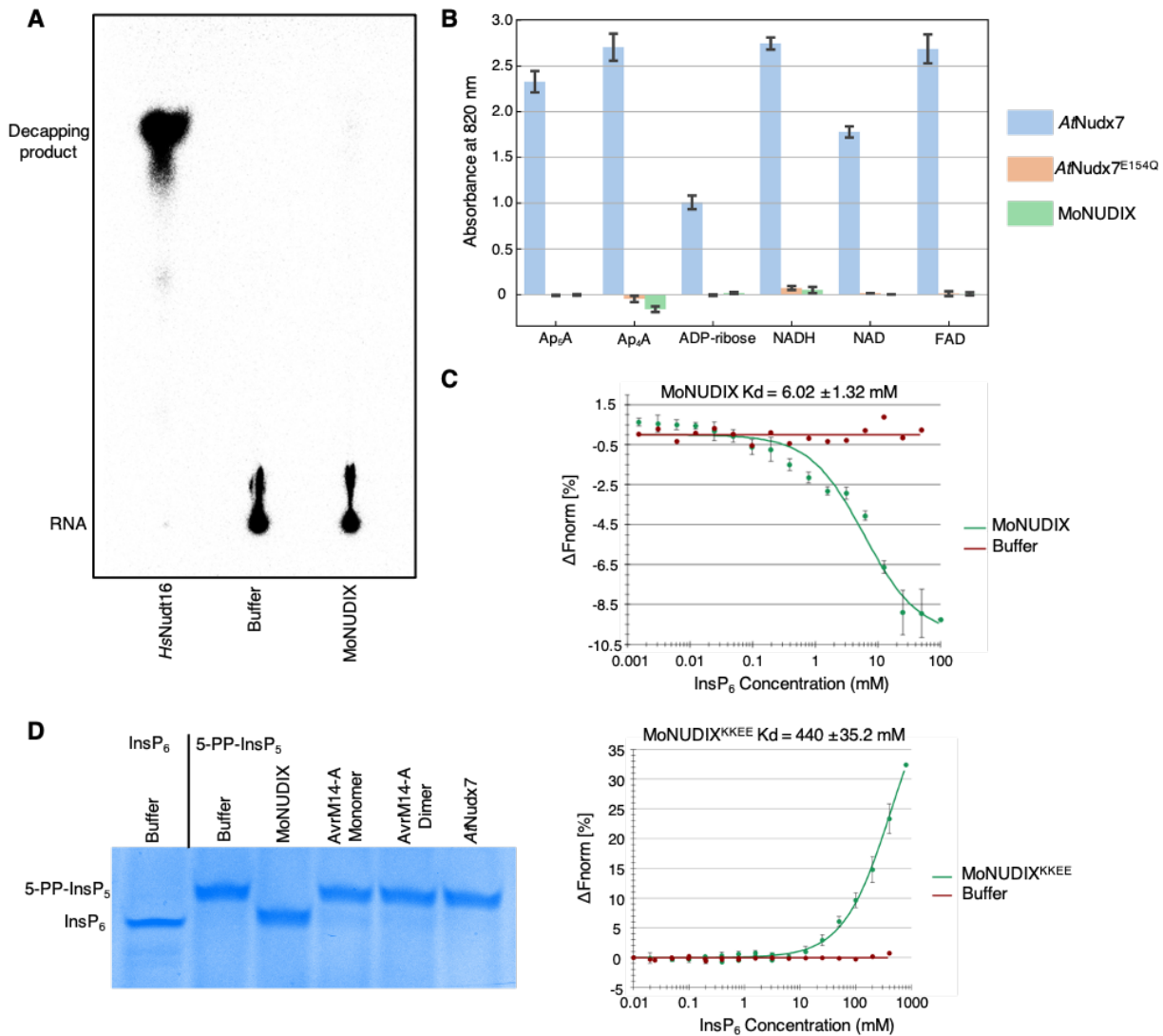


Fig. S5. MoNUDIX specifically hydrolyses inositol pyrophosphates and active site lysines are involved in inositol polyphosphate binding.

(A) Purified proteins (*HsNudt16*, a known mRNA decapping enzyme (88) and MoNUDIX) were incubated with ^{m7}Gp₃₂pp-RNA and the reaction products analysed by thin-layer chromatography (TLC). Capped RNA remains at the origin of the TLC plate, whereas decapping products migrate up the plate. (B) Purified proteins (*AtNudx7*, *AtNudx7^{E154Q}*, and MoNUDIX) were incubated with 2 mM of the indicated substrate at 37 °C for 30 minutes. Substrate hydrolysis was detected via the production of a blue-coloured phosphomolybdate complex that absorbs light with a wavelength of 820 nm. Results are mean absorbance \pm SD (n = 3). A buffer only control without any Nudix hydrolase protein was used to blank the spectrophotometer before measurement. *AtNudx7* and *AtNudx7^{E154Q}* were used as positive and negative controls, respectively. (C) Normalized microscale thermophoresis (MST) binding curves of MoNUDIX (top) and MoNUDIX^{KKEE} (bottom) in the presence of InsP₆, alongside a protein storage buffer control. The binding curve yields a Kd of $6.02 \pm 1.32 \text{ mM}$ for MoNUDIX and a Kd of $440 \pm 35.2 \text{ mM}$ for MoNUDIX^{KKEE}.

Protein concentrations were kept constant while the InsP_6 concentration varied. **(D)** Purified protein (MoNUDIX, AvrM14-A monomer, AvrM14-A homodimer, *AtNudx7*) at a concentration of 5 μM was incubated with 5-PP- InsP_5 for 60 minutes at 37 °C. As a control, buffer-only reactions were completed with InsP_6 and 5-PP- InsP_5 . All reaction products were separated using a polyacrylamide gel and visualised by staining with toluidine blue.

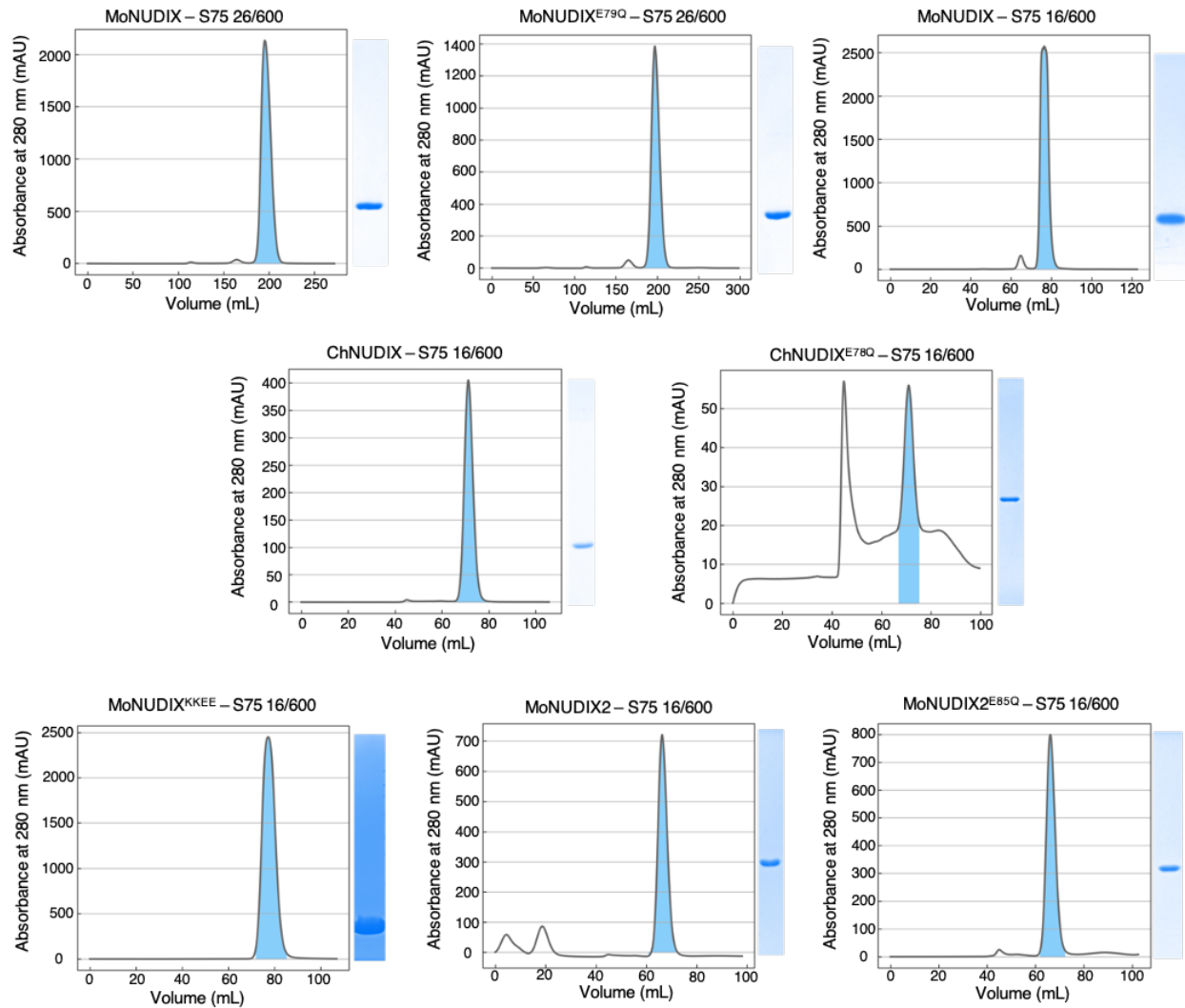


Fig. S6. All effector proteins used in enzymatic assays were purified to homogeneity.
 Size exclusion chromatography (SEC) profiles for all effector proteins purified in this study. The label at the top of each profile indicates the protein and the Highload Superdex column (Cytiva) used in the purification process. The area under the peak shaded blue indicates the volume collected for each effector. Alongside each profile is a Coomassie-stained SDS-PAGE gel demonstrating the purity of the final protein sample collected following SEC and used in enzyme assays.

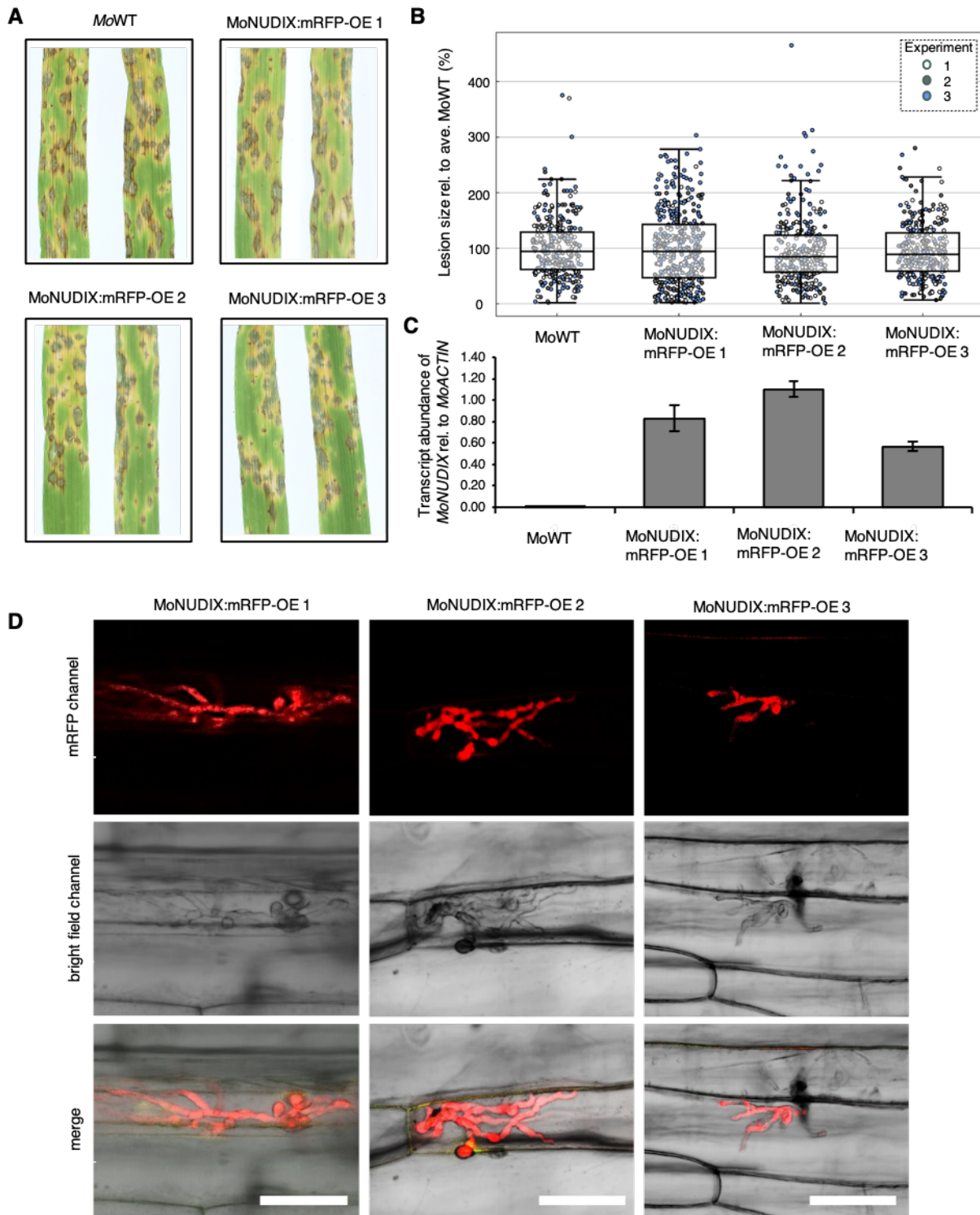


Fig. S7: Constitutive expression of MoNUDIX:mRFP in *M. oryzae* Guy11.

(A) To assess the impact of constitutive expression of MoNUDIX:mRFP on virulence, conidia of wild-type *M. oryzae* (MoWT) and three mutants (MoNUDIX:mRFP-1/-2/-3) were spray inoculated on seven-day old barley leaves. Representative images of each interaction at seven days post inoculation are shown. (B) For each interaction, the size of ~ 100 lesions across 5 leaves for

three independent experiments was determined using ImageJ and visualized in a box-plot diagram. No significant differences between any treatments were identified (Kruskal-Wallis H test, $P = 0.34$). **(C)** To verify expression of MoNUDIX:mRFP, transcript abundance in hyphae grown on PDA was quantified by qPCR. **(D)** For localization, confocal laser-scanning microscopy was performed 72 hpi using all mutants, MoNUDIX:mRFP-1/-2/-3. Scale bar: 10 μm .

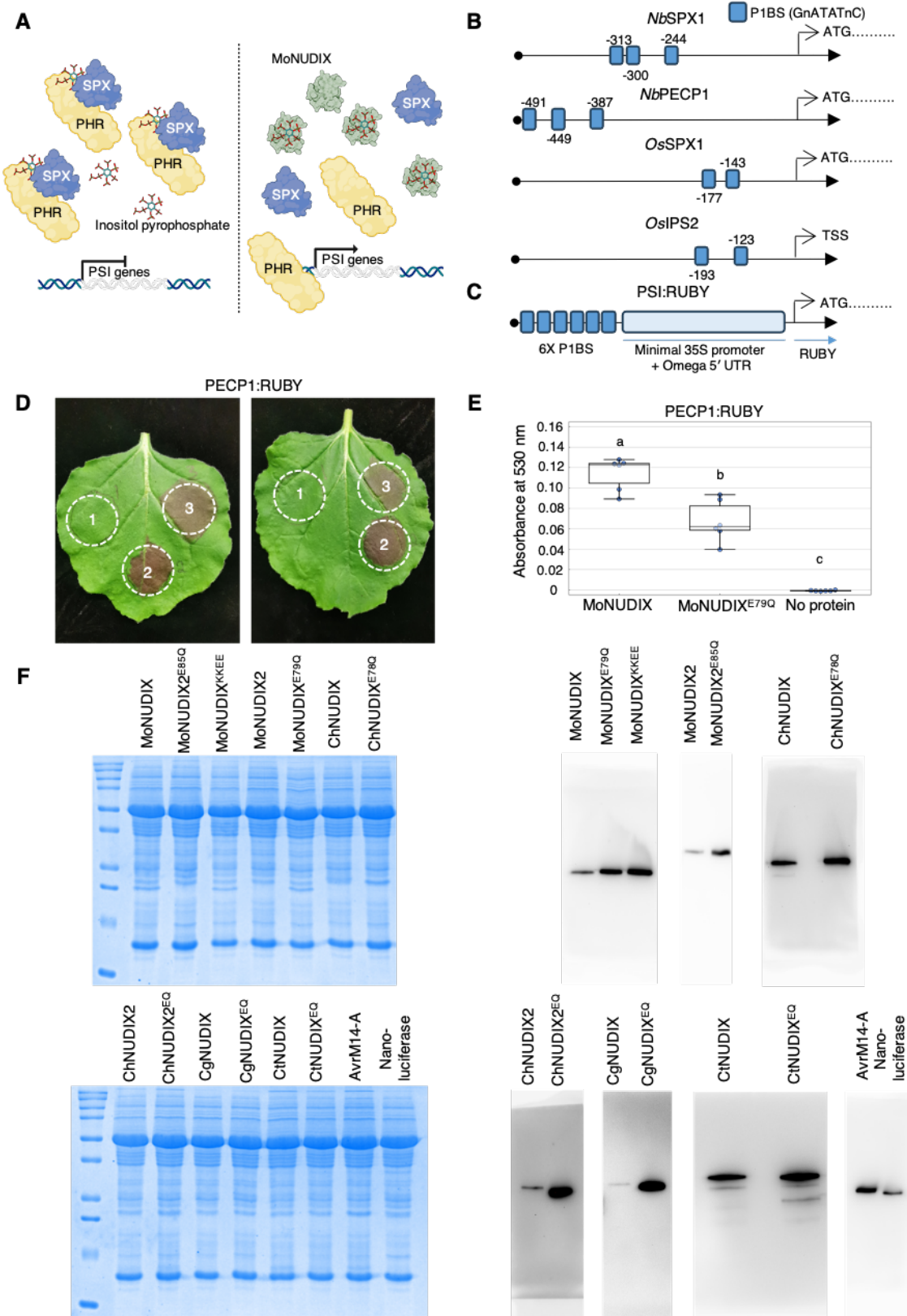


Fig. S8. Assessing phosphate starvation induction by the Nudix effectors in *N. benthamiana*

(A) The hydrolysis of PP-InsP by MoNUDIX in plant cells should activate the expression of phosphate starvation induced (PSI) genes in plants by releasing PHRs from SPX proteins. **(B)** A schematic of the 500 base pairs upstream of the *NbSPX1*, *NbPECP1*, and *OsSPX1* start codons with the PHR1-binding site (P1BS) elements indicated. The 500 bp promoter of *OsIPS2* is also shown; however, as IPS2 is a long non-coding RNA and does not have a clearly defined start codon, the predicted transcriptional start site (TSS) is indicated instead. **(C)** A schematic of the PSI:RUBY promoter and 5' UTR. The synthetic gene contains six P1BS elements in the promoter, a minimal 35 S sequence, and the Omega 5' UTR sequence from the Tobacco Mosaic Virus. Only the start of the RUBY CDS is depicted. Not to scale. **(D)** Representative leaf images demonstrating production of the red betalain pigment in *N. benthamiana* leaf tissue co-transformed with the PEPC:RUBY promoter/reporter and wild-type MoNUDIX (labelled as 2), MoNUDIX^{E79Q} (labelled as 3), or no effector (labelled as 1). **(E)** The absorbance at 530 nm of extracts from transformed *N. benthamiana* leaves. There were 6 biological replicates for each treatment, as indicated by the dots beneath the boxplots. Letters denote significant differences between treatments, as determined by a one-way ANOVA followed by Tukey's post-hoc test; $P < 0.001$. **(F)** (Left) Coomassie-stained SDS-PAGE protein gels demonstrate equivalent total protein amounts in the soluble *N. benthamiana* protein extracts from the agroinfiltrated plant tissue used for western blotting. The effector that should be present in each sample is indicated along the top of the gel; the first lane of both gels contains the Precision Plus Protein Dual Color Standards (Biorad, Hercules, California). (Right) Total protein extracts from *N. benthamiana* leaf tissue agroinfiltrated with a construct to express a HA-tagged protein, as labelled along the top of each blot, were analysed by western blotting. Blots were probed with mouse anti-HA HRP-conjugated antibodies.

Table S1. The *Magnaporthe* and *Colletotrichum* Nudix effector family. The names, species, host plant, protein sequences, and accession IDs of identified *Magnaporthe*, *Colletotrichum*, and *Ceratocystis* Nudix effectors.

<Table S1 in excel sheet >

Table S2. Sequences of the purified proteins used in this study.

<Table S2 in excel sheet >

Table S3. Sequences of all proteins expressed in *N. benthamiana* in this study.

<Table S3 in excel sheet >

Table S4. Promoter sequences discussed in this study.

<Table S4 in excel sheet >

Table S5. Crystallography data collection and structure refinement statistics for 8SXS

<Table S5 in excel sheet >

Table S6. Primer sequences used throughout this study.

<Table S6 in excel sheet >